



University of  
**Southern  
Queensland**

**MODELLING FLOODPLAIN VEGETATION RESPONSES TO  
CATCHMENT HYDROLOGY UNDER DIFFERENT  
CLIMATE CHANGE SCENARIOS**

A Thesis submitted by

**Newton Muhury**

B.Sc. Agril. Engg.

MSci (Res)

For the award of

**DOCTOR OF PHILOSOPHY**

**2023**

## ABSTRACT

The floodplain ecosystems are the most ecologically and economically significant areas increasingly becoming vulnerable and facing severe challenges due to climate change. Understanding how floodplain vegetation responds to changes in climate is essential for effective conservation and management strategies. This study was conducted in an Australian floodplain, with the following objectives: 1) to assess the relationship between surface water interannual variability and responses of different vegetation types in floodplain areas; 2) to evaluate the spatiotemporal impacts of groundwater dynamics on floodplain vegetation; and 3) to model floodplain vegetation responses under different climate change scenarios. To address the first objective, a hydrological model was set up in the Burrinjuck sub-catchment area and calibrated against daily rainfall and streamflow data to simulate catchment runoff. Model performance was evaluated against the Nash Sutcliffe Coefficient of efficiency (NSE) value of 0.95, indicating very good performance. The modelling results show high positive relationships ( $r=0.85$ ,  $0.82$ , and  $0.81$ ) between the observed and predicted NDVI values of grass-type vegetation (distant from the stream) against the rainfall, runoff, and streamflow, respectively, during the dry season. However, these relationships were reduced by 26.8% ( $r=0.60$ ) and 33.33% ( $r=0.54$ ) against runoff and streamflow during the wet season. For the second objective, different floodplain vegetation types in the study area were analysed against groundwater dynamics at the catchment level using ArcSWAT. The SWAT model was calibrated and validated in SWAT-CUP software using ten years (2001–2010) of monthly streamflow data. The modelling results show high positive relationships ( $r = 0.76$ ,  $0.73$ , and  $0.81$ ) between the measured and predicted NDVI values of all vegetation in the sub-basin against the groundwater flow (GW), soil water content (SWC), and combination of these two variables, respectively, during the dry season. For the third objective, the SWAT model was simulated against future time series of climate data projections under RCP4.5 and RCP8.5 climate scenarios. The modelling results reveal that vegetation greenness (LAI) decreased by 147.8% during winter and increased by 5.3% in the summer. The MODIS satellite imagery has been proven effective in studying floodplain vegetation at the catchment level, as evidenced by this study. Additionally, the study emphasises how climate change will affect future floodplain vegetation sustainability. The strategic information gathered from this study regarding current and future floodplain vegetation in Australia will be valuable for long-term planning and management of floodplain vegetation in the country.

## **CERTIFICATION OF THESIS**

I, Newton Muhury, declare that the PhD Thesis entitled '*Modelling Floodplain Vegetation Responses to Catchment Hydrology under Different Climate Change Scenarios*' is not more than 100,000 words in length, including quotes and exclusive of tables, figures, appendices, bibliography, references, and footnotes. The thesis contains no material that has been submitted previously, in whole or in part, for the award of any other academic degree or diploma. Except where otherwise indicated, this thesis is my own work.

Date: 20 December 2023

Endorsed by:

Prof. Armando A. Apan  
Principal Supervisor

Prof. Tek N. Maraseni  
Associate Supervisor

Student and supervisors' signatures of endorsement are held at the University.

## **ACKNOWLEDGEMENTS**

I acknowledge the Ngunnawal, Wiradjuri, Jagera, Giabal, Jarowair, Walgalu, and Ngarigo people as the traditional custodians of the land on which I conducted research of this thesis and published it. I pay my respect to Elders past, present and emerging, for they hold the knowledge, rich traditions, and bold ambitions of Australia's First Peoples.

This thesis is the result of more than three years of intensive work journey that I have been accompanied and navigated by some nice personalities. I want to express my heartfelt gratitude to those amazing individuals for their constant support and guidance during this work.

Firstly, I greatly appreciate my principal supervisor, Professor Armando A. Apan, for his conscientious motivation and guidance and for amazing encouragement and continuous support throughout my research study. I am truly grateful to Professor Armando for his endless effort in guiding me to complete the PhD journey.

I am also thankful to my associate supervisor, Professor Tek Maraseni, for his effort in guiding me to learn scientific writing skills.

I would also like to extend my special thanks to the University of Southern Queensland for all the research support and awarding me a full scholarship to pursue my PhD program.

I thank Dr. Barbara Holmes and Nicole Zimmerle for proofreading the manuscript and for their valuable suggestions to improve writing style and readability.

I am also grateful to the Bureau of Meteorology for climate data and the United States Geological Survey for providing the remote sensing data that I applied for hydrological modelling. I thank the University of Waikato for their open-source WEKA that I used for the machine learning and linear regression modelling. I am also thankful to Johan Norad in providing technical information on LPJ dynamic vegetation model.

I am grateful to my parents for all their love, support, and encouragement for my study since childhood. Finally, I would like to extend my sincere thanks to my wife, Arupa Sarkar and loving son, Avro Muhury, for all their support and sacrifice.

The Australian Government Research Training Program Scholarship has supported this research.

# DEDICATION

To the

**Australian people**

The UniSQ scholarship was funded  
through the tax payments they made  
and

To my wife, **Arupa**,

my son **Avro**,

my parents,

**Narayan Muhury and Nilima Muhury**

For their endless love and support

# TABLE OF CONTENTS

ABSTRACT.....	i
CERTIFICATION OF THESIS.....	ii
ACKNOWLEDGEMENTS.....	iii
DEDICATION.....	v
LIST OF TABLES.....	xi
LIST OF FIGURES.....	xii
ABBREVIATIONS.....	xiv
<b>CHAPTER 1: INTRODUCTION.....</b>	<b>1</b>
1.1. Overview.....	1
1.2. Background.....	3
1.3. Statement of the problem.....	6
1.4. Significance of this study.....	7
1.5. Research questions, aims, and objectives.....	9
1.6. Scope of the study.....	11
1.7. Conceptual framework.....	12
1.8. Organisation of the dissertation.....	13
<b>CHAPTER 2: LITERATURE REVIEW.....</b>	<b>15</b>
2.1. Introduction.....	15
2.2. Climate change impacts floodplain vegetation dynamics.....	15
2.2.1. Climate change impacts catchment hydrology.....	19
2.2.2. Surface hydrology and climate change.....	20
2.2.3. Climate change impacts groundwater recharge.....	22
2.3. Surface water availability impacts floodplain vegetation.....	23
2.3.1. Surface runoff modelling at catchment level.....	23
2.3.2. Vegetation growth responses to surface water availability.....	24
2.4. Groundwater dependent vegetation.....	25
2.4.1. Groundwater modelling at catchment level.....	26
2.4.2. Vegetation growth responses to groundwater.....	26
2.5. Remote sensing technology.....	28
2.5.1. Remote sensing for vegetation index analysis.....	29
2.6. Climate change impact.....	30

2.7. Climate models and climate scenarios .....	32
2.8. Summary and knowledge gaps .....	35
<b>CHAPTER 3: RESEARCH METHODS .....</b>	<b>37</b>
3.1. Introduction.....	37
3.2. The study area .....	37
3.3. Data acquisition, processing, and analysis.....	41
3.3.1. Vegetation response to surface water (Objective 1) .....	41
3.3.2. Vegetation response to groundwater (Objective 2) .....	43
3.3.3. Vegetation response to future climate projections (Objective 3).....	45
3.4. Brief description of data processing and analysing .....	46
3.5. Summary .....	48
<b>CHAPTER 4: MODELLING FLOODPLAIN VEGETATION RESPONSE TO</b>	
<b>SURFACE WATER VARIABILITY .....</b>	<b>50</b>
4.1. Introduction.....	50
4.2. The background of floodplain vegetation response modelling to surface water	51
4.3. Materials and methods .....	54
4.3.1. Overview of research methodology .....	54
4.3.2. Study area.....	55
4.3.3. Study period .....	56
4.3.4. Vegetation in the study area.....	57
4.3.5. Data description .....	57
4.3.6. Normalised Difference Vegetation Index (NDVI) .....	59
4.3.7. Rainfall-runoff hydrological modelling.....	59
4.3.8. SIMHYD model calibration and validation.....	60
4.3.9. SIMHYD model performance criteria .....	61
4.3.10. Machine learning algorithms for data processing .....	61
4.3.11. Waikato Environment for Knowledge Analysis (WEKA) tool .....	62
4.3.12. Modelling the relationships between surface water and NDVI.....	62
4.4. Results.....	63
4.4.1. Hydrological model simulated catchment runoff .....	63
4.4.2. Vegetation response to surface water during the dry season .....	65
4.4.3. Vegetation response towards surface water during the wet season .....	67

4.4.4. Vegetation response based on distance from stream .....	69
4.5. Discussion .....	70
4.5.1. Hydrological modelling .....	70
4.5.2. Vegetation response and surface water relations .....	71
4.5.3. Vegetation response based on distance from the stream .....	72
4.6. Conclusion .....	73

**CHAPTER 5: MODELLING FLOODPLAIN VEGETATION RESPONSE TO  
GROUNDWATER VARIABILITY .....** 75

5.1. Introduction.....	75
5.2. Floodplain vegetation responses to groundwater variability .....	76
5.3. Methods.....	79
5.3.1. Study area.....	79
5.3.2. Overview of the methods .....	80
5.3.3. Hydrological model setup .....	81
5.3.4. Data preparation.....	83
5.3.5. Study period .....	84
5.3.6. Sensitivity analysis and hydrological model calibration .....	85
5.3.7. Hydrological model performance evaluation.....	87
5.3.8. Remote sensing data .....	88
5.3.9. Normalised Difference Vegetation Index (NDVI) .....	89
5.3.10. Machine learning algorithms for data analysis .....	90
5.4. Results.....	91
5.4.1. Hydrological model calibration and validation.....	91
5.4.2. Relationships of vegetation responses and groundwater .....	92
5.4.3. Vegetation responses considering their location within the watershed ..	95
5.4.4. Seasonal vegetation responses .....	95
5.5. Discussion .....	100
5.5.1. Relationships between vegetation responses and ArcSWAT model simulated variables.....	100
5.5.2. Seasonal variability in each vegetation type .....	101
5.6. Conclusion .....	102

**CHAPTER 6: MODELLING FLOODPLAIN VEGETATION RESPONSE TO  
CLIMATE CHANGE.....** 104

6.1. Introduction.....	104
6.2. The need for modelling of floodplain vegetation response to climate change .	105
6.3. Materials and methods .....	109
6.3.1. Study area.....	109
6.3.2. Research methods .....	110
6.3.3. An overview of SWAT hydrological model.....	111
6.3.4. Vegetation dynamics modelling in SWAT .....	112
6.3.5. Hydrological model setup at study catchment .....	114
6.3.6. Assessment of model performance criteria.....	115
6.3.7. Trend analysis of time series data .....	116
6.3.8. Data preparation.....	117
6.3.9. Leaf Area Index (LAI).....	118
6.3.10. General Circulation Models (GCMs).....	118
6.3.11. Bias correction .....	120
6.3.12. Climate scenarios .....	120
6.4. Results.....	123
6.4.1. Analysis of the SWAT model output and parameter sensitivity.....	123
6.4.2. Analysis of the SWAT model calibration and validation against streamflow.....	124
6.4.3. Analysis of the SWAT model calibration and validation against MODIS LAI .....	125
6.4.4. The outcomes of the trend analysis of the precipitation (historical and projected) .....	126
6.4.5. Analytical results of LAI responses to the future precipitation changes .... .....	127
6.4.6. Analytical results of LAI responses to future temperature changes .....	128
6.4.7. Trend analysis of LAI in the watershed (historical and simulated).....	132
6.4.8. Analysis of the floodplain vegetation responses to the SWAT variables... .....	133
6.5. Discussion .....	135
6.5.1. Future climate variables impact on vegetation LAI.....	135
6.5.2. Seasonal variability in climate change vegetation responses .....	136
6.5.3. Vegetation responses to SWAT simulated variables under future climate changes.....	137



## LIST OF TABLES

Table 2.1 Global extent of floodplain areas.....	16
Table 2.2: A few Australian Ramsar wetland areas.....	17
Figure 2.1: Conceptual diagram of a river floodplain.....	18
Table 2.3: Different types of radiative forcing pathways .....	34
Table 3.1: List of datasets acquired .....	42
Table 3.2: List of datasets acquired in the fulfilment of objective 3. ....	45
Table 4.1: Annual dry and wet season of the study period.....	56
Table 4.2: Key datasets used, their descriptions, and sources .....	58
Table 4.3: Different types of floodplain vegetation.....	59
Table 4.4: SIMHYD model parameters .....	60
Table 4.5: Datasets prepared to apply in the WEKA model.....	63
Table 4.6: Regression modelling results.....	65
Table 4.7: Regression modelling results produced using RF and SVM .....	69
Table 5.1: The datasets used in this study.....	83
Table 5.2: The table shows the number of parameters .....	87
Table 5.3: The modelling scenarios and results.....	91
Table 5.4: SWAT simulated variables .....	92
Table 5.5: The WEKA-generated modelling results.....	94
Table 5.6: The WEKA machine learning produced modelling results for shrub .....	94
Table 5.7: The WEKA machine learning modelling results for grass .....	94
Table 5.8: The table shows the modelling results for different types of vegetation responses .	98
Table 5.9: The table shows the modelling results during wet season.....	99
Table 6.1: The datasets used in this chapter .....	118
Table 6.2: Performance indices of SWAT model parameters .....	123
Table 6.3: Trend analysis of the precipitation .....	127
Table 6.4: SWAT simulated LAI changes .....	131
Table 6.5: SWAT simulated LAI changes listed against change of predicted temperature ....	132
Table 6.6: Trend analysis of the MODIS LAI .....	132
Table 6.7: The LAI changes in response to Soil Water Content .....	133
Table 6.8: The LAI changes in response to surface water flow.....	134
Table 6.9: The LAI changes in response to groundwater flow .....	135

## LIST OF FIGURES

Figure 1.1: A few floodplain vegetation types.....	5
Figure 2.2: Total annual anthropogenic GHG emissions by gases.....	19
Figure 2.3: A diagram of hydrologic cycle.....	22
Figure 2.4: Annual streamflow in the Murrumbidgee River.....	24
Figure 2.5: Australian groundwater level status.....	27
Figure 2.6: The climate variable changes:.....	31
Figure 3.1: The location map of the study site Burrinjuck sub-catchment.....	38
Figure 3.2: The annual mean rainfall and temperature at Burrinjuck.....	39
Figure 3.3: The Input-process-output model of the study.....	41
Figure 3.4: A glimpse of the Google Earth web interface.....	42
Figure 3.5: Remote sensing data processing tool.....	43
Figure 3.6: The Waikato Environment for Knowledge Analysis.....	43
Figure 3.7: An overview of ArcGIS interface.....	44
Figure 3.8: The Digital Elevation Model (DEM).....	44
Figure 3.9: A soil map prepared to apply.....	45
Figure 3.10: The floodplain vegetation and land area of the Burrinjuck sub-catchment.....	47
Figure 4.1: An overview of the research methodology.....	54
Figure 4.2: The study area, Burrinjuck sub-catchment.....	56
Figure 4.3: The SIMHYD model calibrated and simulated runoff.....	64
Figure 4.4: The SIMHYD model simulated runoff.....	64
Figure 4.5: Graphical representation of different types of vegetation responses.....	66
Figure 4.6: NDVI from different floodplain vegetation types.....	67
Figure 4.7: NDVI from different floodplain vegetation types.....	68
Figure 5.1: Study area of the Burrinjuck sub-catchment.....	80
Figure 5.2: An overview of the research methodology.....	81
Figure 5.3: GIS data for the watershed.....	83
Figure 5.4: The point area.....	89
Figure 5.5: The model calibration and validation.....	91
Figure 5.6: The forest, shrub, and grass type vegetation NDVI.....	93
Figure 5.7: The NDVI collected from the top-point and bottom-point areas.....	95
Figure 5.8: The vegetation responses (NDVI) against the SWC.....	96
Figure 5.9: Seasonal vegetation responses (NDVI).....	97

Figure 6.1: The Burrinjuck sub-catchment watershed area .....	110
Figure 6.2: An overview of the research methods used.....	111
Figure 6.3: The GCMs projected maximum and minimum temperatures .....	121
Figure 6.4: The GCMs projected maximum and minimum temperatures (RCP8.5).....	122
Figure 6.5: Calibration and validation results from SUFI-2 .....	125
Figure 6.6: The calibration and validation of SWAT simulated LAI.....	126
Figure 6.7: SWAT simulated LAI plotted against observed LAI.....	128
Figure 6.8: SWAT simulated LAI plotted against historical LAI and GCM projected average monthly temperature .....	130

## ABBREVIATIONS

IPCC	International Panel on Climate Change
GCM	General Climate Model
DGVMs	Dynamic Global Vegetation Models
NDVI	Normalised Difference Vegetation Index
LAI	Leaf Area Index
MODIS	Moderate Resolution Imaging Spectroradiometer
SIMHYD	Rainfall-Runoff Hydrological Model
WEKA	Machine learning suite developed by the University of Waikato, New Zealand
SWAT	The Soil Water and Assessment Tool
GIS	Geographical Information Systems
NSW	New South Wales
MDB	Murray Darling Basin
CMIP	Coupled Model Intercomparison Project
BOM	Bureau of Meteorology
GDE	Groundwater dependent ecosystem
GDV	Groundwater-dependent vegetation
SRTM	Shuttle Radar Topography Mission
AVHRR	Advanced Very High-Resolution Radiometer
USGS	U.S. Geological Survey
AppEEARS	Application for Extracting and Exploring Analysis Ready Samples
UV	Ultraviolet region
RCP	Representative Concentration Pathways
ENSO	El Nino – Southern Oscillation
IOD	Indian Ocean Dipole
MJO	Madden-Julian Oscillation
OGCM	Ocean General Circulation Model
AGCM	Atmospheric General Circulation Model
AOGCM	Atmospheric-Ocean General Circulation Model
MDBA	Murray Darling Basin Authority

DEM	Digital Elevation Model
LCLU	Land Cover and Land Use
AOI	area of interest
inSAR	Interferometry Synthetic Aperture Radar
RMSE	Root Mean Square Error
NSE	Nash-Sutcliffe Efficiency
SURQ	Surface water flow
SW	Soil water content
GW	Groundwater flow
GNU	General Public License
ML	Machine Learning
SVM	Support Vector Machine
SWAT-CUP	SWAT Calibration and Uncertainty Programs
R <sup>2</sup>	Coefficient of Determination
PBIAS	Percent Bias

# CHAPTER 1: INTRODUCTION

## 1.1. Overview

Vegetation is crucial in ecosystems, influencing soil composition, atmospheric conditions, moisture levels, and other natural elements (Xue et al., 2021). In any ecosystem, vegetation is pivotal in facilitating energy transfers, regulating the water cycle, and influencing biogeochemical processes on the Earth's surface. It plays a vital role in facilitating the exchange of matter and energy among the pedosphere, hydrosphere, and atmosphere (Song et al., 2018). Thus, the interconnection of climate and vegetation is undeniable, with climate exerting a direct influence on vegetation growth (Tang et al., 2021). Over the years, there has been significant interest in studying floodplain vegetation and its dynamic changes (Klein et al., 2017; Li et al., 2020). Hence, the investigation of floodplain vegetation change has gained prominence.

Floodplain is described as 'areas of low-lying land subject to inundation by lateral overflow water from rivers or lakes with which they are associated' (Junk, 1989). According to this definition, a floodplain may be available along with rivers, lakes, deltas, and estuaries. Floodplain vegetation is essential in regulating river flow conditions and providing natural habitats for aquatic and terrestrial animals (Kingsford, 2000). Floodplain vegetation communities provide many environmental benefits, such as reducing catchment runoff, flood protection, erosion control, etc. These floodplain vegetation communities depend on surface and groundwater for their growth, survival, and other biological processes (Tockner & Stanford, 2002). This is in contrast with vegetation communities in the arid regions, where the scarcity of annual precipitation necessitates a dependence on groundwater. In fact, over 30% of global vegetation in dryland areas derives its water primarily from subsurface sources (Fan et al., 2013).

Precipitation is a major factor in floodplain ecosystem functions, as it can have intense impacts on stream flows, shallow subsurface flows, and deep groundwater flows in a hydrological cycle (Finlayson, 2005; Parsons & Thoms, 2013). Precipitation and temperature, which exhibit temporal and spatial variability, are pivotal climate parameters (Wedajo et al., 2019). Precipitation patterns have been changing globally and regionally impacting the growth of floodplain vegetation (Parsons & Thoms, 2013). In Australia, floodplain vegetation communities, such as those dominated by *Eucalyptus camaldulensis*, *Eucalyptus largiflorens*,

and *Acacia stenophylla*, are also becoming endangered due to water scarcity (Doody et al., 2014). Therefore, understanding the floodplain vegetation response to the catchment hydrology is important for better floodplain management.

Conventional methods for monitoring vegetation, demand significant human and material resources, resulting in extended data acquisition cycles and limited coverage areas, posing challenges in acquiring extensive datasets (Xue et al., 2021). In the past, hydrological studies relied on ground-based observation data for modelling purposes. Data anomalies were one of the limitations in this modelling process at large scale, which was eliminated by using higher spatial resolution data to evaluate hydrological processes more accurately (Wanders et al., 2014). Remote sensing technology addressed this issue in hydrological studies as satellites consistently monitor a specified area in regional and global scales (Long et al., 2014). At present, many organisations provide remote sensing data with minimum or no cost, which allow scientists to use spatial datasets for better hydrological modelling (Long et al., 2014). Researchers (Mancini & Corbari, 2014) found that applying remote sensing technology in calculating surface temperature, Leaf Area Index (LAI), soil moisture content, and vegetation cover area helps to improve hydrological modelling. Hence, it is crucial to utilise remote sensing information for precise calculation of groundwater recharge and detection of floodplain vegetation changes in response to climate variations at different locations. This is essential for improving the assessment of water usage efficiency and enhancing water resource management in floodplain areas.

Considering the interconnections between floodplain vegetation and hydrology, as well as the relationship between hydrology and climate, it is valid to hypothesise that climate change is expected to impact on floodplain vegetation. Thus, climate change impacts on floodplain vegetation require a quantitative assessment rather than speculations.

The aim of this study was to model catchment hydrology under climate change, including surface runoff and groundwater recharge, at a spatio-temporal scale and complexity appropriate for understanding its effects on floodplain vegetation mapped using remotely sensed data. This study helped to better understand the relative contribution of ecohydrological parameters in governing groundwater and surface water distribution and their impacts on floodplain vegetation.

## 1.2. Background

Climate is defined by the long-term patterns average of at least 30 years in various weather variables, encompassing temperature, precipitation, atmospheric pressure, humidity, and wind (Noor et al., 2020). At any given time, climate is a function not only of the atmosphere but is rather the response to linkages and couplings between the atmosphere, the hydrosphere, the biosphere, and the geosphere (Hartmann, 2016). In the pre-industrialisation era, the climate system has exhibited variations over decades to millennia, influenced by both internal dynamics and external radiative forcings, leading to the emergence of distinct and prolonged weather patterns (Mann et al., 2021). These external factors encompass fluctuations in solar radiation, alterations in Earth's orbital parameters, intrinsic fluctuations within the climate system, movements of tectonic plates, and modifications caused by volcanic aerosols as well as human-induced changes in atmospheric composition (Zachos et al., 2001; Le Treut et al., 2007; Houghton et al., 2015).

In the past, the Earth has experienced recurring periods of warming and cooling due to disruptions of energy in the climate system (Houghton et al., 2015; Hartmann, 2016). This energy is mainly sourced from solar radiation. The amount of energy reaching the atmosphere each second on a solar facing surface area of one square meter during daytime as sunlight is approximately 1,370 watts (Le Treut et al., 2007). Some 30% of the sunlight reaching the top of the Earth's atmosphere is redirected back into space (Eddy, 2009). Remaining sunlight is reflected via snow, ice, and deserts like areas of the Earth's surface and the small amount of sunlight which is not reflected to space, absorbed by the Earth's surface and atmosphere (Le Treut et al., 2007). Most of this redirection occurs due to clouds and small particles known as 'aerosols' in the atmosphere (Madronich & Flocke, 1999). To maintain equilibrium in energy absorption, Earth must radiate, on average, emit an equivalent amount of energy back into space (Eddy, 2009). The Earth itself, as well as everything on Earth, emit longwave radiation constantly (Schmidt et al., 2010). However, to emit the absorbed energy, the Earth's surface temperature is supposed to be cooler than the mean global surface temperature (Akitt, 2018). The presence of greenhouse gases helps Earth's surface warmer by acting as blanket which is known as natural greenhouse gas effect (Schmidt et al., 2010). Human activities and some natural causes (i.e., bush fire, volcanic eruption etc.) intensify the blanketing effect through the release of greenhouse gases. Compared to pre-industrial era, approximately 35% of carbon dioxide has increased in the atmosphere, which is known due to human activities through fossil fuels combustion and deforestations (Andres et al., 2012). Thus, human activities have been

significantly modifying the chemical compositions of the global atmosphere leading to significant consequences for climate.

In recent history, the atmosphere has experienced extensive and varied effects due to global change, with human-induced climate change posing a significant threat to numerous species, communities, and ecosystems worldwide (Boukal et al., 2019). Among human activities, greenhouse gas emission is considered one of the main reasons that shifts climate conditions dreadfully (Schmidt et al., 2010). The International Panel on Climate Change gives compelling data indicating that over the past thirty years, the average global temperatures of both land and ocean surfaces have consistently surpassed than previous decade since the first record in 1850 (Short et al., 2016). According to IPCC (2007) the global surface temperature has increased by 0.74°C in the last century with an intense increasing rate after World War II. If the greenhouse gas emissions continue increasing, the projection indicates temperature may increase up to 1.5°C by the year 2050 (Allen et al., 2018). This temperature increase is highly correlated to precipitation, which is one of the main sources of fresh water in many arid and semi-arid countries (Xue et al., 2021). Ongoing climate change has been continuously shifting the primary climatic variables such as temperature and precipitation, that directly affect the regional water resources by altering the surface waterflow and groundwater recharge (Jiang & Grafton, 2012).

The low flow period is also important for some species such as waterbirds (e.g. *Ardea ibis*, *Pelecanus conspicillatus*), insects (e.g. *Papilio fuscus*, *Odonata zygopteran*), and microscopic organisms such as zooplankton (*Copepod candacia*) (Kingsford, 2000). The floodplain dominated trees (Figure 1.1), such as river red gum (*Eucalyptus camaldulensis*), black box (*Eucalyptus largiflorens*), coolibah (*Eucalyptus coolabah*) and river cooba (*Acacia stenophylla*), are flood and drought tolerant. These woodlands can survive during the long, dry period but require a wet period for seed germination and seedling management (Patil et al., 2020).



Figure 1.1: A few floodplain vegetation types growing in the study area (Roberts & Marston, 2011).

Climate variability and climate change have a significant influence on the global vegetation response within ecosystems (Xue et al., 2021). The response of vegetation dynamics to climate change varies significantly with various geographical patterns and sensitivity effects to climate factors due to the spatial variability of ecosystems (Zhong et al., 2010). This demonstrates a feedback mechanism in vegetation-climate interactions. The relationship between changes in air temperature and precipitation may influence plant dispersion and vegetation vigour, limiting the length of the growing season (Huang et al., 2016). A warming environment can considerably increase the process of respiration in plants, evapotranspiration, and increase the soil moisture deficit, all of which can influence vegetation development (Foley et al., 2000; Huang et al., 2016).

Moreover, variation in atmospheric temperature significantly influences in the inter-annual variability of vegetation dynamics by indirectly changing the sunlight, solar radiation, and precipitation (Huang et al., 2016). On the other hand, the precipitation change in the Southern Hemisphere most likely contributes drying trends and the resultant vegetation activities in the semi-arid regions e.g., southern part of Chile, Africa, and south-eastern part of Australia (Parsons & Thoms, 2013; Li et al., 2020). Due to the impact of global climate change, specific structural traits of various vegetation types undergo alterations, influencing their associated functions within the Earth-atmospheric system (Huang et al., 2016). Generally, there has been a notable shift in global vegetation cover, which has an impact on species dynamics and grassland conditions (Arora, 2002; Boukal et al., 2019). In reaction to environmental

variables, the world's vegetation types, including native vegetation such as forests, grasslands, and shrublands, are negatively impacted by land, topography, and soil (changing land cover influencing drainage and erosion and decreased cohesion of residual plant) (Foley et al., 2000). Understanding these elements and their effects on vegetation dynamics allows for the implementation of targeted effective mitigation strategies to ensure biodiversity sustainability, including vegetation protection.

### **1.3. Statement of the problem**

Floodplain degradation is widespread and threatens ecosystems in both regional and global scales. Studies have been conducted over time to examine the degradation of floodplains, which is associated with habitat loss and altered ecological processes, with a specific emphasis on changes in land use (Entwistle et al., 2019). However, another crucial aspect that has been overlooked in the previous studies is the climate change impact on floodplain degradation (Mosner et al., 2015). Lewin (2013) documented this degradation, which has been occurring for approximately the last 400 years, including how the geomorphological processes disconnecting rivers from their floodplains. Climate change-induced rainfall reduction makes billabongs dryer, as well as other land features connected to the floodplain (Finlayson, 2005). These billabongs and waterholes provide natural habitats for aquatic species such as frogs, fish, etc. (Reid et al., 2012; Hillman & Shiel, 2017). However, despite a variety of their economic, cultural, and environmental services, floodplain and their related ecosystems have become endangered. Although these concerns lack thorough explanation (Blöschl et al., 2019), they notably highlight the importance of delving into quantifying climate changes' impact on surface and sub-surface water flow, as well as the responses of floodplain vegetation.

Previous study on Australia's largest wetlands, the Lowbidgee floodplain (located downstream of the Murrumbidgee River which covers approximately 217,000 hectares), has focused on reduced river flow to assess floodplain's significant size reduction (Kandasamy et al., 2014). The sub-surface water flow, soil water content, groundwater recharge and runoff were not studied simultaneously. However, flow reduction directly impacts photosynthesis processes by altering environmentally available water in a floodplain system. Water consumption by vegetation depends on various factors including their physiological properties (such as leaf area, depth of root, etc.) and environmental factors, i.e. catchment runoff,

infiltration, groundwater recharge, atmospheric temperature, humidity, and greenhouse gas concentration (Politti et al., 2014; Qaderi et al., 2019). The river regulation is another reason that affects the available amount of water in the environment. River flows are the key to recover floodplain from dying state, with growing interest in managing flows for floodplain. Environment-friendly water allocation methodologies have been developed in few countries, such as North America, South Africa, as a response to higher water demand on the water resource for the survival of flora and fauna, especially in arid and semi-arid areas (Hughes & Rood, 2003). However, based on literature review, no study has claimed that comprehensively examined the concurrent impacts of climate change on both surface and groundwater within the catchment area, alongside changes in the Leaf Area Index (LAI) of floodplain vegetation, under both current and projected future climate scenarios. The insights derived from such investigations are crucial for accurately estimating seasonal and annual vegetation growth under the changing climate conditions (Eccles et al., 2021).

The biophysical effects of vegetation on climate systems have been considered in several studies concerning deforestation and anthropogenic land cover change (Gao et al., 2001; Arora, 2002). Vegetation actively participates in the evapotranspiration process that affects surface energy and water balance in a more effective way than bare soil, as the plant can draw moisture from the soil more quickly (Bruijnzeel, 2004). Previous studies found in bi-directional relation between climate change and vegetation, coupling General Climate Models (GCMs) with Dynamic Global Vegetation Models (DGVMs) (Foley et al., 2000; Arora, 2002). However, previous studies could not provide adequate answers to how vegetation dynamics, i.e., growth and reproduction, respond to extreme climatic variable changes such as intense precipitation or intense atmospheric temperature. This study focused on estimating the impacts of climate change on catchment runoff, groundwater recharge, and vegetation growth by implementing two different hydrological modelling frameworks at a sub-catchment level.

#### **1.4. Significance of this study**

Climate change has been intensifying the hydrological cycle since the last century, which may lead to shifting global drylands (Chen et al., 2017). Compared to other vegetation communities, the floodplain vegetation community is highly sensitive to the river flow for their nutrient supply. Most of Australia's dryland rivers have the most variable flow regimes in the world for their long period of low or no flow, followed by extreme floods (Leigh et al., 2010). These variable and unpredictable flow creates floodplain inundation variability and influencing

floodplain vegetation distribution and productivity (Thapa et al., 2016). Therefore, understanding the pattern of streamflow changes is critically important to understand floodplain vegetation growth in response to surface water availability.

Quantifying the climate change-induced hydrological effects on floodplain vegetation is important to investigate to develop floodplain management policies for both regional and global communities (Mosner et al., 2015). This research offered potential benefits for state and local government agencies, environmental stakeholders, research groups, and any other entities that deal with developing policies for sustainable floodplain vegetation management. This study will generate knowledge for better understanding of climate change's impacts to floodplain vegetation.

The river flow variability influences floodplain ecosystems in various ways. A longer period of the dry condition can lead to a decline in tree conditions, such as leaf mortality and branch dieback to mitigate transpiration demand in response to groundwater depletion, as tree growth significantly improves with a shorter period of inundation (Davies et al., 2012). However, climate change can impact the dry and wet conditions of catchment hydrology, leading to negative responses in floodplain ecosystems (Paillex et al., 2013).

Significantly, groundwater is also important in maintaining floodplain wetlands health (Fu et al., 2020). Shallow aquifers that are connected to the river flow contribute water to the floodplain by storing water during floods (Fu et al., 2020; Wu et al., 2022). Studies suggest that regional groundwater flow may also control floodplain hydrological process when the wetland is in the groundwater discharge zones (Cartwright et al., 2019). Thus, regional groundwater flows influence floodplain nutrients condition and vegetation distribution (House et al., 2016; Cartwright et al., 2019; Fu et al., 2020). However, assessing groundwater flow and floodplain vegetation interactions at sub-catchment level is critical for a river-fed floodplain system. This thesis provides significant insights to understand the underlying relationship between groundwater recharge and floodplain vegetation responses at a sub-catchment level.

This study is one of the comprehensive works on floodplain vegetation responses to future climate change using a set of methods that applied station gauged and remote sensing data and GIS techniques in hydrological modelling to simulate vegetation LAI, as well as investigating the relationships between soil water content, surface runoff, groundwater recharge and floodplain vegetation greenness. Researchers can acquire valuable insights into the intricate dynamics of these ecosystems. Such understanding plays a pivotal role in forecasting and alleviating the effects of climate change on biodiversity, ecosystem services,

and human communities. The methodologies applied in this study can be replicated in a similar floodplain context in different parts of Australia and globally.

### **1.5. Research questions, aims, and objectives**

This study focused on the main research question: *“What is the potential response of different floodplain vegetation communities to the current and future climate-induced hydrological change at a catchment level?”* Using the high-resolution Normalised Difference Vegetation Index (NDVI) imagery and Leaf Area Index (LAI) data derived from MODIS imagery as representation of vegetation greenness, this research specifically has addressed the following research questions, namely:

1. What is the relationship between floodplain vegetation response (measured by remote sensing) and surface water availability in the dry and wet seasons under historical and current climate conditions?
2. How does groundwater dynamics affect floodplain vegetation (measured by remote sensing) during dry and wet conditions using historical and present climate data?
3. What are the projected impacts of future climate change on floodplain vegetation dynamics?

Addressing each of the three research questions in this thesis can significantly contribute to accomplishing the primary goal by providing comprehensive insights, evidence, and analysis. The first research question sets the relationships between surface water availability and floodplain vegetation responses by exploring fundamental concepts, theories, or background information related to the catchment hydrology. Addressing this question allows for a thorough understanding of the catchment and modelling framework surrounding the research area. By addressing this question, the thesis demonstrates a comprehensive understanding of the seasonal surface water availability under climatic conditions.

The second question involves spatial data obtaining and analysis to setup a hydrological model for understanding groundwater dynamics. By addressing this question, the thesis provides empirical evidence to support its hypotheses. This empirical evidence strengthens the validity and reliability of the thesis findings, enhancing its overall credibility. Additionally, addressing this question allows for a deeper understanding of the groundwater floodplain vegetation relationships that contribute to the broader understanding of the research topic.

The third question focuses on future climate projections and their implications to simulate Leaf Area Indices (LAI). Addressing this question allows the thesis to discuss the potential impact of climate change on floodplain vegetation growth. By considering this research question, the thesis moves beyond mere description or analysis to provide meaningful insights that can improve policy-making or further research in this field. This contributes to the broader impact and relevance of the thesis, demonstrating its significance beyond academic discourse.

Ultimately, addressing each of these research questions contributes to accomplishing the main goal of the thesis by providing a comprehensive, evidence-based exploration of the research topic. It establishes a strong theoretical foundation, presents empirical evidence to support hypotheses, and discusses the greater implications of the findings. Together, these components contribute to advancing knowledge in the field and achieving the overall objectives of the thesis.

This study aimed to assess the potential hydrological and climate change impacts on floodplain vegetation communities at the catchment level using remote sensing data and hydrological modelling. In this study, two different hydrological models were used for catchment runoff simulation and groundwater recharge estimation. A series of computational experiments applied using historical runoff and climate data covering both extreme climatic events such as floods and prolonged droughts. A deterministic catchment hydrological model was set up to simulate Leaf Area Index (LAI). The model performance was assessed using LAI data obtained from MODIS satellite imagery to project future floodplain vegetation response. The research was guided by the following specific objectives:

1. to assess the relationship between surface water interannual variability and responses of different vegetation types in floodplain areas using multi-temporal satellite imagery and time series data
2. to evaluate the spatio-temporal impacts of groundwater dynamics on floodplain vegetation through groundwater modelling using remote sensing data and time series data; and
3. to model floodplain vegetation responses under different climate change scenarios using model simulated LAI and GCMs predicted future climate data.

## 1.6. Scope of the study

The scope of this study included the assessment of hydrological analysis of the catchment to understand water availability for vegetation use under future climate change scenarios in relation to surface water and groundwater changes. A simplified version of Hydrolog known as SIMHYD hydrological model was employed at the upstream sub-catchment of the Murrumbidgee River catchment in the south-eastern part of Australia. This model was able to mimic the catchment runoff which was then correlated to NDVI using machine learning tool, WEKA. The Soil Water and Assessment Tool (SWAT) was applied at catchment level to calculate groundwater recharge, which then correlated to the SWAT simulated LAI as vegetation greenness which was then analysed under future climate scenarios to understand the vegetation climate change relationships. Global Circulation Models projected future climate data for a future period from 2030 to 2100 were applied in this study. The proposed methodologies applied in this study, in combination with remote sensing and GIS, to estimate groundwater recharge is a pilot application in the Murrumbidgee River floodplain area. Moreover, this research included different types of vegetation e.g., trees, shrubs, and grasses. In addition, this study focused on understanding how changes in the ecohydrology of the area, specifically groundwater and surface water distribution (introduced by climate variability and change), have impacted floodplain vegetation.

The specific outputs and contributions of this study are the following:

- a. The hydrological modelling applied for both surface water and groundwater at a catchment level, with output modelling result, can be applied for water resource management.
- b. The groundwater recharge estimation applied at a sub-catchment area considering future time series data, can be utilised for water resource allocation policies.
- c. This study produced qualitative and quantitative analysis of vegetation response to future projected climate change, which would be useful for better floodplain vegetation management.
- d. The research methodologies applied for vegetation modelling can be applied to identify future bushfire prone area.

## **1.7. Conceptual framework**

Global climate change is an ongoing phenomenon that can bring negative impacts on floodplain vegetation, such as reducing vegetation growth, changes in growth patterns, and inter-annual variability (Fu et al., 2020). The temperature increase and precipitation change, for instance droughts and excessive rainfall, can adversely affect vegetation growth in Australia (Jiang & Grafton, 2012). This study used hydrological modelling techniques and remote sensing methods to address the potential impacts of climate change in floodplain vegetation dynamics. Firstly, catchment hydrology was analysed using conceptual and deterministic hydrological models to determine surface runoff and groundwater recharge. Secondly, remote sensing methods applied to identify vegetation greenness in the form of NDVI and LAI for different types of vegetation in relation to spatial variations. Finally, under different climate scenarios, the future climate data was applied in the SWAT model to simulate LAI and other variables to determine the vegetation response to future climate change. The conceptual framework of this study is presented in Figure 1.2.

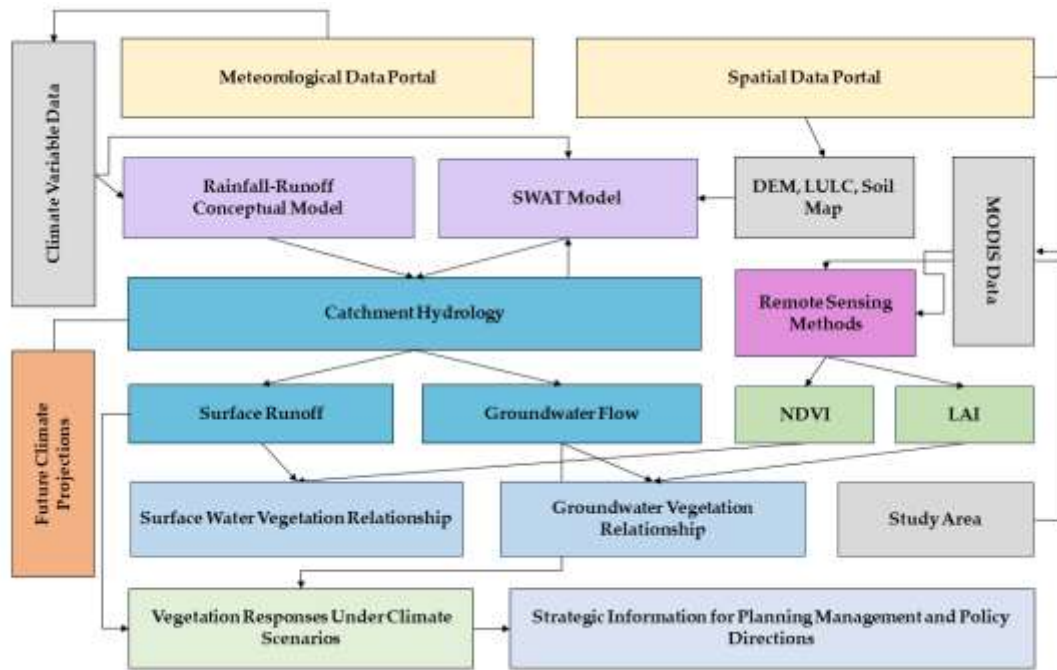


Figure 1.2: A conceptual framework of the study.

## 1.8. Organisation of the dissertation

This thesis is organised into seven chapters. **Chapter 1** (Introduction) outlines the overview and background of the study, identifies the research gaps, provides the significance of the study, enumerates the research questions, aim and specific objectives of the present work, defines the scope and limitations, and describes the conceptual framework of the study.

**Chapter 2** (Review of Literature) provides a review of the current knowledge and gaps relevant to the study. These include the explanations of changing vegetation dynamics due to global climate change, use of remote sensing technology in vegetation mapping, the incidence of climate change and its impacts, the GIS-based techniques in hydrological modelling, and the use of MODIS LAI data in modelling the future response of vegetation in relation to climate change incidence. **Chapter 3** delves into the Research Methods employed in this study, providing insights into the study area, the overarching study design, and the essential elements of data, including acquisition, pre-processing, and data analysis.

**Chapter 4** and **Chapter 5** discuss the floodplain vegetation response to the environmental water availability at the catchment level. **Chapter 4** addresses the first objective of this study. It presents the use of MODIS NDVI imagery in mapping the floodplain vegetation in the Burrinjuck sub-catchment, NSW, Australia, and the surface runoff simulation using

hydrological model and time-series climate data to model the relationship. **Chapter 5** addresses the second objective of the study. It explains the projection of groundwater variability and modelling floodplain vegetation response using the ArcSWAT model, MODIS NDVI data, and Machine Learning.

**Chapter 6** addresses the third objective of the study. This chapter discusses the projection of future climate data and simulation of leaf area index (LAI) and other SWAT variables under climate change scenarios using the ArcSWAT model. In addition, an analysis of model performances against LAI and streamflow is also presented in this chapter.

Lastly, **Chapter 7**, presents the overall conclusions, implications, explains the overall summary, findings, research contributions of the study, and finally enumerates the recommendations for future studies.

## **CHAPTER 2: LITERATURE REVIEW**

### **2.1. Introduction**

The preceding chapter introduced the comprehensive framework of the study. This framework highlighted the imperative of examining catchment hydrology, forecasting floodplain vegetation distribution, and projecting future climate impacts. These analyses aim to furnish crucial insights for strategic planning, effective floodplain management, and informed policymaking, particularly addressing the challenges posed by climate change. In this second chapter, a literature review was conducted on floodplain vegetation responses to water availability, the importance of floodplain vegetation, the application of remote sensing technology in hydrological modelling, the impact of climate change on floodplain vegetation, and the floodplain vegetation response under future climate scenarios. The specific and detailed literature reviews for each objective are presented in **Chapters 4 to Chapter 6**.

### **2.2. Climate change impacts floodplain vegetation dynamics**

Floodplains are environmentally sensitive and ecologically viable areas important for catchment hydrology that provide many natural functions and services. (Dudgeon et al., 2006; Acreman & Ferguson, 2010). Despite significant contributions to biodiversity and ecosystem functions, their global endangerment is attributed to human activities, including hydrological alterations and land use changes (Tockner & Stanford, 2002; Mosner et al., 2015). Besides these anthropogenic influences on the floodplains, the ongoing changing climate conditions additionally affect the floodplain ecosystem negatively by changing hydrological conditions (Chen et al., 2017). Table 2.1 shows the largest floodplain areas around the world, including the main river system and major impacts of the floodplains.

Table 2.1 Global extent of floodplain areas that remain predominantly undisturbed in their functionality.

<b>Region</b>	<b>Large River system</b>	<b>Floodplain area (km<sup>2</sup>)</b>	<b>% of the global total</b>	<b>Major impacts</b>
Africa	Congo Basin, Nile, Niger	310, 000	13.85	Hydrological change
Europe	Danube and Volga deltas	40, 000	1.78	Embankment
North America (USA)	Mississippi	240, 000	10.7	Hydrological change
South America	Amazonian Basin	1, 100, 000	49.11	Deforestation
Asia	Mekong, Irrawaddy	400, 000	17.86	Hydrological change
Australasia	Fly River, Paroo River, and Cooper Creek	150, 000	6.7	Hydrological change

Source: Tockner and Stanford (2002)

Previous studies applied different approaches to estimate climate change and hydrological influences on vegetation dynamics in various floodplains, including arid, semi-arid, and Mediterranean regions (Rivaes et al., 2013; Kopeć et al., 2014; Leauthaud et al., 2018). Cienciala and Pasternack (2017) used remote sensing data for vegetation productivity assessment and later correlated floodplain inundation with hydroclimatic conditions, flow regulations, and floodplain vegetation productivity. Other studies (Adamson et al., 2009; Kirby et al., 2013; Qureshi & Whitten, 2014; Zhu et al., 2015) have done modelling to estimate the impact of hydrological and climate change at different catchments within the Murray Darling Basin (MDB). Similar hydrological modelling studies have also been completed in the Murrumbidgee River catchment to find climate change effects and adaptation options (Dyer et al., 2014; Qureshi & Whitten, 2014; Reinfelds et al., 2014; Ren & Kingsford, 2014). Understanding hydrological changes accurately is crucial for modeling their impact on floodplain vegetation.

In this research, Coupled Model Intercomparison Project (CMIP) Phase 5 and climate models data applied for vegetation modelling, which is different from previous studies, presented in Chapter 6. CMIP5 is a set of coordinated climate model experiments to produce a state-of-the-art multi-model dataset designed to advance our knowledge of climate variability and climate change (Taylor et al., 2012). In recent years, the assessment of LAI has been considered as one of the useful ways in vegetation modelling, which is important for the photosynthesis process and plant growth (Clough et al., 2000; Gu et al., 2017). These indices help to correlate terrestrial ecosystem structures, their functions, and their interactions with the environment (Fang et al., 2019). Understanding the LAI dynamics is significant to the

enhancement of ecosystem service under the context of global climate change (McLaughlin & Cohen, 2013). Australia has many ecosystems and wetlands which require better water management for their floodplain vegetation. Table 2.2 shows a few Australian Ramsar wetland areas, including their featured flora and fauna.

Table 2.2: A few Australian Ramsar wetland areas including featured flora and fauna.

<b>Name</b>	<b>Area in hectares</b>	<b>Vegetation</b>	<b>Fauna</b>
Apsley Marshes	880	Swamp Paperbark	White-bellied Sea eagle, Australian Bittern
Currawinya Lakes	151,300	Gidgee, Yapunyah, Mulga	Pelicans, Gulls, Terns, Swans
Fivebough and Tuckerbil Swamps	620	Grasses and salt-tolerant succulents	Australian Bittern, Brolga, Painted Snipe, Glossy Ibis
Gwydir Wetlands	102,120	Coolibah	Black-necked Stork, Jacana, Australian Bittern
Kakadu National Park	1,979,766	Grasses, Paperbark swamps	Freshwater and saltwater crocodiles, pig-nosed turtle, whistling-duck, Radjah shelduck
Kerang Wetlands	9,419	Black Box, River Red Gum, tangled lignum	White ibis, straw-necked ibis
Lake Warden System	1,999	Melaleuca trees, Acacia, Banksia	Australian Shelducks, Black Swans, Grey Teals
Riverland	30,640	River Red Gum, Black Box	Regent Parrot, Southern Bell Frog, Freckled Duck

The structure and function of floodplain ecosystems are predominantly reliant on surface water hydrology, and modifications to the hydrologic system are often indicative of disturbed and endangered floodplain ecosystems (Figure 2.1) (Vörösmarty et al., 2010; Capon & Reid, 2016). Climate change is anticipated to worsen current challenges and produce various immediate impacts on floodplain biodiversity and ecological systems (Capon et al., 2013; Capon et al., 2016). Specifically, many areas around the world, particularly in arid and semi-arid climatic zones, are expected to experience more frequent, prolonged, and intense droughts (Nielsen & Ball, 2015). Therefore, it is widely anticipated that alterations to floodplain vegetation composition, disappearance of native species, and notably, the proliferation of exotic invasions will occur in response (Catford et al., 2014).

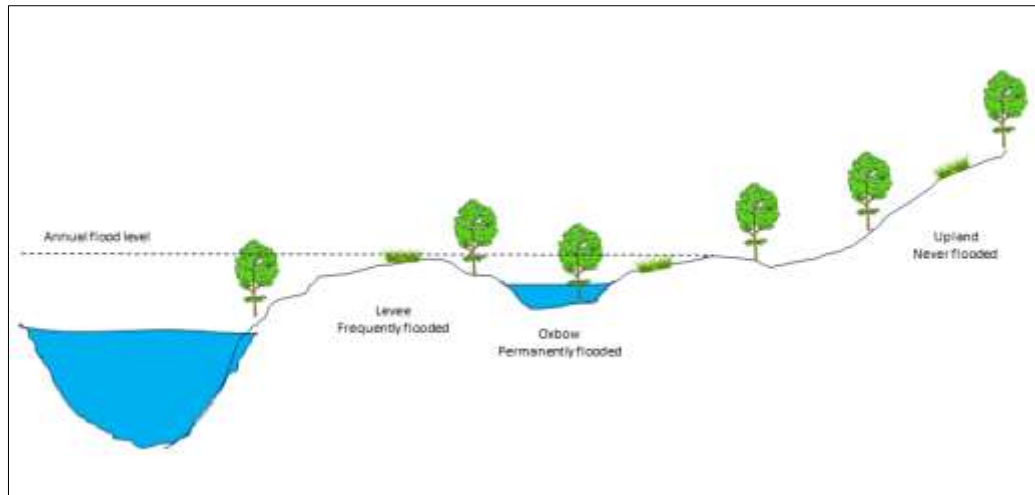


Figure 2.1: Conceptual diagram of a river floodplain area adopted from Craft (2022).

Floodplains offer a dynamic array of plant habitats, which change in response to intricate topographical gradients ranging from river channels to floodplain edges (Capon & Reid, 2016). These habitats may encompass diverse wetland depressions and other geological characteristics, flood tolerant species occupying wetter areas and drought tolerant or perennial plants dominating drier areas (Brock et al., 2003). The variability in survival and regeneration mechanisms among floodplain plant species enables the vegetation in these dynamic environments to adapt flexibly to a wide range of hydrological conditions. Arid floodplain vegetation is likely to exhibit remarkable resilience to climate change, including mega-droughts, owing to its adaptation to substantial hydrologic variability, which has encompassed previous extended drought periods (Capon & Reid, 2016).

Water resources and the hydrological cycle are linked with climate, and any changes in climate variables directly influenced water availability and quality (Yang et al., 2021). Global climate change and its impact on hydrological cycle causes the redistribution of water resources in time and space (Nan et al., 2011). This redistribution and changes of water resources at geographical location will cause the ecosystem to change greatly (Yang et al., 2021). Previous studies documented that ecosystems are highly sensitive to global warming, and as climate change is continuing, the ecosystems are facing degradation in size, reducing their services (Boukal et al., 2019; Entwistle et al., 2019; Fu et al., 2020). Furthermore, integrating vegetation dynamics responses to soil water content, groundwater recharge, and surface water flow into climate change studies is imperative for enhancing ecosystem management. This research gap has been addressed in Chapter 6 of the Thesis.

### 2.2.1. Climate change impacts catchment hydrology

The Intergovernmental Panel on Climate Change (IPCC) Fifth Assessment Report identifies that climate has changed in the last 50 years, and most regions have noticed an increase in air temperatures by 0.85 °C between 1880 and 2012 (IPCC, 2014). Anthropogenic greenhouse gas emissions have been the primary driver of climate change since the pre-industrial era (Figure 2.2). Global warming potentially influences the catchment hydrological cycle, resulting in changes in the spatial and temporal distributions of regional water resources (Boer et al., 2000; Nijssen et al., 2001; Labat et al., 2004; Ramanathan et al., 2005). Likewise, Australia is no exception to a changing climate, which was proven by significant heatwave experienced in the south-east of Australia at the beginning of 2020. Over the past 150 years, human activity has exacerbated geological, hydrological, and ecological processes driven by highly variable climates through time and across the Murray Darling Basin (MDB) (Goss, 2003; Williams, 2017). These extreme climatic conditions characterise the MDB of the recent past, and these conditions are expected to be an increasing part of future climate change (Pall et al., 2011; Ummenhofer & Meehl, 2017). Hence, the assessment of climatic influence on water resources and their corresponding ecosystem would provide better modelling opportunity under future climate scenarios.

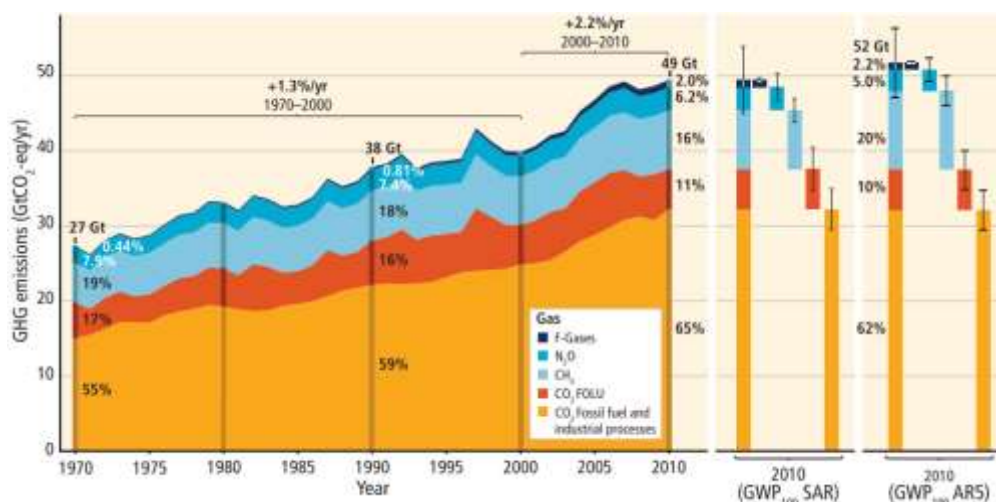


Figure 2.2: Total annual anthropogenic GHG emissions by gases 1970-2010 (IPCC, 2014).

The potential effects of climate change on the river basin hydrological cycles have been extensively analysed in various regions around the world, based on different emission scenarios and climate models (Wang et al., 2008; Raje et al., 2014; Kim et al., 2016; Mengistu et al., 2023; Probst & Mauser, 2023). The changing climate variability such as increasing temperatures can lead to high evaporation and transpiration rates, and changes in precipitation

patterns, could potentially reduce the amount of water available for surface runoff and the groundwater recharge. Given the significance of this data for floodplain ecosystem water resources management, it is imperative to assess the degree to which alterations in climate variability influence hydrological conditions.

To evaluate the climate change impact on hydrology, various approaches have been developed over time, which can be categorised into three distinct groups. These are paired catchments approach, time series analysis or statistical method, and hydrological modelling, among which hydrological models provide comprehensive analysis from limited data (Li et al., 2009). A dependable method for assessing the impact of climate change on catchment hydrology involves simulating basin hydrology using multiple hydrological models across various scenarios. Several studies have been conducted to evaluate the impact of climate change on catchment water availability (Lauri et al., 2012; Kim et al., 2013; Khoi & Hang, 2015; Shrestha et al., 2018). These studies suggest an almost certain temperature increase in the future, however the direction of change in precipitation and streamflow remains uncertain and depends entirely on the climate models and the downscaling methods. It is important to include both temperature and precipitation in the catchment hydrology modelling, so that vegetation response to catchment hydrology analysis provide a better understanding for ecosystems management.

### ***2.2.2. Surface hydrology and climate change***

Hydrological modelling results depend on model selection considering the catchment type, which means climate change impact analyses should be included in the modelling. Precipitation and snowmelt constitute the principal sources of water flow within a catchment area, while changes in precipitation patterns and temperature serve as the primary catalysts for variations in water availability for both surface and groundwater resources (Hamlet & Lettenmaier, 1999). Cuo et al. (2013) explained that any changes in observed streamflow were due to the combined effects of changes in precipitation, evapotranspiration, rainfall runoff, and baseflow, and were caused primarily by climate change. Over the past few decades, notable advancements have been made in the advancement of hydrologic models incorporating integrated features. These models effectively parameterise runoff generation processes and employ soil-vegetation-atmosphere transfer schemes to proficiently regulate water and energy balances at the land surface (Raje et al., 2014). Most of the hydrological model simulations rely on the model calibration with historical stream flow and climate data. Therefore, creating

an adaptive hydrological model that can account for future climate and catchment conditions not currently observable is a challenging task (Kim et al., 2016).

Rainfall-runoff model refers to hydrological models that replicate the flow of water in a catchment outlet by utilising input time series data of rainfall. Figure 2.3 outlined the water transformation cycle between atmosphere, lithosphere, and hydrosphere in a catchment hydrological cycle. In a balanced rainfall-runoff hydrological model, the volume of water available as surface water and ground water resources are the excess of precipitation over evapotranspiration (Beare & Heaney, 2002). This evapotranspiration fluctuates by the potential impact of climatic factors such as temperature, solar radiation, wind, and humidity. The other factors that influence evapotranspiration are catchment vegetation, vegetation type and vegetated area with the catchment (Zhang et al., 1999). However, the relationship between vegetation cover and transpiration becomes more significant as precipitation levels rise, thereby mitigating the immediate effects of climate change (Zhang et al., 1999; Zhang et al., 2022). As vegetation growth increase, so does their impact on atmospheric carbon dioxide, leading to higher levels of carbon dioxide. This increase in carbon dioxide, in turn, enhances water use efficiency, resulting in reduced transpiration. Alternatively, climate factors like elevated temperatures, alterations in rainfall distribution, and variations in soil moisture levels may either amplify or counteract the advantages conferred by increased carbon dioxide levels on plant physiology (Zhang et al., 2022). Hence, gaining insights into the correlation between plant physiology and water availability at the catchment level would be an advantage in devising effective floodplain water management strategies. Chapter 4 describes the relationship between floodplain vegetation and surface water availability at catchment level.

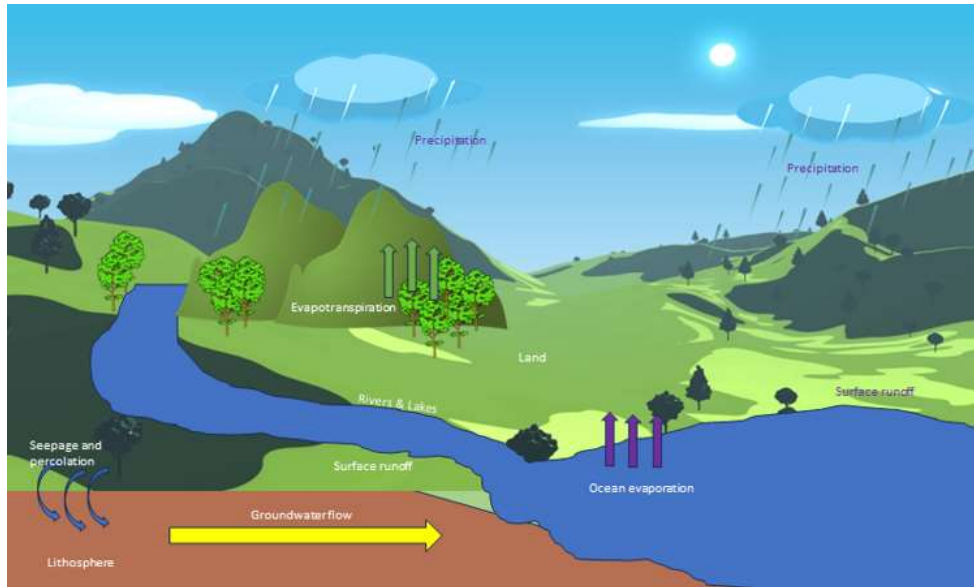


Figure 2.3: A diagram of hydrologic cycle showing the water transfer cycle between surface, ocean, and atmosphere adopted from Singh and Singh (2021).

### **2.2.3. Climate change impacts groundwater recharge**

Global warming also impacts groundwater dynamics, such as the rate and timing of groundwater recharge, and seasonal mean and annual groundwater depth variations by the distribution of precipitation (Panwar, 2013). These impacted changes in groundwater recharge may be larger than changes in precipitation (Mackay, 2008). Precipitation is one of the main sources of groundwater recharge through infiltration, depending on soil particles and land cover (i.e. vegetated land has a higher infiltration rate than bare soil) (Adhikari et al., 2020). This infiltration rate is also being influenced by several factors like the gradient of the land and size and textures of the soil particles. Infiltration rate is less on stiff land where runoff is high compared to flat land; and sand dominated soil has higher infiltration capacity than clay soil (Ziadat & Taimeh, 2013). Many studies showed that infiltration rate relates to climate change that eventually changes groundwater table. Ducci and Tranfaglia (2008) applied remotely sensed data for hydrological modelling and showed an average of 30% decrease in infiltration rate under the current climate change scenario. Ali et al. (2012), by applying Global Climate Model's (GCMs) projections, found that groundwater recharge increases by 50% in wet conditions (summer), 10-25% in semi-wet (autumn), and decreases in dry condition (winter) by 2050, compared to present values.

Regional reduction of groundwater resources or lowering the groundwater table is now recognised as a global scale problem (Konikow & Kendy, 2005). This reduction directly

impacts groundwater-dependent vegetation communities as well as environmental water availability. The future climate change prediction for less precipitation exacerbates this groundwater lowering issue by influencing groundwater recharge (Gurdak et al., 2012). Thus, for better floodplain management, the natural fluctuations in groundwater levels caused by climate variability must be considered (Dey & Mishra, 2017); Chen et al., 2004). This study aimed to evaluate the alterations in groundwater flow and subsurface water flow under projected future climate scenarios, which is discussed in Chapter 5 and Chapter 6 of the thesis.

### **2.3. Surface water availability impacts floodplain vegetation**

Surface water plays an important role in floodplain vegetation dynamics by naturally changing flooding pattern in the dry and wet season. Flooding is considered important in structuring river floodplain vegetation as it enhances the sediment and nutrient transport to the vegetation (Harvey et al., 2009). Redistribution of sediment and other nutrients is the key process for productive floodplain vegetation, including adjacent channels productivity (Kretz et al., 2021). Climate-induced hydrological alteration influences the rate and timing of surface water flow (subsequently impacting river-floodplain systems), making it one of the key environmental problems for many river basins around the world (Rosenberg et al., 2000; Grafton & Horne, 2014; Dang et al., 2016). Climate change mitigation policies require better water management to protect floodplain ecosystems for their environmental and socio-economic services (Doody et al., 2015). There are no sufficient studies found on streamflow and floodplain vegetation correlation (e.g. flow intensity and floodplain vegetation resistance) which gives a better understanding of sediment transport in shallow floodplain ecosystem (Alsdorf et al., 2007; Harvey et al., 2009).

#### **2.3.1. Surface runoff modelling at catchment level**

Surface water flow is very much influenced by catchment runoff, driven by precipitation and evapotranspiration. In a rainfall dominated hydrological system, climate change is critical because of its direct influence on precipitation and evaporation. Potter and Zhang (2009) demonstrated the severity of climate change using rainfall-runoff model in the Murray-Darling Basin. There were significant reductions in rainfall and runoff observed during the dry period in the catchment. McMahon et al. (2007) compared this high variability with

similar river system around the world. Further, a rainfall-runoff hydrological model named Simplified Hydrolog (SIMHYD) was successfully used with statistically downscaled data and gridded catchment rainfall time series data for surface water modelling (Fu et al., 2013). In this study, SIMHYD rainfall-runoff hydrological model was employed at the study catchment to assess the surface runoff (in Chapter 4 of the Thesis).

### **2.3.2. Vegetation growth responses to surface water availability**

Understanding floodplain vegetation response to water resource availability at various spatial and temporal scales encourages the rebuilding of floodplain management strategies (Yin et al., 2015). In arid and semi-arid areas, river flows proportionately fluctuate with precipitation intensity and timing. According to Bureau of Meteorology (BOM, 2021a), the annual stream flow is highly variable in the Murrumbidgee River (Figure 2.4). Scientists (Broich et al., 2018) discovered that precipitation and flooding are key drivers of vegetation distribution in dryland area floodplain. According to Sims and Colloff (2012) study of the Paroo River wetlands, vegetation greenness expanded after enormous floods. However, coupled hydrological climate change factors applying at catchment level shows that vegetation greenness mostly depends on precipitation than streamflow (Wen et al., 2013). Additionally, flooding causes bigger vegetation greenness than precipitation; likewise, flooding is essential in keeping up heterogeneous spatial-temporal pattern of floodplain vegetation (Parsons & Thoms, 2013; Broich et al., 2018). Vegetation types, distribution, and their water reliance inside floodplain channel inundation are mostly controlled by seasonal flooding (Fu & Burgher, 2015; Broich et al., 2018).

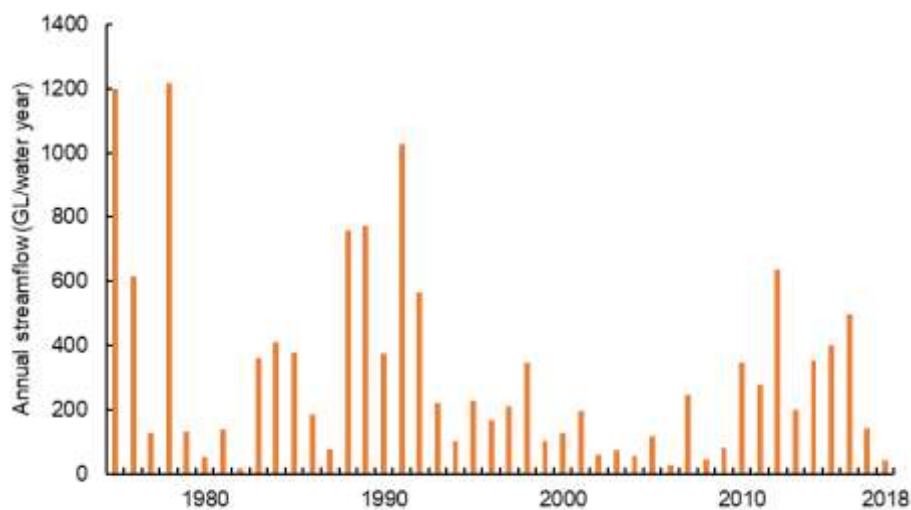


Figure 2.4: Annual streamflow in the Murrumbidgee River (BOM, 2021b).

Many of the papers that have been published primarily focused on the hydraulic connectivity between rivers and wetlands, with a specific emphasis on how rivers respond to flood pulses and their significant impact on both water dynamics within floodplain wetlands (Kingsford, 2000; Harvey et al., 2009; Kim et al., 2016). Alterations in the hydrological cycle could potentially lead to significant ecological consequences within freshwater ecosystems, primarily influenced by variations in water flow patterns, particularly regarding seasonality and extreme events (Andersen et al., 2006). Exploring the relationships among river flow and vegetation in floodplain wetlands can be challenging, primarily due to the intricate nature of hydrological processes, making reliance through field observations often difficult (Fu et al., 2020). As a result, instead of conducting comprehensive wetland studies, numerical simulations which involve modelling hydrological processes have been applied to effectively examining hydrological patterns in wetlands (Thompson et al., 2009; House et al., 2016). Nonetheless, studies that solely depended on models have a limited ability to connect model outcomes to diverse wetland patterns. Consequently, studies have introduced remote sensing data as a means to analyse the hydrological patterns within floodplains, as they provide a direct depiction of alterations in wetlands (Wu et al., 2017). Thus, applying remote sensing data in the hydrological model would provide better model performances.

#### **2.4. Groundwater dependent vegetation**

Groundwater dependent ecosystems (GDEs) use groundwater to fulfil their water requirements permanently or temporarily to support their flora, fauna and processes (Richardson & Pysek, 2012). Hydrological condition changes may directly affect floodplain ecosystem. Groundwater is known as water available under the surface, which provides an alternative source of freshwater, facing extreme pressures for excessive water demand. Lowering the groundwater table and flow rate change can be caused by human water consumption, and this groundwater reduction directly impacts groundwater-dependent floodplain vegetation (Cui et al., 2020). In recent years, increasing awareness of the groundwater-dependent ecosystem's importance encourages to understand groundwater-dependent vegetation response under hydrological and climatic change condition (Kløve et al., 2014). River-fed groundwater hydrological characteristics are crucial for groundwater-dependent vegetation (GDV) and to manage groundwater resources efficiently, including aquifers, rivers, and floodplains (Huang et al., 2019).

#### **2.4.1. Groundwater modelling at catchment level**

Groundwater recharge is the water infiltration, mostly from precipitation, through the surface to reach the groundwater storage. It is not possible to accurately and directly measure the rate of groundwater recharge due to complex infiltration process and hydrogeological settings (Gemitzi et al., 2017). The reliable indirect method is hydrological modelling for groundwater recharge estimation, in addition to the climate change impact assessment on recharge (van Dijk et al., 2013; Gemitzi et al., 2017). Researchers (Crosbie et al., 2012) found that groundwater recharge dynamics greatly fluctuates with uncertainties during dry and wet conditions from GCM-predicted climate scenarios. In general, groundwater studies report a decrease of potential groundwater recharge globally, including most of Australia (except the northern part) (Gemitzi et al., 2017). According to Taylor et al. (2012), groundwater recharge is highly related to the spatio-temporal distribution of precipitation, although higher precipitation with increased temperature, which accelerates evapotranspiration, may also cause a reduction.

There are several approaches available to estimate groundwater recharge which are categorised into physical, chemical and numerical modelling approach (Adhikari et al., 2020). Soil and Water Assessment Tool (SWAT) is a semi-distributed hydrological model which is used for analysing flow dynamics, plant growth, sediment and nutrients move with groundwater recharge rate (Awan & Ismaeel, 2014; Vigiak et al., 2015; Adhikari et al., 2020). Hydrological modelling calibration over a long period requires continuous data which involves the use of remotely sensed data for hydrologic and climate variables (Mohanty et al., 2013; Fang & Lakshmi, 2014). However, the use of other spatial data, such as digital elevation model (DEM), land use, soil map and temporal data for runoff, air temperature, precipitation, solar radiation, relative humidity and wind speed, provides better modelling results (Hallouz et al., 2019). This study employed a distributed hydrological model using ArcGIS tool applying spatial and temporal data to model catchment hydrology including groundwater recharge, which later applied for groundwater vegetation response modelling.

#### **2.4.2. Vegetation growth responses to groundwater**

In wetland ecosystems, groundwater-dependent vegetation mostly takes water from both soil moisture and groundwater system (Naumburg et al., 2005). The groundwater depth decreases with hydrological factors may cause the extinction of groundwater dependent

vegetation communities in the drylands (Braatne et al., 2008). Groundwater reduction can also limit water flow in the downstream facing water shortage. This water shortage caused degradation of groundwater-dependent vegetation as nearly 30% of all global vegetation communities in arid and semi-arid areas (Fan et al., 2013). According to the Bureau of Meteorology (BOM, 2021b), the groundwater status is mostly average to below average in the upper, middle, and lower aquifer groups across Australia (Figure 2.5). Studies around the world, including Australia, concluded that changes in groundwater depth affect dependent vegetation communities by inducing changes in vegetation dynamics (Huang et al., 2019).

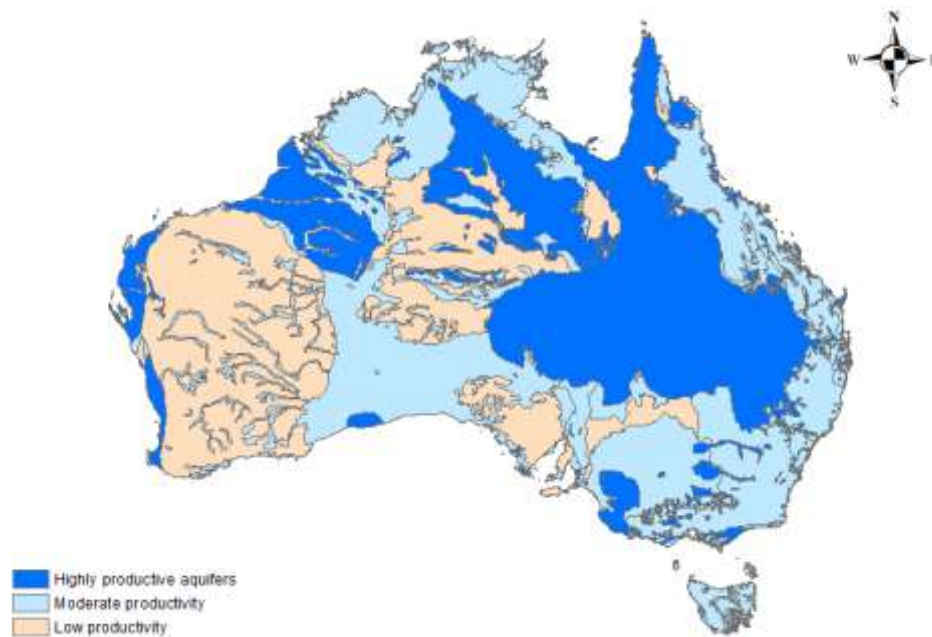


Figure 2.5: Australian groundwater level status (BOM, 2021b).

The significant groundwater depletion is one of the rising global concerns due to increasing demand, human consumption, irrigation, and groundwater-dependent ecosystems, especially during droughts. The global-scale nature of the depletion of regional groundwater resources is widely acknowledged (Konikow & Kendy, 2005). Numerous groundwater sources exhibit limited to non-renewability over significant time spans, impacting both human society and dependent ecosystems. Anticipated climate change is expected to exacerbate these concerns in various regions globally, as it will lead to decreased precipitation and heightened evapotranspiration. Both of these factors are likely to reduce groundwater recharge and potentially elevate groundwater withdrawal rates (Green et al., 2011). Thus, the growing recognition of the significance of wetlands and other groundwater-dependent ecosystems

(GDEs) has prompted more attention on gaining a better understanding of groundwater-ecosystems interactions in the face of a shifting climate (Kløve et al., 2014).

## **2.5. Remote sensing technology**

Remote sensing technologies such as satellite imaging provide a wide range of information that can be applied to hydrological studies. Knowledge of remote sensing technology has improved over the last decades, which can provide spatial information on maximum surface fluxes. In recent years, satellite remote sensing techniques have attracted researchers because of data availability and easiest retrieval process in a spatially contiguous manner (Liou & Kar, 2014). This technology helps researchers to develop various algorithms to utilise remotely sensed data, in conjunction with additional ground-based observations, to estimate hydrological parameters.

Landsat 8 images provide relatively higher spatial resolution and wider coverage data covering historical and current observations of natural resources in assessing long-term wetland changes (Jia et al., 2018). In the last few decades, remote sensing technology was applied in many wetlands related research, such as carbon cycle and climate warming in floodplain environments, land use and land cover changes, and hydrological processes in wetlands (Schmidt & Skidmore, 2003; Yuan et al., 2005; Gu et al., 2017). Besides Landsat, floodplain studies include the use of Shuttle Radar Topography Mission (SRTM), Moderate Resolution Imaging Spectroradiometer (MODIS) and Advanced Very High-Resolution Radiometer (AVHRR) data. The Aqua and Terra satellites provide daily, nearly repeated coverage of the Earth's surface with different spectral bands (Gu et al., 2017). Among them, seven bands work for land remote sensing with a spatial resolution of 250m for band 1 and band 2, while 500m for band 3 to band 7 (Pflugmacher et al., 2012). Satellite images provide an efficient tool for monitoring water areas and flood inundation extent on a large coverage (Gu et al., 2017). Most of the remotely sensed data providers included additional features in their data portals. For example, U.S. Geological Survey (USGS) data portal included Application for Extracting and Exploring Analysis Ready Samples (AppEEARS) data pre-processing tool.

Researchers have used MODIS data to monitor spatio-temporal variations of surface water and flood area in a small and large area (Chen et al., 2017). Huang et al. (2014) generated a flood inundation map, including spatial and temporal patterns of inundation, in the MDB using MODIS data. Applying the same technique, a flood inundation model was developed to

assess for overbank losses on the Murrumbidgee River Floodplain (Dutta et al., 2013). AVHRR time series and NDVI data also used to analyse the length of growing period including seasonal changes of wetland in previous study (Vrieling et al., 2013). Therefore, applying high resolution remote sensing data in mapping floodplain vegetation dynamics at the catchment level offers a promising approach, which is addressed in Chapter 4 and Chapter 5 of the thesis.

### **2.5.1. Remote sensing for vegetation index analysis**

Remote sensing of vegetation primarily involves acquiring electromagnetic wave reflectance data from canopies using passive sensors. The spectral reflectance or emission characteristics of vegetation, which pertain to how vegetation interacts with the electromagnetic spectrum, are influenced by the chemical and morphological characteristics of the surface of organs or leaves (Xue & Su, 2017). The primary uses of remote sensing for vegetation primarily rely on the following light spectra: (i) the ultraviolet region (UV), between 10 to 380 nm; (ii) the visible spectra, which are composed of the blue (450–495 nm), green (495–570 nm), and red (620–750 nm) wavelength regions; and (iii) the near and mid infrared band (850–1700 nm) (Rahim et al., 2016; Xue & Su, 2017). The indices derived from this light spectrum range can be associated with various characteristics beyond just measuring plant growth and vigour (Foley et al., 1998). These vegetation characteristics include water content, pigments, sugar and carbohydrate levels, protein content, aromatics, and more. On the other hand, the reflectivity of plants in the thermal infrared spectral range (8–14 $\mu$ m) conforms to the principles of the blackbody radiation law, enabling us to interpret plant emissions as a direct reflection of their temperature (Karwa, 2020). Therefore, indices derived from this spectral range can serve as a surrogate to evaluate the dynamics of stomata regulation, which can be used as a proxy to assess plant health.

The assessment of changes in the health of forest cover over time typically relies on ecological indicators, including total leaf area, respiration, canopy cover, biomass, and photosynthesis (Makumbura & Rathnayake, 2022). Further, the Leaf Area Index (LAI) exhibits a robust correlation with the interchange of water, energy, and CO<sub>2</sub> within forests and the environment (Rajib et al., 2020). Vegetation information from remotely sensed images primarily relies on analysing variations and alterations in the green foliage of plants and the spectral attributes of the canopy. The primary validation method typically involves establishing direct or indirect correlations between acquired Vegetation Indices (VIs) and the corresponding

in-situ measurements of vegetation attributes, including but not limited to vegetation cover, LAI, biomass, growth, and vigour assessment (Xue & Su, 2017).

Remote sensing technology helps to analyse vegetation dynamics from satellite images (Fu & Burgher, 2015). Normalised Difference Vegetation Index (NDVI) is one of the most reliable sources to characterise vegetation growth and their distribution on the ground along the catchment scale (Groeneveld, 2008; Sims & Colloff, 2012). According to Gao et al. (2001), NDVI utilises the contrast of strong reflectance in the near-infrared region and the strongly absorbed reflectance in the red wavelength region. Mathematically, NDVI is calculated from the difference between the red and near-infrared bands and normalising it over the sum of red and near-infrared bands. The NDVI analysis can be applied to reflect the density and greenness of the vegetation distributions in a selected area, which also helps to identify the relationship between vegetation and groundwater depth at catchment scale (Zhu et al., 2015). Xiaomei et al. (2007) derived suitable groundwater depth for vegetation growth from NDVI using groundwater depth histogram and pixels of NDVI. They also analysed NDVI frequency distribution for different types of vegetation with different groundwater depth. This vegetation index was also used to draw a linear relationship between vegetation growth and antecedent precipitation in arid and semi-arid regions (Fu & Burgher, 2015; Han et al., 2018). However, it is essential to apply remotely sensed vegetation data in vegetation-water relationship modelling under future climate scenarios. This study addressed this research gap in Chapter 6.

## **2.6. Climate change impact**

According to IPCC (2014), the global mean surface temperature change for the end of the 21st century (2081–2100) in relation to 1850-1900 is projected to likely exceed 1.5°C for RCP4.5, RCP6.0 and RCP8.50 (Figure 2.6). However, according to RCP8.5 scenario precipitation increases in high latitude regions and decreases in mid-latitude to sub-tropical dry regions, while many mid-latitude wet regions are characterised by high levels of precipitation are projected under same climate scenario (Figure 2.6) (IPCC, 2014). Anthropogenic greenhouse gas emissions have been the primary driver of climate change since the pre-industrial era.

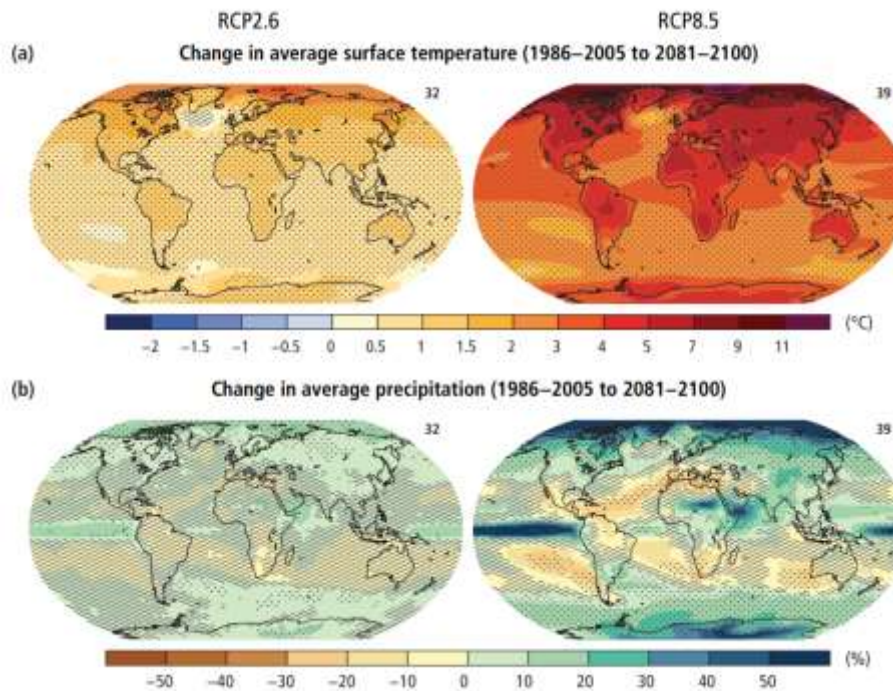


Figure 2.6: The climate variable changes: (a) Change in average surface temperature and (b) change in average precipitation, based on multi-model mean projections for 2081–2100 relative to 1986–2005 under the scenarios RCP2.6 (left) and RCP8.5 (right) (IPCC, 2014).

Evidence shows that future climate variable change related incidence is apparent. Climate change leads to shifts in average temperatures, fluctuations in climate patterns, and an increase in extreme weather events, such as droughts, exceptionally high or low temperatures, heavy rainfall, and floods (Mengistu et al., 2023). Since regional climate has a significant effect on catchment hydrology, floodplain ecosystem will become a susceptible area (Li et al., 2016). Any alteration in temperature and precipitation patterns will have a ripple effect on land and water systems, ultimately impacting vegetation communities (Fu et al., 2020). Additionally, the agricultural sector confronts a range of other challenges, including but not limited to pests and diseases, water supply issues, waterlogging, salinity, soil degradation, heat stress, drought, and the unsuitability of current planting areas (Arndt & Tarp, 2017). The impact of climate change on the geographic distribution and growth of plant species will vary based on factors such as the vegetation type (annual or perennial) and their growth patterns (Anderegg, 2015).

Australia's climate has remarkable variability, primarily attributed to the influences of several major atmospheric phenomena, including El Niño – Southern Oscillation (ENSO), the Indian Ocean Dipole (IOD), the Madden-Julian Oscillation (MJO), and the Southern Annular Mode (SAM) (King et al., 2014; Chung & Power, 2017). Due to extreme climate variability, floodplain ecosystems in Australia are sensitive to long term climatic conditions (Howden et

al., 2010). The temperature increases due to climate change in Australia higher than other countries and the pattern and intensity of precipitation are changing (Garnaut, 2011). Considering climate change impact on catchment hydrology, the negative impact of climate change in Australia could lower the floodplain vegetation growth in the future. These gaps are addressed in Chapter 5 and Chapter 6 of the Thesis.

## **2.7. Climate models and climate scenarios**

Understanding the nature of future climate and its variability is important for policy making to improve environmental resource management, mitigating the impact of future climate scenarios. One of the best tools that can simulate the entire Earth's climate, is known as Global Climate Model. These climate models are developed by using mathematical representations of climate systems that adhere to the fundamental principles of physics, and extensively corroborated with historical observations (IPCC, 2014). These models exhibit relatively low spatial resolutions, with grid spacings of up to 300 kilometres, equivalent to a single theoretical value per grid cell measuring 300 kilometres by 300 kilometres. They encompass a spectrum of complexity, ranging from basic one-dimensional models to intricate three-dimensional models, commonly referred to as General Circulation Models (GCMs). GCMs can be additionally classified into oceanic GCMs (OGCM) and atmospheric GCMs (AGCM), which can be integrated to dynamically simulate interactions between the oceans, atmosphere, and land surface, collectively referred to as Atmospheric-Ocean General Circulation Models (AOGCMs) (Abiodun & Adedoyin, 2016).

General Circulation Models (GCMs) are one of the primary tools for understanding forthcoming climate projections. As of now, the Coupled Model Intercomparison Project (CMIP) has entered Phase 6 (CMIP6). CMIP6 represents a greater expansion over Phase 5 (CMIP5) and provides higher spatial resolution and improved physical parameters, which can support a larger number of simulations. The primary distinction between CMIP5 and CMIP6 lies in their future scenarios. While CMIP5 relied on the Representative Concentration Pathways (RCPs), CMIP6 employs a fresh set of emission scenarios known as the Shared Socioeconomic Pathways (SSPs). These SSPs encompass a range of anticipated economic and social shifts based on various socioeconomic premises. Several analyses have indicated that CMIP6 models exhibit superior performance in simulating future climate compared to CMIP5 models. For instance, Hamed et al. (2022) conducted a comparison between two scenarios from

CMIP5 (RCP4.5 and RCP8.5) and their counterparts in CMIP6 (SSP2-4.5 and SSP5-8.5) specifically in Egypt. Their findings revealed that CMIP6 demonstrated reduced uncertainty in modeling seasonal air temperatures and rainfall changes compared to CMIP5. Similarly, Wu et al. (2019) evaluated the performance of CMIP5 and CMIP6 models across various metrics such as daily precipitation patterns on both global and regional scales, tropospheric air temperatures in East Asia, and long-term trends in surface air temperatures in the Pacific Ocean. Their analysis indicated significant enhancements in CMIP6 compared to CMIP5. However, it is worth noting that certain studies have also pointed out instances where CMIP6 models exhibited poorer performance than CMIP5 models. For example, Zhu and Yang (2020) observed inferior simulation results in CMIP6 models concerning air temperature and precipitation in the humid regions of the Tibetan Plateau when compared to CMIP5 models. Similarly, Song et al. (2021) simulated future changes in precipitation and air temperature in South Korea using scenarios from both CMIP5 (RCP4.5 & RCP8.5) and CMIP6 (SSP2-4.5 & SSP5-8.5). Their findings highlighted higher uncertainty in precipitation simulations under SSP projections, whereas RCP projections displayed greater uncertainty in predicting air temperature.

In these experiments four different representative concentration pathways (RCP) were performed using various coupled GCMs developed by several international climate modelling groups from around the world (Sharmila et al., 2015). In contrast to CMIP3, CMIP5 models exhibit improvements in terms of representing model physics, vertical resolution, and the incorporation of atmospheric aerosols (Taylor et al., 2012; Sperber et al., 2013)

Numerous studies have already investigated the overall future climate changes in global monsoonal precipitation using multi-model ensemble and selected CMIP5 models under different range of RCP scenarios (Table 2.3) (Lee & Wang, 2012; Kitoh et al., 2013; Wang et al., 2014), that suggest notable increase in global monsoonal precipitation during 21st century due to temperature increase. However, considering the future projections between RCP 4.5 (intermediate) and RCP 8.5 (extreme) scenarios, it becomes evident that significant differences in climate outcomes are anticipated based on the chosen emission pathways . Kitoh et al. (2013) suggested that the global monsoon response to atmospheric warming is larger and more robust in a warmer world (RCP 8.5) among the models. Moreover, GCMs have been used predicting future climate variable changes until end of the 21st century developed by various specialised institutions in climate research.

Table 2.3: Different types of radiative forcing pathways from greenhouse gas emissions from human activities, with radiative forcing of 2.6, 4.5, 6.0 and 8.5 W/m<sup>2</sup> by 2100.

<b>RCP</b>	<b>Radiative forcing</b>	<b>Atmospheric CO2 equivalent (parts per million)</b>	<b>Pathway shape</b>
8.5	>8.5 W/m <sup>2</sup> in 2100	>1370 (in 2100)	Rising
6	~6 W/m <sup>2</sup> at stabilisation after 2100	~850 (at stabilisation after 2100)	Stabilisation without overshoot
4.5	~4.5 W/m <sup>2</sup> at stabilisation after 2100	~650 (at stabilisation after 2100)	Stabilisation without overshoot
2.6	peak at ~2.6 before 2100 and then decline	peak at ~490 (before 2100 and then decline)	Peak and decline

Source: (IPCC, 2014)

## 2.8. Summary and knowledge gaps

Reviewing the literature prompts a fundamental need for remote sensing-based approach to climate change studies in mapping different floodplain vegetation areas and in projecting vegetation responses to the future climate variable changes presented in this thesis. The key findings of this review are summarised as follows:

1. Essential research remains necessary to evaluate how floodplain vegetation will respond to future climate conditions, particularly given the ongoing and escalating occurrence of extreme weather events that pose threats to floodplain ecosystems and associated environments (Mosner et al., 2015; Eccles et al., 2021).
2. Hydrological modelling-based approaches are grounded in theory of ecosystem management to face the climate change effects on water resources, which have become more complex and comprehensive. Therefore, estimating surface and groundwater availability using different hydrological models at catchment level that directly influence vegetation growth (Moxham et al., 2019). This hydrological assessment would be appropriate to identify vegetation-water correlations by examining the changes in vegetation indices.
3. MODIS satellite imagery data provides opportunity to identify vegetation conditions by gathering different types of vegetation over the year. These time series data have been successfully applied in previous studies (Cao et al., 2015). Therefore, using a pre-processing tool in generating time series vegetation indices data could provide a better understanding the seasonal variability in the floodplain vegetation response to climate scenarios.
4. Studying the reactions of floodplain vegetation to changes in water availability caused by climate change can aid in the management of floodplain ecosystems by predicting the effects of climate change in the future (Mosner et al., 2015; Moomaw et al., 2018).
5. Given the impact of climate change in Australia, floodplain ecosystems are placed in a vulnerable position due to their enhanced sensitivity to extreme climatic events. Therefore, it is important to study climate change impact on floodplain vegetation in Australia (Xu et al., 2023).

6. Floodplain vegetation is dependent on catchment hydrology, thus any changes in water availability can put floodplain vegetation at risk depending on the types of vegetation and its distribution. The greenness of floodplain vegetation may be influenced by climatic variability, as climate change is the sole factor driving changes in catchment hydrology (Burandt et al., 2024). Nevertheless, there is a lack of research examining the various vegetation types and their proximity to the stream. It is imperative to address this research gap in order to comprehend the potential for crop management.
7. Floodplain vegetation is vulnerable to climatic stresses such as drought and floods. According to climate projections, Australia is expected to encounter climatic pressures due to rising temperatures, alterations in precipitation patterns, and a reduction in precipitation in the forthcoming period. There is a knowledge gap regarding vegetation response to soil water content including extreme events in future time spans.
8. Understanding the vegetation responses to future extreme climatic conditions based on vegetation types and distance from the water outlet will provide an opportunity to develop crop productions with efficient irrigation systems. This can be addressed through vegetation response modelling with remote sensing data, especially in the under-sampled drylands of the world where irrigation is difficult due to water scarcity.

This thesis aims to address the research gaps identified by the literature review and outlined in detail in Chapter 1.

## **CHAPTER 3: RESEARCH METHODS**

### **3.1. Introduction**

The previous two chapters provided an overview of the key problems of the ongoing issues in floodplain ecosystems, specifically in overcoming the challenges of climate change. In addition, those chapters presented the works that have been done so far to understand the climate change impact on floodplain vegetation. Chapter 1 also discussed the overall framework of the study and identified the current research gaps on topics that need to be addressed. These knowledge gaps were considered the basis for developing the objectives of this research study. The present chapter elaborates on the methodologies of the study adopted to achieve the objectives enumerated in Chapter 1. It should be noted, however, that specific methods are discussed in the ensuing chapters corresponding to the specific objectives of this study in Chapters 4, 5, and 6. This present chapter describes the following subsections: i) Description of the Study Area, ii) Research Design, iii) Data acquisition, processing, and analysis, and iv) Summary. More specific discussion of the methods can be found in Chapters 4 to 7, corresponding to the four specific objectives of this Thesis.

### **3.2. The study area**

The study area, the Burrinjuck sub-catchment, is located in New South Wales (NSW), the southeast part of Australia, within the upper catchments of the Murrumbidgee River basin in the mountains of the Great Dividing Range. It is geographically situated between latitude 34.53°S to 35.14°S and longitude 148.31°E to 148.55°E (Figure 3.1). The area of interest, the Burrinjuck sub-catchment, is approximately 115 kilometres north-west of Canberra, Australia's capital. The name Burrinjuck comes from the Aboriginal words “booren yiack”, meaning precipitous mountain. The primary character of the Burrinjuck Dam and its environs is rural, featuring a township in Yass and smaller communities in Binalong, Bookham, Bowning, Gundaroo, Murrumbateman, Sutton, and Wee Jasper.

The topography of the Burrinjuck sub-catchment area consists of gentle and moderate slopes, and the elevation varies from 373 to 934 m (Saha et al., 2013). The climate of the study area is characterised as temperate, as classified by the Köppen-Geiger climate classification system, with a predominantly warm summer and an absence of a long dry season, featuring an average temperature of 22°C during the hottest months (Peel et al., 2007). The average annual rainfall of the catchment is 675mm, but the average monthly rainfall has high year-to-year variation. The mean annual rainfall in the Murrumbidgee region varies significantly due to its diverse climate, with an average rainfall of 1700mm in the Snowy Mountains area and less than 600mm in the Wagga Wagga.

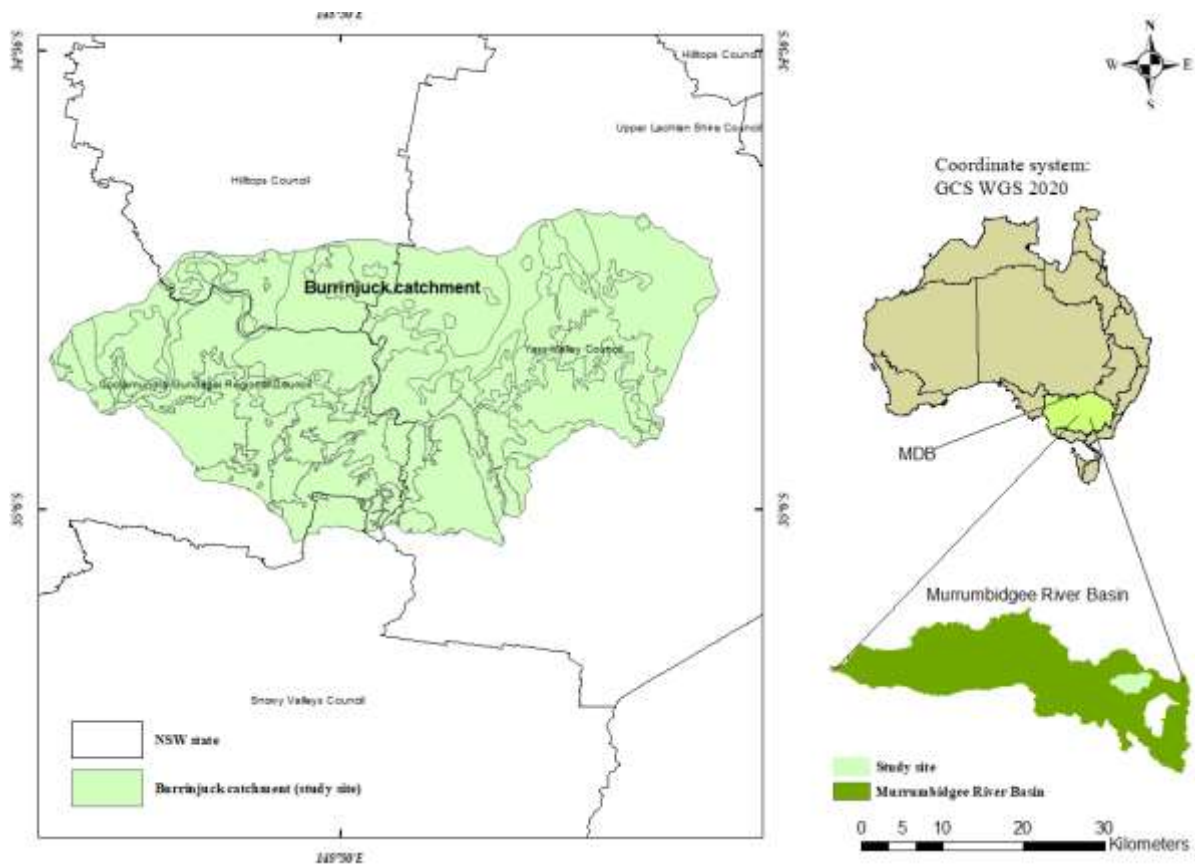


Figure 3.1: The location map of the study site Burrinjuck sub-catchment. Inset: Australia map showing Murray Darling Basin (green) and Murrumbidgee River Basin (olive).

The annual rainfall of the Burrinjuck sub-catchment area is 926.6mm (average from 1908 to 2023) (BOM, 2023). The highest rainfall was observed in the month of July (100.1mm) and the lowest in February (56.1mm) as the driest month (Figure 3.2). In the winter months of June to August, rainfall varies from 96mm to 100mm, and summer rainfall from December to February varies from 56.1mm to 63.1mm (BOM, 2023). The mean temperatures throughout the year in this region exhibit variations, with the annual maximum and minimum temperatures at 20.7 and 9.2, respectively. Specifically, the highest maximum mean temperature occurs in January and February, fluctuating between 29.8°C and 29.0°C (BOM, 2023). In contrast, the lowest mean temperatures of the year, ranging from 12.5°C to 11.7°C, are experienced in June and July.

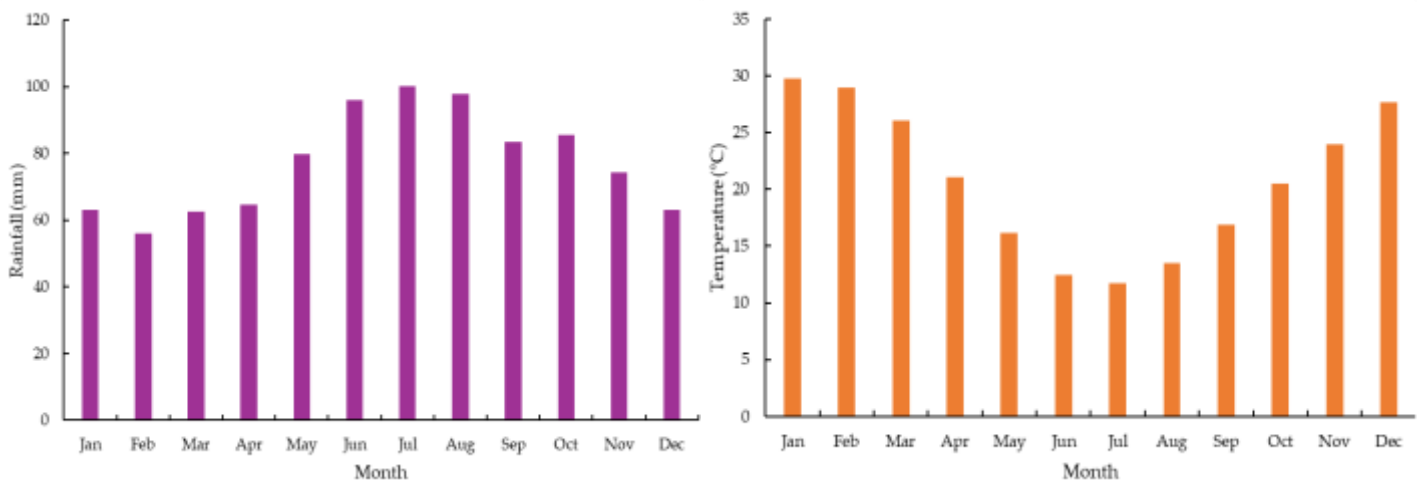


Figure 3.2: The annual mean rainfall and temperature at Burrinjuck sub-catchment (Station ID 073007), NSW, Australia. Source: BOM (2023).

The climate of the Murrumbidgee River catchment is more diverse in the New South Wales (NSW) than in the Australian Capital Territory (ACT) section, with cooler upstream located in the high alpine to the dry and hot plain in the downstream (Wen et al., 2013). The evapotranspiration also varies from upstream to downstream.

The Burrinjuck sub-catchment covers approximately 12,950km<sup>2</sup>, which is sub-catchment of the Murrumbidgee River catchment. The Murrumbidgee River catchment covers an area of 84,000km<sup>2</sup> (about 8% of MDB), having 6,749km length of streams (Norris et al., 2001). The Murrumbidgee River is an important water source for many wetlands, among them sixteen wetlands listed as nationally significant (MDBA, 2023). For instance, Fivebough and Tuckerbill swamps are important waterbird habitats listed under the Ramsar convention. The

Lowbidgee floodplain is the largest wetland in the Murrumbidgee region. It includes the second-largest red gum forest in Australia, with significant black box, lignum, and reed-bed communities (Rogers et al., 2013).

The southeastern region of Australia is distinguished by the higher runoff generation in the catchment of the Murrumbidgee River (Vaze et al., 2011). In September 2009, the lowest flow observed was 30 ML/Day, while in November 2016, the highest flow reached at 31,224 ML/Day, as reported by the Bureau of Meteorology (Simpson, 2022). The annual surface water availability in the Murrumbidgee River catchment is about 4,000 GL (Gonzalez et al., 2020). This flow rate is low in the alpine region at Tharwa and higher in the downstream of the Murrumbidgee River area at Balranald (western part of the catchment). The annual runoff coefficient (i.e. the amount of runoff to the amount of precipitation received) in the downstream area is less than 2% (Khan et al., 2005). This climate variability changes the river dynamics through the river network and periodically inundates the wetland and floodplain areas.

The Wiradjuri people constitute the largest Aboriginal nation residing in the slopes and plains of the Murrumbidgee catchment. Their nation stretches from the River Murray to areas beyond Dubbo in the northern region, and extends westward to Balranald. Alongside the Wiradjuri, there exist several smaller nations situated at the western extremity of the catchment, namely the Barapa Barapa, Muthi Muthi, Nari Nari, Nyeri Nyeri, Wadi Wadi, Wamba Wamba, Weki Weki, and Wolgalu. Conversely, the Ngunawal and Ngarigo nations claim the mountainous territories located at the eastern end of the Murrumbidgee catchment (MDBA, 2023).

The arrival of Europeans in the 1820s marked the initiation of a transformative process on the landscape, impacting the vegetation, soils, and rivers (Starr, 1999; Olley & Wasson, 2003). This process continues to resonate to this day. By 1825, the catchment area had already witnessed the introduction of sheep and cattle, which began grazing activities. Whilst grazing has historically been the predominant agricultural activity, the initial settlers also cultivated small portions of land for the purpose of growing cereals, vegetables, and orchards. As a result of the burgeoning livestock industry, stock numbers rapidly increased, with some properties experiencing a thirty-fold multiplication within the first decade of settlement (Olley & Wasson, 2003). During the pastoral period, small towns emerged to support the grazing industry. Presently, Canberra stands as the most prominent urban hub within the catchment area, boasting a population of nearly 470,000. Since 1954, the city has experienced rapid growth. The catchment area now accommodates extensive grazing lands for sheep and cattle, alongside limited sections dedicated to commercial softwood plantations. Currently dryland grazing and

cereal crop production comprise approximately 75% of the land use in this region. Rice and grape cultivation thrive in this area, contributing to 50% of Australia's rice production and 42% of New South Wales's grape production. Commercial forestry occupies a mere 3% of the catchment in the eastern part of the region (MDBA, 2023).

### 3.3. Data acquisition, processing, and analysis

A depiction of the data inputs, processes, and study outputs can be observed in Figure 3.3. The data capture and acquisition details and methods for each technical chapter are discussed in the subsequent sections of this Thesis. This section only describes the general overview of the data acquisition, processing, and analysis in Figure 3.3, as these processes are different for each technical chapter.

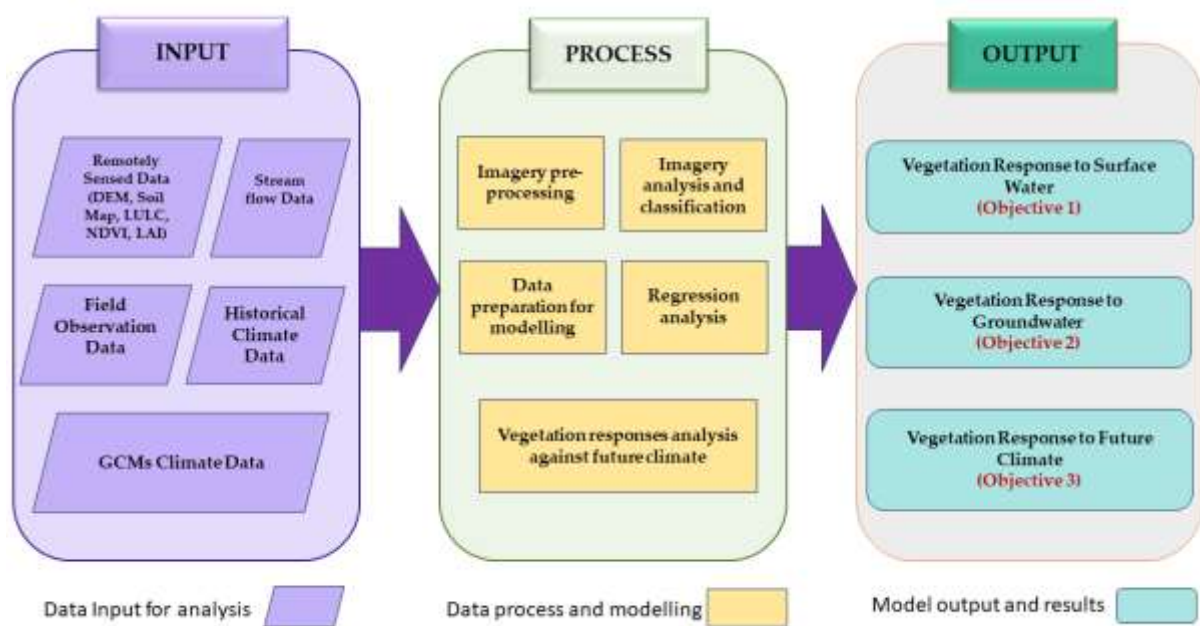


Figure 3.3: The Input-process-output model of the study.

#### 3.3.1. Vegetation response to surface water (Objective 1)

The datasets used to achieve vegetation and surface water modelling consist of remotely sensed NDVI datasets, Climate data, and Google Earth data. A screenshot of the Google Earth interface is presented in Figure 3.4. A list of datasets, their descriptions, and the acquisition

period is listed in Table 3.1. The NDVI data was pre-processed using the AppEEARS tool which is accessible via the EarthData web portal (Figure 3.5). The simulated and predicted results were modelled using the WEKA machine learning tool. A screenshot of the WEKA tool interface is presented in Figure 3.6.

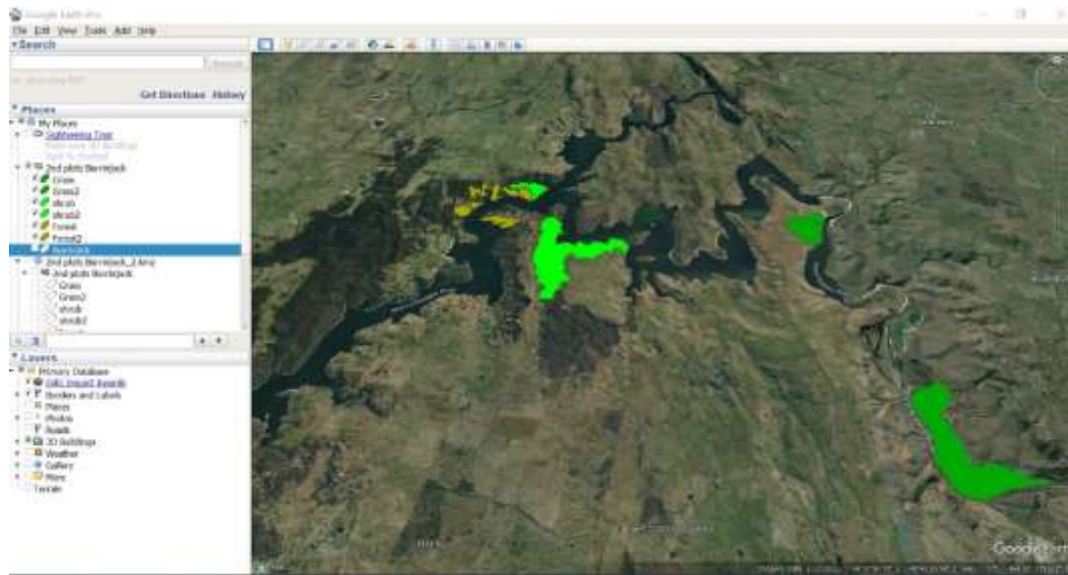


Figure 3.4: A glimpse of the Google Earth web interface.

Table 3.1: List of datasets acquired in the fulfilment of Objective 1.

<b>Dataset</b>	<b>Description</b>	<b>Acquisition year/period</b>
MODIS imagery	Application-ready NDVI with spatial resolution of 250 m.	August, 2021
Precipitation	Station-gauged daily data	March, 2021
Temperature	Station-gauged daily data	March, 2021
Evapotranspiration	Satellite-derived, 0.05 degree (approximately 5 x 5 km)	March, 2021
Runoff	Satellite-derived, 0.05 degree (approximately 5 x 5 km)	April, 2021
Streamflow (discharge)	Station gauged, temporal	April, 2021

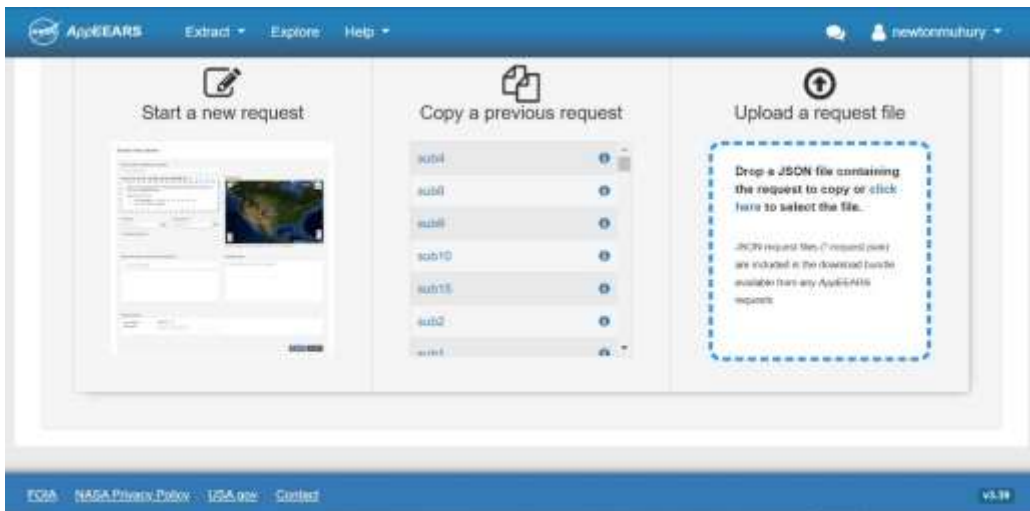


Figure 3.5: Remote sensing data processing tool, AppEEARS interface captured from EarthData web portal.



Figure 3.6: The Waikato Environment for Knowledge Analysis (WEKA) tool interface.

### 3.3.2. Vegetation response to groundwater (Objective 2)

This objective required hydrological analysis to understand the catchment's groundwater properties, which achieved by SWAT model setup using remotely sensed Digital elevation Model (DEM), soil map, and land use and land cover map. These datasets were processed in ArcGIS tool (Figure 3.7). The processed DEM and soil map are presented in Figures 3.8 and 3.9, respectively.



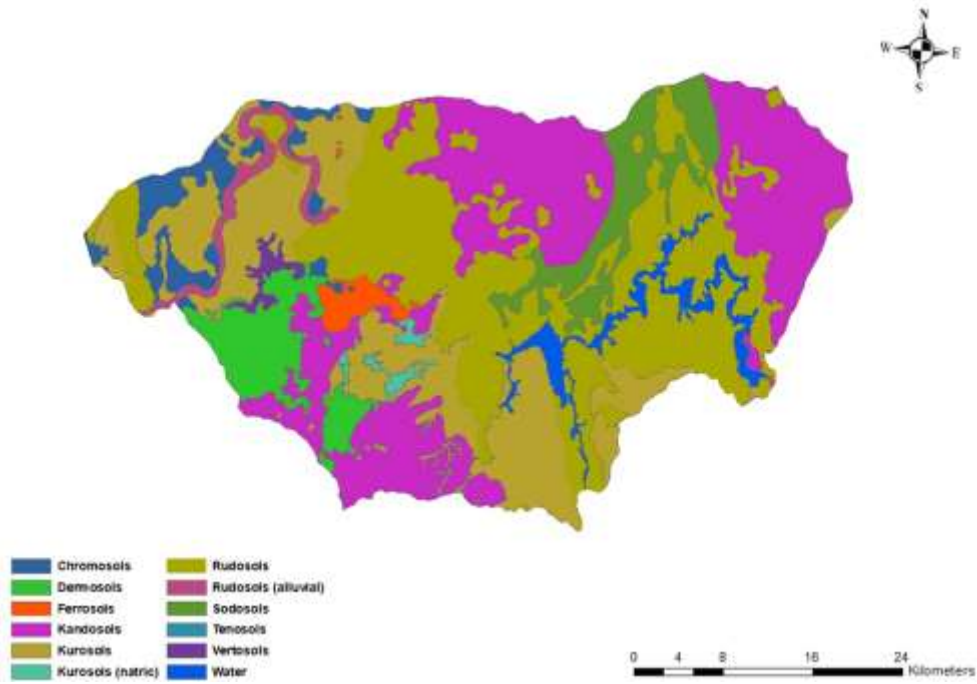


Figure 3.9: A soil map prepared to apply for the study catchment delineation using ArcSWAT.

### 3.3.3. Vegetation response to future climate projections (Objective 3)

The datasets used to achieve vegetation response to catchment water availability under future climate change consist of remotely sensed vegetation index, DEM, soil map, LCLU map datasets, and Climate data. A list of datasets, their descriptions, and the acquisition period is listed in Table 3.2.

Table 3.2: List of datasets acquired in the fulfilment of objective 3.

Data	Frequency	Description	Acquisition year/period
Precipitation	Daily	Station gauged, temporal	January, 2022
Temperature	Daily	Station gauged, temporal	January, 2022
Relative Humidity	Daily	Station gauged, temporal	January, 2022
Wind speed	Daily at 9 am	Station gauged, temporal	January, 2022
Solar radiation	Daily average	Spatial	January, 2022
Streamflow (discharge)	Daily	Station gauged, temporal	February, 2022
MODIS NDVI	16-Day	250 m spatial resolution	February, 2022
DEM	-	30 m spatial resolution	February, 2022
Soil Map	-	250 m spatial resolution	February, 2022
LCLU map	-	50 m spatial resolution	February, 2022

### 3.4. Brief description of data processing and analysing

Briefly, the data acquisition for Objective 1 (i.e., vegetation and surface water modelling) consists of satellite imagery datasets, namely time-series MOD13Q1 (version V006) imagery, and Google Earth data. A short field survey (Figure 3.10) was conducted to determine the vegetation types available in the area of interest (AOI) with the guidance of higher resolution Google Earth. This process helped to build confidence about the satellite data interpretation, as well as to be more familiar with vegetation and other landscape attributes. A total of 480 MOD13Q1 NDVI images were computed for each vegetation plot category over the 21-year period. The MODIS NDVI time-series data was pre-processed in AppEEARS tool, was then analysed to prepare these data applicable to the WEKA machine learning tool.

Missing data or data gap is one of the common occurrences in time series climate data in the research field (Afrifa-Yamoah et al., 2020; López et al., 2021; Fagandini et al., 2023). Thus, the analysis of any time series data that contains missing data, may not be statistically robust compared to the complete series of data. However, in practice, it is not possible for different reasons such as, error in the sensors, malfunctions, absent of the staff for manual observations. Many studies described and implemented gap filling homogenisation techniques to deal with this problem, which require the use of neighbouring station data (Jeffrey et al., 2001; Hofstra et al., 2008; Mekis & Vincent, 2011; Vincent et al., 2012). Few studies mentioned about the general specified threshold or 'rule of thumb', for example, the missing data must be less than 5% of daily values in a month (Zubieta et al., 2017). In this study, about 0.28% missing data identified in the climate time series data, which have been filled using the K-nearest neighbour technique (Lu & Qin, 2014).

For Research Objective 2 (Remote sensing-based vegetation groundwater relationship modelling), Shuttle Radar Topography Mission (SRTM) imagery data collected using Interferometry Synthetic Aperture Radar (inSAR) from the Space Shuttle Endeavour, were evaluated for the topography of the study catchment. This 30m resolution Digital Elevation Model (DEM) imagery files were processed in ArcGIS with Burrinjuck sub-catchment area shapefiles. The catchment parameters such as gradient and length of the slope, the stream network characteristics including slope, width, and length of the channel information have been derived from the SRTM DEM data. Additional catchment data, such as Land Use and Land Cover (LULC) from the NSW Office of Environment and Heritage, was acquired alongside a soil map sourced from the Digital Atlas of Australian Soil.

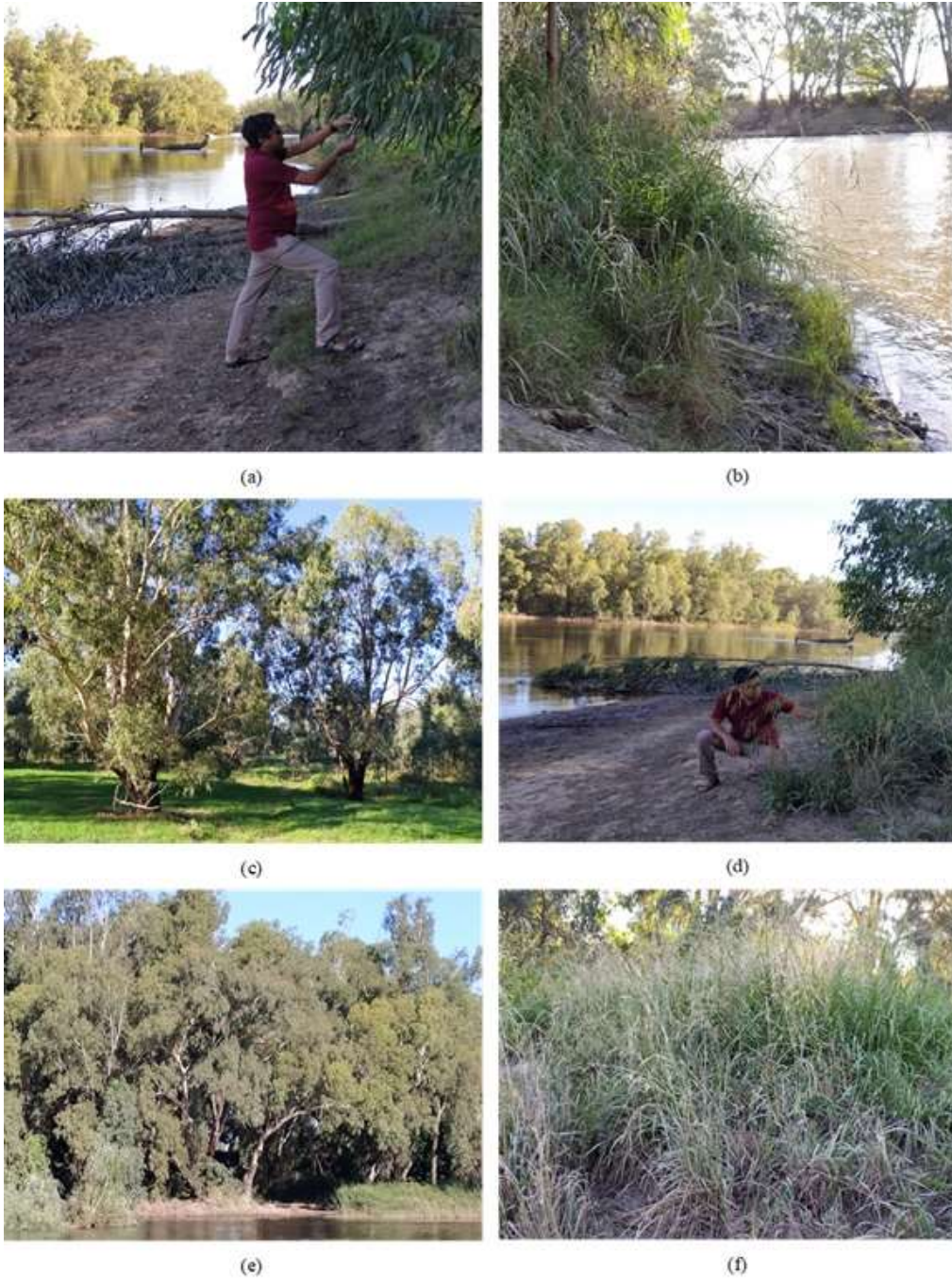


Figure 3.10: The floodplain vegetation and land area of the Burrinjuck sub-catchment of the Murrumbidgee River catchment – a) shrubs near the stream flow, b) grasses near the stream flow, c) sparse shrubs in the floodplain, d) sparse grasses, e) trees near the streamflow, f) grasses situated far from the stream flow.

The MODIS NDVI data were obtained for each sub-basin delineated from ArcSWAT hydrological analysis, similarly, derived in Objective 1 to predict and map vegetation conditions in the study area. The regression analysis was accomplished using the traditional linear regression and machine learning algorithms. The model prediction accuracy was assessed using the root mean square error (RMSE) and correlation coefficient (r) of predicted and observed values using a 10-fold cross-validation, which is a leave-one-out approach from leave-one-out cross-validation method. The pre-processing of MODIS imagery, as well as the derivation of vegetation indices, were executed within USGS data portal using AppEEARS data pre-processing tool. The vegetation response modelling/regression analysis and model assessment were done in WEKA Machine Learning Software (Hall et al., 2009).

In Objective 3 (vegetation responses to future climate change), the same study area for hydrological alteration under future climate change was evaluated in context to both surface water and groundwater. The relationship of vegetation responses with modelled data was also determined using correlation analysis. The hydrological analysis was computed under two climate change scenarios RCP4.5 and RCP8.5 according to CMIP5. The trend analysis was completed using the non-parametric Mann-Kendall trend test and Sen's slope to identify the trends and quantify the change for historical and GCMs projected future rainfall at the study site. A similar trend analysis was achieved for remotely sensed LAI and SWAT simulated LAI under GCMs projected climate data. The accuracy of SWAT model performance was also analysed using model simulated data calibrated with observed stream flow and MODIS LAI data. The accuracy was determined by Nash-Sutcliffe Efficiency (NSE) and coefficient of determination, known as  $R^2$  (R-squared) values. Statistical tests (correlation) were attained using the IBM SPSS tool, determining the vegetation responses to surface water flow (SURQ), soil water content (SW), and groundwater flow (GW). The detail of the process was explained in Chapter 6 of the Thesis.

### **3.5. Summary**

As the detailed methods are discussed in the subsequent technical chapters (i.e., Chapters 4, 5, and 6), a brief overview of the methods applied is presented herein. In summary, the floodplain vegetation response to catchment water was determined by using time-series MODIS 250 m NDVI imagery in two different analytical approaches: regression analysis using ML algorithms; and the trend analysis of the time-series datasets. The projected future

floodplain vegetation responses to climate change in Australia was carried out by using catchment hydrological modelling and MODIS vegetation indices data under different emission-based climate scenarios. The responses were determined by modelling using linear regression and machine learning algorithms, and GIS-based implementation.

The following technical chapters include the thorough descriptions of methodologies in determining floodplain vegetation responses to climate change:

Chapter 4 presents the first technical chapter of the thesis and discusses the floodplain vegetation response to available surface water at catchment level. It also includes the results on the potential different types of vegetation responses with regard to their distance from the streamflow.

Chapter 5 uses field observations and remotely sensed data to analyse catchment hydrological units. This chapter encompasses an analysis of the distribution of vegetation across various locations on the slope, as well as their respective responses to the surface water and ground water recharge.

Chapter 6 applies station gauged climate data, remotely sensed data, and projected future climate data to consider regional variation in the responses between floodplain vegetation sensitivity in a semi-arid floodplain ecosystem in Australia.

# **CHAPTER 4: MODELLING FLOODPLAIN VEGETATION RESPONSE TO SURFACE WATER VARIABILITY**

## **4.1. Introduction**

Chapter 2 highlighted the knowledge gaps in the comprehension of floodplain vegetation responses to surface water modelling at the catchment level using remotely sensed data and machine learning algorithms. The gap in the relationship of vegetation response with the plant biophysical variables, such as the Normalised Difference Vegetation Index (NDVI), was also emphasised. This information provides essential foundations for diverse applications, including the mapping of vegetation types, the estimation of surface water availability, and the estimation of NDVI for different vegetation types. Within this chapter, briefly discussed on the grass vegetation, shrub vegetation, and tree vegetation of the floodplain ecosystem, as well as their proximity to the streamflow (both near and distant from the stream).

This chapter is structured into five distinct sections. The first section, Background, presents and deliberates on the information pertaining to previous works conducted on the topic, as well as the knowledge gaps surrounding vegetation responses to surface water availability. These knowledge gaps were utilised as a foundation to establish the objectives of the study. The subsequent section, Methods, outlines the approaches and methodologies employed to attain the objectives. The Results, as well as the Discussion sections, ensue. Finally, the chapter ends with the Conclusion, highlighting the novel knowledge and insights derived from this study on vegetation growth.

This Chapter presents the first objective of the study, which encompass the following aspects: a) an analysis of all floodplain vegetation types and their respective distances from the streamflow, which have only been partially examined in previous studies; b) the characterisation of catchment hydrological variables and their associations with vegetation; and c) the application of diverse machine learning algorithms to model the vegetation responses to seasonal variability. Additionally, this Chapter provides the inaugural report on the vegetation responses of the floodplain ecosystem in south-east Australia.

## **4.2. The background of floodplain vegetation response modelling to surface water**

Climate change that relates to global warming is affecting socio-economic and ecological systems around the world (Hein et al., 2009; van der Velde et al., 2012; Herrera-Pantoja & Hiscock, 2015). This changing climate has been directly impacting water resources due to the direct relationship between the climate system and the hydrological cycle of the region, especially in arid and semi-arid regions across the world, by altering rainfall patterns, increasing potential evapotranspiration and surface runoff (Prosser et al., 2021). Research predicts that future climate change will lead to extreme temperatures and precipitation in frequency and severity (Fischer & Knutti, 2015; Liu et al., 2021). These temperatures and precipitation change directly impact vegetation greenness in arid and semi-arid regions where precipitation is the key factor in promoting vegetation growth (Thomey et al., 2011; Zhang et al., 2016). Therefore, understanding the vegetation and surface water relationship is important for vegetation-water resource management in arid and semi-arid regions (Wu et al., 2022).

According to the current climate change projections, finer resolution modelling shows the average temperature in Australia could rise between 0.5°C and 2.5°C in the next 50 years (IPCC, 2021). The temperature change directly affects solar radiation and humidity, indirectly influencing evapotranspiration and precipitation. In Australia, approximately 90% of the precipitation returns to the atmosphere via the evapotranspiration process (by which ecosystems return water from Earth's surface, including soil and plant surfaces in the form of water vapor to the atmosphere), with the remainder amount contributing to groundwater recharge and stream flows through runoff (Li et al., 2007; Glenn et al., 2011). On the other hand, the average annual 45mm runoff in Australia is the lowest among all continents: one-fourth of Africa, one-seventh of Asia, Europe and North America, and one-fourteenth of South America (Saha et al., 2013). Australia is generally an arid continent, and a large portion of its natural vegetation depends on rainfall. Therefore, any changes in the annual amount of precipitation may amplify two to three times larger variations in the annual runoff (Shi et al., 2007). For example, a 20% reduction in rainfall may typically lead to a 40% to 60% reduction in runoff (Chiew et al., 2018). However, an understanding of floodplain vegetation responses to the runoff change is vital for an efficient floodplain vegetation and water management system (Merritt et al., 2010). Therefore, it is necessary to model the relationship between vegetation response and surface water variables on a small catchment scale for sustainable

land management and in developing policies that could ensure efficient water use in arid region.

Likewise, floodplain ecosystems in arid regions are highly influenced by climate changes (Zhang et al., 2016). Floodplain comprises low-lying land areas subject to inundation by lateral overflow water from rivers or lakes with which they are associated (Junk, 1989). According to this definition, a floodplain is usually visible along rivers, lakes, deltas, and estuaries worldwide. Floodplain vegetation plays an essential role in regulating river flow conditions and for providing natural habitats for aquatic and terrestrial animals (Kingsford, 2000). In addition, these vegetation communities offer many environmental benefits, such as reducing catchment runoff, flood protection and erosion control (Peters et al., 2016). However, the floodplain vegetation depends on surface and groundwater for their growth, survival and other biological processes (Tockner & Stanford, 2002).

The rapidly changing climate globally makes these vegetation communities vulnerable by altering hydrogeological cycles, causing a significant reduction in surface and sub-surface water flows, and resulting in drastic changes in the size, morphology, and ecology of many floodplains around the globe (Aguiar et al., 2016). This floodplain degradation is widespread and it is linked with biodiversity loss and loss of ecosystems function and structure (Entwistle et al., 2019). Lewin (2013) documented the geomorphological process that has been occurring for the last 400 years, and how this process disconnects rivers from their floodplains. In addition, climate change-induced rainfall reduction makes 'billabongs' (oxbow lakes) dryer, as well as affecting other land features connected to the floodplains (Finlayson, 2005). These billabongs and waterholes provide natural habitats for aquatic species such as frogs and fish (Reid et al., 2012; Hillman & Shiel, 2017). However, as explained above, floodplains and their related ecosystems have been endangered regionally and globally despite their valuable economic and environmental services.

In the past, hydrological studies relied on ground-based observation data for modelling purposes. Data anomalies are one of the limitations for the modelling process, although these can be eliminated by using higher spatial resolution data to evaluate hydrological processes more accurately for restoration purposes (Wanders et al., 2014). Remote sensing technology could also address data anomaly issues as satellites consistently monitor a specified area on regional and global scales (Long et al., 2014). At present, many organisations provide remote sensing data with minimum or no cost, which allows scientists to use spatial datasets for better hydrological modelling (Dutta et al., 2015). Researchers (e.g., (Mancini & Corbari, 2014; Sutanudjaja et al., 2014)) have found that applying remote sensing data in hydrology such as

Normalised Difference Vegetation Index (NDVI), Leaf Area Index (LAI), soil moisture content, and vegetation cover map can help to improve surface water modelling results. Therefore, using remote sensing data to model the relationship between surface water variables and floodplain vegetation responses at a sub-catchment level is essential for effective floodplain vegetation and water resource management. Several researchers have examined the relationships between vegetation response and rainfall under climate change at regional and global scales (Pei et al., 2019; Chi et al., 2020). Researchers also have applied machine learning algorithms or artificial neural network to understand vegetation and soil water relationships (Okujeni et al., 2015; Yuan et al., 2019; Virnodkar et al., 2020; Chen et al., 2021; Habibie et al., 2022; Lees et al., 2022; Li et al., 2022; Zhou et al., 2022). However, none of the previous studies focused on modelling the relationships between floodplain vegetation responses and seasonal surface water variability under changing climate conditions. Based on the literature review, there was a knowledge gap identified for regression modelling between floodplain vegetation and available surface water variables. According to this desktop research, none of the previous studies has considered assessing the response of different vegetation types to hydrological model simulated runoff (surface and sub-surface runoff).

This study aims to analyse and build regression models for the relationships between seasonal surface water variability and floodplain vegetation responses using Moderate Resolution Imaging Spectroradiometer (MODIS) derived NDVI data and machine learning algorithms. The specific objectives of this study are: i) to understand different types of vegetation responses against surface water availability at the catchment level; and ii) to build regression models for the relationship between different vegetation response (as measured by NDVI) and seasonal surface water availability. For these purposes, a simplified version of the Hydrolog (SIMHYD) known as rainfall-runoff hydrological model, has been employed to infer catchment runoff followed by regression models to correlate the vegetation response and seasonal surface water availability. The novelty of this paper lies in the assessment of different types of floodplain vegetation responses (of different types and proximity to stream) using satellite imagery at different seasons (dry season and wet season) and locations (distance from the stream flow) for a period of more than 20 years.

### 4.3. Materials and methods

#### 4.3.1. Overview of research methodology

An overview of research methods implemented in this study is presented in Figure 4.1. The required data have been obtained from various data portals, such as the Australian Bureau of Meteorology (BOM) and the U.S. Geological Survey (USGS) web portals. The rainfall, temperature and streamflow data were processed in Microsoft Excel (Microsoft Corporation, 2018) and converted files into CDT format to apply to the SIMHYD hydrological model (Chiew et al., 2002). Similarly, satellite-derived evapotranspiration, runoff, and MODIS data were processed using ArcGIS (ESRI, 2019) and AppEEARS tools. After data preparation, the SIMHYD model was calibrated with daily rainfall, evapotranspiration, and streamflow data. The same calibration parameters were used for model simulation and the simulated results validated against remotely sensed runoff data. The SIMHYD simulated runoff data along with NDVI, temperature, and rainfall data, were applied to the WEKA machine learning tool for regression analysis to understand the relationships.

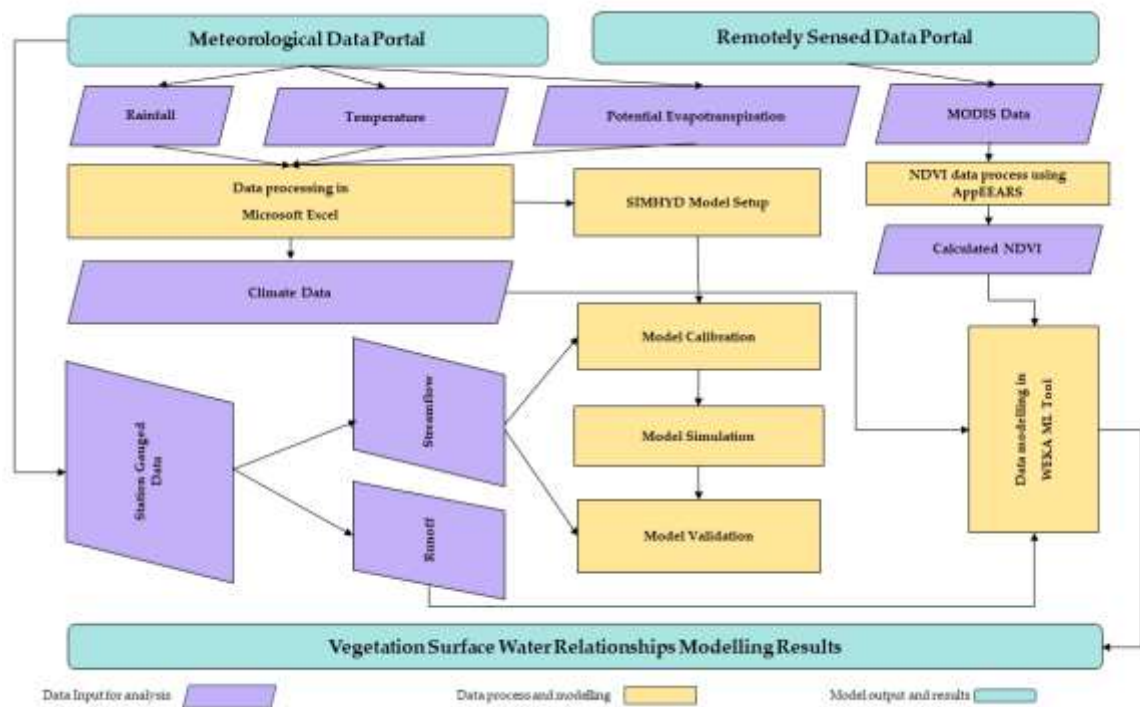


Figure 4.1: An overview of the research methodology for modelling different types of floodplain vegetation responses and seasonal surface water variability using machine learning tool and remote sensing data.

### **4.3.2. Study area**

The study area covers the Burrinjuck sub-catchment area, which is situated within the upper catchment of the Murrumbidgee River basin in the Great Dividing Range (Figure 4.2). It is about 55 kilometres south-west of Yass in New South Wales (NSW), Australia, and roughly 330 kilometres south-west of Sydney, with latitude and longitude of 34.53°S-35.14°S and 148.31°E-148.55°E. The Burrinjuck Dam was built to develop the Murrumbidgee irrigation project after the devastating drought in 1901-1902. It is the main water storage for the 660,000-hectare irrigation area in Riverina, NSW, and with its capacity of 1,026 gigalitres is double that of the Sydney harbour. The Burrinjuck sub-catchment and surrounding area is predominantly rural, with a township at Yass and villages at Binalong, Bookham, Bowning, Gundaroo, Murrumbateman, Sutton, and Wee Jasper. The total population in this area is 17,321 (ABS, 2019). This rural land is largely used for agriculture, especially sheep grazing. Also important for tourism and viticulture. The area's elevation varies from 373 to 934m, while the average annual rainfall is 675mm. The Murrumbidgee River catchment has the most diverse climate in the upper and lower Murrumbidgee, with an annual average rainfall of 1,500mm in the alpine area to less than 400mm in the Riverina plains. In the Burrinjuck Dam and surrounding area, 24% of rainfall appears as runoff, contributing to the maximum river flow (Chiew et al., 2002). As part of the upper Murrumbidgee catchment with higher elevation and relatively higher rainfall, this part of the river contributes significant water flow into Lake Burrinjuck.

The catchment's land gradient decreases downstream of the Burrinjuck Dam, and the floodplain width increases between 5 and 20 km. The Murrumbidgee River catchment accounts for 22% of the Murray Darling Basin's (MDB) surface water diverted for irrigation and urban use. It contributes 25% of fruit and vegetable production, 42% of grapes in New South Wales, and half of Australia's rice production. Agricultural production within the MDB has a value of over AUD23.6 billion annually, or 40.2% of Australia's gross value of agricultural production (ABS, 2021). The Murrumbidgee River normally recharges from the annual rain in the upper catchment regions. However, several studies have shown that there is a notable change compared to historical data in climate variables such as rainfall and evapotranspiration in this region, which impact recharge and water flows (Adamson et al., 2009; Connor et al., 2009; Goesch et al., 2009).

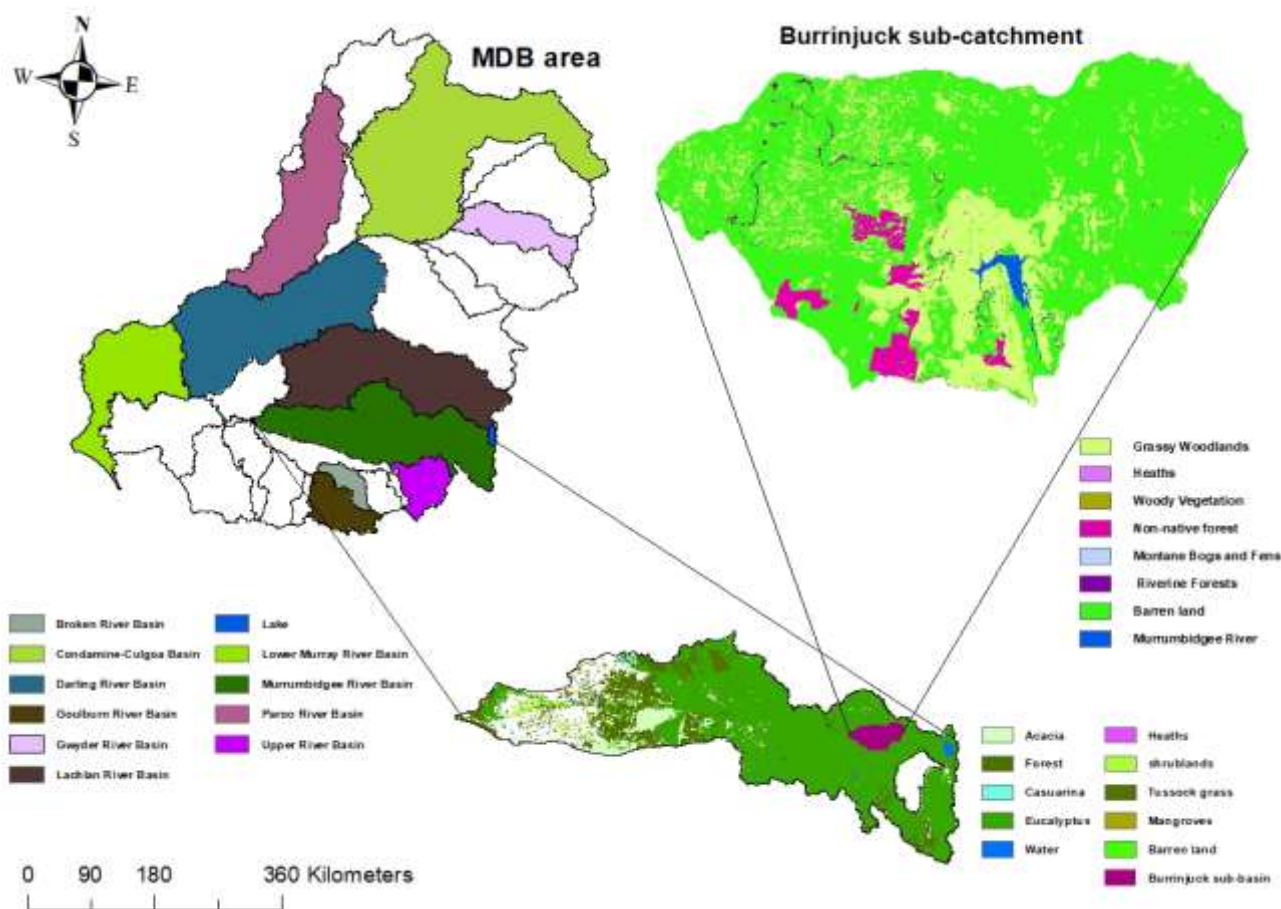


Figure 4.2: The study area, Burrinjuck sub-catchment on the right which is located within the Upper Murrumbidgee River catchment. The top left section shows the vegetated area of the Murray Darling Basin (MDB), highlighting the location of the Murrumbidgee River catchment. Bottom left describes the vegetated area in the Murrumbidgee River Catchment.

#### 4.3.3. Study period

The study period (2000-2020) was selected to include both a long-term drought (2001-2006) and flooding (2009-2011) phases. Both dry and wet phases were included in the study to ensure that any long-term change in the vegetation condition was captured by NDVI data. The annual data were divided into two seasons: i) dry season and ii) wet season, which were categorised based on rainfall and temperature anomalies (Table 4.1). The average monthly dry season rainfall is 35.73mm and 163.77mm in the drought and flooding periods, respectively and average wet season rainfall is 73.32mm in the study area.

Table 4.1: Annual dry and wet season of the study period

Dry season	Sep	Oct	Nov	Dec	Jan	Feb
Wet season	Mar	Apr	May	Jun	Jul	Aug

#### **4.3.4. Vegetation in the study area**

The Burrinjuck floodplain study area resides within the Burrinjuck natural reserve, possesses a diversity of vegetation types which can be categorised into six distinct forest ecosystems. These ecosystems are i) Apple box – Norton’s box moist grass forest, ii) Wee Jasper Norton’s box – Poa grass forest, iii) Brittle Gum – Broad-Leaved Peppermint Poa grass forest, iv) Dwyer’s Gum heathy low open woodland, v) Long Leaved Box (Black Cypress Pine) heath shrub forest, and vi) Blue Gum – Broad-Leaved Peppermint dry grass shrub forest. Some of the dominant tree, shrub, and grass types of vegetation in the study area are *Eucalyptus nortonii* (Norton’s box), *Eucalyptus mannifera* (Brittle gum), *Eucalyptus albens* (White box), *Acacia dealbata* (Silver wattle), *Platylobium formosum* (Pea bush), *Geranium solanderi* (Native geranium), *Joycea pallida* (Silver top wallaby grass) etc.

The vegetation types used for the analysis in this study were selected from these ecosystems. The grass type vegetation near the stream (FV1) and distant from the stream (FV4) are member of Apple box – Norton’s box moist grass forest, Wee Jasper Norton’s box – Poa grass forest, and Blue Gum – Broad-Leaved Peppermint dry grass shrub forest ecosystems. The shrub-type vegetation found near the stream (FV2) and at a distance from the stream (FV5) consists of ecosystems characterised by Long-Leaved Box (Black Cypress Pine) heath shrub forest and Blue Gum – Broad-Leaved Peppermint dry grass shrub forest. The tree type vegetation near the stream (FV3) and distant from the stream (FV6) are members of the Apple box – Norton’s box moist grass forest, Wee Jasper Norton’s box – Poa grass forest, Brittle Gum – Broad-Leaved Peppermint Poa grass forest, Long Leaved Box (Black Cypress Pine) heath shrub forest, and Dwyer’s Gum heathy low open woodland ecosystems.

#### **4.3.5. Data description**

The climate, hydrological and remote sensing datasets applied in this study, were sourced from Australia’s Bureau of Meteorology (BoM), New South Wales (NSW) Office of Water and the U.S. Geological Survey (USGS) (Table 4.2). A combination of station gauged, and satellite derived data were used as input parameters in the hydrological model for catchment runoff simulation. During the catchment hydrological modelling, 22 missing data identified out of 7,665 daily rainfall data. These missing data have been filled using the K-nearest neighbour technique (Lu & Qin, 2014).

Table 4.2: Key datasets used, their descriptions, and sources

<b>Data</b>	<b>Frequency</b>	<b>Description</b>	<b>Source</b>
Precipitation	Daily	Station gauged, temporal	Bureau of Meteorology
Temperature	Daily	Station gauged, temporal	Bureau of Meteorology
Evapotranspiration	Daily	Satellite-derived, 0.05 degree (approximately 5 x 5 km)	Bureau of Meteorology
Runoff	Daily	Satellite-derived, 0.05 degree (approximately 5 x 5 km)	Bureau of Meteorology
Streamflow (discharge)	Daily	Station gauged, temporal	NSW Office of Water
MODIS NDVI	16-Day	250 m spatial resolution	U.S. Geological Survey

### ***Meteorological data***

The daily precipitation and temperature data were downloaded for the period 2000 to 2020 from the Australian Bureau of Meteorology (BOM, 2021a, 2021b) to analyse seasonal intensity and identify prolonged drought and flood events. The potential evapotranspiration and runoff data were obtained from the Australian Water Resources Assessment Landscape model available from the BOM website and later processed using ArcGIS. This historical runoff data was applied for hydrological model calibration.

### ***Remotely sensed data***

In this study, the MODIS (Terra) 16-Day Global 25m composite product of MOD13Q1 (version V006) was used to identify vegetation conditions. The NDVI values were selected from the available vegetation indices in the MOD13Q1 product from 2000 to 2020. There were 480 images of MOD13Q1 NDVI for the 21 years that have been calculated for each type of vegetation plot. The average annual and seasonal NDVI data for the study period were calculated from this 21-year dataset which minimised the cloud cover correlation for the vegetation response. In the plot selection, supervised classification technique was applied to select eighteen plots for six different vegetation types (such as grass, shrub, and tree) from the study area (Table 4.3). The plots were selected by vegetation survey and using Google Earth tool to identify the density of each vegetation type in the plotted area. These selected plots have been converted into polygons in the Google Earth Pro and then saved as KML files which were later processed into shapefile in ArcGIS (ESRI, 2019). A pre-processing tool named

Application for Extracting and Exploring Analysis Ready Samples (AppEEARS) has been selected to obtain pre-processed NDVI time-series data for those shapefiles prepared earlier. The average NDVI data from three plots were used for each vegetation response.

Table 4.3: Different types of floodplain vegetation used in this objective 1

Series	Floodplain vegetation type (FVT) description	Distance from the stream (m)	Short name
1	Grasses near the stream	0 – 913	FVT1
2	Shrubs near the stream	0 – 638	FVT2
3	Trees near the stream	0 – 904	FVT3
4	Grasses far from the stream	3303 -7079	FVT4
5	Shrubs far from the stream	2506 – 5011	FVT5
6	Trees far from the stream	5040 -10456	FVT6

#### 4.3.6. Normalised Difference Vegetation Index (NDVI)

The healthy vegetation mostly absorbs light from the red spectrum and reflects light from the near-infrared (NIR) spectrum. NDVI utilises the contrast of strong reflectance in the near-infrared region and the strongly absorbed reflectance in the red wavelength region. NDVI calculation was performed by applying the difference between the red and near-infrared bands and normalising it over the sum of red and near-infrared bands (Equation 1).

$$NDVI = \frac{(Near\ Infrared - Visible\ red\ light)}{(Near\ Infrared + Visible\ red\ light)} \quad (1)$$

Satellite sensors captured about 20% red and 60% near-infrared reflected light from the chlorophyll pigments (Martiny et al., 2007). The difference between the contrast of the two bands allowed for quantifying the energy received by vegetation through leaves identifying the vegetation conditions (Tucker, 1979). These vegetation conditions also depend on climate variability and catchment hydrology.

#### 4.3.7. Rainfall-runoff hydrological modelling

The SIMHYD hydrological model is the simplified version of the Hydrolog rainfall-runoff model, previously used in the Murray Darling Basin (MDB) area for hydrological modelling (Chiew & McMahon, 2002; Chiew et al., 2002). The SIMHYD model requires only three types of daily time series input data such as rainfall, evapotranspiration, and streamflow

data for calibration. After successful calibration, the model was run to simulate daily catchment runoff from the daily precipitation and potential evapotranspiration data.

The catchment hydrology is highly influenced by rainfall that drains in evapotranspiration and runoff (Saha et al., 2013). Like other catchments, SIMHYD simulates little to no infiltration excess runoff. Therefore, the optimisation of maximum infiltration loss (default value is 200) and infiltration loss exponent (default value is 1.5) were not used in this study as the Burrinjuck sub-catchment is not considered to be a tropical catchment.

In the SIMHYD model, daily rainfall first fills the interception storage, which is emptied each day by evaporation. The excess rain is then subjected to an infiltration function that determines the infiltration capacity. The excess rainfall that exceeds the infiltration capacity becomes infiltration excess runoff. Finally, infiltrating moisture is subjected to a soil moisture function that diverts the water to the stream (interflow), groundwater storage (recharge) and soil moisture storage. Interflow is first estimated as a linear function of the soil wetness (soil moisture level divided by soil moisture capacity) (Beven, 2012). The default values applied for the SIMHYD model are listed in Table 4.4.

Table 4.4: SIMHYD model parameters and their boundary values

<b>Parameter</b>	<b>Default value</b>	<b>Minimum</b>	<b>Maximum</b>
Baseflow Coefficient	0.3	0.0	1.0
Impervious Threshold	1	0	5
Infiltration Coefficient	200	0	400
Infiltration Shape	3	0	10
Interflow Coefficient	0.1	0.0	1.0
Pervious fraction	0.9	0.0	1.0
Rainfall Interception Store Capacity	1.5	0.0	5.0
Recharge Coefficient	0.2	0.0	1.0
Soil Moisture Store Capacity	320	1	500

#### **4.3.8. SIMHYD model calibration and validation**

Selecting a calibration period is critical to cover both extremely dry and wet periods, and average annual streamflow must be similar for the whole period of record. The calibration period was selected for 2001 to 2009, which covers both extremely dry and wet conditions.

A period of nine years (2001-2009), including one year of warmup, was selected as a calibration period, while eight years (2009-2016) was chosen for model validation. The modelling was performed for 0.05° x 0.05° grid cells to allow a better representation of the spatial patterns and gradient in rainfall. The same set of parameter values were used for all 0.05° x 0.05° grid cells for the Burrinjuck area. Once the model was trained, applied parameter settings to simulate runoff for the period from 2000 to 2020.

#### **4.3.9. SIMHYD model performance criteria**

The value of the objective function for the calibration of parameters can be used as the model performance statistics. Nash-Sutcliffe efficiency (NSE) was used as the objective function (Nash & Sutcliffe, 1970), which can be described as equation 2:

$$NSE = 1 - \frac{\sum_{i=1}^n (Q_{obs,i} - Q_{sim,i})^2}{\sum_{i=1}^n (Q_{obs,i} - \bar{Q}_{obs})^2} \quad (2)$$

where n is the number of time steps,  $Q_{obs,i}$  is the observed flow at time step i (daily here),  $\bar{Q}_{obs}$  is the mean of the observed flow, and  $Q_{sim,i}$  is the simulated flow. The range of NSE is  $[-\infty, 1]$ , where 1 represents a perfect match between the observed and simulated flow.

The SIMHYD model was run on daily time series data, and model performance was measured by the Nash Sutcliffe Coefficient of efficiency (NSE). The NSE value with a range of 0 to 1 ('0' means no similarity and '1' means similar) describes the agreement between the calibrated and observed daily runoffs. NSE values greater than 0.6 suggest a reasonable modelling of runoff, while NSE values greater than 0.8 means good modelling of runoff for the catchment (Peel et al., 2000).

#### **4.3.10. Machine learning algorithms for data processing**

A machine learning (ML) algorithm is a set of computational codes that can process a large amount of data in a complex way (Sarker, 2021). The algorithms read and process data to learn the maximum possible patterns about the data (Cracknell & Reading, 2014). In this study, two ML tools (i.e., RF and SVM) were selected for creating regression and classification models, as they are widely used supervised learning techniques in remote sensing and vegetation studies (López-Serrano et al., 2016; Stas et al., 2016; Chen et al., 2021; Li et al., 2021). The impact of a collection of explanatory variables (Xs), including rainfall,

temperature, runoff, and streamflow, on a target variable (Y) was modelled, i.e., NDVI, which is in the context of supervised learning (SL).

#### **4.3.11. Waikato Environment for Knowledge Analysis (WEKA) tool**

In modelling the relationships between surface water and NDVI, the Waikato Environment for Knowledge Analysis (WEKA) tool developed by the University of Waikato, New Zealand (Hall et al., 2009; Eibe et al., 2016). The WEKA tool is free software licensed under the General Public License (GNU) and able to run the selected classifier compared to other open-source data mining tools (Sharma et al., 2015). WEKA is user-friendly well-known machine learning (ML) suits that supports typical data mining activities such as data pre-processing, clustering, classification, regression, visualisation, and feature selection (Marin et al., 2021). In this study WEKA is employed for machine learning (ML) applications which has been considered in previous studies (Sharma et al., 2015; Abdurahman, 2017; Kitessa et al., 2021; Kushwaha et al., 2021; Marin et al., 2021).

#### **4.3.12. Modelling the relationships between surface water and NDVI**

Firstly, the WEKA tool was setup to run a random forest model using 36 different datasets. These datasets included the combination of rainfall, runoff, streamflow, and different types of vegetation responses (NDVI values). Each dataset was initially set for linear regression to find the collinear and non-collinear variables. Secondly, the machine learning tool was prepared to run a support vector machine (SVM) model using the same datasets.

The performance of all models has been assessed in two ways: a) using a 10-fold cross-validation, which is a leave-one-out approach, and b) using the 80 and 20 per cent split method. These two approaches were performed to compute the Root Mean Square Error (RMSE) and correlation coefficient (r) between the observed and predicted vegetation response (NDVI value) of each model. Among them the models with higher correlation coefficient (r) values and smaller RMSEs were selected to analyse the relationship against rainfall, runoff, and streamflow. A lag time factor was applied between NDVI and rainfall, runoff, and streamflow to test if there are differences in response considering vegetation growth time. Table 4.5 shows how the dataset was prepared with no lag in the time series of NDVI data, and 1-month, 2-month, 3-month lagged NDVI time series data against rainfall (e.g., rainfall in May corresponds with NDVI value in June for a 1-month lagged).

Table 4.5: Datasets prepared to apply in the WEKA model with and without lagged NDVI time-series data

No lag		1-month lagged NDVI		2-month lagged NDVI		3-month lagged NDVI								
Rain	NDVI	Rain	NDVI	Rain	NDVI	Rain	NDVI							
Sep-00	4.53	0.64	Sep-00	4.53	Oct-00	0.55	Sep-00	4.53	Nov-00	0.55	Sep-00	4.53	Dec-00	0.48
Oct-00	4.16	0.55	Oct-00	4.16	Nov-00	0.55	Oct-00	4.16	Dec-00	0.48	Oct-00	4.16	Jan-01	0.34
Nov-00	3.88	0.55	Nov-00	3.88	Dec-00	0.48	Nov-00	3.88	Jan-01	0.34	Nov-00	3.88	Feb-01	0.35
Dec-00	0.89	0.48	Dec-00	0.89	Jan-01	0.34	Dec-00	0.89	Feb-01	0.35	Dec-00	0.89	Mar-01	0.38
Jan-01	1.15	0.34	Jan-01	1.15	Feb-01	0.35	Jan-01	1.15	Mar-01	0.38	Jan-01	1.15	Apr-01	0.39
Feb-01	3.10	0.35	Feb-01	3.10	Mar-01	0.38	Feb-01	3.10	Apr-01	0.39	Feb-01	3.10	May-01	0.38
Mar-01	2.23	0.38	Mar-01	2.23	Apr-01	0.39	Mar-01	2.23	May-01	0.38	Mar-01	2.23	Jun-01	0.45
Apr-01	1.79	0.39	Apr-01	1.79	May-01	0.38	Apr-01	1.79	Jun-01	0.45	Apr-01	1.79	Jul-01	0.51
May-01	0.38	0.38	May-01	0.38	Jun-01	0.45	May-01	0.38	Jul-01	0.51	May-01	0.38	Aug-01	0.56

## 4.4. Results

### 4.4.1. Hydrological model simulated catchment runoff

The result shows that the SIMHYD model has simulated catchment runoff with an acceptable NSE value of 0.95, indicating good modelling outcomes for the catchment. The default parameters used in the calibration where infiltration coefficient 348.95, recharge coefficient 0.28 and soil moisture store capacity value was 486.78.

Two optimisation options, i.e., the generic algorithm and the pattern search multi-start, were applied for the SIMHYD calibration. Among these two calibration methods, the pattern search multi-start option has produced better results with higher NSE value (NSE=0.95 and 0.83, respectively). Figure 4.3 describes the comparison between observed, calibrated, and simulated daily runoff at Burrinjuck sub-catchment study area.

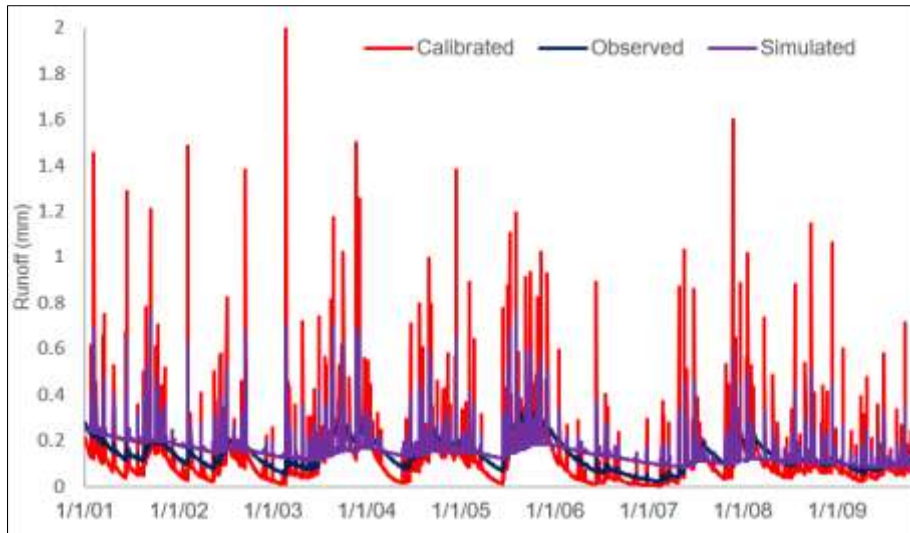


Figure 4.3: The SIMHYD model calibrated and simulated runoff data plotted against the observed data (daily timestep results displayed). The data presented in daily time series from 2001 to 2010.

The rainfall is the main dominating factor in changing the simulated runoff. The SIMHYD model has been calibrated with 10% increased rainfall as well as 10% decreased rainfall (increased and decreased observed rainfall data by 10%). Figure 4.4 shows that simulated runoff was not equally sensitive to changing rainfall intensity. The result shows the average simulation runoff has increased by 54% when rainfall data was increased, and average runoff decreased by 87% when model was calibrated with decreased rainfall data. The analysed results show that runoff is more sensitive with reduced rainfall than that of increment.

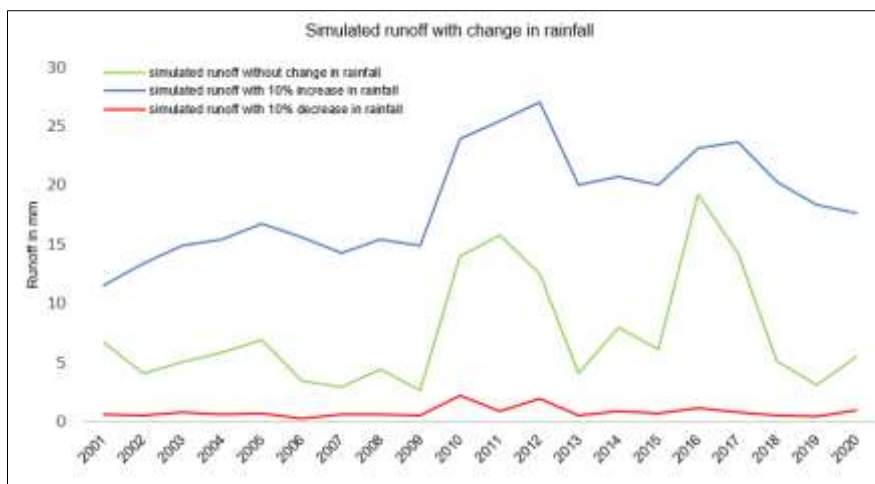


Figure 4.4: The SIMHYD model simulated runoff (mm) data (no change) plotted (colour in green) against simulated runoff with 10% increased rainfall (colour in blue), and simulated runoff with 10% decreased rainfall data (colour in red).

#### 4.4.2. Vegetation response to surface water during the dry season

The vegetation response (NDVI values) modelling results from both random forest (RF) and support vector machine (SVM) algorithms during the dry season are presented in Table 4.6 and Figure 4.5. The overall RMSE varies between 0.03 and 0.12 (3% to 12%) for the dry season, indicating high model performances. The modelling results show that grass vegetation type distant from the stream (FVT4) was highly responsive to rainfall, runoff, and streamflow ( $r=0.85, 0.82,$  and  $0.81,$  respectively) during the dry season when applied 1-month lagged NDVI time series data (Table 4.6). The modelling results also explained that grass vegetation type near the stream (FVT1) had high positive relationships with rainfall and runoff ( $r=0.75,$  and  $0.71$  respectively) when applied 1-month lagged NDVI time series data (Table 4.6). Furthermore, the results show that shrub and tree vegetation types both near (FVT2 and FVT3) and distant (FVT5 and FVT6) from the stream were highly responsive to catchment runoff ( $r=0.77, 0.71, 0.75,$  and  $0.76$  respectively) during the dry season (Table 4.6). In the modelling result, over 83% of the calculated area had RMSE  $<10\%$ . The RMSE values were different for RF (RMSE= 0.08, 0.09, and 0.08 respectively) and SVM (RMSE=0.07, 0.08, and 0.087 respectively) while the model was run against rainfall, runoff, and streamflow.

Table 4.6: Regression modelling results produced using RF and SVM machine learning algorithms without lagged time and with 1-month lagged time during the dry season.

Type	Random forest						SVM					
	Rainfall		Runoff		Streamflow		Rainfall		Runoff		Streamflow	
	r	RMSE	r	RMSE	r	RMSE	r	RMSE	r	RMSE	r	RMSE
FVT1	<b>0.71</b>	0.09	0.67	0.09	0.66	0.09	<b>0.68</b>	0.09	0.63	0.09	0.66	0.09
FVT2	0.66	0.05	<b>0.77</b>	0.04	0.66	0.05	<b>0.70</b>	0.05	<b>0.70</b>	0.05	<b>0.70</b>	0.05
FVT3	0.64	0.05	<b>0.71</b>	0.05	0.64	0.05	0.65	0.05	0.65	0.05	0.55	0.06
FVT4	<b>0.67</b>	0.13	<b>0.77</b>	0.11	<b>0.70</b>	0.13	0.65	0.13	<b>0.68</b>	0.13	<b>0.69</b>	0.13
FVT5	<b>0.67</b>	0.09	<b>0.75</b>	0.08	<b>0.69</b>	0.08	0.65	0.09	0.60	0.04	0.62	0.09
FVT6	0.58	0.05	<b>0.76</b>	0.04	0.56	0.05	0.51	0.05	0.55	0.05	0.58	0.05
1-Month lagged time												
FVT1	<b>0.75</b>	0.09	<b>0.71</b>	0.09	<b>0.68</b>	0.09	<b>0.79</b>	0.07	<b>0.72</b>	0.08	<b>0.73</b>	0.08
FVT2	0.52	0.06	0.63	0.05	0.46	0.06	0.56	0.05	0.53	0.06	0.49	0.06
FVT3	0.53	0.05	0.64	0.05	0.39	0.06	0.50	0.06	0.49	0.06	0.45	0.06
FVT4	<b>0.85</b>	0.09	<b>0.82</b>	0.10	<b>0.81</b>	0.10	<b>0.84</b>	0.09	<b>0.81</b>	0.10	<b>0.81</b>	0.10
FVT5	<b>0.79</b>	0.08	<b>0.75</b>	0.08	<b>0.74</b>	0.08	<b>0.81</b>	0.07	<b>0.73</b>	0.08	<b>0.75</b>	0.08
FVT6	0.49	0.05	<b>0.72</b>	0.05	0.45	0.06	0.31	0.06	0.35	0.07	0.19	0.06

From the results, it was also found that responses of grass vegetation type near the stream (FVT1) were increased by 5.1%, 7.5%, and 4.6% ( $r=0.75, 0.71,$  and  $0.68$  respectively) when 1-month lagged NDVI datasets applied against rainfall, runoff, and streamflow

compared to no-lag data (Table 4.6). On the other hand, the responses of shrub and tree vegetation types near the stream (FVT2 and FVT3) were decreased by 18% and 8.5% ( $r=0.77$ ,  $0.71$ ,  $0.63$ , and  $0.64$  respectively) when model was run against runoff without lag time and 1-month lagged NDVI datasets. However, the modelled results were slightly different for RF and SVM ( $r=0.77$ ,  $0.71$ , and  $0.70$ ,  $0.65$ , respectively) when runoff was used as a relative factor (Table 4.6).

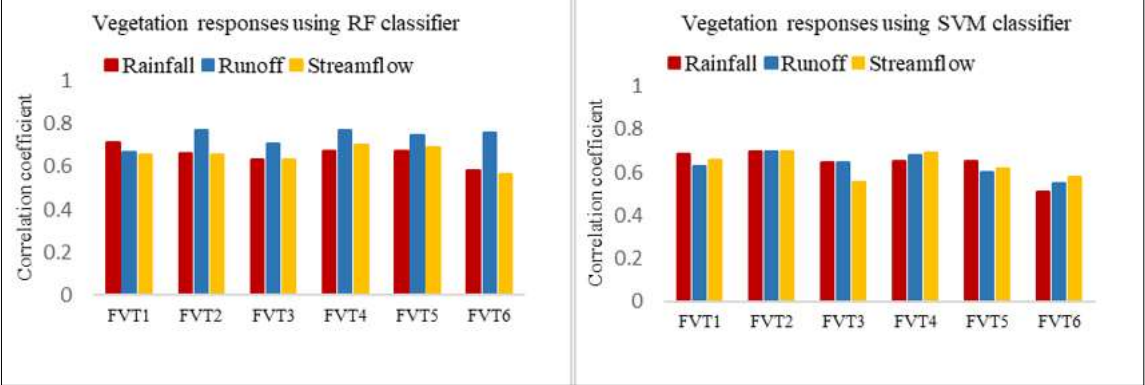


Figure 4.5: Graphical representation of different types of vegetation responses (NDVI values without lagged time) against rainfall, runoff, and streamflow using random forest and support vector machine classifiers in WEKA model.

The Figure 4.6 shows the graphical distributions of different types of observed floodplain vegetation (NDVI) responses against the average mean monthly rainfall, runoff, and streamflow.

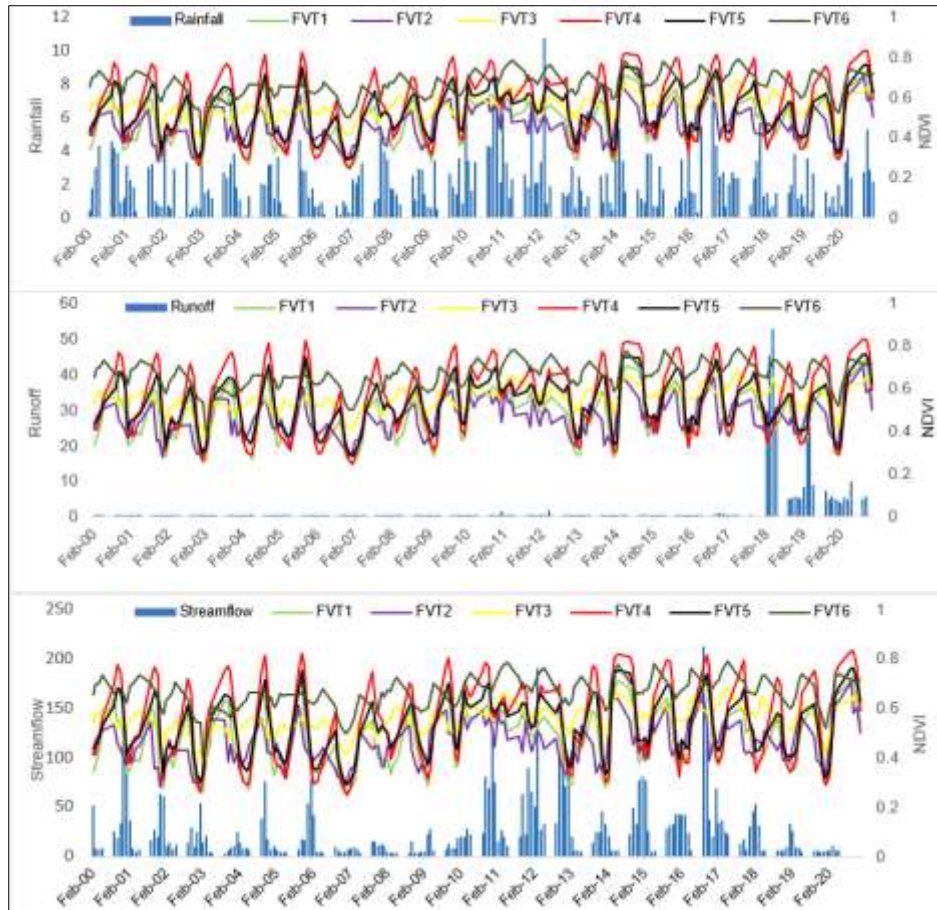


Figure 4.6: NDVI from different floodplain vegetation types plotted against catchment rainfall, runoff, and streamflow during the dry season.

Moreover, the modelling results show that FVT1 ( $r=0.71$ ) was highly sensitive to climatic factors such as rainfall and temperature compared to FVT2 ( $r=0.50$ ) and FVT3 ( $r=0.54$ ) during dry season.

#### 4.4.3. *Vegetation response towards surface water during the wet season*

Different vegetation responses were also analysed during the wet season. Figure 4.7 graphically represents the NDVI values of selected six different vegetation types against the average mean monthly rainfall, runoff, and streamflow between March and September from 2000 to 2020.

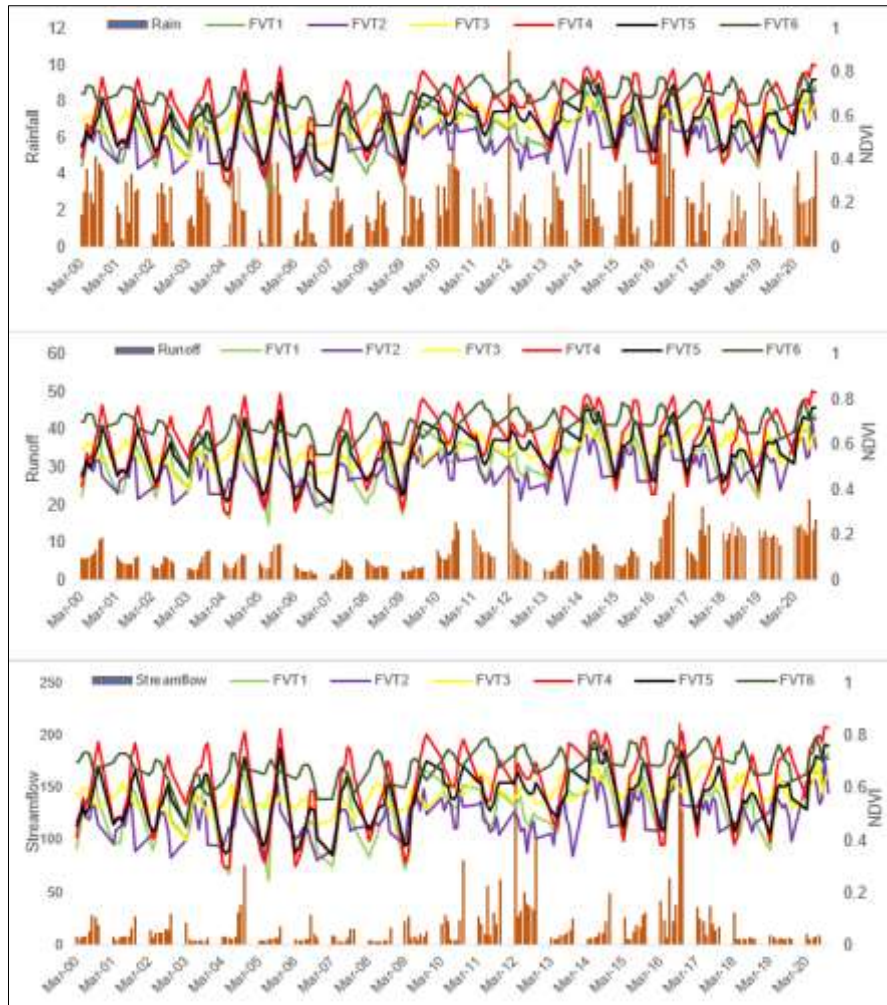


Figure 4.7: NDVI from different floodplain vegetation types plotted against catchment rainfall, runoff, and streamflow during the wet season.

The modelling result shows that all three vegetation types near the stream (FVT1, FVT2, and FVT3) and two vegetation types far from the stream (FVT4 and FVT5) were highly responsive to runoff ( $r=0.75, 0.79, 0.70, 0.71,$  and  $0.75$  respectively) during the wet season (Table 4.7). The models predicted grass and tree vegetation types far from the stream (FVT4 and FVT6) were highly responsive to rainfall ( $r=0.85$ ) and runoff ( $r=0.71$ ) when applied 1-month lagged NDVI time series dataset during the wet season (Table 4.7).

Table 4.7: Regression modelling results produced using RF and SVM machine learning algorithms without lagged time and 1-month lagged time during the wet season.

Type	Random forest						SVM					
	Rainfall		Runoff		Streamflow		Rainfall		Runoff		Streamflow	
	r	RMSE										
FVT1	0.4591	0.1029	<b>0.7508</b>	0.0747	0.4669	0.0991	0.4393	0.098	<b>0.5116</b>	0.0947	<b>0.6272</b>	0.0892
FVT2	0.5966	0.0448	<b>0.7972</b>	0.0339	0.4775	0.048	<b>0.5774</b>	0.0431	<b>0.6058</b>	0.0445	<b>0.6975</b>	0.0422
FVT3	0.4279	0.0558	<b>0.7036</b>	0.0436	0.438	0.0564	0.4709	0.0477	<b>0.5489</b>	0.0451	<b>0.6107</b>	0.0503
FVT4	<b>0.6712</b>	0.127	<b>0.715</b>	0.1079	<b>0.5101</b>	0.1288	<b>0.6515</b>	0.1277	0.4953	0.1316	<b>0.5184</b>	0.1238
FVT5	0.4679	0.0932	<b>0.7551</b>	0.0681	0.4955	0.0874	0.4319	0.0939	0.4893	0.087	<b>0.5691</b>	0.0874
FVT6	0.5835	0.0514	0.5002	0.0517	<b>0.5455</b>	0.0498	<b>0.5817</b>	0.0521	0.4908	0.0487	<b>0.5852</b>	0.0492
1-Month lagged time												
FVT1	<b>0.618</b>	0.088	0.5239	0.0959	0.5122	0.0993	0.5832	0.0878	0.5763	0.0896	0.5413	0.091
FVT2	0.3912	0.0479	0.4572	0.0438	0.3204	0.0484	0.4298	0.0476	0.4714	0.0465	0.3748	0.0491
FVT3	0.36	0.0502	0.4592	0.0455	0.3977	0.0481	0.3281	0.051	0.3972	0.0496	0.3052	0.0514
FVT4	<b>0.8512</b>	0.0901	<b>0.6014</b>	0.1246	0.5425	0.1279	<b>0.8438</b>	0.0895	<b>0.6306</b>	0.117	<b>0.6161</b>	0.1186
FVT5	0.5759	0.0808	0.511	0.0847	0.4085	0.0922	0.5509	0.0822	0.5725	0.0808	0.4844	0.0861
FVT6	0.4872	0.0526	<b>0.7137</b>	0.0584	0.3683	0.0689	0.3344	0.0559	0.1668	0.0903	0.1883	0.0737

The WEKA machine learning tool was able to model available surface water variables and vegetation responses for 21 years despite the drought years (2002 and 2006) and extreme wet years (2010 and 2016). Likewise, the correlation coefficient of catchment runoff and NDVI values of FVT2 and FVT3 were highly positive ( $r=0.79$  and  $0.70$ , respectively) when temperature was used as a relative factor (Table 4.7). The  $r$ -value of the FVT2 response against runoff was 3.7% higher in the wet season than dry season. However, the  $r$ -values were reduced by 10.6% and 27.7% when the model was run against rainfall and streamflow. Furthermore, the reductions in  $r$ -values were higher by 33.3% and 31.7%, respectively, when a 1-month lagged datasets were applied between NDVI-rainfall and NDVI-streamflow correlation analysis (Table 4.7).

#### 4.4.4. Vegetation response based on distance from stream

The machine learning (ML) modelling results show that vegetation types, based on proximity to the stream, responded differently to surface water availability. Overall, their responses were better during the dry season compared to the wet season. FVT4 (grass vegetation far from the stream), FVT5 (shrub vegetation far from the stream), and FVT6 (tree vegetation far from the stream) showed variations in their responses from moderate to a highly positive manner against all three types of surface water resources. However, the values of  $r$  increased for FVT4 and FVT5 by 26.81% and 16.8%, respectively, and decreased by 7.4% for FVT6 when models were run with a 1-month lagged NDVI-rainfall datasets (Table 4.6).

During the wet season, the degree of responses became smaller between FVT5-rainfall and FVT5-streamflow correlations compared to dry season. Results also show that the correlation coefficient value ( $r$ ) was 0.51, which indicated 27% lower than dry season when ML tool was applied between the NDVI (FVT4) and streamflow during wet season. There was a significant change noticed in the modelling results between FVT6 and runoff, which decreased by 33.3% compared to the  $r$  value (0.75) during the dry season. However, correlation coefficient ( $r$ ) values between modelled and actual NDVI for FVT5 against rainfall and streamflow have decreased by 26.9% and 46%, respectively, when applied 1-month lagged NDVI datasets (Table 4.7).

## **4.5. Discussion**

### **4.5.1. Hydrological modelling**

Hydrological modelling is important for better understanding of catchment water availability and its movement. The selection of model is the key factor of the hydrological modelling which depends on available catchment data, spatial representation, operational technique, robustness, and climate condition (Pechlivanidis et al., 2011). The SIMHYD model requires fewer parameters to run compared to other rainfall-runoff hydrological models such as HBV and GR4J. In hydrological modelling, calibration is an integral part of the process, though practically, it is impossible to mimic and measure all hydrological properties of a catchment. The SIMHYD was calibrated against daily rainfall, streamflow, and potential evapotranspiration which generated 0.95 NSE value. This result explained that the calibration techniques applied in this study have improved the modelling results (Zhang et al., 2009).

The SIMHYD model calibration with reduced and increased rainfall conditions were considered in this study, ranging from -10% to +10%. Figure 4.4 shows that runoff was not equally sensitive to change in rainfall intensity. For example, runoff was more sensitive to the rainfall reduction than increased rainfall. This result outcome supports the previous findings that runoff patterns are not equally varied with change in rainfall patterns (Potter et al., 2010). However, the magnitude of the runoff increased by 37% to 82% with increased rainfall and reduced by 77% to 94% with decreasing rainfall. According to Chiew (2006), the runoff elasticity of rainfall is approximately 2-3 times but the study results show that runoff was 4-6 times more sensitive to the change. The different outcome in the results could be due to other conditions of the study area such as soil moisture content, land use, land cover, and elevation. Further results show that calibrated runoff decreased by a minimum of 15% to a maximum of

62% in the wet season, and 8% to a maximum of 29% in the dry season. These results support the previous finding that runoff reduction is more severe in the southern Murray Darling Basin area than the reduction in annual rainfall (Potter et al., 2010). Moreover, this study analysed the long-term (from 2000 to 2020) seasonal rainfall variability in the study area using high quality datasets from Australian BoM. The main variations of rainfall in this south-eastern part of Australia were clearly season-dependent. For example, occasional high volume rainfall events occur in winter (Montazerolghaem et al., 2016). These occasional high volume rainfall events can also contribute to increasing catchment's surface and subsurface runoff (Saha & Zeleke, 2014).

Previous studies have reported that the change in catchment vegetation condition may greatly affect the rate of actual evapotranspiration and runoff (Sun et al., 2017). Furthermore, runoff coefficients also vary with water availability; for example, it may increase in the flood season and decrease in the non-flood season (Liang et al., 2015). The evapotranspiration rate is lower in the winter season due to lower temperature, and shedding of leaves of tree species results in increased streamflow (Sun et al., 2017). However, hydrological modelling helps to understand the relationship between catchment water balance and the vegetation. This knowledge would help to explain the interactions between vegetation dynamics and the water cycle (Yang et al., 2009). In hydrological modelling, high flows are easy to predict during model calibration. However, for better understanding, low flow also requires consideration in the model calibration. The model used in this study, SIMHYD, has the ability to observe low flow characteristics (Chiew et al., 2018). The results of this study had important environmental implications for arid sub-catchments elsewhere with similar environmental conditions.

#### **4.5.2. Vegetation response and surface water relations**

The relationship modelling results show that the correlation coefficient ( $r$ ) values are highly positive (0.75, 0.79, 0.70, 0.71, and 0.75 etc.) for grass and shrub type vegetation (FVT1, FVT2, FVT4 and FVT5) while model was run against runoff during the wet season. Furthermore, only grass vegetation type far from the stream (FVT4) had a high positive correlation coefficient ( $r$ ) with rainfall ( $r=0.85$ ) than other vegetation types during the wet season. However, the correlation coefficient ( $r$ ) values were lower by 36.6%, 10.6%, and 26.9% for all three types of vegetation (FVT1, FVT2, and FVT3) near the stream, while the model was run against rainfall compared to the dry season. These seasonal variations may be related to the inter-seasonal temperature difference.

However, grass vegetation type is highly responsive to catchment runoff than rainfall during the wet season. Therefore, the average NDVI value of grass near the stream (FVT1) is 11.53% higher in wet season than in dry season. Furthermore, the rainfall pattern is influenced by El Nino and La Nina in the study region, which leads to irregular patterns of floods and droughts. Thus, considering the climate scenario of the study region should give more accurate results for vegetation response and surface water relationship.

The analysis of the results revealed that shrub and tree vegetation types near the stream (FVT2 and FVT3) in the study area have greater relationships with catchment runoff than rainfall. The  $r$  values predicted by RF algorithm for FVT2-rainfall and FVT3-rainfall relationships were lower as 0.59 and 0.42 (compared to 0.66 and 0.63, respectively during dry season). Interestingly, the value of  $r$  significantly decreased for all three vegetation types (FVT1, FVT2, and FVT3) when applied lagged NDVI-runoff datasets. Moreover, most of the trees in the floodplain are phreatophytes, that is, their long root absorbs water from the groundwater or the capillary fringe just above the groundwater table (Naumburg et al., 2005). Additionally, in some floodplain areas, the groundwater tables are expected to be close to the surface (Martinetti et al., 2021). Thus, including groundwater assessment in future studies can be a good option. In this study, the modelling relationships between vegetation response and surface water availability using the machine learning tools were simulated correlations. These correlations could be further improved in future studies by introducing other factors in relationships modelling, such as soil moisture content, soil water holding capacity, and land gradient.

#### ***4.5.3. Vegetation response based on distance from the stream***

Overall, significant changes in correlation coefficient ( $r$ ) were observed for grass and shrub vegetation distant from the stream (FVT4 and FVT5) during the study period when 1-month lagged NDVI datasets applied in the relationship analysis. The correlation coefficient ( $r$ ) values were increased by 26.8% and 16.8% against rainfall, 6.1% and 1% against runoff, and 15.6% and 8% against streamflow, compared to the model run without lagged time in the NDVI datasets during the dry season. In contrast, for trees far from the stream (FVT6), the correlation coefficient ( $r$ ) between NDVI and runoff was highly positive ( $r=0.75$ ) during the dry season without lag time in the dataset. Thus, the correlation was decreased by 5.5% when model was run with 1-month lagged NDVI datasets. This result reflects that tree type vegetation far from the stream grow well when runoff increases in the dry season.

Furthermore, this type of vegetation does not respond well to the runoff during the wet season. Similar analysis showed that grass vegetation (FVT4) responds better than shrub vegetation (FVT5) during the wet season, and relationships were positively increased by 26.8% and 23%, respectively, when 1-month lagged NDVI datasets applied in the analysis. Thus, in this study the modelled results support the previous finding on higher sensitivity of grass vegetation towards surface water availability (Kath et al., 2019).

#### **4.6. Conclusion**

This study showed contrasting vegetation responses to seasonal surface water variability. The result section revealed that grass vegetation type, either near the stream or distant from the stream, is more sensitive to rainfall than runoff and streamflow. This study suggests that the grass vegetation type is highly dependent on summer rainfall and winter runoff for their growth, and any instability or long-term drought can negatively affect these floodplain vegetation communities. The vegetation and surface water variability relationships describe that responses vary on vegetation types and their locations. Floodplain ecosystem management authorities need to review the current basin water management policies in the semi-arid region to include flexible water use strategies to allow for adjustment under seasonal requirements.

The relationship between floodplain vegetation and catchment hydrology is two-way, and any change in the environment can directly influence the vegetation response to surface water. For example, suitable growing temperature and available water can increase the potential evapotranspiration rate and land cover, with grass vegetation type reducing the catchment runoff. The hydrological modelling results suggested that rainfall dominates the catchment's water balance, in which streamflow increases in the wetting period between May and August when the evapotranspiration rate is lower. Any changes in the streamflow directly impact the condition of floodplain vegetation during the wet season. These potential changes in the condition of vegetation are required to be included in hydrological modelling. A coupled hydrological modelling option can be considered in future studies, for instance the use of LAI values in the modelling tool. Furthermore, in a rainfall dominated catchment hydrology, any prediction of future change in the rainfall pattern should also be considered carefully for better floodplain management.

In the next chapter, Chapter 5, the vegetation responses to groundwater resources in the floodplain area using ArcSWAT hydrological model, MODIS imagery for vegetation mapping, and machine learning algorithms are presented.

# CHAPTER 5: MODELLING FLOODPLAIN VEGETATION RESPONSE TO GROUNDWATER VARIABILITY

## 5.1. Introduction

Chapter 4 analysed the floodplain vegetation responses to surface water availability at the catchment level using remotely sensed vegetation data and machine learning algorithms. Correlation analysis in Chapter 4 also unveiled the connection between the response of vegetation and surface water. As stated in Chapter 2, utilising satellite imagery data in catchment hydrological modelling would enhance the model's ability to replicate catchment hydrology with greater precision on broader geographical scales. The recent development in satellite technology provides an opportunity to access a vast amount of new-generation imagery data in the present and coming years. While literature is growing on the use of remotely sensed imagery data, remote sensing applications for vegetation response modelling with catchment hydrology in a floodplain in temperate zones are still not reported in the literature.

The correlation between the vegetation response and the water present beneath the soil surface is analysed in this research using Terra's Moderate Resolution Imaging Spectroradiometer (MODIS), Normalised Difference Vegetation Index (NDVI) and soil water content (SWC) data. The Soil & Water Assessment Tool (SWAT) interface known as ArcSWAT was used in ArcGIS for the groundwater analysis. The specific objectives of this study are the following: a) to understand the relationship between different types of vegetation responses (NDVI) and groundwater variables as simulated by SWAT model at the basin level; b) to assess the correlation between the vegetation response (as measured by NDVI) and SWAT simulated variables at different positions (top and bottom) within the sub-basin; and c) to model seasonal vegetation responses to groundwater variables at the basin level using the WEKA machine learning tool. The Digital Elevation Model derived from the SRTM imagery and vegetation indices (e.g., NDVI) derived from MODIS Terra and Aqua sensors were developed and evaluated. This study attempted to contribute to developing sustainable water resource management for the dry and wet seasons in an efficient way. The modelling results may be used to improve domestic agricultural production by selecting appropriate crops and plants that can grow commercially in similar regions.

This Chapter is structured into six sections. Section 1 outlines the objectives of the Chapter, while Section 2 examines the background literature and previous research on utilising

satellite data to study vegetation groundwater relationships in floodplain areas. Section 3 outlines the Methods employed to accomplish the objectives of the Chapter. Section 4 showcases the outcomes of the correlation and regression analyses conducted on SWAT-simulated groundwater variables and MODIS NDVI data. Additionally, it models the associations between simulated and predicted NDVI, which were generated using the machine learning algorithms employed in this study. Section 5 examines and analyses the findings in light of the identified objectives and research gaps outlined in Section 2. The Chapter culminates in Section 6 by presenting the implications of the results and providing recommendations for future studies.

This study presents the utilisation of MODIS imagery data in the modelling of the relationship between vegetation and groundwater in a floodplain, employing machine learning algorithms.

## **5.2. Floodplain vegetation responses to groundwater variability**

Floodplain vegetation plays an important role in catchment hydrology and energy flow. Floodplain vegetation distribution is directly influenced by several factors, including rainfall, temperature, and groundwater (Ponting et al., 2021). Rainfall, temperature, and groundwater are highly variable in arid and semi-arid regions (Mohammed et al., 2020). The annual rainfall in arid regions is much less than the annual potential evapotranspiration and surface water flows (i.e., surface runoff), which provides a limited water supply for vegetation systems (Condon et al., 2020). Therefore, groundwater becomes the only water source in arid regions, affecting the spatial and temporal distribution of soil water content (SWC), which, in turn, affects the growth of vegetation (Huang et al., 2019). An accurate understanding of the distribution of SWC in arid regions is important since water deficit is gradually becoming one of the major factors limiting agricultural productivity and ecological development (Cheng et al., 2020). As one of the driest continents in the world, Australia has been facing severe droughts over the last 50 years, noticeably in the south-eastern part of the country (Ma et al., 2015). This area will become drier in the coming decades due to increasing annual average temperatures and decreasing rainfall (Dai, 2011). Therefore, understanding the vegetation response to SWC is critical for sustainable ecosystem improvements in arid regions (Wang et al., 2011).

SWC can be estimated using both direct and indirect methods. The direct method, such as the oven drying technique, is widely used because of its reliability and simplicity (Schmugge et al., 1980); however, the direct method is labour-intensive, time-consuming, and costly for continuous application in large catchments. On the other hand, hydrological simulation and remote sensing techniques can be used for the same purpose at a catchment or global scale (Uniyal et al., 2017). SWC can also be estimated for previous years using remote sensing techniques, which is not possible to obtain from experimental measurements (Uniyal et al., 2017). Therefore, model-simulated results can fulfil temporal and spatial data requirements and improve SWC and vegetation response relationship studies.

The SWC also influences vegetation productivity and water stress (Porporato et al., 2004; Tian et al., 2019). The amount of soil water availability in drought regions for vegetation intake affects the length of the growing period (Leenaars et al., 2018). However, groundwater is the main source of water for vegetation growth in arid regions (Zhu et al., 2004). Any changes in the groundwater tables decrease the accessibility of the dependent vegetation and may create water stress (Naumburg et al., 2005). Moreover, water stress can trigger a longer growing period and photosynthesis reduction, thereby resulting in reduced productivity and increased vegetation mortality (Tian et al., 2019). The reduction in accessible soil water availability under a changing climate may exaggerate ecological droughts during the plantation season (Schlaepfer et al., 2017). Researchers have identified that the change in groundwater depth affects the vegetation physiology and dynamics (Tomlinson & Boulton, 2010; Zhu et al., 2016). Another study also focused on individual vegetation responses by examining the leaf, tree, canopy, and population (Eamus et al., 2015). However, according to current knowledge, accessible water in soil and vegetation response modelling is still lacking. This research focuses on SWC that is accessible to floodplain vegetation and understanding their relationship in a seasonal context.

The Soil and Water Assessment Tool (SWAT) is a physically based and semi-distributed hydrological model widely used for quantitative hydrological modelling (Arnold et al., 2012; Adhikari et al., 2020). Many researchers have used SWAT for evaluating soil water at the catchment scale (Pisinaras et al., 2010; Francesconi et al., 2016; Cuceloglu et al., 2017). Previous studies have shown that changes in the water balance components, specifically soil water storage, evapotranspiration, land use/land cover dynamics, and water yield, are more sensitive under wet climate and heterogeneous soils (Silva Jr et al., 2021; Yonaba et al., 2021). The SWAT model has also been successfully applied in the U.S. to estimate SWC for drought monitoring and predicting crop production (Narasimhan & Srinivasan, 2005). However, the

SWAT application in the Australian region is limited (Saha & Zeleke, 2014). In this study, a SWAT model was used to estimate SWC for the Burrinjuck sub-catchment within the Murrumbidgee River catchment. The suitability of the model simulation for long-term SWC datasets was assessed using a combination of physically measured and remotely sensed data. This type of simulation helps to correlate with long-term historical vegetation data.

The Normalised Difference Vegetation Index (NDVI), which can be derived from remote sensing, is frequently applied for studies on vegetation dynamics over large scales (Park et al., 2014; Fu & Burgher, 2015; Nouri et al., 2017; Mallick et al., 2021). Researchers used NDVI to understand the relationships between terrestrial vegetation and climate (Nouri et al., 2017). Several studies found a linear relationship between NDVI and climate variables in arid regions (Groeneveld et al., 2007; Wen et al., 2013; Nanzad et al., 2019). Relationships also were investigated for NDVI and groundwater levels and groundwater flow discharge (Aguilar et al., 2012; Seeyan et al., 2014; Bhanja et al., 2019). However, none of these previous studies analysed the relationship between NDVI and hydrological model simulated SWC in an arid region.

This study aims to analyse and model the relationships between seasonal SWC variability and floodplain vegetation responses using MODIS-derived NDVI data and machine learning algorithms for 20 years (2001–2020). In this study WEKA machine learning tool was applied in selection of various machine learning algorithms, developed by the University of Waikato, New Zealand (Hall et al., 2009; Eibe et al., 2016). The WEKA tool is a collection of machine learning algorithms for data mining activities that supports data pre-processing, clustering, classification, regression, and visualisation (Marin et al., 2021). This software can be run under the General Public License (GNU) with a selected classifier compared to other data mining tools (Sharma et al., 2015).

The results of this study provide qualitative information on catchment hydrology and water resources on temporal and spatial dimensions at the sub-catchment level. A calibrated model at this scale can be used for various analyses such as sedimentation, water pollution, and future stream flow prediction. This study also contributes to developing sustainable water resource management for the dry and wet season in an efficient way. The modelling results may be used to improve domestic agricultural production by selecting appropriate crops and plants that can grow commercially in similar regions. An understanding of seasonal vegetation water requirements from this study can be implemented to review the floodplain water management policies for better water management.

## **5.3. Methods**

### **5.3.1. Study area**

The study area resides within the Upper Murrumbidgee catchment (Figure 5.1) in the south-east of the Murray Darling Basin (MDB), in south-eastern Australia. The Burrinjuck sub-catchment area size is 12,950 km<sup>2</sup> (approx.) which is one-seventh that of the Murrumbidgee River catchment (Brown et al., 2007). The latitude and longitude of the study area are 34.53° S–35.14° S and 148.31° E–148.55° E. The Burrinjuck sub-catchment is situated within the upper catchment of the Murrumbidgee River basin, which was built (1910–1927) to develop an irrigation project after the devastating drought in 1902. The Murrumbidgee River rises at an altitude of around 1500 m in Kosciuszko National Park and flows approximately 316 km before entering Burrinjuck Reservoir at an altitude of 370 m (approx.). The topography of the Burrinjuck sub-catchment area is described in Chapter 3. The upper mountainous section of the Murrumbidgee River flow is regulated by dams for hydroelectric power generation and water supply (Wallbrink et al., 1996).

The main land use in this part is forest and pasture. However, this area also contributes to agricultural production by growing wheat and cereals (Verstraeten et al., 2007). Having a diverse climate in the upper and lower Murrumbidgee, the mean annual rainfall varies 350 mm in the Riverina plains and 1700 mm in the Snowy Mountains (Green et al., 2011). The Burrinjuck sub-catchment and surrounding area contribute to the maximum river flow by adding 24% of the total rainfall as runoff (Cracknell & Reading, 2014). The climate has enriched the Burrinjuck reserve possesses a high diversity of vegetation types and ecosystems. The detail climatic characteristics of the study area is described in the Chapter 3.

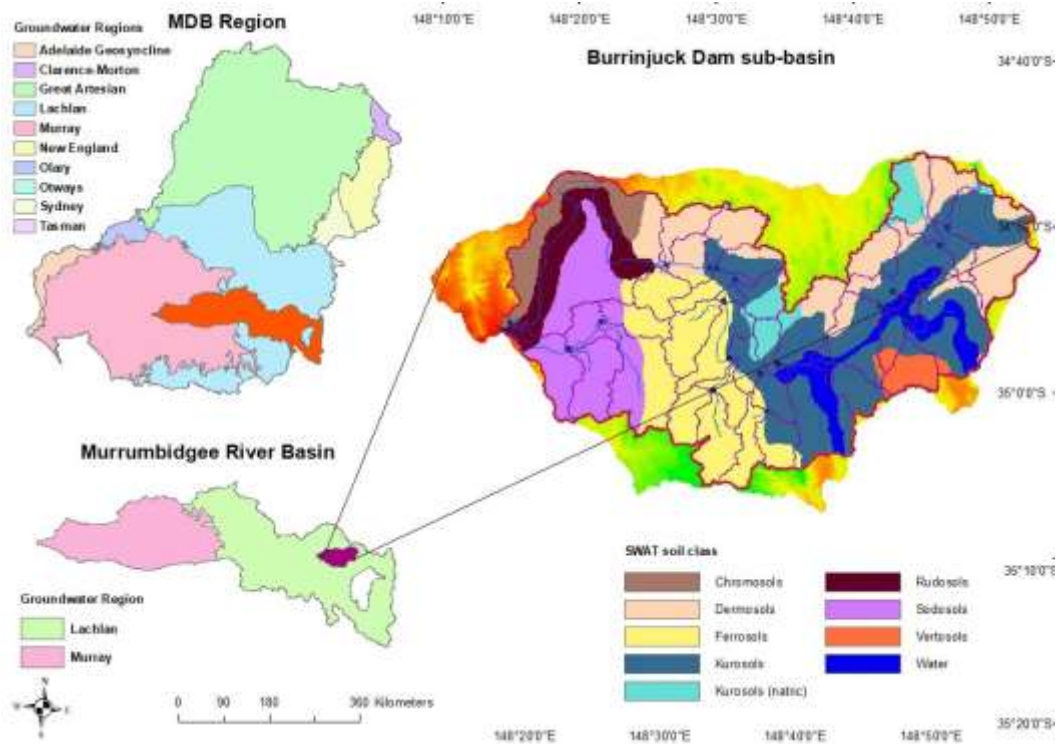


Figure 5.1: Study area of the Burrinjuck sub-catchment situated in the Murrumbidgee River catchment within the Murray-Darling Basin region.

### 5.3.2. Overview of the methods

The overall data processing described in the Chapter 3. Figure 5.2 presents an overview of the research methods applied in this study. The SWC and groundwater flow (GW) were simulated in ArcSWAT. The datasets used in this study were obtained from various local and international data portals, such as the Australian Bureau of Meteorology (BOM) and U.S. Geological Survey (USGS). This study used the ArcGIS tool (ESRI, 2019) and Microsoft Excel (Microsoft Corporation, 2018) for spatial and attribute data pre-processing and formatted the data to apply in the ArcSWAT hydrological model. A detail of data processing tools described in Chapter 3. Further, this study analysed the model output data using the WEKA machine learning tool with different vegetation responses as measured by MODIS NDVI values (Smith & Frank, 2016). Different machine learning algorithms have been applied to model the relationships between vegetation types, and their location within the sub-basin and seasonal groundwater variability.

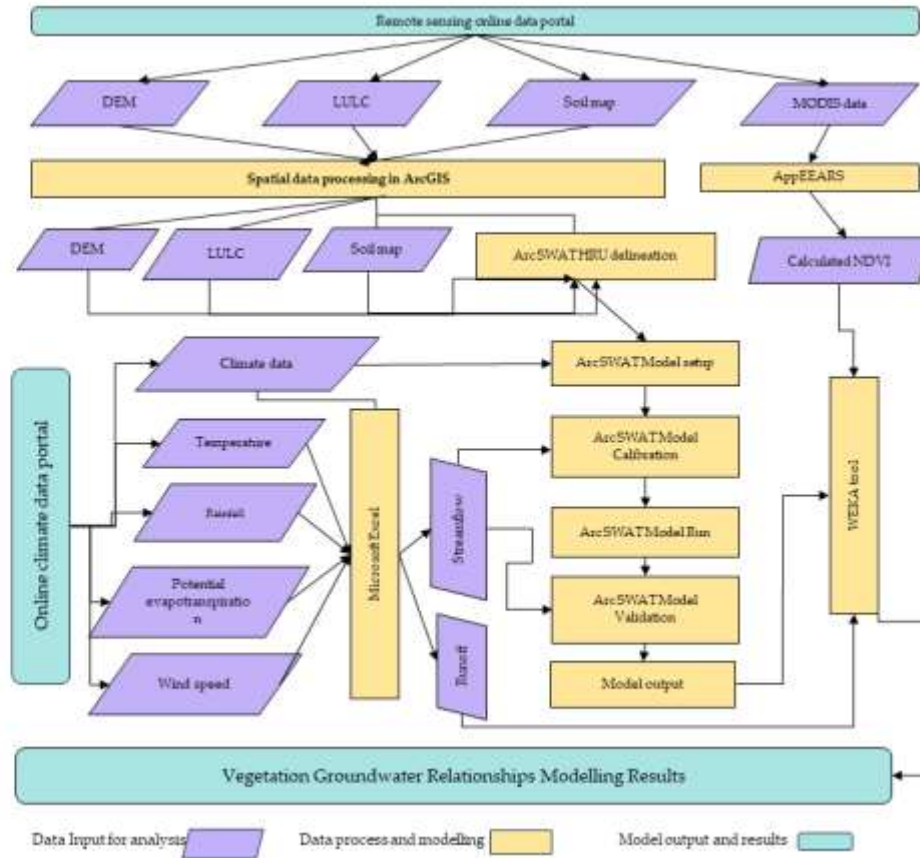


Figure 5.2: An overview of the research methodology for vegetation responses and groundwater variables modelling using machine learning algorithms.

### 5.3.3. Hydrological model setup

An ArcSWAT interface of the SWAT2012 model was used in this study (Arnold et al., 2012). The SWAT2012 compatible ArcGIS version 10.6 was installed on a desktop to run SWAT model from the user interface. The SWAT model is a continuous physically based distributed parameter model that operates on a daily time-step. This model is capable of simulating catchment hydrology, land use impact on water, sediments, plant growing, agricultural-chemical yields, etc., within agricultural watersheds (Neitsch et al., 2011; Arnold et al., 2012). SWAT divides the watershed into multiple sub-basins based on spatial characteristics. These sub-basins are further subdivided into hydrological response units (HRUs) that consist of unique land use, soils, and slope characteristics (Gassman et al., 2014). Each HRU is simulated for SWC, groundwater flow, nutrient cycles, sedimentation, crop growth, and management practices (Saha et al., 2013). The simulated results from the HRUs represent the sub-basin scale. SWAT (Neitsch et al., 2011) simulates the hydrological cycle based on the following daily water balance equation:

$$SW_t = SW_0 \sum_{i=0}^t (R_{day} - Q_{surf} - E_a - W_{seep} - Q_{gw})_i \quad (1)$$

Where  $SW_t$  is the ultimate water content in (mm),  $SW_0$  is the amount of water content on the first soil of the day  $i$  (mm),  $t$  is time (days),  $R_{day}$  is the amount of rainfall on day  $i$  (mm),  $Q_{surf}$  is the amount of surface runoff on specific day  $i$  (mm),  $E_a$  is the amount of evapotranspiration on day  $i$  (mm),  $W_{seep}$  is the amount of water percolated into the vadose zone from the soil profile on day  $i$  (mm), and  $Q_{gw}$  is the amount of return flow on day  $i$  (mm).

The SWAT model was delineated from a 30m resolution digital elevation model (DEM) (Figure 5.3 (c)). A threshold drainage area of 1342 km<sup>2</sup> was selected based on the DEM and Murrumbidgee River network to divide the watershed into 43 sub-basins, which were later categorised into 350 HRUs depending on land cover and land use, soil types, and slope. The model was run for 20 years of data, starting from 2001 and ending in 2020. The SWC data for Australia was obtained from the Australian Water Resource Assessment Landscape water balance model (AWRA-L), which was calibrated against the streamflow data. It is not best practice to use data from a different model simulation to run a hydrological model as it may not provide good modelling results. To avoid this confusion, the model was calibrated and validated against observed streamflow data instead of SWC.

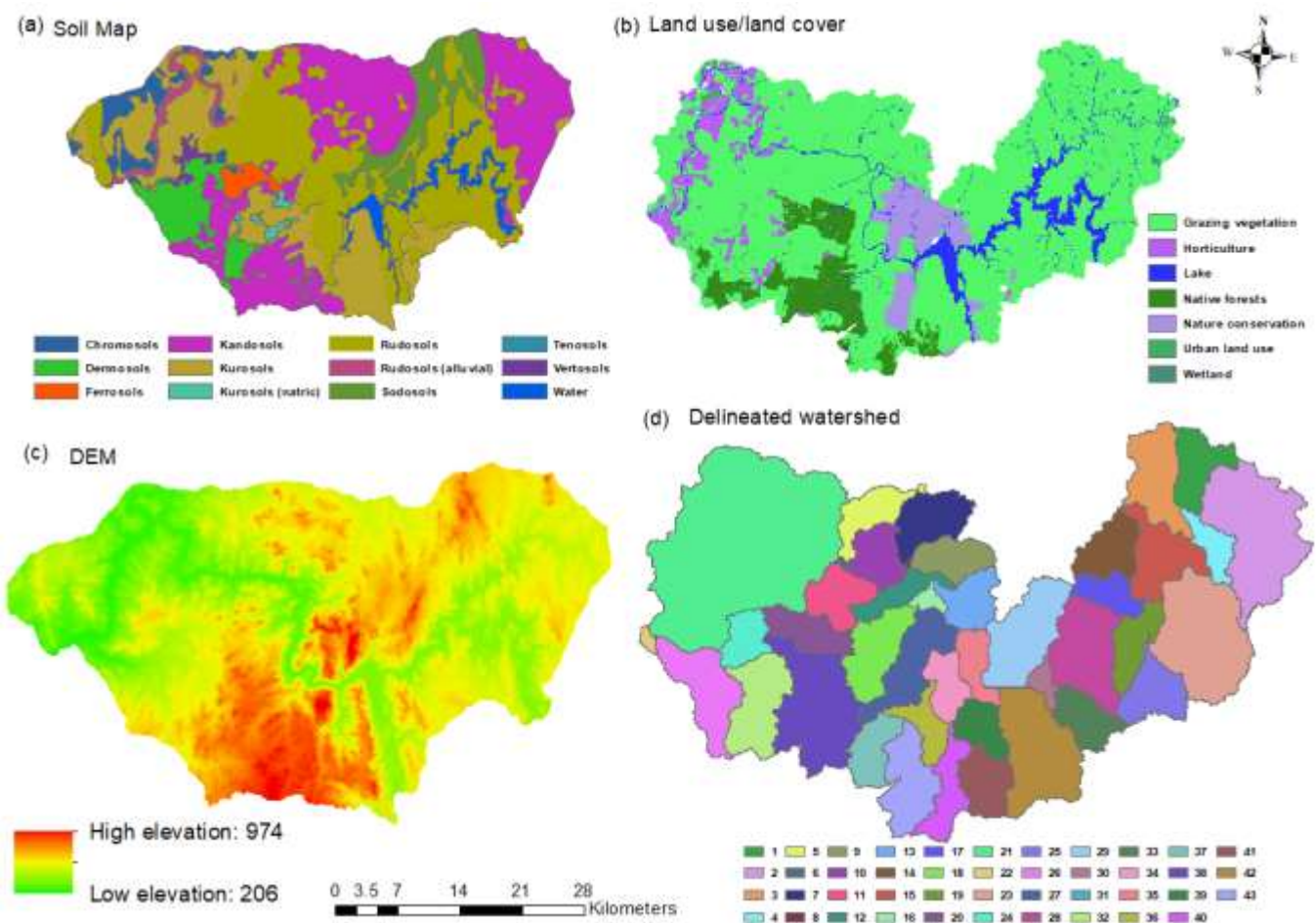


Figure 5.3: GIS data for the watershed. In the above figure, four images are captured: (a) Study area soil map, (b) Land use/land cover map, (c) DEM, and (d) Delineated watershed.

### 5.3.4. Data preparation

A combination of climatological and land properties data was required to develop a semi-distributed model using the ArcSWAT interface (Chapter 3). Some data such as DEM, soil, land use, and weather data are mandatory to run the dynamics of the watershed; however, streamflow, reservoir information, sediment, water quality, chemical, and pesticide data are non-mandatory. The data used in this study and their sources are listed in Table 5.1.

Table 5.1: The datasets used in this study including their descriptions and sources.

Data	Frequency	Description	Source
Precipitation	Daily	Station gauged, temporal	Bureau of Meteorology
Temperature	Daily	Station gauged, temporal	Bureau of Meteorology
Relative Humidity	Daily	Station gauged, temporal	Bureau of Meteorology
Wind speed	Daily at 9 am	Station gauged, temporal	Bureau of Meteorology
Solar radiation	Daily average	Spatial	Bureau of Meteorology
Streamflow (discharge)	Daily	Station gauged, temporal	NSW Office of Water

MODIS NDVI	16-Day	250 m spatial resolution	U.S. Geological Survey
DEM	-	30 m spatial resolution	U.S. Geological Survey
Soil Map	-	250 m spatial resolution	Digital Atlas of Australian Soil
Land cover/land use map	-	50 m spatial resolution	NSW Office of Environment and Heritage

### **5.3.5. Study period**

The study period (2001–2020) was selected to include a long-term drought (2001–2006) and flooding (2007–2010) phases. Both dry and wet phases were included in the study to ensure any long-term change in the vegetation condition was identified in the NDVI data. The annual data were divided into two seasons: (i) dry and (ii) wet, which were categorised based on rainfall and temperature anomalies. The average dry season (Oct–Mar) and wet season (Apr–Sep) rainfall are 52.4 mm, 66.45 mm and 70.74 mm, 73.91 mm in the drought and flooding periods, respectively.

#### **DEM**

The sub-basin parameters (gradient and length of the slope) and stream network characteristics (slope, width, and length of the channel) were obtained from the DEM file. For this study, a 30 m resolution DEM downloaded from the Shuttle Radar Topography Mission (SRTM) using the USGS data portal (USGS, 2021). DEM for the Burrinjuck sub-catchment study area was masked for the SWAT application (Figure 5.3(c)).

#### **Land Use/Land Cover Data**

The land use data for the study area used in the ArcSWAT HRU delineation was developed by the NSW Office of Environment and Heritage. These satellite imagery data were derived for the period of 2001 to 2005 and verified with Google Earth and a field survey of specific land cover types. The raster files were processed in ArcGIS to reclassify for the SWAT model (Figure 5.3(b)).

#### **Soil Data**

The SWAT model requires soil information of the basin area including a database table of soil texture, pH number, available water content, hydraulic conductivity, bulk density, and organic carbon content for each soil type (Setegn et al., 2009; Saha et al., 2013). The soil map of the study area was downloaded from the Digital Atlas of Australian Soil (ASRIS, 2014) (Figure 5.3(a)). A ‘usersoil’ database table was prepared for this study from the available soil

information and lookup tables, and then replaced the default ‘usersoil’ table in the SWAT database.

### ***Climate Data***

The climate data used in this study included daily rainfall, temperature (maximum and minimum), wind speed, solar radiation, and relative humidity. They were obtained from the Australian Bureau of Meteorology (BOM, 2021a). The climate data was obtained for a period of 21 years (from 2000 to 2020) in daily time series format. These data were processed using the Microsoft Excel tool to fill 0.2 of the missing data by the linear interpolation method (Fassò et al., 2020).

### ***5.3.6. Sensitivity analysis and hydrological model calibration***

This study applied sensitivity analysis following the guidelines explained in the previous studies (Andrade et al., 2019), using the SWAT Calibration and Uncertainty Programs (SWAT-CUP). The SWAT-CUP has five algorithm options for model calibration (SUFI-2, PSO, GLUE, ParaSol, and MCMC), eleven functions (mult, sum,  $R^2$ , chi2, NS, br2, ssqr, PBIAS, KGE, RSR, MNS) and integrated features such as plot visualisation (Abbaspour et al., 2018). The sensitivity analysis was done using SUFI-2, considering One-At-A-Time method of 15 parameters related to the processes of streamflow, recharge, evapotranspiration, percolation, infiltration from the list to identify the most sensitive ones for the model simulations at the Burrinjuck sub-catchment. According to previous studies (Abbaspour et al., 2015), the Curve Number for moisture condition II (CN2) and the coefficient of water percolation to the deep aquifer (RCHRG\_DP) were identified as the two most important sensitive parameters. Based on literature review, among the two sensitive parameters, CN2 was chosen for the model calibration of this study. However, some other parameters such as Surface runoff lag coefficient (SURLAG), and Manning’s roughness coefficient (CH\_N2) were also analysed, which found not as sensitive in the previous modelling done by Saha and Zeleke (Saha et al., 2013). The fact is that the previous study was done in the Yass River gauging station, which was upstream of the Burrinjuck sub-basin, while the present study focuses on the whole basin. Acquiring knowledge from several previous studies that applied SWAT model close to the study area helps parameter selection for sensitivity analysis. Thirteen parameters were chosen to do sensitivity analysis (Table 5.2) based on previous SWAT model application

in the Kyeamba Creek basin (Saha & Zeleke, 2014) and Yass River basin (Saha et al., 2013). The difference in basin scale could interfere in the sensitivity analysis. Therefore, the parameters used for calibration in this study are not necessarily the same proposed by Saha (Saha et al., 2013).

In this study, the Sequential Uncertainty Fitting algorithm (SUFI-2) and selected the Nash–Sutcliffe model efficiency (NSE) coefficient was used as target function for calibration procedures. In calibration process, SUFI-2 captures the uncertainties of the model run. The six parameters applied in the calibration process were selected from sensitivity analysis table based on their ranking (Table 5.2). A researcher (Abbaspour et al., 2015) found that the calibration process and uncertainties are closely related, and identifying these relationships are important. In the SUFI-2 interface, the input parameter uncertainty is expressed as ranges, whereas output parameter's uncertainties are expressed from the 95 PPU (95% probability distribution), which is calculated using the Latin American Hypercube Sampling from the cumulative distribution of an output variable at 2.5% and 97.5%. The adjustment between the simulation results and the observed data can be done by *p-factor* (the fraction of measured data bracketed by the 95PPU band) and the *R-factor* (ratio of the average width of the 95PPU band and the standard deviation of the measured variable) known as statistical indices (Abbaspour et al., 2015). The *p-factor* value  $> 0.7$  and *R-factor* value  $< 1.5$  are desirable for streamflow discharge depending on the situation (Abbaspour et al., 2004).

The SWAT model was calibrated (2004-2007) and validated (2008-2010) with a warm-up period of three year (2000-2002). The calibration and validation processes have been done in monthly timestep at two different points within the watershed, starting from the upstream of the streamflow station (Yass station) and then to the downstream station (Burrinjuck Dam station).

Table 5.2: The table shows the number of parameters applied, their definitions, and ranking in the SWAT-CUP simulation.

Parameter Definition	Value Range	Unit	Method	Par.inputfile	Ranking
Initial SCS runoff curve number for moisture condition	35–89	%	r	CN2	1
Effective hydraulic conductivity in the main channel alluvium	0–500	mm/h	v	CH_K2.rte	13
Manning’s <i>n</i> value for the main channel	0–0.3	—	v	CH_N2.rte	12
Base flow alpha factor	0–1	days	v	ALPHA_BF.gw	5
Groundwater delay	30–500	days	v	GW_DELAY.gw	10
Groundwater “revap” coefficient	0.02–0.2	—	v	GW_REVAP.gw	11
Threshold depth of water in the shallow aquifer for return flow to occur	0–5000	mm H <sub>2</sub> O	v	GWQMN.gw	3
Threshold depth of water in the shallow aquifer required for “revap” to occur	0–1	mm H <sub>2</sub> O	v	REVAPMN.gw	8
Soil evaporation compensation factor	0–0.65	-	v	ESCO.bsn	2
Average slope length	10–150	m	r	SLSUBBSN.hru	9
Surface runoff lag coefficient	0.05–24	—	v	SURLAG.bsn	15
Available water capacity of the soil layer	–0.5–0.5	mm H <sub>2</sub> O/mm	r	SOL_AWC.sol	4
Depth from the soil surface to layer bottom	–0.5–0.5	mm	r	SOL_Z.sol	6
Peak rate adjustment factor for sediment routing	1–2	-	r	ADJ_PKR.bsn	14
Maximum canopy storage	0–100	mm H <sub>2</sub> O	v	CANMX.hru	7

\*Method r=Relative and v=Replace

\*\*Input file rte=Route, gw=Groundwater, hru=Hydrological Response Unit, bsn=Basin, sol=Soil

### 5.3.7. Hydrological model performance evaluation

In this study, the model calibration performance was assessed using the coefficient of determination ( $R^2$ ), Nash-Sutcliffe Efficiencies (NSE), and percent bias (PBIAS) quantitative statistics which were used in previous studies (Moriassi et al., 2007; Setegn et al., 2009; Zhang et al., 2009). Moreover, fifteen parameters were applied in SWAT-CUP simulation and ranking them following the model performance acceptance guidelines documented by Arnold (Moriassi et al., 2007) which is presented in Table 5.2.

The Nash–Sutcliffe simulation efficiency (NSE) coefficient is a dimensionless statistic, indicating the accuracy of simulated versus observed data against the 1:1 line (Nash & Sutcliffe, 1970). NSE is the most widely used statistical indicator for hydrological model performance, in which NSE value 1 represents observed and simulated values are the same, while negative NSE value means simulations are extremely poor. NSE is defined as:

$$NSE = 1 - \frac{\sum_{i=1}^n (Q_{obs,i} - Q_{sim,i})^2}{\sum_{i=1}^n (Q_{obs,i} - \overline{Q_{obs}})^2} \quad (2)$$

where  $n$  is the number of time steps,  $Q_{obs, i}$  is the observed flow at time step  $i$  (daily here),  $\bar{Q}_{obs}$  is the mean of the observed flow, and  $Q_{sim, i}$  is the simulated flow. The range of  $NSE$  is  $[-\infty, 1]$ , where 1 represents a perfect match between the observed and simulated flow.

A hydrological model with higher  $R^2$  is considered as a good result (Wu et al., 2022).  $R^2$  is defined as:

$$R^2 = \left\{ \frac{\sum_{i=1}^n (Q_i^{obs} - \bar{Q}^{sim})(Q_i^{sim} - \bar{Q}^{sim})}{\sum_{i=1}^n (Q_i^{obs} - \bar{Q}^{obs})^2 \sum_{i=1}^n (Q_i^{sim} - \bar{Q}^{sim})^2} \right\}^2 \quad (3)$$

where,  $Q_i^{obs}$  and  $Q_i^{sim}$  are representing the measured and simulated data for  $i^{\text{th}}$  observation and  $\bar{Q}^{obs}$  and  $\bar{Q}^{sim}$  are the mean of the measured and simulated data, respectively.

The percent bias ( $PBIAS$ ) determines the average tendency to be greater or smaller simulated values than their observed data (Moriasi et al., 2007). The maximum  $PBIAS$  value is zero, indicating the simulation is exactly the same as the observed data. In general, a smaller  $PBIAS$  value signifies accurate model simulation.  $PBIAS$  is calculated as:

$$PBIAS = \frac{\sum_{i=1}^n (Q_i^{obs} - Q_i^{sim}) * 100}{\sum_{i=1}^n Q_i^{obs}} \quad (4)$$

Where  $Q_i^{obs}$  and  $Q_i^{sim}$  are representing the measured and simulated data for the  $i^{\text{th}}$  observation, respectively.

### 5.3.8. Remote sensing data

Moderate Resolution Imaging Spectroradiometer (MODIS) data are available from the U.S. Geological Survey website for free of cost (USGS, 2021). This study used the MODIS (Terra) 16-Day Global 250 m composite product of MOD13Q1 (version V006) to identify vegetation condition. The NDVI values were selected from the available vegetation indices in the MOD13Q1 products from imagery acquired during the period 2001 to 2020. Six plots of different vegetation types (such as grass, shrub, and tree) were selected (average size between 1 and 2 km<sup>2</sup>) within the Burrinjuck sub-catchment. These plots were selected randomly (i.e., stratified random sampling) based on specific vegetation types dominated in the selected plot area. Further point areas (500 m radius) were also selected at the bottom and top of each sub-basin (Figure 5.4). The total of sixty areas (point area) were calculated for 40 sub-basins (three sub-basins were too small to create point). These plots have been converted into polygons in

the Google Earth Pro and then saved as KML files which were later processed into shapefiles in ArcGIS (ESRI, 2019). A pre-processing tool named Application for Extracting and Exploring Analysis Ready Samples (AppEEARS) was selected to obtain pre-processed NDVI time-series data for those shapefiles prepared earlier.

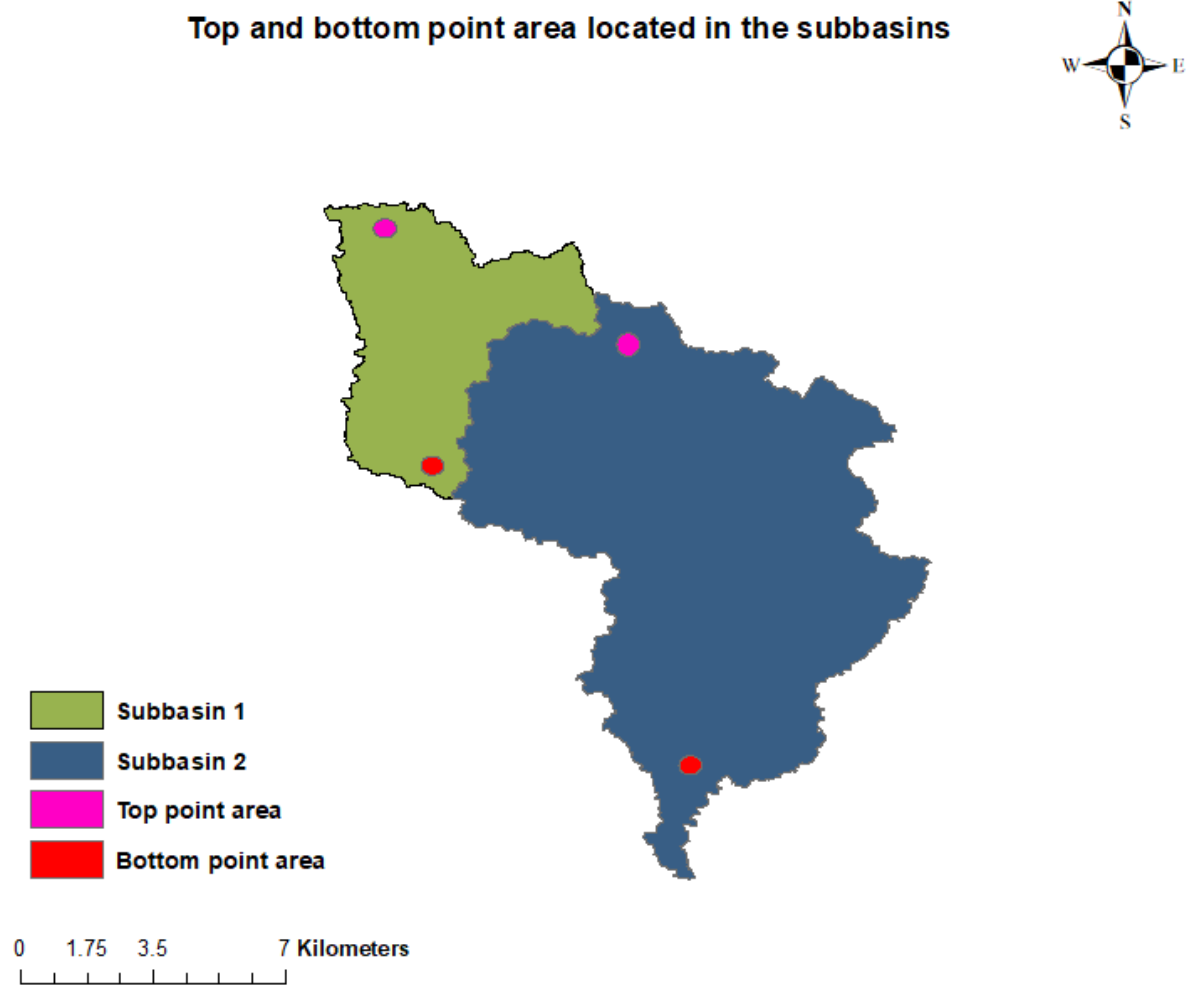


Figure 5.4: The point area with a radius of 500m selected both from the top and bottom locations within sub-basins. The pink circles and red circles representing point area of the top location and bottom locations, respectively.

### **5.3.9. Normalised Difference Vegetation Index (NDVI)**

The NDVI data were processed using the AppEEARS tool (EarthData, 2021). MODIS sensor captures a range of broad spectrum of reflected sunlight from tree leaves. The healthy vegetation mostly absorbs light from the red spectrum and reflects light from the near-infrared

(NIR) spectrum. NDVI utilises the contrast of strong reflectance in the near-infrared region and the strongly absorbed reflectance in the red wavelength region. NDVI calculation was performed applying the difference between the red and near-infrared bands and normalising it over the sum of red and near-infrared bands (Equation 5).

$$\text{NDVI} = \frac{(\text{Near Infrared} - \text{Visible red light})}{(\text{Near Infrared} + \text{Visible red light})} \quad (5)$$

Three types of vegetation indices were obtained using the Google Earth map and U.S. Geological Survey website. Firstly, the plots were selected for forest type vegetation within the watershed in Google Earth Pro and saved into KML files. These KML files were then processed in ArcGIS to convert into shapefiles and later used to obtain 20 years (2001–2020) of NDVI data from USGS. These similar steps were followed to obtain NDVI data for shrub and grass type vegetation within the watershed. The NDVI was calculated for each of the 43 sub-basins for the same period (2001–2020).

### **5.3.10. Machine learning algorithms for data analysis**

A machine learning (ML) algorithm is a set of computational codes that can process a large amount of data in a complex way (Sarkar, 2021). It is also known as data-driven methods that build models based on evidence obtained from a sample data set. The algorithms read and process data to learn the maximum possible patterns about the data (Cracknell & Reading, 2014). In this study, the Waikato Environment for Knowledge Analysis (WEKA) tool was applied, developed by the University of Waikato, New Zealand (Hall et al., 2009; Eibe et al., 2016). Firstly, the WEKA tool was set up to run a random forest model using 43 different datasets. These datasets included the combination of SWC and groundwater flow towards stream, and different types of vegetation responses (NDVI values). Each dataset was initially set for linear regression to find the collinear and non-collinear variables. Secondly, the machine learning tool was prepared to run a support vector machine (SVM) model using the same datasets.

The performance of all models was assessed in two ways: (a) using a 10-fold cross-validation, which is a leave-one-out approach, and (b) using the 80 and 20 per cent split-sample method. These two approaches were performed to compute the root mean square error (RMSE) and correlation coefficient ( $r$ ) between the SWAT output variables (SW and GW) and predicted vegetation response (NDVI value) of each model. The model selection was based on higher correlation coefficient ( $r$ ) values and smaller RMSEs to analyse the relationship against soil

water content (SWC) and groundwater flow (GW). This study also analysed these relationships based on rainfall intensity such as dry season (October to March) for less intensity and wet season (April to September) for high intensity.

## 5.4. Results

### 5.4.1. Hydrological model calibration and validation

In section 5.3.10 under sensitivity analysis, Table 5.2 shows the sensitivity ranking of the different model parameters and their ranges applied during the calibration. The model was calibrated and validated at two different stations (Figure 5.5), for which the results are listed in Table 5.3. The results explained that manual calibration performed better than auto-calibration. The NSE value 0.79 for the manual calibration, as a performance parameter can be marked as ‘very good’ for the SWAT model developed in the study area, which was able to simulate about 79% of the variance on observed streamflow data.

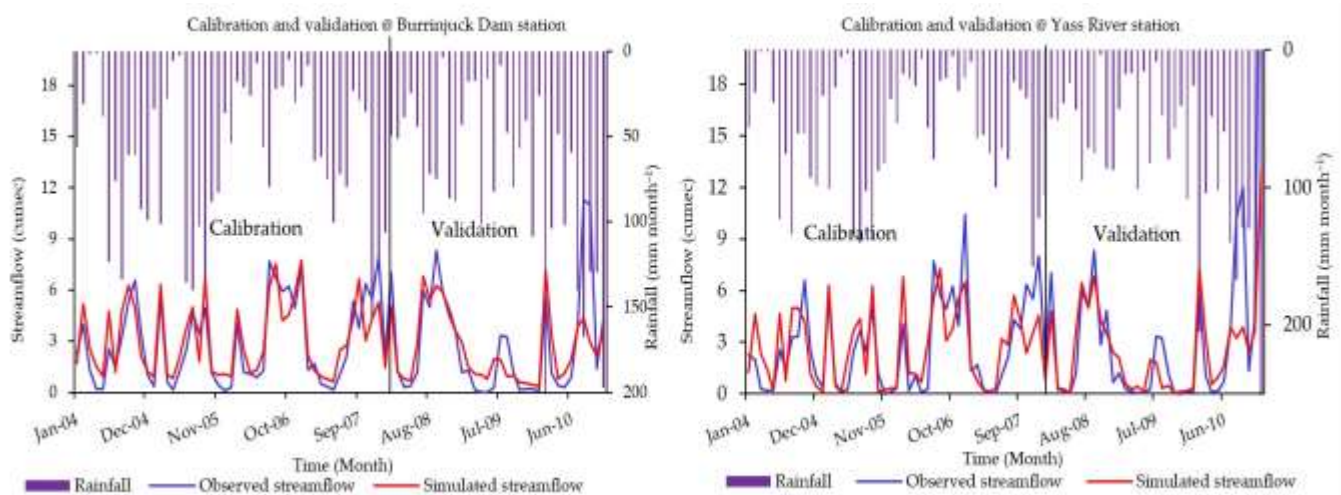


Figure 5.5: The model calibration and validation at two different locations based on the available station, (i) Burrinjuck Dam, and (ii) Yass River station

Table 5.3: The modelling scenarios and results.

Scenario	NSE	R <sup>2</sup>	PBIAS
Default	0.64	0.69	30.9
Manual calibration	0.79	0.82	26.3
SUFI-2	0.65	0.72	29.1

The statistical indicators reflected a regression between observed and simulated streamflow for those two stations with NSE 0.76, PBIAS 18.7,  $R^2$  0.76, p-factor 0.82 and NSE 0.67, PBIAS 31.5,  $R^2$  0.67, and p-factor 0.46, respectively. The hydrographs showed that the observed and simulated values have a noticeable difference in the plots. Additionally, the model slightly overestimated the low flow during the calibration and validation periods.

#### **5.4.2. Relationships of vegetation responses and groundwater**

The average monthly SWC and groundwater data were presented in Table 5.4. The average correlation coefficient of different vegetation types and SWAT model output variables over the study period is shown in Figure 5.6. The different correlation patterns of responses of vegetation types and SWC suggested that vegetations were considerably influenced by SWC. The linear regression results showed that shrub vegetation NDVI was highly correlated ( $R^2=0.82$ ) to SWC than forest and grass type vegetation NDVI ( $R^2=0.78$ , and  $R^2=0.72$ , respectively). However, grass type vegetation response was higher ( $R^2=0.59$ ) to groundwater (GW) compared to forest vegetation ( $R^2=0.24$ ) and shrub vegetation ( $R^2=0.25$ ).

Table 5.4: SWAT simulated variables. Soil water content (SWC) and groundwater flow (GW) data presented as average monthly for the study area.

<b>Variable</b>	<b>January</b>	<b>February</b>	<b>March</b>	<b>April</b>	<b>May</b>	<b>Jun</b>	<b>July</b>	<b>August</b>	<b>September</b>	<b>October</b>	<b>November</b>	<b>December</b>
SWC	86.28	98.54	93.18	96.25	112.64	130.79	131.11	129.71	122.23	106.23	100.48	78.14
GW	6.07	3.72	5.10	4.59	4.60	9.13	21.15	29.00	28.73	24.57	15.01	10.96

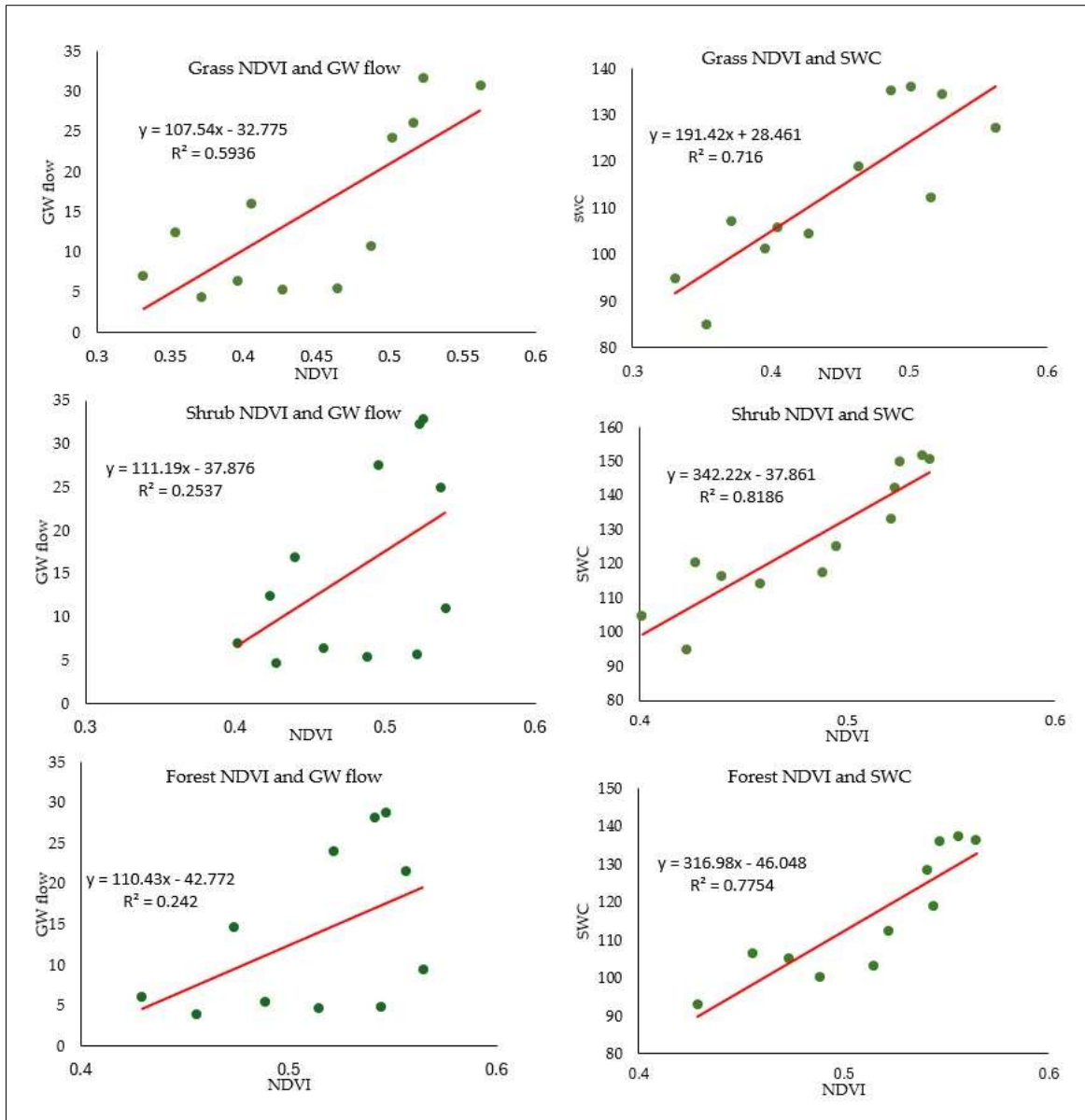


Figure 5.6: The forest, shrub, and grass type vegetation NDVI datasets are plotted against model-simulated surface runoff and groundwater flow (GW) to calculate the co-efficient of determination ( $R^2$ ).

The WEKA modelling results show that sub-basin NDVI (including all vegetation types within the sub-basin no 28) was highly responsive ( $r=0.78$ ) compared with forest NDVI ( $r=0.61$ ) when the ML algorithms were applied against SWC and GW (Table 5.5). Similarly, sub-basin NDVI (including all vegetation types within the sub-basin no 19 and 28) was highly responsive ( $r=0.76$  and  $r=0.74$  respectively) than shrub and grass type vegetation ( $r=0.67$  and  $r=0.56$  respectively) (Tables 5.6 and 5.7).

Table 5.5: The WEKA-generated modelling results for forest, sub-basin, top-point, and bottom-point NDVI against SWAT-simulated variables, SWC and GW. The r represents the correlation coefficient.

Sub-Basin		GW			SWC			SWC and GW		
# 28		r	RMSE	RRSE	r	RMSE	RRSE	r	RMSE	RRSE
FOREST	SVM	0.373	0.064	91%	0.592	0.055	79%	0.610	0.055	78%
	RF	0.219	0.076	110.42%	0.446	0.067	91%	0.540	0.060	85%
SB_NDVI	SVM	0.597	0.075	80%	0.710	0.066	70%	0.781	0.059	62%
	RF	0.484	0.088	94%	0.604	0.079	84%	0.736	0.064	68%
TP_NDVI	SVM	0.471	0.072	89%	0.624	0.063	78%	0.660	0.061	75%
	RF	0.407	0.080	98%	0.624	0.063	78%	0.631	0.064	79%
BP_NDVI	SVM	0.267	0.072	96%	0.513	0.064	85%	0.521	0.063	85%
	RF	0.132	0.085	113%	0.330	0.078	104%	0.434	0.070	93%

Table 5.6: The WEKA machine learning produced modelling results for shrub vegetation NDVI from sub-basin, top point, and bottom point against the SWAT simulated SWC and GW. The r represents the correlation coefficient in the below results.

Sub-Basin		GW			SWC			SWC and GW		
# 19		r	RMSE	RRSE	r	RMSE	RRSE	r	RMSE	RRSE
SHRUB	SVM	0.533	0.059	82%	0.681	0.051	70%	0.671	0.052	72%
	RF	0.596	0.056	77.96%	0.625	0.055	74%	0.626	0.054	74%
SB_NDVI	SVM	0.579	0.073	82%	0.689	0.064	72%	0.759	0.058	65%
	RF	0.462	0.084	94%	0.577	0.076	85%	0.685	0.066	74%
TP_NDVI	SVM	0.674	0.078	74%	0.697	0.075	71%	0.812	0.061	58%
	RF	0.609	0.087	82%	0.571	0.090	86%	0.772	0.067	64%
BP_NDVI	SVM	0.247	0.082	97%	0.456	0.075	89%	0.451	0.075	89%
	RF	0.041	0.098	117%	0.267	0.091	108%	0.363	0.082	97%

Table 5.7: The WEKA machine learning modelling results for grass type vegetation NDVI (sub-basin combined, vegetation located at the top point, and vegetation located at the bottom point) against SWAT variables. The correlation coefficient (r) for the random forest and support vector machine algorithms are listed in the below table.

Sub-basin		GW			SWC			SWC and GW		
# 23		r	RMSE	RRSE	r	RMSE	RRSE	r	RMSE	RRSE
GRASS	SVM	0.4642	0.1116	84.57%	0.5342	0.105	79.28%	0.5629	0.1024	76.98%
	RF	0.4876	0.1094	.83.15%	0.4607	0.112	82.75%	0.4955	0.1088	80.10%
SB_NDVI	SVM	0.6004	0.1071	80.63%	0.649	0.1007	75.75%	0.7431	0.0889	66.92%
	RF	0.5369	0.1171	88.10%	0.4353	0.1299	97.78%	0.6522	0.1025	77.11%
TP_NDVI	SVM	0.6528	0.1276	75.90%	0.6729	0.1238	73.62%	0.7883	0.1035	61.55%
	RF	0.581	0.1422	84.62%	0.4665	0.1605	95.47%	0.7031	0.121	71.97%
BP_NDVI	SVM	-0.0069	0.1265	101.07%	0.1134	0.1242	99.19%	0.2045	0.1223	97.67%
	RF	-0.0646	0.1519	121.35%	0.0884	0.1438	114.89%	0.1552	0.1312	104.79%

### 5.4.3. Vegetation responses considering their location within the watershed

The results shown in Figure 5.7 were calculated from the average data for 40 sub-basins. The monthly average correlation coefficient result shows that vegetation in the top-point location in a sub-basin is more sensitive ( $R^2=0.77$ ) to SWC when compared with vegetation in the bottom point location ( $R^2=0.72$ ). On the other hand, vegetation in the bottom point location is more correlated to groundwater ( $R^2=0.62$ ) than vegetation in the top point location ( $R^2=0.57$ ).

The average correlation coefficient of top-point (distant from outlet) and bottom-point (close to outlet) NDVI and SWC is shown in Figure 5.7. The modelling results show that vegetation in the top-point location of the sub-basin has moderate  $r$  values against GW and SWC (0.67 and 0.69 respectively) compared with vegetation in the bottom location (0.25, and 0.46 respectively). Moreover, the result shows strong correlations for the top point vegetation NDVI against these two variables ( $r=0.81$  and  $r=0.79$ , respectively) (Tables 5.6 and Table 5.7). The negative value of  $r$  ( $-0.0069$ ) shows that vegetation in the bottom location of sub-basin #23 has no response to the GW (Table 5.7).

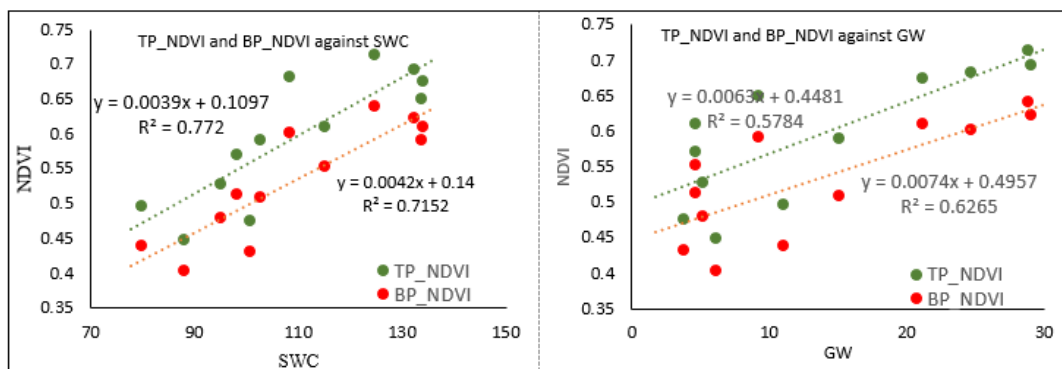


Figure 5.7: The NDVI collected from the top-point and bottom-point areas as vegetation responses are plotted against the Soil Water Content (SWC) and groundwater flow (GW) to calculate the coefficient of determination ( $R^2$ ).

### 5.4.4. Seasonal vegetation responses

The results of the linear regression analysis for different vegetation types for two distinct seasons are shown in Figure 5.8. The correlation results show that shrub and forest vegetations are highly correlated ( $R^2=0.89$  and  $R^2=0.82$ , respectively) to SWC during the wet season compared with grass type vegetation ( $R^2=0.47$ ). However, grass vegetation shows a better response during the dry season ( $R^2=0.52$ ) compared with the shrub and forest ( $R^2=0.45$  and  $R^2=0.43$ , respectively).

The vegetation responses were observed for different locations within the sub-basin (Figure 5.9). The regression analysis shows that vegetation in the top point and bottom point locations of the sub-basin are highly correlated to GW in the dry ( $R^2=0.79$  and  $R^2=0.84$ , respectively) and wet season ( $R^2=0.81$  and  $R^2=0.85$ , respectively). However, vegetation in these two locations is moderately correlated to SWC during the wet season ( $R^2=0.66$  and  $R^2=0.71$ , respectively) than the dry season ( $R^2=0.51$  and  $R^2=0.54$ , respectively).

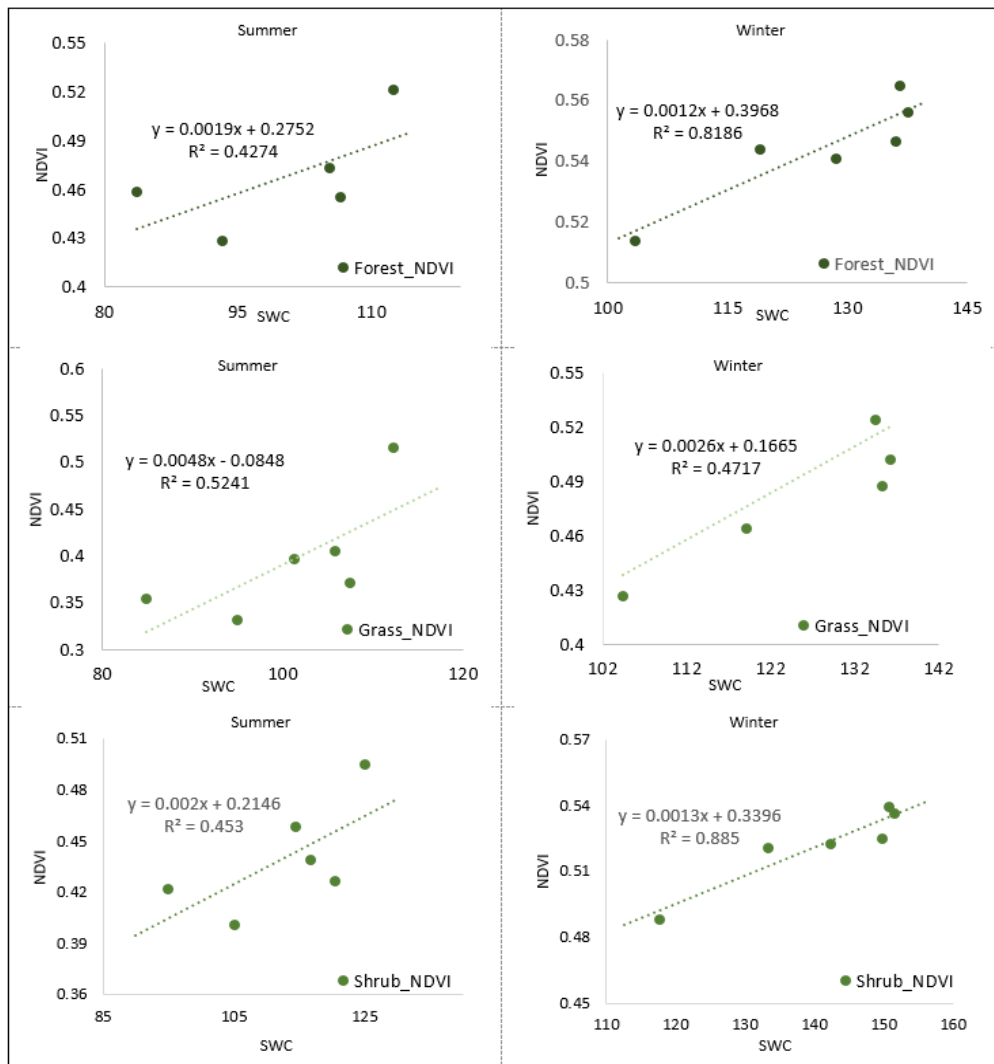


Figure 5.8: The vegetation responses (NDVI) against the SWC in dry and wet seasons in the study area are plotted to calculate the coefficient of determination ( $R^2$ ).

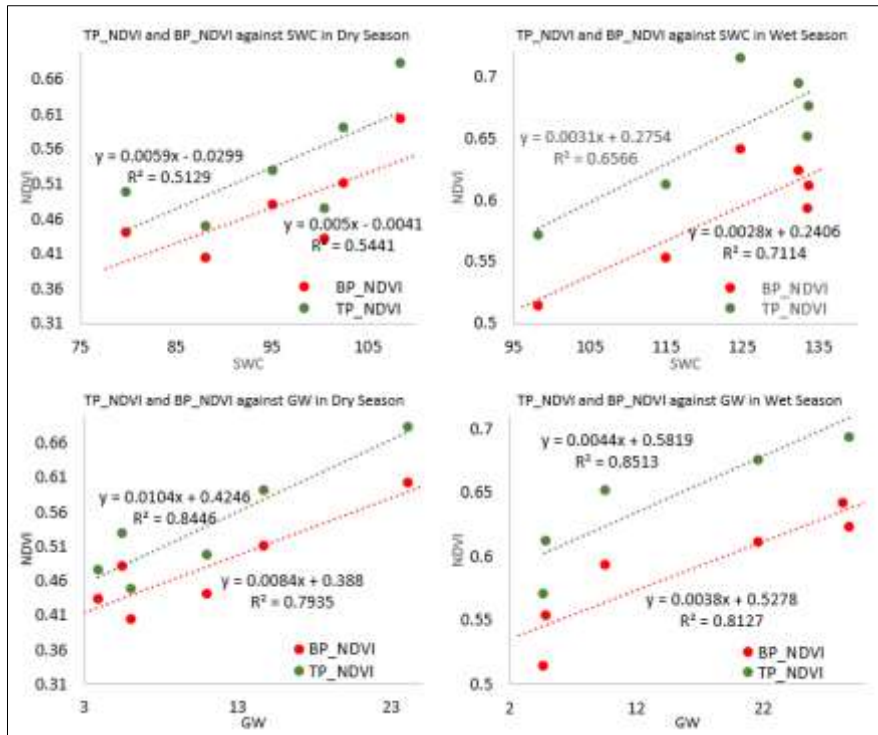


Figure 5.9: Seasonal vegetation responses (NDVI) from different locations (top point and bottom point) against soil water content (SWC) and groundwater flow are plotted to identify the coefficient of determination ( $R^2$ ).

The WEKA modelling results show that shrub vegetation is moderately responsive to GW and SWC ( $r=0.62$  and  $r=0.63$ , respectively) in the dry season. However, forest and grass type vegetation are less responsive to GW and SWC ( $r=0.52$ ,  $r=0.48$ ,  $r=0.27$ , and  $r=0.38$ , respectively) in the dry season (Table 5.8). All three types of vegetation were less responsive to GW and SWC in the wet season.

Table 5.8: The table shows the modelling results for different types of vegetation responses and vegetation located at different points in the sub-basin. This result shows the relationship during the dry season. The r value shows the correlation coefficient of the modelling results.

Sub-Basin		GW			SWC			SWC and GW		
# 28		r	RMSE	RRSE	r	RMSE	RRSE	r	RMSE	RRSE
FOREST	SVM	0.527	0.053	0.837	0.481	0.056	0.871	0.594	0.051	0.792
	RF	0.581	0.053	0.828	0.317	0.068	1.074	0.560	0.054	0.844
SB_NDVI	SVM	<b>0.730</b>	0.058	0.674	0.570	0.071	0.815	0.782	0.054	0.625
	RF	<b>0.702</b>	0.062	0.716	0.434	0.084	0.974	0.750	0.058	0.666
TP_NDVI	SVM	0.564	0.068	0.817	0.539	0.070	0.840	0.649	0.063	0.753
	RF	0.592	0.069	0.826	0.379	0.085	1.017	0.637	0.065	0.777
BP_NDVI	SVM	0.362	0.061	0.921	0.368	0.061	0.917	0.403	0.060	0.901
	RF	0.420	0.063	0.944	0.254	0.073	1.099	0.403	0.062	0.935
Sub-basin		GW			SWC			SWC and GW		
# 19		r	RMSE	RRSE	r	RMSE	RRSE	r	RMSE	RRSE
SHRUB	SVM	0.629	0.048	0.777	0.631	0.048	0.799	0.666	0.046	0.766
	RF	0.627	0.048	0.7660%	0.604	0.050	0.784	0.633	0.048	0.771
SB_NDVI	SVM	0.755	0.052	0.650	0.731	0.054	0.676	0.812	0.046	0.580
	RF	0.736	0.054	0.671	0.744	0.053	0.660	0.763	0.510	0.636
TP_NDVI	SVM	0.780	0.060	0.594	0.697	0.075	0.713	0.729	0.066	0.687
	RF	0.777	0.060	0.623	0.789	0.059	0.605	0.789	0.059	0.605
BP_NDVI	SVM	0.424	0.062	0.892	0.322	0.065	0.958	0.442	0.061	0.893
	RF	0.184	0.071	1.070	0.269	0.068	1.023	0.254	0.068	1.031
Sub-basin		GW			SWC			SWC and GW		
# 23		r	RMSE	RRSE	r	RMSE	RRSE	r	RMSE	RRSE
GRASS	SVM	0.271	0.094	0.967	0.382	0.090	0.920	0.412	0.088	0.902
	RF	0.301	0.100	1.023	0.212	0.108	1.115	0.473	0.087	0.897
SB_NDVI	SVM	0.696	0.088	0.728	0.571	0.098	0.811	0.756	0.078	0.648
	RF	0.572	0.101	0.837	0.442	0.116	0.956	0.730	0.083	0.682
TP_NDVI	SVM	0.708	0.109	0.709	0.575	0.124	0.808	0.763	0.100	0.649
	RF	0.553	0.133	0.860	0.503	0.140	0.907	0.737	0.103	0.671
BP_NDVI	SVM	-0.128	0.116	1.025	-0.206	0.116	1.026	0.008	0.123	1.092
	RF	-0.111	0.138	1.225	-0.139	0.138	1.227	-0.202	0.118	1.043

In contrast to the sub-basin level, the vegetation NDVI is highly responsive to GW and SWC ( $r=0.75$  and  $r=0.73$ , respectively) in the dry season. Furthermore, the sub-basin NDVI shows a strong relationship with SWC and GW ( $r=0.81$ ) (Table 5.8) in the dry season, and moderate relation ( $r=0.62$ ) in the wet season (Table 5.9). This result clearly indicates that the vegetation in the sub-basin is positively influenced by groundwater flow both in the dry and wet seasons.

Table 5.9: The table shows the modelling results during wet season for different types of vegetation responses and vegetation located at different points in the sub-basin. The r value shows the correlation coefficient of the modelling results.

Sub-basin # 28		GW			SWC			SWC and GW		
		r	RMSE	RRSE	r	RMSE	RRSE	r	RMSE	RRSE
FOREST	SVM	0.163	0.050	98%	0.372	0.047	93%	0.356	0.048	0.934
	RF	0.230	0.055	107%	0.182	0.058	114%	0.242	0.053	1.035
SB_NDVI	SVM	0.501	0.060	86%	0.623	0.054	78%	0.710	0.049	0.699
	RF	0.530	0.066	94%	0.458	0.067	96%	0.640	0.055	0.785
TP_NDVI	SVM	0.246	0.057	96%	0.371	0.054	92%	0.358	0.055	0.927
	RF	0.361	0.058	99%	0.060	0.071	121%	0.092	0.076	1.288
BP_NDVI	SVM	0.089	0.058	99%	0.245	0.057	97%	0.203	0.057	0.981
	RF	0.159	0.063	108%	0.028	0.071	121%	0.048	0.066	1.120
Sub-basin # 19		GW			SWC			SWC and GW		
		r	RMSE	RRSE	r	RMSE	RRSE	r	RMSE	RRSE
SHRUB	SVM	0.346	0.045	93%	0.431	0.044	90%	0.445	0.043	0.892
	RF	0.460	0.044	90.10%	0.501	0.042	87%	0.474	0.043	0.889
SB_NDVI	SVM	0.478	0.062	87%	0.630	0.055	77%	0.623	0.056	0.778
	RF	0.568	0.060	84%	0.637	0.055	77%	0.629	0.055	0.779
TP_NDVI	SVM	0.612	0.072	79%	0.612	0.072	79%	0.749	0.060	0.658
	RF	0.640	0.072	79%	0.578	0.078	85%	0.676	0.068	0.746
BP_NDVI	SVM	-0.037	0.076	101%	0.173	0.075	99%	0.114	0.076	1.013
	RF	-0.002	0.087	116%	0.118	0.086	114%	0.142	0.079	1.052
Sub-basin # 23		GW			SWC			SWC and GW		
		r	RMSE	RRSE	r	RMSE	RRSE	r	RMSE	RRSE
GRASS	SVM	0.228	0.120	97%	0.350	0.117	94%	0.339	0.117	0.946
	RF	0.159	0.138	111%	0.071	0.145	117%	0.063	0.138	1.117
SB_NDVI	SVM	0.470	0.102	88%	0.519	0.099	85%	0.601	0.092	0.795
	RF	0.460	0.109	94%	0.337	0.119	102%	0.510	0.103	0.885
TP_NDVI	SVM	0.621	0.109	78%	0.567	0.115	82%	0.709	0.098	0.701
	RF	0.608	0.116	83%	0.353	0.142	102%	0.627	0.111	0.795
BP_NDVI	SVM	0.197	0.115	98%	-0.281	0.117	100%	0.173	0.117	0.995
	RF	-0.062	0.144	123%	-0.174	0.148	126%	-0.043	0.134	1.143

The vegetation in the top-point location within the sub-basin is also highly responsive to GW and SWC ( $r=0.78$  and  $r=0.70$ , respectively) than vegetation in the bottom-point location ( $r=0.42$  and  $r=0.32$ , respectively) in the dry season. The vegetation in the top-point location has a higher r value ( $r=0.79$ ) when correlated against GW and SWC in the dry season. However, vegetation in the top-point location has moderate responses to GW and SWC ( $r=0.64$  and  $r=0.61$ , respectively), and highly responsive ( $r=0.75$ ) against these two variables together (Table 5.8).

## 5.5. Discussion

### 5.5.1. Relationships between vegetation responses and ArcSWAT model simulated variables

This study presents a robust analysis of the relationships between groundwater availability and vegetation responses vigour in the floodplain zone. The hydrological model simulated different groundwater variables by calculating a range of meteorological variables, which were later analysed in relation to NDVI using different machine learning algorithms. Among random forest (RF) and support vector machine learning (SVM) algorithms, the SVM represented higher  $r$  values ( $r=0.78$ ,  $r=0.75$ ,  $r=0.74$  etc.) compared with RF ( $r=0.73$ ,  $r=0.68$ , and  $r=0.65$  etc.) when analysed by different types of vegetation NDVI. Previous studies also mentioned outperformance of random forest in terms of vegetation and water relationship modelling (Erdal & Karakurt, 2013; Muñoz et al., 2018). Before the analysis, the SWAT model calibration was completed and produced the 0.51 NSE value. This might reflect high volume of groundwater loss and disconnection of deep aquifer in SWAT (Uniyal et al., 2017). The analysis result found that the simulated variables (SWC and GW) and vegetation NDVI relationships vary with vegetation types when considered data from the same sub-basin (watershed). The shrub-type vegetation is highly correlated to SWC over forest and grass vegetation; however, grass vegetation shows a high correlation to GW compared to forest and shrub vegetation (Jiao et al., 2020). The first objective of this study, to understand different types of vegetation responses to SWC and groundwater, is thus successful. Previous studies have found a strong correlation between different types of vegetation and SWAT-simulated SWC (Park et al., 2014). However, in their studies, different types of floodplain vegetation such as forest, shrub, or grass vegetation responses have not been included.

This study identified that the vegetated location within the sub-basin also impacts these relationships to SWC and GW. The vegetation located in the top point within the sub-basin, which are distant to the water outlet or stream, showed higher response to SWC ( $r = 0.69$ ,  $0.78$  etc.). The SWC volume rate is generally high near the water outlet, and that is why the vegetation located in the bottom point zone can easily access SWC for their growth. This saturated soil enables surface and sub-surface flows and activates connectivity between soils and streams (Von Freyberg et al., 2014; Van Meerveld et al., 2015). Moreover, vegetation located in the top point showed higher response to GW ( $R = 0.62$ ) than vegetation located in the bottom point. The modelling results also showed the correlation coefficient ( $r$ ) value has increased by 42% against GW for vegetation located at the top point compared to the bottom

point. The correlation coefficient ( $r$ ) was highly positive (0.81) for top-point vegetation when SWC and GW variables were considered together as relationship predictors. This means vegetation located in the top point can grow well when SWC and groundwater flow increases within the sub-basin.

### **5.5.2. Seasonal variability in each vegetation type**

In the seasonal domain, the vegetation responses become stronger in the wet season when rainfall increases in the study area. As rainfall is the main source of water in the area of interest, the average SWC and GW values increased by 22% and 32.68%, respectively, during the wet season. Considering the inter seasonal water variability, the vegetation responses to SWC and groundwater flow varied over different types of vegetation. Further analysis found the grass vegetation response decreased by 10.6% in the wet season compared to the dry season. This variation may also be related to inter-seasonal temperature differences, which negatively impacts vegetation growth in winter months (Lin et al., 2012; He et al., 2017). However, forest and shrub vegetation types are highly responsive to the sub-basin's SWC during the wet season. Therefore, forest and shrub responses were increased by 48.8% and 49.43%, respectively, in the wet season when compared to the dry season.

Similarly, vegetation responses and groundwater relationships against SWC and groundwater flow were analysed during the dry season using machine learning algorithms. The vegetation NDVI (including all vegetation in the sub-basin) against GW and SWC produced highly positive correlation coefficient values ( $r$ ) (0.76, and 0.73 respectively). However, when the model was run against GW and SWC together, the  $r$  value becomes higher (0.81). The overall RF model performance was 7.3% better against runoff over the SVM classifier. The result shows that the RF classifier performs better than the SVM algorithm in the predictions. This result supports the findings of other studies where RF is widely used for crop mapping, urban studies and particularly for land use/land cover applications (Sheykhmousa et al., 2020). In this study, the WEKA model produced different  $r$  values when considered a combined vegetation NDVI dataset at the sub-basin level. For example, the values of  $r$  between the sub-basin NDVI and GW, SWC were 0.75, 0.73, and 0.81, respectively. This means that vegetation in the sub-basin within a floodplain is highly responsive to groundwater flow and SWC during the dry season.

Not surprisingly, it was found that shrub and forest type vegetation are highly responsive to GW ( $r = 0.63$  and  $0.58$ , respectively) compared to grass ( $r = 0.30$ ). These results

support that woody vegetation type is highly responsive to groundwater, while the non-woody vegetation type immediately responds to rainfall by seed or rhizome regeneration (Sandi et al., 2020). However, both shrub and forest vegetation were moderately responsive to SWC and GW ( $r = 0.66$  and  $0.59$ , respectively). This means tree and shrub vegetation can grow well when SWC and groundwater flow increase after the rainfall in dry season. Moreover, this study suggests the grass vegetation type is highly dependent on groundwater during the dry and winter season for their growth, and any instability or long-term drought can negatively affect these floodplain vegetation communities.

A comprehensive documentation of different types of vegetation and groundwater relationships can be prepared for efficient floodplain vegetation management based on the results of this study. Agricultural production in similar regions around the world can be increased by selecting appropriate crops based on their seasonal response to groundwater. Authors should discuss the results and how they can be interpreted from the perspective of previous studies and of the working hypotheses. The findings and their implications should be discussed in the broadest context possible. Future research directions may also be highlighted.

## **5.6. Conclusion**

The analytical findings underscore the profound interrelationship between the vegetation system and groundwater hydrology, particularly emphasising the pronounced dependency on groundwater hydrology during the dry season. More specifically, shrub and grass type vegetation that are located distant from the water outlet in the HRU, highly responsive to groundwater availability during summer period. However, similar type vegetation that are located near the water outlet, become less responsive to groundwater flow. This suggests that small and medium-rooted vegetation, for instance, quince, feijoa, wheat, and oats etc., can grow well in similar floodplains globally, with possible implications for water management during the dry season.

The results of the study conclude interdependence between floodplain vegetation and catchment hydrology is reciprocal, and alterations in the surroundings can have a direct impact on the vegetation's response to groundwater. For example, suitable growing temperature and available water can boost vegetation growth which, in turn, contributes to increasing the potential evapotranspiration rate. On the other hand, grass type vegetation growth helps to increase the infiltration. The hydrological simulation results suggested that rainfall dominates the study area catchment water balance, in which groundwater flow increases in the wetting

period between April and September. Any alterations in the groundwater condition within the basin region can have a direct influence on the state of vegetation, which need to be included in future studies applying LAI in the hydrological modelling. As rainfall dominates the catchment hydrology, any future changes in the rainfall pattern need to be considered carefully for better floodplain management. Measuring the field soil moisture data and applying that data for model calibration could be another option to compare model simulation to support the output results.

This study contributes scientific insights into groundwater-vegetation relationship and outlines a methodology for modelling the relationship in contrast to seasonal groundwater variations. The findings of this research have the potential to aid in the development of sustainable floodplain vegetation systems in both temperate and semi-arid environments. The study analysed various vegetation types and their proximity to streamflow, while also evaluating their responses to groundwater variables. However, there could be other factors, e.g., vegetation density and depth of root can be included in the future studies. Further research should consider improving the modelling results applying more data for intense rainfall and extreme drought years. Thus, the multiple regression including a time lag, temperature, or rainfall frequency as well as future climate projections may give better understanding on ecosystem hydrology.

The next chapter, Chapter 6, will present and discuss the vegetation response modelling under future changing climate at catchment level.

# CHAPTER 6: MODELLING FLOODPLAIN VEGETATION RESPONSE TO CLIMATE CHANGE

## 6.1. Introduction

Chapter 5 discussed the floodplain vegetation responses to groundwater variability at the catchment level in the floodplain using SWAT hydrological modelling, remotely sensed leaf area index (LAI) data, and machine learning algorithms. This preceding chapter revealed the connections between the response of vegetation and groundwater through correlation analysis.

The analysis of the hydrological cycle can be conducted with greater accuracy by utilising remotely sensed data, as indicated by the literature review presented in Chapter 2. The incorporation of satellite imagery data in catchment hydrological analysis would augment the model's capacity to simulate catchment hydrology on larger geographical scales accurately. The recent advancements in satellite technology have paved the way for a substantial opportunity to access a vast amount of new-generation imagery data in the present and upcoming years. The literature on remotely sensed imagery data is expanding, however, there is currently no reported use of such data for model calibration and vegetation response modelling within temperate floodplain ecosystems.

The future climate projections from three GCMs were considered under two climate scenarios, RCP4.5 and RCP8.5 for a future period from 2031 to 2100. The correlation between the response of vegetation and the water present beneath the sub-surface is analysed in this research using Terra's Moderate Resolution Imaging Spectroradiometer (MODIS) leaf area index (LAI) and groundwater flow (GW) data. A semi-distributed hydrological model was employed to simulate leaf area index (LAI), as well as assessing the catchment hydrological variables. The Digital Elevation Model (DEM) derived from the SRTM imagery, in addition to remotely sensed vegetation indices data (e.g., LAI) generated from MODIS Terra and Aqua sensors, was developed, and evaluated using ArcGIS tool.

The findings of this study can be used for sustainable floodplain conservation, restoration, land-use planning, policy-making, and to help floodplain communities better prepare for and respond to changing flood patterns and related challenges under changing climate. The modelling results reveal that rainfall pattern is fluctuating under future projections

in the study area, in which the warmer season is more effective for the vegetation greenness. Moreover, the modelling results highlighted the increase in the average projected future winter temperature, can be potential opportunities for cultivating vegetation during the winter season.

This Chapter is organised into six sections. Section 1 outlines the scope of the Chapter, while Section 2 examines the literature on the use of satellite data for model calibration and correlation analysis between vegetation greenness and groundwater in floodplain regions. Section 3 discusses the Methods required to achieve the objectives of the Chapter. In section 4, the results of the correlation and regression analyses were conducted on SWAT-simulated groundwater variables and MODIS LAI data under GCM's future climate projections. Section 5 thoroughly evaluates and analyses the discoveries in relation to the established objectives and research gaps identified in Section 2. The Chapter concludes in Section 6 by elucidating the consequences of the outcomes and offering suggestions for forthcoming investigations.

## **6.2. The need for modelling of floodplain vegetation response to climate change**

Global climate change has been a great concern to researchers due to its impact on human and vegetation dynamics (Biggs et al., 2017; Callaghan et al., 2020). It is now well documented that climate change impacts on vegetation dynamics have negatively influenced global ecosystems; thus, ecosystem vulnerability has become one of the highlighted topics in earth science and ecological studies (Reichstein et al., 2013; Zhou et al., 2014; Xu et al., 2020). According to IPCC (2014), the continuous human-induced greenhouse gas emissions may exaggerate further warming and increase the climate change. This changing climate will significantly impact vegetation, particularly in floodplain areas, as it alters river flow and flood regimes. Therefore, understanding the floodplain ecosystem vulnerability in the context of climate change is one of the important issues of the current climate change study.

A floodplain is usually situated along rivers, lakes, deltas, and estuaries that harbors great diversification because of large spatio-temporal heterogeneity (Ward et al., 1999; Mosner et al., 2015). It is known as a resource-rich area in terms of soil nutrients that help to grow vegetation, and thousands of species make their habitat in the floodplain area worldwide. The floodplain vegetation provides an important role in catchment hydrology, as well as contributing to regulate carbon cycle (Kingsford, 2000; Adepoju et al., 2019). The physiological properties of the vegetation such as stomatal resistance leaf area index, rooting

depth, albedo, and soil moisture use influence the climate (Glenn et al., 2008). Moreover, floodplain vegetation protects riverbank erosion by reducing overland flow speed and increasing infiltration (Liu et al., 2018). On the other side, vegetation links atmosphere and hydrosphere by transpiration processes and its dynamics help maintaining the functions of the earth's ecosystems (Adepoju et al., 2019). However, floodplain systems are directly influenced by precipitation that causes high flows and inundates floodplains during an extensive 'wet' season and makes them waterless in 'dry' season (Ward et al., 2014). In addition, the ecosystem functions entirely depend on the duration, timing, strength, and seasonal variability of floodplain inundation (Junk & Wantzen, 2004). These inundation characteristics rely on climatic factors, and among them the most important factor is precipitation, its pattern has been changed globally due to climate change (Brown et al., 2017; Jiang et al., 2017). Thus, it is important to understand vegetation responses to climate change for sustainable floodplain conservation and restoration.

In general, vegetation dynamics is directly influenced by two important factors, climate variability and land use change (Adepoju et al., 2019). It can be simplified that land use change is more likely to change the hydrological processes, whereas climate change is the main actor in changing phenology, evapotranspiration, and ecological balance (de Jong et al., 2011). Previous studies also explained that temperature increase due to climate change can prolong vegetation growth season and promote vegetation productivity (Qu et al., 2020). However, in the arid and semi-arid region, increasing temperature may cause water stresses and inversely affect the vegetation growth, especially in the floodplain areas (Muhury et al., 2022). Researchers have addressed the biophysical effects of vegetation on climate in numerous studies by investigating deforestation (Lawrence et al., 2022), land use and land cover change (Santos et al., 2023), changes in physiological vegetation characteristics (Lian et al., 2022), and impact on monsoonal circulations (Spracklen et al., 2018). However, several studies found that vegetation growth was strongly affected by global climate change in the last few decades in arid and semi-arid regions (Tucker et al., 2001; Xu et al., 2014). Australia is a continent where both arid and semi-arid characteristics can be found in its different regions. Water stress is prominent for over the last few decades in the south-eastern part of Australia, and future climate predictions show a decreasing rainfall pattern (Muhury et al., 2023). The floodplain vegetation response to changing climate is not linear and it is very important to quantify the influence of various climate-induced factors on floodplain vegetation considering the spatial and temporal heterogeneity of a given area. Therefore, quantifying the responses at sub-catchment level

helps to assist floodplain ecosystems to prepare and respond to changing flood patterns and related challenges.

The global climate has changed rapidly in the last century that caused temperature increasing by  $0.74^{\circ}\text{C}$ , as well as changing the precipitation patterns and its intensity (Jiang et al., 2017). In addition, the mean precipitation is also decreasing in the arid and semi-arid areas leading to droughts in these regions (Jiang et al., 2017; Wu et al., 2022). Australia is mostly an arid region and highly sensitive to precipitation changes, and this precipitation change caused streamflow reduction in southeast Australia (Head et al., 2014). In recent decades, the precipitation in southeast Australia has declined, more precisely it is noticeably changing during the winter season (McKay et al., 2023). This winter precipitation decline has impacted agricultural production by reducing river flow in the Murrumbidgee River which is one of the main rivers in the Murray-Darling Basin (MDB) (Prosser et al., 2021). The summer precipitation trend in this area is highly variable that makes it difficult to understand the significance of long-term trends in the southeast Australian precipitation (Prosser et al., 2021; Muhury et al., 2023). Research studies suggest that rainfall patterns are likely to change across the MDB in the near future, with a projected rainfall decrease by 15% to 20% in the Basin area (Muhury et al., 2023).

Precipitation trends rely on both climate dynamics and thermodynamics changes; thus, it is difficult to understand how anthropogenic force will influence southeast Australian precipitation (Marvel et al., 2019; Bonfils et al., 2020). However, the climate system is very complex, and it is reasonable why climate change studies are focused on specific climate components of the global climate change. Therefore, in this study climate components such as precipitation and temperature effects were considered in relation to vegetation leaf area index (LAI).

Leaf area index (LAI) provides information about the density and spatial arrangement of leaves within a vegetation canopy, which is essential for understanding various ecological processes and estimating primary productivity (Kumar et al., 2019; Mohammadi Igder et al., 2022). Moreover, LAI is a measurement, commonly used in ecology and remote sensing to describe the amount of leaf area per unit of ground area in a plant or vegetation canopy that represents the potential leaf surface area for photosynthesis (Fang et al., 2019). LAI has been used in eco-hydrological studies as this vegetation attribute correlates with plant phenological development (Alemayehu et al., 2017). Among few hydrological models, the Soil and Water Assessment Tool (SWAT) has been widely applied for plant growth study, catchment water balance modelling as well as other hydrological features (Mekonnen et al., 2018; Duan et al.,

2019; Tan et al., 2020). SWAT model simulates the seasonal leaf area index (LAI) by employing a day length threshold and heat unit theory using a simplified version of the Environmental Policy Impact Climate (EPIC) growth module (Chen et al., 2023). Besides, this attributable EPIC module ignores spatiotemporal heterogeneity of vegetation, resulting in poor simulation of vegetation dynamics (Chen et al., 2023). Introducing precipitation in the SWAT model to track vegetation for new growing season, the simulation of vegetation dynamics in SWAT model has been improved (Strauch & Volk, 2013; Valencia et al., 2022). Previous studies have successfully applied SWAT model globally for drought monitoring and vegetation growth predictions (Muhury et al., 2022). However, to date, there has been no study on vegetation greenness modelling by SWAT hydrological model under future climate scenarios, based on projected minimum and maximum temperature and precipitation.

In previous climate studies, General Circulation Models (GCMs) have been applied for future climate projections in the hydrological modelling (Muhury et al., 2023). There are several GCMs available under the Coupled Model Intercomparison Project Phase 5 (CMIP5) to address the various climatic issues, which is not always feasible due to limitation of resources (Sa'adi et al., 2020). Therefore, the selection of GCM is necessary for a specific catchment to project future climate according to CMIP5 under RCP scenarios (Ouyang et al., 2015; Sa'adi et al., 2020). There are various statistical and multicriteria decision-making (MCDM) techniques applied for GCMs performance assessment (Sa'adi et al., 2020; Jose & Dwarakish, 2022). However, it is not often easy to select suitable GCMs based on standard statistical Multi-Criteria Decision Making (MCDM) technique (Jose & Dwarakish, 2022). In this study, the selection of GCMs was based on their ability to simulate historical rainfall, their country of origin, and their application in the previous studies.

By applying different GCMs projected climate data to the hydrological model in simulating LAI and analysing the relationship among climate factors, SWAT variables and LAI, this study constructed the vegetation growth in a floodplain area with moderate slope. Then, this study focused on analysing vegetation greenness shifting in response to long term climate change under various climate scenarios to identify the outcomes that can be utilised in similar areas around the world.

This research seeks to assess the impacts of climate change variability on floodplain vegetation in the Burrinjuck sub-catchment in the south-east part of Australia. To achieve this goal, a hydrological modelling framework was used to simulate LAI under future climate variability and evaluate future vegetation growth under two different emission scenarios (RCP 4.5 and RCP 8.5). The specific objectives of this study are the following: (1) to understand the

potential impacts of future climate change on the floodplain vegetation dynamics using a hydrological model simulated Leaf Area Index (LAI) and GCMs projections under two scenarios i.e., RCP 4.5 and 8.5; (2) to compare changes in vegetation dynamics monthly and seasonally in relation to different GCM and RCP scenarios; and (3) to assess vegetation responses to SWAT-simulated hydrological variables under future climate scenarios and assessing vegetation greenness responses towards them.

### **6.3. Materials and methods**

#### **6.3.1. Study area**

The Burrinjuck sub-catchment, which is part of the Upper Murrumbidgee River catchment in the south-east part of Australia (Figure 6.1), was selected as the study area. This area is located within 34.53° S and 148.31° E and -35.14° S and -148.55° E. The Burrinjuck Dam was built on the Murrumbidgee River in 1927 to improve the agricultural irrigation in the southern part of New South Wales (NSW) (Muhury et al., 2023). This Murrumbidgee River begins its journey from Kosciuszko National Park with an altitude of 1500m and flows around 316km to enter the Burrinjuck Reservoir. The Burrinjuck sub-catchment was considered as the study area due to the plant diversity in this floodplain with moderate slopes and varying elevation from 373m to 934m (Muhury et al., 2022). The land use and land cover in this area is mostly dominated by forest and pasture, however, wheat and cereals also grow well in this area that contribute to the national agricultural production (Muhury et al., 2023). Moreover, the diverse rainfall in the lower and upper Murrumbidgee makes this floodplain suitable. The detailed climatic characteristics of the study area were described in the previous chapter (Chapter 3). Overall, the Burrinjuck sub-catchment has a diverse range of vegetation types and land use classes (Figure 6.1) that makes this area unique within the Murrumbidgee River catchment.

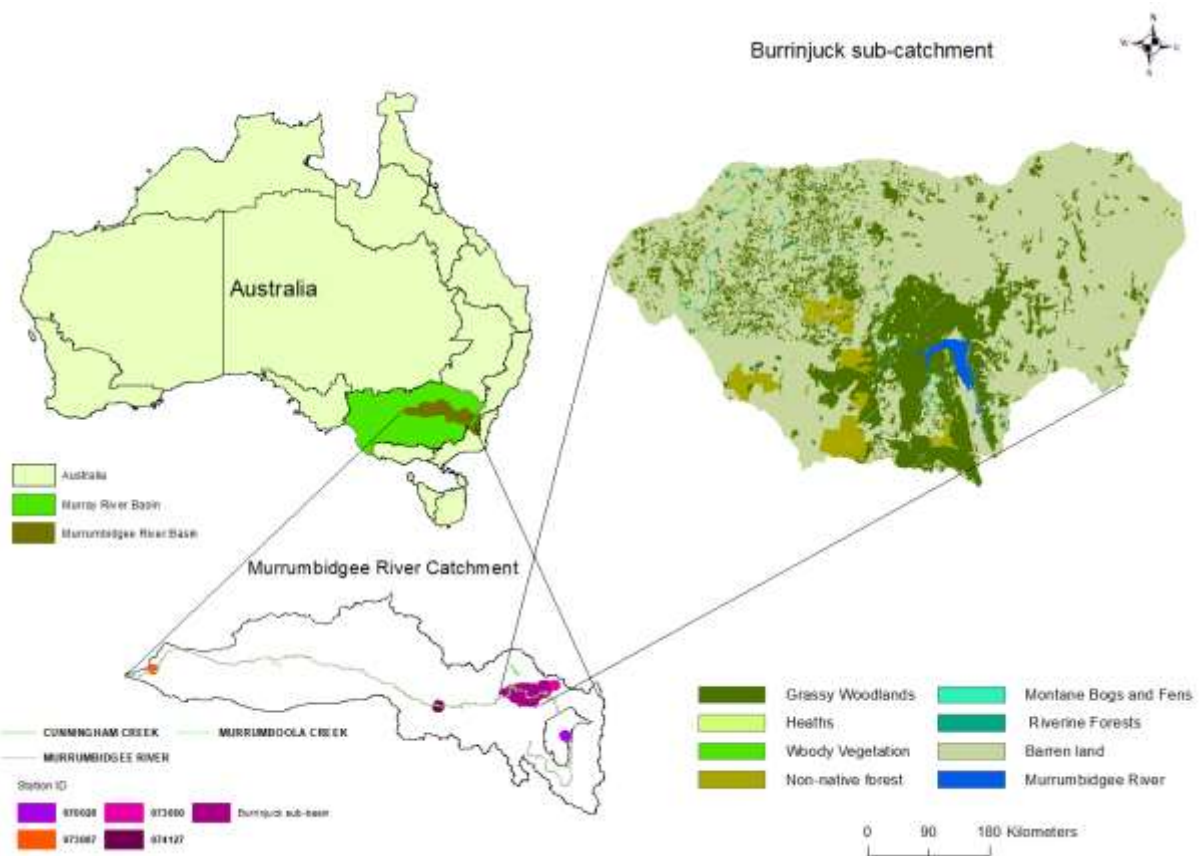


Figure 6.1: The Burrinjuck sub-catchment watershed area on the right (generated by SWAT model) is located within the Murrumbidgee River basin on the bottom left.

### 6.3.2. Research methods

Chapter 3 has largely explained about the methods required in the current chapter. On the other hand, the specific methods applied in this present study have been outlined in Figure 6.2. The SWAT model was setup using ArcGIS (ArcMap) to mimic the Burrinjuck sub-catchment hydrology. The model input datasets used in this study were obtained from governmental data portals, such as Climate Change in Australia, Bureau of Meteorology (BOM), and U.S. Geological Survey (USGS). For data analysis, Microsoft Excel and Tableau tool were used. The model simulated LAI has been calibrated and validated against the Moderate Resolution Imaging Spectroradiometer (MODIS) LAI data. The SWAT model was also calibrated and validated using the SWAT-CUP tool with station-gauged streamflow data.

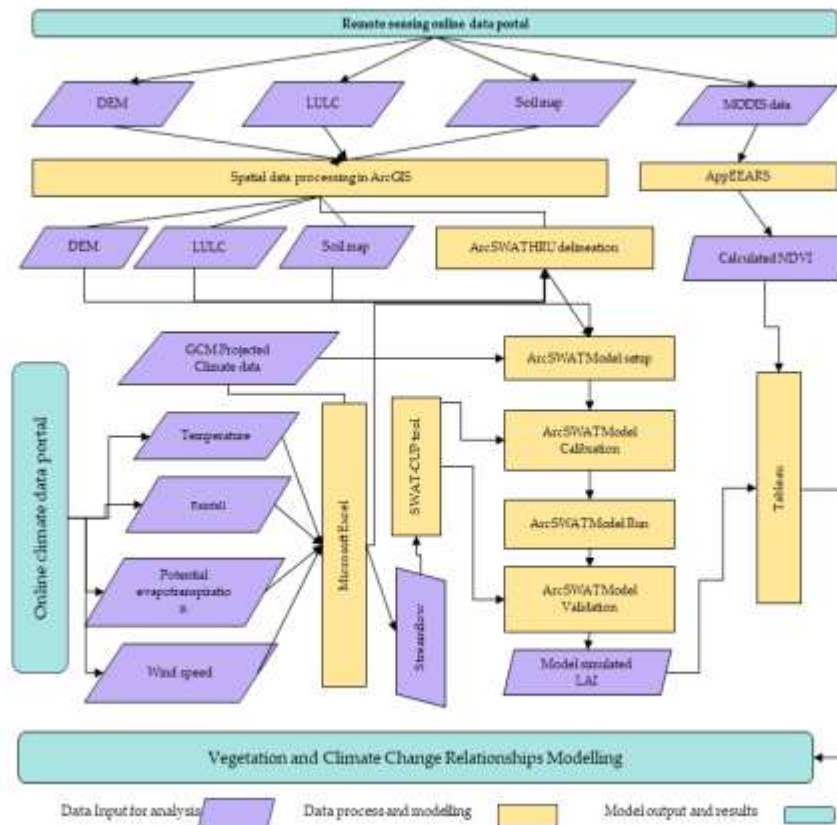


Figure 6.2: An overview of the research methods used for modelling vegetation responses and future climate change.

### 6.3.3. An overview of SWAT hydrological model

The Soil & Water Assessment Tool (SWAT) is a semi-distributed, physically based watershed model that simulates the major water balance components continuously at a daily time step (Arnold et al., 1998). In the SWAT model, a watershed is being delineated into multiple sub-basins based on spatial characteristics. These sub-basins are further subdivided into Hydrological Response Units (HRUs) according to individual land use, soil, and topography (Neitsch et al., 2011; Gassman et al., 2014). Each HRU is simulated for vegetation growth, soil water content, groundwater flow, nutrient cycles, sedimentation, and land management practices, in which the outputs are aggregated at the sub-basin scale through channel processes (Arnold et al., 2012; Saha et al., 2014). In this study, the primary focus is on vegetation growth at the level of HRUs. The water balance calculations at HRU level include surface runoff, infiltration, evaporation, plant uptake, lateral flow, and percolation to lower layers (Neitsch et al., 2011). SWAT estimates surface runoff and infiltration from daily precipitation using the Soil Conservation Service (SCS) and Curve Number (CN) method (Zhang et al., 2019). The hydrological cycle in the watershed can be mimicked by SWAT

simulation, where model calculation is based on the following water balance equation (Neitsch et al., 2011):

$$SW_t = SW_0 \sum_{i=0}^t (R_{day} - Q_{surf} - E_a - W_{seep} - Q_{gw})_i \quad (1)$$

Where  $SW_t$  is the ultimate water content in (mm),  $SW_0$  is the amount of water content on the first soil of the day  $I$  (mm),  $t$  is time (days),  $R_{day}$  is the amount of rainfall on day  $i$  (mm),  $Q_{surf}$  is the amount of surface runoff on specific day  $i$  (mm),  $E_a$  is the amount of evapotranspiration on day  $i$  (mm),  $W_{seep}$  is the amount of water percolated into the vadose zone from the soil profile on day  $i$  (mm), and  $Q_{gw}$  is the amount of return flow on day  $i$  (mm).

SWAT provides three methods to estimate potential evapotranspiration (PET): i) Priestley–Taylor, ii) Penman–Monteith, and iii) Hargreaves method. In this study Penman–Monteith method was applied to calculate PET (Penman, 1948; Xiang et al., 2020). The Penman–Monteith equation used in SWAT can be expressed as:

$$\lambda E = \frac{\Delta (H_{net} - G) + \rho_{air} * c_p * [e_z^0 - e_z] / r_a}{\Delta + \gamma (1 + \frac{r_c}{r_a})} \quad (2)$$

where  $\lambda E$  is the flux density of latent heat ( $\text{MJm}^{-2} \text{d}^{-1}$ ),  $E$  the depth rate evaporation ( $\text{mmd}^{-1}$ ),  $\Delta$  refers to gradient of saturation vapor pressure temperature curve ( $\text{kPa}^\circ\text{C}^{-1}$ ),  $H$  the net radiation ( $\text{MJm}^{-2} \text{d}^{-1}$ ),  $G$  the ground heat flux density ( $\text{MJm}^{-2} \text{d}^{-1}$ ),  $c_p$  the specific heat ( $\text{MJkg}^{-1} \text{ }^\circ\text{C}^{-1}$ ),  $\rho_{air}$  refers to air density ( $\text{kgm}^{-3}$ ),  $e_z$  the water vapor pressure of air at elevation (kPa),  $e_z^0$  the saturation vapor pressure of air at elevation  $z$  (kPa),  $r_c$  the plant canopy resistance ( $\text{sm}^{-1}$ ),  $\gamma$  the psychrometric constant ( $\text{kPa}^\circ\text{C}^{-1}$ ), and  $r_a$  the aerodynamic resistance ( $\text{sm}^{-1}$ ). Plant growth is estimated in  $r_c$  by dividing the minimum effective stomatal resistance for a single leaf,  $r_l$  ( $\text{sm}^{-1}$ ) by one-half of the leaf area index (LAI):

$$r_c = \frac{r_l}{0.5 \cdot \text{LAI}} \quad (3)$$

Further details regarding the water balance and ET equations can be found in the SWAT documentation (Neitsch et al., 2011).

#### **6.3.4. Vegetation dynamics modelling in SWAT**

SWAT model incorporates the simplified version of the Erosion Productivity Impact Calculator (EPIC) plant growth module to simulate the annual vegetation growth (Neitsch et

al., 2011; Ma et al., 2019). In the EPIC plant growth module, the LAI was simulated as a function of canopy height, which is required to calculate the canopy resistance and the aerodynamic resistance (Neitsch et al., 2011). At the initial stage of plant growth, canopy height and leaf area development are controlled by the optimal leaf area development function. The function of the optimal leaf area development is listed as:

$$fr_{LAI_{max}} = \frac{fr_{PHU}}{fr_{PHU} + \exp(l_1 - l_2 * fr_{PHU})} \quad (4)$$

$$fr_{PHU} = \frac{\sum_{i=1}^d HU}{PHU} \quad (5)$$

Where  $fr_{LAI_{max}}$  is the fraction of the plant's maximum leaf area index for the plant,  $l_1$  and  $l_2$  are the shape coefficients,  $fr_{PHU}$  is the fraction of potential heat units for a certain period during the growing season,  $HU$  is the heat units accumulated on a given day ( $d$ ) which can be only positive value, and  $PHU$  is the potential heat units required for each plant maturity. PHU refers to the number of days between budding and leaf senescence. For annuals and perennials plant growth, before the LAI reaches its maximum value, the leaf area added on day  $i$  is calculated as follow:

$$\Delta LAI_i = (fr_{LAI_{max,i}} - fr_{LAI_{max,i-1}}) * LAI_{max} * \{1 - e^{[5*(LAI_{i-1} - LAI_{max})]}\} \quad (6)$$

which is then used to calculate total leaf area index as follows:

$$LAI_i = LAI_{i-1} + \Delta LAI_i \quad (7)$$

In the above equations,  $\Delta LAI_i$  is the leaf area added on day  $i$ ,  $LAI_i$  and  $LAI_{i-1}$  are the leaf area index on day  $i$  and leaf area index on previous day,  $fr_{LAI_{max,i}}$  and  $fr_{LAI_{max,i-1}}$  are the fraction of the plant's maximum leaf area for day  $i$  and  $i-1$ , respectively.  $LAI_{max}$  is the maximum leaf area index of the plant.  $LAI_{max}$  for grown trees can be adjusted by considering the age of the trees and the time required for the plant species to reach full growth (Neitsch et al., 2011). However, the actual LAI calculated for each day may differ from optimal growth due to variation in the availability of temperature, soil water, and other factors.

By default, SWAT uses a fundamental feature, named dormancy, at which plants do not grow during the shortest days of the year. During dormancy, a portion of biomass changes to residue where LAI is set to minimum for related plant. Dormancy also resets a fraction of potential heat units to zero, thus, a new growing cycle begins when length of the day reaches the latitude-specific threshold. However, tropical plants do not become dormant and heat units and fraction of potential heat units accumulate continuously throughout the whole simulation period. As SWAT only simulates plant growth when the plant reaches at maturity (instead of dormancy), the model requires a management configuration “kill” option for stopping a growing season and triggering a new one. In this study, the plant growing season was considered to start from the beginning of the simulation for trees. This model setting forced SWAT to consider one growing cycle in the first year of the 8-year long simulation period. In the remaining seven years, the potential heat units increased continuously since there is no reset mechanism without dormancy. Therefore, the LAI simulations in SWAT, based on scheduled management operation, represent higher value in summer and lowest in winter (Strauch & Volk, 2013).

### ***6.3.5. Hydrological model setup at study catchment***

SWAT2012 can be run using GIS tool in Windows operating system. This study utilised ArcMap v10.6 (Desktop version) to execute SWAT2012 Revision 681. The watershed was delineated using a 30 m resolution digital elevation model (DEM). A total drainage area of 872 km<sup>2</sup> was selected in the Burrinjuck sub-basin with the help of DEM and the Murrumbidgee River network, thus, it divided the watershed into 18 Sub-basins and then categorised into 158 HRUs depending on the unique land use, soil, and slope. After completion of the SWAT setup, it was initially run for 21 years including 2 years of warmup period from 2000 to 2020. The SWAT model was calibrated against observed streamflow data obtained from the Australian Bureau of Meteorology (BOM) using additional SWAT Calibration and Uncertainty Programs (SWAT-CUP) tool. Moreover, the SWAT model was also calibrated using remotely sensed LAI data processed from 500 m spatial resolution and 8-day temporal dataset of MODIS LAI type MOD15A2H, for each HRU by spatial aggregation.

### 6.3.6. Assessment of model performance criteria

Hydrological model performance evaluation is crucial to assess model accuracy and reliability in simulating the behaviour of the hydrological system. There are different metrics and methods for model performance evaluation, however, the selection of evaluation criteria may depend on the specific objectives of the modelling and the available data. In this study, a few statistical metrics were considered for model evaluation, such as the coefficient of determination ( $R^2$ ), Nash-Sutcliffe efficiencies (NSE), and percent bias (PBIAS) quantitative statistics (Moriassi et al., 2007; Setegn et al., 2009; Zhang et al., 2009). Moreover, twenty one SWAT parameters were applied in the SWAT-CUP simulation and ranked them according to the model performance acceptance guidelines suggested by Arnold et al., (Arnold et al., 2012) which are presented in the latter section.

The Nash-Sutcliffe Efficiency (NSE), also known as the Nash-Sutcliffe coefficient, is a widely used dimensionless statistical metric to assess the performance of hydrological models or other environmental models. It was proposed by Nash and Sutcliffe in 1970 (Nash & Sutcliffe, 1970). NSE is particularly useful for evaluating models that simulate time series data, such as streamflow or water level. The NSE compares the predictive performance of a model with the performance of a simple benchmark model, usually represented by the mean of the observed data. The NSE ranges from negative infinity to 1, with 1 representing a perfect match between the predicted and the observed data, 0 indicating that the model performs no better than the mean of the observed data, and negative values indicating that the model performs worse than the mean. NSE is defined as:

$$NSE = 1 - \frac{\sum_{i=1}^n (Q_{obs, i} - Q_{sim, i})^2}{\sum_{i=1}^n (Q_{obs, i} - \bar{Q}_{obs})^2} \quad (8)$$

In the above equation,  $n$  is the number of time steps,  $Q_{obs, i}$  is the observed flow at time step  $i$  (daily here),  $\bar{Q}_{obs}$  is the mean of the observed flow, and  $Q_{sim, i}$  is the simulated flow.

The coefficient of determination, known as  $R^2$  (R-squared), is a statistical metric used to assess how well a regression model fits the observed data. In the context of regression analysis,  $R^2$  quantifies the proportion of the variance in the dependent variable that is predictable from the independent variable(s) in the model. It provides a statistical measure of the goodness-of-fit of the regression model. The  $R^2$  value ranges from 0 to 1, where 0 indicates that the regression model explains none of the variance in the dependent variable, meaning it

does not fit the data at all. A hydrological model with higher  $R^2$  is considered as a good result (Wu et al., 2022).  $R^2$  is defined as:

$$R^2 = \left\{ \frac{\sum_{i=1}^n (Q_i^{obs} - \bar{Q}^{sim})(Q_i^{sim} - \bar{Q}^{sim})}{\sum_{i=1}^n (Q_i^{obs} - \bar{Q}^{obs})^2 \sum_{i=1}^n (Q_i^{sim} - \bar{Q}^{sim})^2} \right\}^2 \quad (9)$$

where,  $Q_i^{obs}$  and  $Q_i^{sim}$  are representing the measured and simulated data for  $i^{\text{th}}$  observation and  $\bar{Q}^{obs}$  and  $\bar{Q}^{sim}$  are the mean of the measured and simulated data, respectively.

The percent bias (PBIAS) provides a measure of the systematic tendency of the model to greater or smaller simulated values than their observed data (Arnold et al., 2012). The maximum *PBIAS* value is zero, indicating the simulation is unbiased and similar to the observed data. In general, a smaller *PBIAS* value signifies accurate model simulation. *PBIAS* is calculated as:

$$PBIAS = \frac{\sum_{i=1}^n (Q_i^{obs} - Q_i^{sim}) * 100}{\sum_{i=1}^n Q_i^{obs}} \quad (10)$$

In the above equation,  $Q_i^{obs}$  and  $Q_i^{sim}$  are representing the measured and simulated data for the  $i^{\text{th}}$  observation, respectively.

### 6.3.7. Trend analysis of time series data

In this study, a non-parametric statistical test known as the Mann-Kendall trend test was applied to examine the presence or absence of monotonic trend in time series data (Mann, 1945; Hamed, 2009). This test is particularly useful when the traditional parametric test is less appropriate, or the time series data do not meet the normality assumptions. This Mann-Kendall test is commonly used in different research studies including earth science, hydrology, climatology etc. to understand whether there is a significant increasing or decreasing trend, as well as to quantify the strength of that trend. The following equation (11) is used to determine the Mann-Kendall test statistic.

$$S = \sum_{i=1}^{n-1} * \sum_{j=i+1}^n \text{sign}(X_j - X_i) \quad (11)$$

Where  $X_j$  and  $X_i$  represent sequential data in the time series,  $n$  represents the size of the time series. In the above equation  $j > i$  and  $i=1, 2, 3 \dots n-1$ ,  $k = 2, 3, 4 \dots n$ . The  $sign(X_j - X_i)$  is calculated using following equation (12)

$$sign(X_j - X_i) = \begin{cases} +1 & \text{if } (X_j - X_i) > 0 \\ 0 & \text{if } (X_j - X_i) = 0 \\ -1 & \text{if } (X_j - X_i) < 0 \end{cases} \quad (12)$$

The variance of  $S$  can be calculated from the following equation:

$$Var(S) = \frac{S(n-1)(2n+5) - \sum_q^p t_p(t_p-1)(2t_p+5)}{18} \quad (13)$$

Where,  $q$  is the number of tied groups in the datasets,  $t_p$  is the number of data in the  $p^{th}$  tied group,  $n$  is the total number of data in the time series. A positive value of  $S$  indicates that an increasing and negative value of  $S$  is decreasing trend of time series data. The following equation (4) is used to calculate the Mann-Kendall test statistics.

$$Z_s = \begin{cases} \frac{S-1}{\sqrt{var(S)}} & \text{if } S > 0 \\ 0 & \text{if } S = 0 \\ \frac{S+1}{\sqrt{var(S)}} & \text{if } S < 0 \end{cases} \quad (14)$$

The degree or rate of change can be calculated using the Thiel-Son slope method. Equation (X) is used to calculate the Theil–Sen slope ( $\beta$ ).

$$\beta = median\left(\frac{X_j - X_i}{j - i}\right) \quad (15)$$

Where  $X_j$  and  $X_i$  represent sequential data in the time series,  $i=1,2,3 \dots n-1$  and  $j > i$ .

### 6.3.8. Data preparation

SWAT requires a combination of both climate and land properties data to build a hydrological model. These data requirements can be categorised into essential such as DEM, soil map, land use map, and weather data (precipitation, temperature, windspeed, solar radiation, and relative humidity), and non-essential such as streamflow, reservoir information, sediment transfer, water quality, chemical and pesticide data. The datasets used in this study, including their source of availability, are listed in the Table 6.1. A detailed description about the SWAT input data was outlined by (Muhury et al., 2022).

Table 6.1: The datasets used in this chapter including the frequency, source, and description.

Data	Frequency	Description	Source
DEM	-	30 m spatial resolution	U.S. Geological Survey
Land cover/land use map	-	50 m spatial resolution	NSW Office of Environment and Heritage
Soil Map	-	250 m spatial resolution	Digital Atlas of Australian Soil
MODIS LAI	8-Day	500 m spatial resolution	U.S. Geological Survey
Temperature	Daily	Station gauged, temporal	Bureau of Meteorology
Solar Radiation	Daily	Station gauged, temporal	Bureau of Meteorology
Precipitation	Daily	Station gauged, temporal	Bureau of Meteorology
Relative humidity	Daily	Station gauged, temporal	Bureau of Meteorology
Wind speed	Daily	Station gauged, temporal	Bureau of Meteorology
Streamflow (discharge)	Daily	Station gauged, temporal	NSW Office of Water

### 6.3.9. Leaf Area Index (LAI)

The LAI is widely used in research studies to assess the amount of leaf area in an ecosystem, which is a dimensionless and time-dependent vegetation parameter (De Bock et al., 2023). Watson (1947) defined LAI as the ratio of one-sided leaf area in the canopy per unit ground surface area [ $\text{m}^2 \text{m}^{-2}$ ]. It is dynamic and subject to change in relation to internal and external factors such as plant type, orientation, seasonality, nutrition availability, diseases, etc. (Fang et al., 2019). LAI is considered a critical parameter in processes such as respiration, rainfall interception, transpiration (ET), and biophysical cycles in ecosystems. Therefore, LAI has been extensively used in agriculture and forestry research to estimate vegetation growth, yield, biomass, energy, and water balances in the ecosystems. For broad leaf plant, LAI = leaf area/ground area,  $\text{m}^2/\text{m}^2$ , has a value range from 0 to 10 depending on plant physiology and growth phase (Pérez et al., 2022).

### 6.3.10. General Circulation Models (GCMs)

In contrast to Phase 3 (CMIP3), CMIP5 models exhibit improvements in terms of representing model physics, vertical resolution, and the incorporation of atmospheric aerosols (Taylor et al., 2012; Sperber et al., 2013). However, on the premise of CMIP5, CMIP6 incorporates a more complex global carbon cycle, airborne impacts, atmospheric chemistry, terrestrial and marine biogeochemistry, and other processes, further perfecting and improving the physical process of each model and improving the model's simulation ability. Moreover, it

is worth noting that certain studies have also pointed out instances where CMIP6 models exhibited poorer performance than CMIP5 models. For example, Zhou et al. (2022) observed inferior simulation results in CMIP6 models concerning air temperature and precipitation in humid regions of the Tibetan Plateau when compared to CMIP5 models. GCMs have been valuable tools for assessing climate change and for generating climate projections (Brown et al., 2017). This study applied GCMs of CMIP5 which adopted carbon cycle models and a dynamic vegetation model (Jia et al., 2019). Among these GCMs, eight of them have been identified as the best performance model by Australian Government Climate Agencies. However, few models are recommended for representing the “best”, “worst”, and “maximum consensus” scenarios for any region. In this study, two climate scenarios RCP 4.5 and RCP 8.5 were considered for future climate projections. RCP 4.5 is a medium-low stabilisation scenario in which radiative forcing stabilises at  $4.5 \text{ Wm}^2$  by the year of 2100 with 650 ppm  $\text{CO}_2$  concentration (Xu et al., 2014; Chang et al., 2023; Muhury et al., 2023). However, RCP 8.5 represents extremely high emission scenario, indicating high radiative forcing pathway that leads to  $8.5 \text{ Wm}^2$  by the year 2100 with  $\text{CO}_2$  concentration. Substantial uncertainty is present in the analyses when using GCM data. Climate projections, for example, are dependent on different Greenhouse Gas (GHG) emission scenarios, which involve a range of economic and technological development conditions, as well as the interaction between global and local growth dynamics (Reshmidevi et al., 2018). The selection of a single GCM has been repeatedly pinpointed as the primary source of uncertainty in overall analyses, based on previous research (Chen et al., 2011). Given the significant uncertainty associated with GCMs, it is imperative to exercise caution when interpreting climate change impacts derived from the utilisation of a single GCM. Therefore, numerous multi-model ensemble climate simulations have been utilised in a variety of recent studies (Jung et al., 2013).

After conducting a robust literature review, the outputs of three GCMs, i.e., ACCESS1.0, MK3.6, and MIROC5, were used to assess the future climate change impact on the Burrinjuck sub-basin vegetation community. ACCESS1.0, MK3.6, and MIROC5 were selected to project future climate variables such as temperature and precipitation that directly correlate to vegetation growth, for the two emission scenarios RCP 4.5, and RCP 8.5. However, ACCESS1.0 (known as maximum consensus scenario model), which defined as the future climate populated by the highest number of models, that number must be greater than one-third of the total number of available GCMs (Muhury et al., 2023).

### 6.3.11. Bias correction

Biases in climate model simulation are common which can be detected through validation. This involves comparing the model's output with observations and conducting various analyses, such as calculating the mean and other complex computations. In this study, bias corrected application-ready data was utilised, employing the quantile mapping method.

The utilisation of the quantile mapping approach is favored for its simplicity and effectiveness in correcting biases in climate models' outputs. This approach, also referred to as 'probability mapping' and 'distribution mapping', involves establishing a statistical relationship between observed and model-simulated outputs (Gupta et al., 2019). This is achieved by substituting the simulated values with observed values at corresponding cumulative density function (CDF) positions within the chosen distribution, based on the climate variable being analysed. Precipitation values above 0 are adjusted for bias by aligning the daily precipitation values for each month with the Gamma distribution, which specifically considers values exceeding 0. The correction for precipitation bias is determined through the utilisation of the following equation (Ines & Hansen, 2006);

$$\bar{x}_{ms.corr} = \begin{cases} F_{oh}^{-1}(F_{mh}(x_{ms})), & x_{ms} \geq x_{th} \\ 0, & x_{ms} < x_{th} \end{cases} \quad (16)$$

Similarly, temperature values vary from negative to positive. Therefore, normal distribution fits best for temperature data. The equation utilised for correcting temperature data bias can be defined as (Li et al., 2010);

$$\bar{x}_{ms.corr} = x_{ms} + F_{oh}^{-1}(F_{ms}(x_{ms})) - F_{mh}^{-1}(F_{ms}(x_{ms})) \quad (17)$$

where  $x$  is climatic variable,  $x_{ms.corr}$  is bias corrected model simulated data; to categories between the wet and the dry day threshold value  $x_{th}$  is used (day with precipitation greater than 1 mm is assumed to be a wet day);  $F$  is CDF, whereas  $F^{-1}$  is its inverse. (o = observed, m = model, h = historical period, and s = simulation period). Here, the simulated period can either be historical or a future period.

### 6.3.12. Climate scenarios

GCMs future projections for two climate scenarios are considered in this study and have been assessed for future periods, i.e., (i) 2031–2055, (ii) 2056–2075, and (iii) 2076–2100. These scenarios are defined by daily time series of climate data based on historical rainfall, and temperature from 2031 to 2100. Scenario 1: Representative Concentration Pathway (RCP) 4.5

projections for 2031–2055, 2056–2075, 2076–2100. Scenario 2: Representative Concentration Pathway (RCP) 8.5 projections for 2031–2055, 2056–2075, 2076–2100.

Figure 6.3(a) shows the average maximum temperatures according to ACCESS1.0 model, which are close to the historical maximum temperature under RCP 4.5. However, the minimum temperatures are slightly above the average historical minimum temperature shown in Figure 6.2(d). According to MIROC5 and MK3.6 climate models projection, the average maximum temperature from January to May decrease, and from June to December the maximum temperature shows an increasing trend (Figure 6.3b, 6.3c). These two climate models predicted minimum temperature decreases for January to June and increases from July to December over three future time spans according to RCP 4.5 climate scenarios (Figure 6.3e & 6.3f).

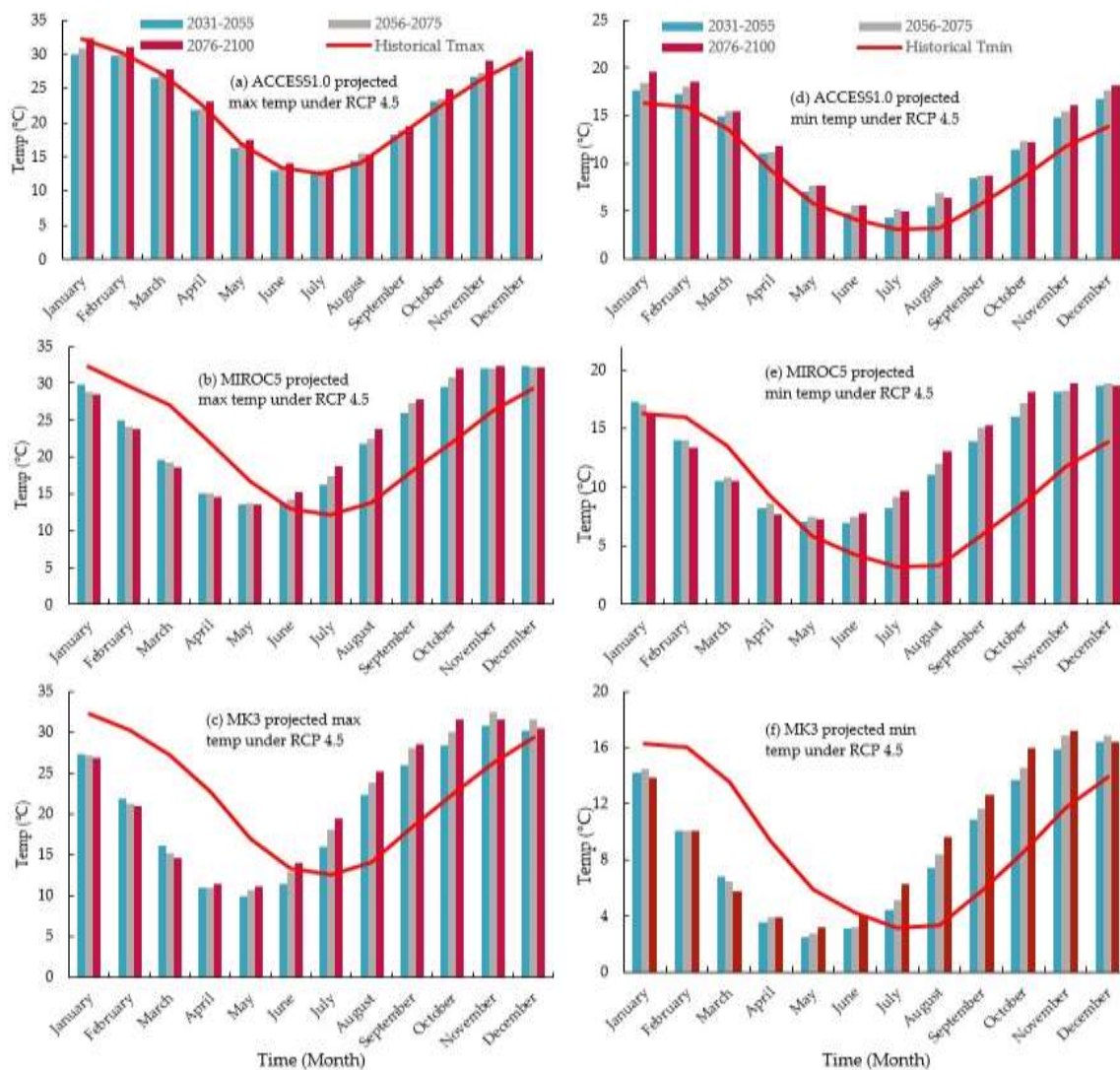


Figure 6.3: The GCMs projected maximum and minimum temperatures plotted against observed (2000-2020) minimum and maximum temperatures in three different time periods (e.g., 2031-2055, 2056-2075, 2076-2100) under climate scenario RCP 4.5.

In contrast to climate scenario 8.5, the ACCESS1.0 GCM predictions show that the average maximum and minimum temperatures will be increased compared to the historical averages, when considering for the future time frames (Figure 6.4a & 6.4d). Likewise, MIROC5 and MK3.6, both predict the average maximum temperatures from January to June are below the historical average maximum and July to December average temperatures are above the historical average (Figure 6.4b & 6.4c). However, the average minimum temperatures under MIROC5 for the first five months of the year are close to the historical average minimum, whereas the rest of the month's average is higher than the historical average minimum temperature (Figure 6.4e). Considering the MK3.6, January to May temperature projections are below the historical average, and July to December predictions are above the historical average temperature (Figure 6.4f).

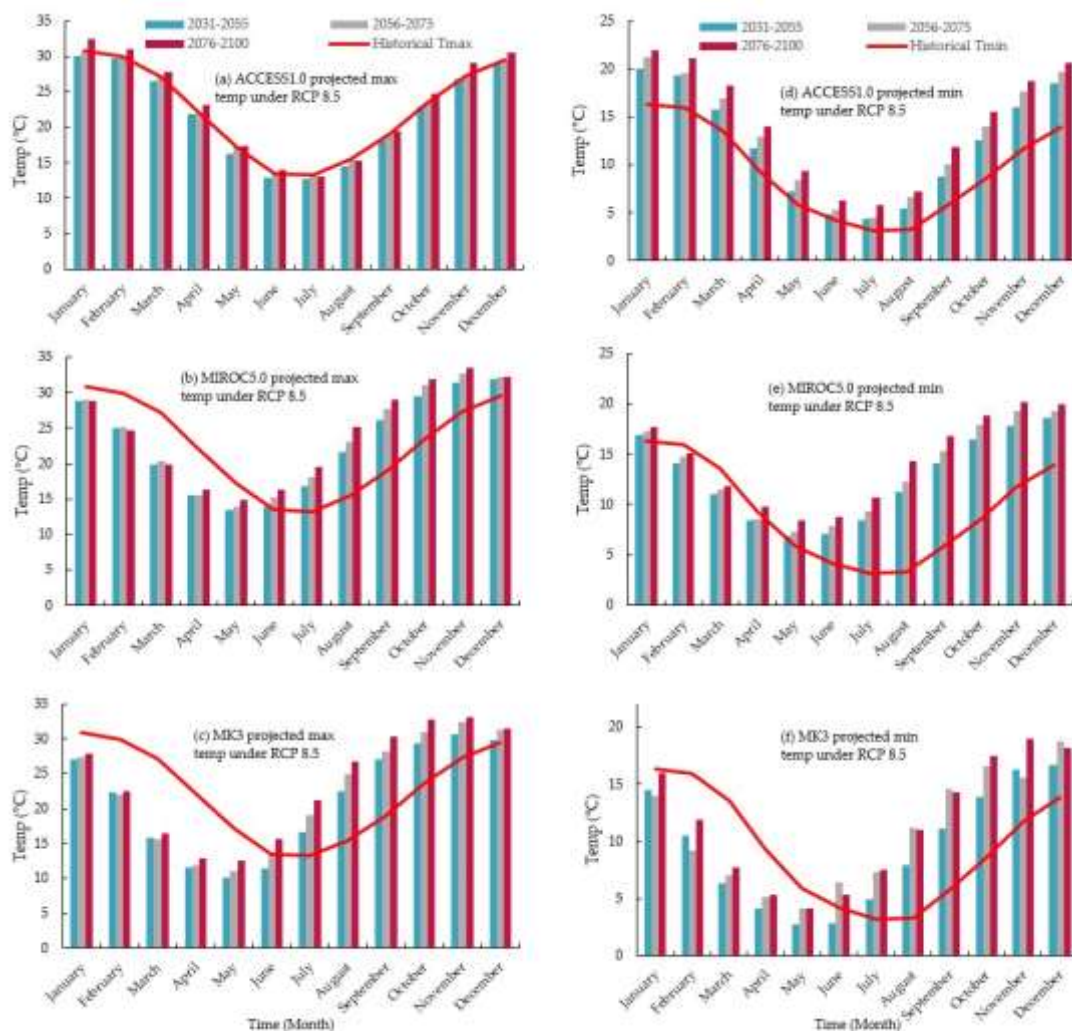


Figure 6.4: The GCMs projected maximum and minimum temperatures (RCP8.5) are plotted against observed (2000-2020) minimum and maximum temperatures in three different time periods (e.g., 2031-2055, 2056-2075, 2076-2100) under climate scenario RCP 8.5.

## 6.4. Results

### 6.4.1. Analysis of the SWAT model output and parameter sensitivity

In this study, a SWAT model was built using the ArcGIS interface (ArcSWAT) in the study area based on remotely sensed data for high resolution DEM, soil map, and LULC map. A pre-calibration parameter selection was done according to previous SWAT model run for hydrological and vegetation analysis. The model was run using monthly climate data from 2000 to 2020 which covered both drought and flood conditions in the study area. Table 6.2 listed the sensitivity ranking including the descriptions of the parameters. The five parameters according to the list were CH\_N1, SOL\_AWC, ESCO, GW\_REVAP, REVAPMN (Table 6.2).

Table 6.2: Performance indices of SWAT model parameters

Parameter Name	Description	t-Stat	P-Value	Sensitivity Rank
CH_N1.sub	Channel Manning's n	3.03	0.06	1
SOL_AWC.sol	Available water capacity in the soil	-2.68	0.08	2
ESCO.hru	Soil evaporation compensation factor	2.02	0.14	3
GW_REVAP.gw	Ground water revap coefficient	-1.89	0.16	4
REVAPMN.gw	Threshold depth of water in the shall aquifer for revap to occur [mm]	1.67	0.19	5
CH_K2.rte	Hydraulic conductivity of the chan [mm/hr]	1.61	0.21	6
CN2.mgt	Curve Number	-1.58	0.21	7
SURLAG.bsn	Surface runoff lag coefficient	1.45	0.24	8
CANMX.hru	Maximum canopy storage [mm]	1.39	0.26	9
HRU_SLP.hru	Average slope steepness [m/m]	1.29	0.29	10
SOL_Z.sol	Depth of the soil layer [mm]	-1.12	0.34	11
SLSUBBSN.hru	Average slope length [m]	-1.11	0.35	12
SLSOIL	Slope length for lateral subsurface flow	-1.10	0.35	13
ALPHA_BNK.rte	Baseflow alpha factor for bank storag (day <sup>-1</sup> )	1.06	0.37	14
ALPHA_BF.gw	Base flow alpha factor (day <sup>-1</sup> )	1.06	0.37	15
EPCO.hru	Plant uptake compensation factor	0.87	0.45	16
RCHRG_DP.gw	Deep aquifer percolation fraction [fraction]	-0.83	0.47	17

SOL_K(..).sol	Saturated hydraulic conductivity of the soil [mm/hr]	-0.78	0.49	18
GWQMN.gw	Threshold depth of water in the shallow aquifer required for return flow to occur [mm]	0.75	0.51	19
GW_DELAY.gw	Ground water delay [days]	-0.23	0.83	20
CH_N2.rte	Manning's coefficient of the channel	0.02	0.98	21

#### **6.4.2. Analysis of the SWAT model calibration and validation against streamflow**

The parameters according to the sensitivity ranking were applied for model validation. Further, the calibration and validation results were analysed to assess the model performance, which outlined NSE values 0.79 and 0.67 for the calibration and validation, respectively. These performance results can be marked as 'good' for the SWAT model developed in the study area. According to the results, the model in the study area was able to simulate about 79% of the variance on observed streamflow data. Moreover, 'R' values also confirm good correlation between observed and simulated streamflow during calibration and validation. The 'R' value shows very good performance (R=0.82) for calibration and satisfactory (R=0.67) for validation. Furthermore, the SWAT model exhibited a significant improvement in statistical indices.

Figure 6.5 shows calibration (2002 to 2006) and validation (2007 to 2010) results using SUFI-2 compared to the observed and simulated streamflow. These results confirm that the SWAT model was able to simulate streamflow relatively close to the observed values which is a fundamental criterion for SWAT watershed applications (Gassman et al., 2007; Strauch & Volk, 2013). The hydrographs show that the observed and simulated values have a noticeable difference in the plots. Additionally, the model slightly overestimated the low flow during the calibration and validation periods.

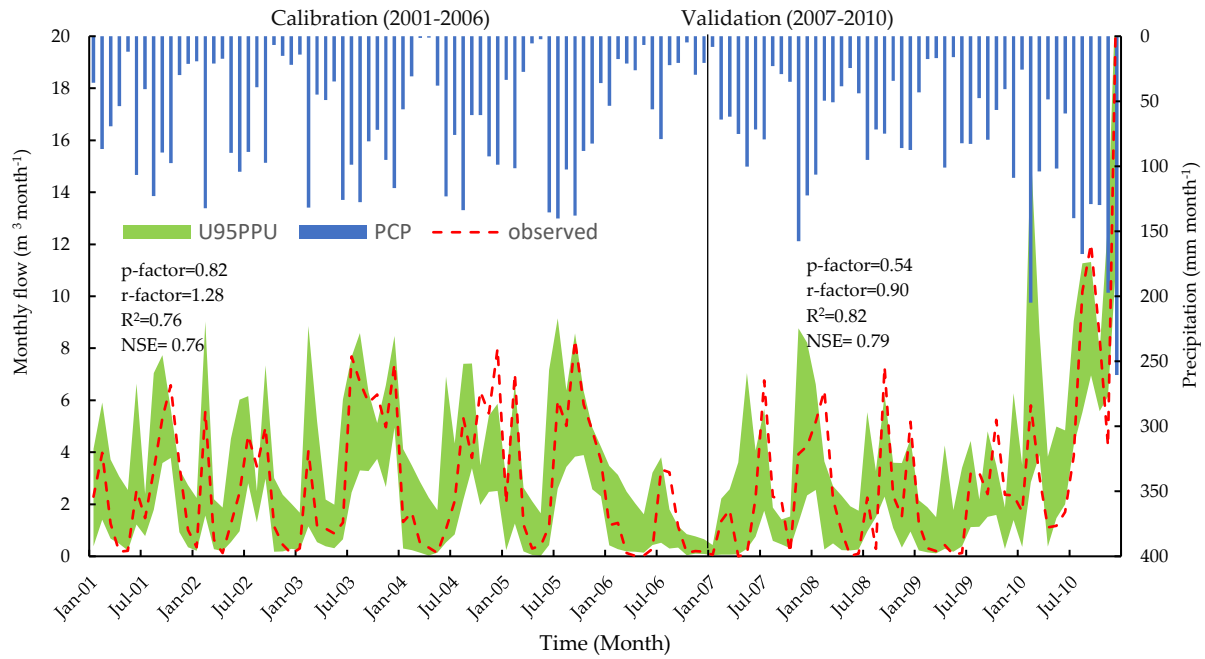


Figure 6.5: Calibration and validation results from SUFI-2 comparing observed and simulated streamflow from 2002 to 2006 and 2007 to 2010.

### 6.4.3. Analysis of the SWAT model calibration and validation against MODIS

#### LAI

In this study, a manual calibration was performed between SWAT simulated LAI and MODIS LAI. To do this, the MODIS LAI data was downsampled to match the basic calculation units of the SWAT model. The linear interpolation method was applied to segregate the 8-day MODIS LAI data into daily time series data and then aggregated to monthly data. Further the monthly average LAI was calculated for the entire watershed based on the downsampled and original MODIS LAI datasets. The two datasets had the same patterns of seasonal variations, where the LAI was highest in December and January and lowest in June. While for the original SWAT model, the LAI reaches the peak value in December. In almost every month, the original SWAT simulated value was noticeably higher than the remotely sensed LAI. Figure 6.6 shows the calibration and validation results between the SWAT LAI and MODIS LAI for ten years from 2001 to 2010.

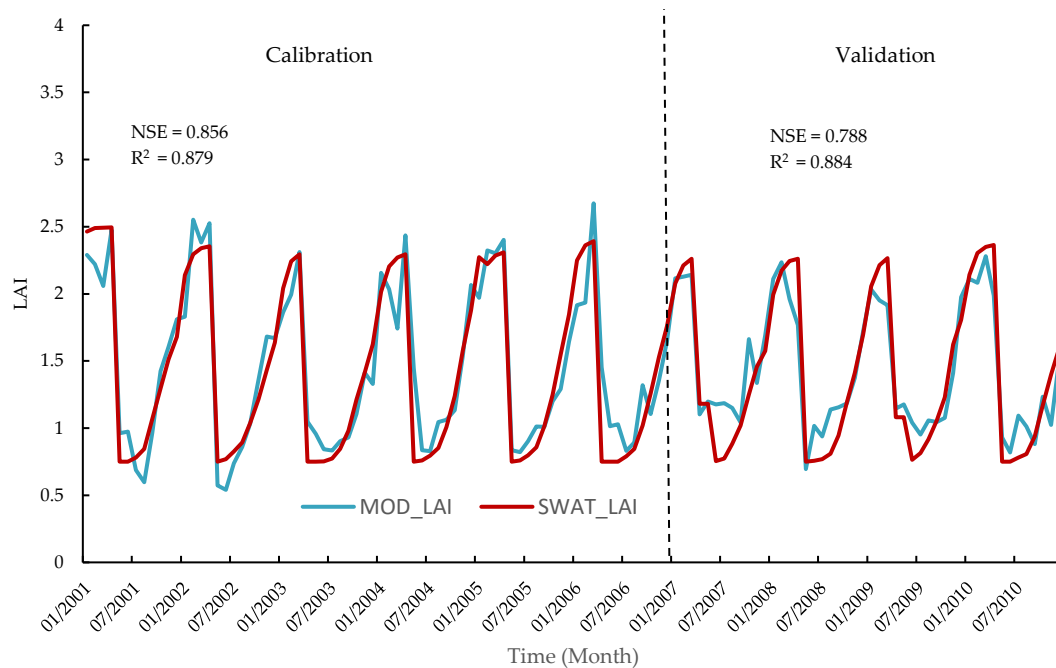


Figure 6.6: The calibration and validation of SWAT simulated LAI using remotely sensed MODIS LAI data. The calibration period from 2001 to 2006 and validation period 2007 to 2010.

#### **6.4.4. The outcomes of the trend analysis of the precipitation (historical and projected)**

In this study, a python script was created to calculate non-parametric Mann-Kendall trend test and Sen's slope to identify the trends and quantify the changes for GCMs projected future rainfall at the Burrinjuck sub-catchment. The trend analysis was consolidated into baseline (1980-2020), near (2031-2055), mid-century (2056-2075), and distant (2076-2100) periods of time spans. Table 6.3 shows that, except for MIROC5, the ACCESS1.0 and MK3.6 GCMs projected the annual rainfall with significant decrease by 1.96 to 2.51mm under RCP 8.5. Moreover, according to MK3.6, the autumn, and winter rainfall would also decrease significantly by 2.45mm, and 3.76mm respectively under the same climate scenario. However, the MIROC5 projections showed that the rainfall would increase during autumn, winter, and spring under RCP 4.5 and RCP 8.5 climate scenarios.

Table 6.3: Trend analysis of the precipitation for historical (1980-2020) and three GCM's predicted for future time span (2031-2055).

Model	Scenarios	Annual			Summer			Autumn			Winter			Spring		
		p	Zs	$\beta$	p	Zs	$\beta$	p	Zs	$\beta$	p	Zs	$\beta$	p	Zs	$\beta$
Historical	Baseline	0.098	-1.65	-5.94	0.451	0.75	0.35	0.645	-0.46	-0.185	<b>0.0172</b>	<b>-2.381</b>	<b>-1.089</b>	0.597	-0.527	-0.288
ACCESS1.0	RCP 4.5	0.194	-1.297	-1.326	0.440	-0.770	-0.175	0.050	-1.956	-0.164	0.251	1.145	0.135	0.282	-1.074	-0.188
ACCESS1.0	RCP 8.5	<b>0.0491</b>	<b>-1.967</b>	<b>-1.777</b>	0.795	-0.258	-0.0527	0.152	-1.429	-0.137	0.516	-0.648	-0.080	0.0515	-1.946	-0.255
MIROC5	RCP 4.5	0.737	-0.334	-0.482	0.090	-1.693	-0.334	0.298	1.039	0.137	0.594	0.532	0.100	0.715	0.365	0.067
MIROC5	RCP 8.5	0.116	1.571	2.203	0.605	0.517	0.095	0.114	1.576	0.192	0.167	1.378	0.196	0.437	0.775	0.185
MK3	RCP 4.5	0.130	-1.510	-1.128	0.411	-0.821	-0.116	0.155	-1.419	-0.081	<b>0.026</b>	<b>-2.225</b>	<b>-0.111</b>	0.405	-0.831	-0.102
MK3	RCP 8.5	<b>0.011</b>	<b>-2.51</b>	<b>-1.350</b>	0.863	0.172	0.016	<b>0.014</b>	<b>-2.453</b>	<b>-0.157</b>	<b>0.0001</b>	<b>-3.761</b>	<b>-0.189</b>	0.293	-1.049	-0.101

*p*-value (*p*) is a statistical measure; Z-score (Zs) is a standardized score;  $\beta$  (beta) represents the slope coefficient. The bold numbers are accepted values in the trend analysis.

#### 6.4.5. Analytical results of LAI responses to the future precipitation changes

Precipitation is another important climate variable that makes water available in the soil as soil water content for vegetation growth. To visualise the impacts of the precipitation, the average monthly precipitation was plotted against the SWAT simulated LAI in three different future time spans (Figure 6.7). The plotted results showed that winter and spring rainfall has positive impacts on LAI for all GCMs under both climate scenarios for future time spans. However, the LAI had a slight increase and lateral movement during summer and autumn where average rainfall was below 45 mm. Moreover, the simulated LAI for all GCMs under both scenarios, from February to April, was higher than the MODIS LAI in all three future time spans (Figure 6.8).

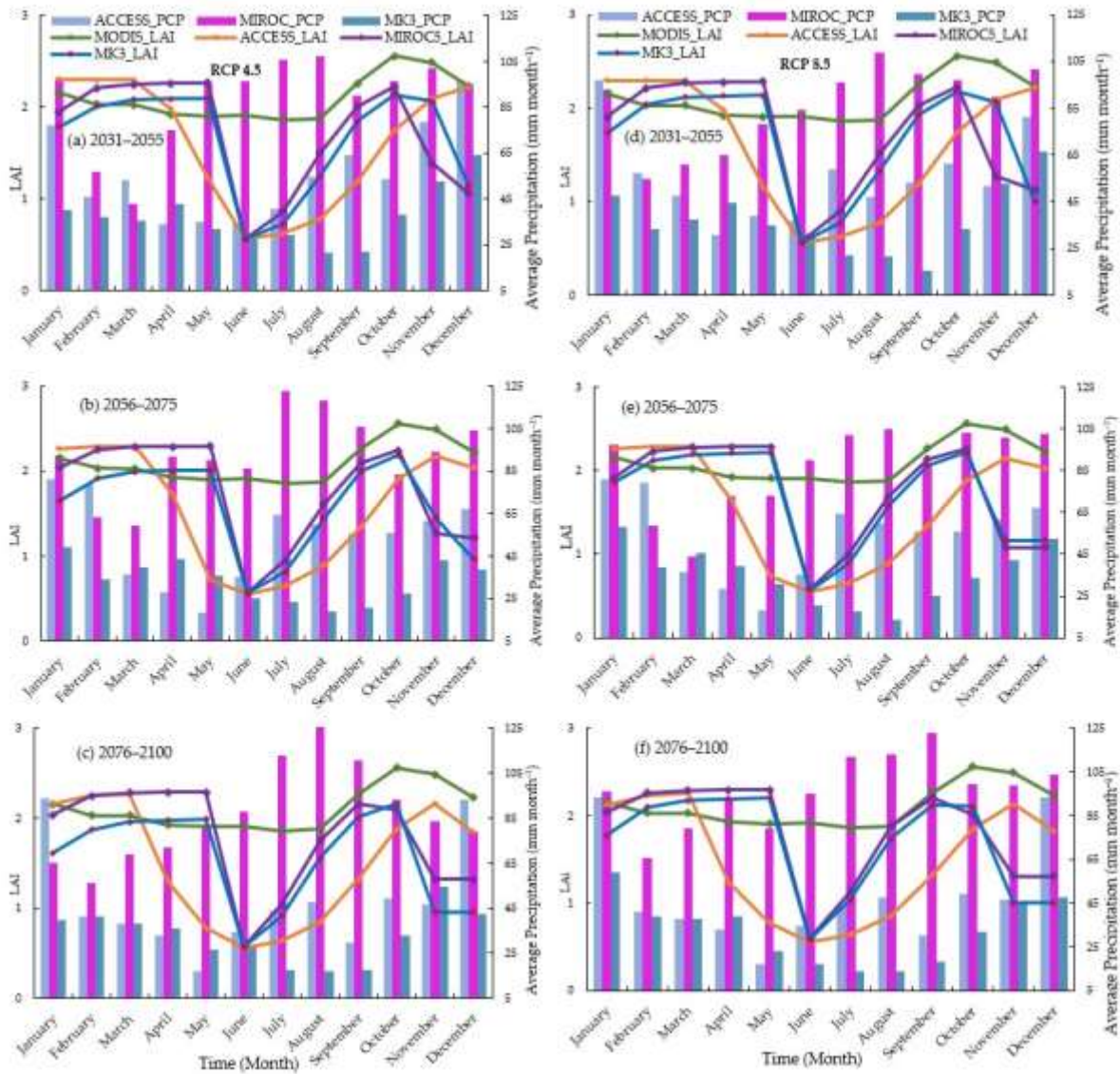


Figure 6.7: SWAT simulated LAI plotted against observed LAI (obtained from MODIS) and projected precipitation for the future time spans.

#### 6.4.6. Analytical results of LAI responses to future temperature changes

To understand vegetation responses to future climate variables, the SWAT simulated LAI values were analysed against GCMs projected temperatures (Figure 6.8). Considering ACCESS1.0 GCM projections, the simulated LAI decreased along with decrease in temperature from January to June in the future time spans under climate scenario RCP 4.5 and RCP 8.5. However, LAI increased from July to December when temperature was also increased in the study area under the same climate scenario (Figure 6.8). Further, the simulated LAI using MIROC5 and MK3.6 climate data, presented a positive increase from June to October and then decreased until December under both climate scenarios and for all the future time spans (Figure 6.8).

The SWAT simulated LAI data were analysed under two different future climate scenarios, RCP 4.5, and RCP 8.5, against MODIS LAI. In the analysis, the average MODIS LAI data from 2001 to 2020 was considered as benchmark to quantify the future LAI changes. The SWAT simulated LAI showed mostly a decreasing trend for all future time spans except January to April in 2031-2055, January to March in 2056-2075, and February to March in 2076-2100 according to ACCESS1.0. The highest LAI was increased according to ACCESS1.0 is 10.86% during the period of 2031-2055 (Table 6.4).

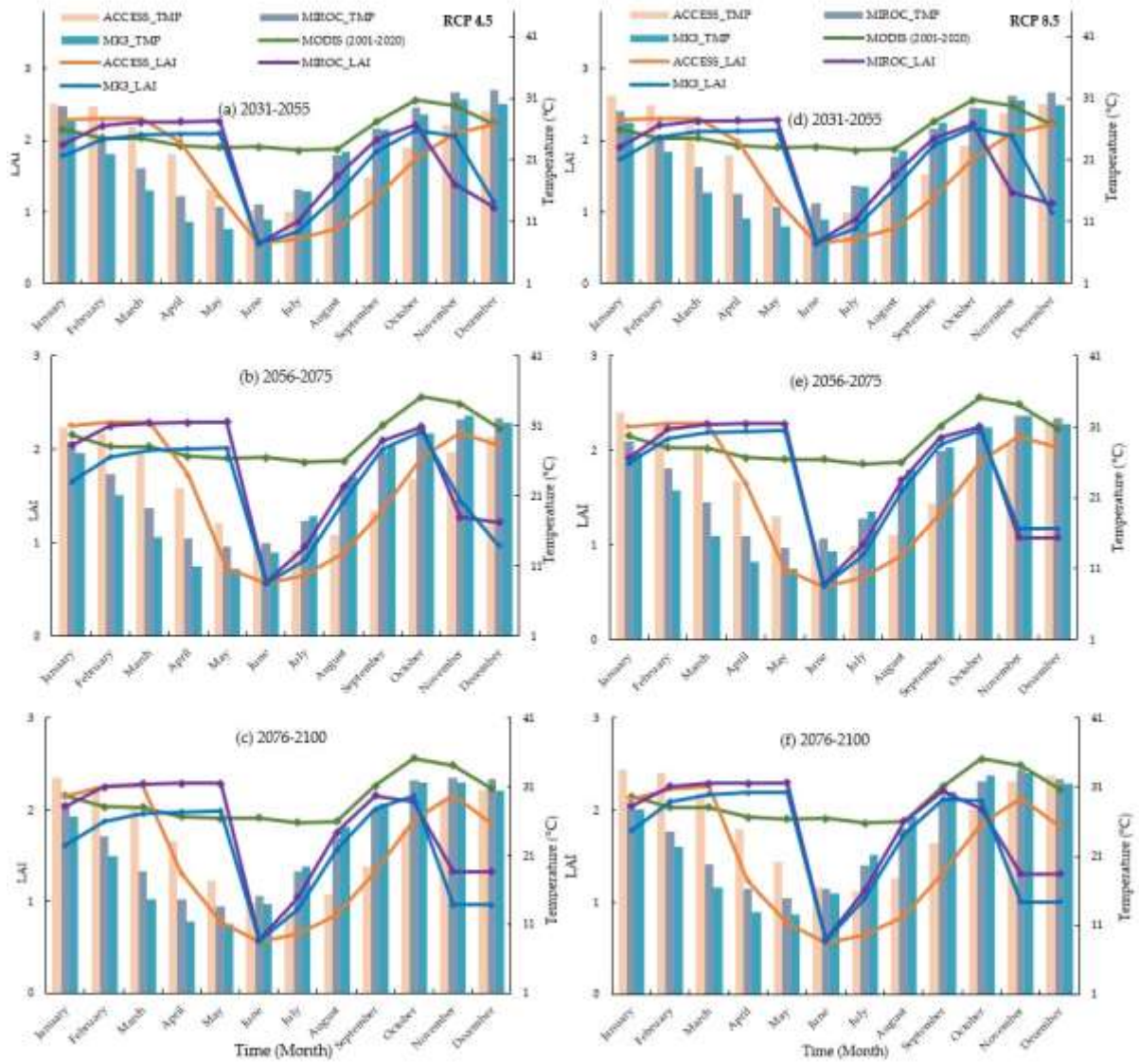


Figure 6.8: SWAT simulated LAI plotted against historical LAI and GCM projected average monthly temperature under climate scenario RCP 4.5 and RCP 8.5 for the future time spans.

Table 6.4: SWAT simulated LAI changes (percent of change compared to MODIS LAI data) listed against change of predicted temperature. The SWAT model was prepared using GCM's predicted climate data input under climate scenario RCP 4.5.

RCP 4.5	ACCESS1.0						MIROC5						MK3.6					
	2031-2055		2056-2075		2076-2100		2031-2055		2056-2075		2076-2100		2031-2055		2056-2075		2076-2100	
Month	TMP	LAI																
Jan	-2.33	5.75	-4.24	4.28	0.65	-0.01	-7.60	-9.70	-10.60	-5.03	-11.40	-5.26	-15.18	-18.63	-5.09	-27.36	-16.83	-29.96
Feb	1.28	10.72	1.07	10.23	5.05	8.79	-15.65	7.30	-18.46	9.02	-19.47	8.91	-26.12	-1.17	-8.39	-5.46	-29.41	-7.67
Mar	-2.03	10.86	0.39	10.56	2.79	9.74	-27.36	9.04	-28.64	10.30	-30.93	10.23	-40.43	2.35	-11.88	-1.66	-46.10	-3.25
Apr	-1.24	2.57	-0.20	-10.34	4.76	-41.26	-31.70	13.67	-32.17	14.69	-34.01	14.63	-50.34	7.38	-11.16	3.71	-48.69	2.47
May	1.60	-47.44	3.49	-127.57	5.00	-115.24	-18.57	14.59	-17.10	15.51	-17.73	15.47	-40.71	8.40	-5.92	4.93	-33.47	3.92
Jun	1.73	-179.24	3.73	-178.90	7.87	-178.40	5.44	-175.74	10.02	-173.46	16.53	-171.00	-12.70	-178.49	-0.10	-176.18	7.40	-175.25
Jul	2.18	-151.22	8.66	-141.16	6.99	-145.16	34.30	-93.97	43.01	-78.61	54.53	-65.92	31.36	-123.07	5.93	-102.43	59.80	-84.43
Aug	10.73	-112.95	11.86	-90.35	10.77	-97.87	57.91	-22.07	62.49	-14.96	71.83	-6.50	61.40	-43.48	10.07	-26.69	82.10	-18.03
Sep	4.09	-77.03	5.15	-59.58	7.63	-61.46	44.10	-11.59	51.63	-7.21	54.02	-4.39	43.37	-20.21	10.06	-11.80	58.29	-11.41
Oct	5.82	-41.77	6.55	-30.85	12.69	-32.69	33.91	-14.15	39.68	-12.92	45.29	-20.59	28.64	-18.15	8.01	-15.56	43.44	-17.28
Nov	8.71	-16.91	4.08	-13.08	10.81	-13.91	21.93	-68.93	21.73	-82.67	23.51	-76.21	17.34	-18.62	6.21	-62.77	20.49	-131.88
Dec	2.63	-0.28	0.69	-8.44	4.48	-18.89	10.24	-92.64	9.60	-71.44	9.65	-59.11	2.90	-81.69	2.22	-108.62	4.13	-109.38

In contrast to RCP 8.5, the simulated LAI generated from MIROC5 and MK3.6 data showed a downward trend starts in June. Moreover, a significant decrease was found in June by 179.24%, 175.74%, and 178.85% according to all three GCMs, respectively. Likewise, a decrease in LAI continued until December. However, an increasing trend was found in LAI from February to May under MIROC5 and MK3.6 projections (Table 6.4).

Table 6.5: SWAT simulated LAI changes listed against change of predicted temperature. The SWAT model was prepared using GCM's predicted climate data input under climate scenario RCP 8.5.

RCP 8.5	ACCESS1.0						MIROC5						MK3.6					
	2031-2055		2056-2075		2076-2100		2031-2055		2056-2075		2076-2100		2031-2055		2056-2075		2076-2100	
Month	TMP	LAI	TMP	LAI	TMP	LAI	TMP	LAI	TMP	LAI	TMP	LAI	TMP	LAI	TMP	LAI	TMP	LAI
Jan	-2.33	5.74	2.58	4.17	4.27	-1.66	-10.41	-11.61	-10.17	-11.15	-10.27	-4.85	-15.87	-21.39	-15.12	-13.88	-13.43	-19.01
Feb	1.28	10.72	4.92	10.19	11.92	8.22	-15.72	7.53	-14.72	8.04	-16.74	9.22	-24.51	0.26	-25.45	3.93	-24.11	2.69
Mar	-2.03	<b>10.86</b>	3.11	10.54	11.37	9.40	-26.83	9.74	-24.58	10.01	-26.53	10.46	-41.82	3.91	-42.13	6.78	-39.32	6.00
Apr	-1.24	2.57	5.89	-14.64	12.94	-48.29	-30.14	14.34	-29.54	14.52	-26.13	14.82	-47.69	9.02	-46.11	11.76	-41.52	11.14
May	1.60	-55.05	10.87	-123.86	21.65	-116.21	-19.24	<b>15.20</b>	-16.20	15.35	-10.17	15.62	-38.84	<b>9.98</b>	-33.55	12.74	-24.44	12.23
Jun	1.73	-179.24	14.60	-178.90	25.94	-178.40	7.03	-173.63	17.18	-170.02	24.93	-167.60	-12.14	-178.68	3.22	-175.93	19.64	-172.07
Jul	2.18	-151.22	17.47	-141.15	31.44	-145.16	38.47	-87.49	49.00	-71.39	61.35	-55.10	36.93	-112.26	56.50	-88.20	74.38	-66.14
Aug	10.73	-112.95	13.96	-90.34	28.94	-97.87	56.42	-20.58	67.21	-10.00	82.13	0.09	63.34	-35.35	80.62	-17.25	93.74	-7.42
Sep	4.09	-77.03	12.05	-59.77	26.94	-61.56	44.39	-10.66	53.47	-5.29	60.67	-2.14	49.85	-15.57	56.13	-8.82	67.78	-6.06
Oct	5.82	-42.05	11.12	-32.80	26.21	-34.91	33.46	-13.80	41.33	-12.54	44.87	-24.83	32.93	-16.03	40.77	-14.49	48.36	-19.93
Nov	8.71	-17.18	8.99	-14.26	21.70	-15.38	19.93	-82.56	24.39	-109.87	27.81	-78.43	16.89	-18.61	23.94	-96.43	25.89	-123.44
Dec	2.63	-0.38	8.45	-9.04	11.85	-19.91	8.82	-83.63	10.16	-89.50	10.17	-61.12	2.05	-102.91	7.18	-77.38	7.68	-101.76

#### 6.4.7. Trend analysis of LAI in the watershed (historical and simulated)

The Mann-Kendall trend test and Sen's slope were conducted to discover the trends in the SWAT simulated LAI for the future time spans under two climate scenarios RCP 4.5 and RCP 8.5. In this calculation, MODIS LAI data from 2002 to 2020 was considered as baseline including two climate scenarios for each climate model which were outlined in Table 6.6. The analysis showed a decreasing trend for MODIS LAI during summer and spring by 2.86 and 1.99, respectively. Similarly, according to MIROC5 and MK3.6 climate projections, SWAT simulated LAI increased in winter by 1.99 (mm), 2.59 (mm), 2.31 (mm), and 2.09 (mm) respectively, under both climate scenarios. However, the results also showed the LAI decreases during spring by 2.17 (mm) according to MIROC5 under RCP 4.5; and 3.17 (mm), and 2.29 (mm) according to MK3.6 under RCP 4.5 and RCP 8.5, respectively.

Table 6.6: Trend analysis of the MODIS LAI (2002-2020) and three GCM's predicted climate variables induced SWAT simulated LAI for future time span (2031-2055).

Model	Scenarios	Annual			Summer			Autumn			Winter			Spring		
		p	Zs	β	p	Zs	β	p	Zs	β	p	Zs	β	p	Zs	β
MODIS	Baseline	0.888	-0.139	-0.0005	<b>0.004</b>	-2.868	-0.009	0.833	0.209	0.008	0.420	-0.805	-0.0008	<b>0.045</b>	-1.995	-0.005
ACCESS1.0	RCP 4.5	0.17	-1.35	-0.005	0.070	-1.805	-0.004	0.128	-1.518	-0.013	0.906	0.117	0.0	0.261	-1.123	-0.002
ACCESS1.0	RCP 8.5	0.350	-0.934	-0.004	0.083	-1.728	-0.003	0.233	-1.191	-0.007	0.888	0.140	0.0002	0.981	0.023	6.666
MIROC5	RCP 4.5	<b>0.029</b>	-2.175	-0.007	0.052	-1.938	-0.015	<b>0.015</b>	-2.416	-0.001	<b>0.045</b>	1.996	0.002	<b>0.029</b>	-2.175	-0.012
MIROC5	RCP 8.5	0.907	0.116	0.0003	0.925	0.093	0.0007	0.522	0.638	7.291	<b>0.009</b>	2.593	0.004	0.797	-0.256	-0.001
MK3	RCP 4.5	0.440	-0.770	-0.003	0.833	0.210	0.003	0.725	-0.350	-0.001	<b>0.020</b>	2.312	0.003	<b>0.001</b>	-3.177	-0.007
MK3	RCP 8.5	0.605	0.516	0.001	0.386	0.865	0.005	0.637	0.471	0.0013	<b>0.035</b>	2.097	0.002	<b>0.021</b>	-2.297	-0.004

p-value (p) is a statistical measure; Z-score (Zs) is a standardized score; β (beta) represents the slope coefficient.

#### 6.4.8. Analysis of the floodplain vegetation responses to the SWAT variables

In this study, the vegetation responses to SWAT simulated variables were analysed using LAI changes (%) in relation to soil water content (SW), surface water flow (SURQ) and ground water flow (GW). The LAI increases from 0.16% to 58.13% by ACCESS1.0, 0.35% to 136.05% by MIROC5, and 0.87% to 84.92% according to MK3.6 (Table 6.7). However, SW data showed a decreasing trend for all the future time spans according to ACCESS1.0. The highest decrease for SW was identified in the month of May according to ACCESS1.0 during mid future time span (2056-2075). According to MIROC5, the SW shows positive values from January to May during 2031-2055, and 2056-2075. Among these future time spans, the highest SW increased by 24.84% and 42.14% under RCP 4.5 and RCP 8.5, respectively.

Table 6.7: The LAI changes in response to Soil Water Content (SW) that are simulated using climate data predicted from three different GCMs under RCP 4.5.

RCP 4.5	ACCESS1.0						MIROC5						MK3.6					
	2031-2055		2056-2075		2076-2100		2031-2055		2056-2075		2076-2100		2031-2055		2056-2075		2076-2100	
	SW	LAI	SW	LAI	SW	LAI	SW	LAI	SW	LAI	SW	LAI	SW	LAI	SW	LAI	SW	LAI
Jan	-3.15	<b>-9.79</b>	-11.77	-11.12	-10.56	-19.21	<b>24.843</b>	-30.903	21.48	-23.01	3.93	-23.36	-43.18	-38.79	-45.21	-38.28	-48.67	-39.70
Feb	-21.74	-8.26	-18.82	-9.72	-30.89	-17.45	11.625	-26.192	13.59	-18.84	-2.10	-19.95	-42.73	-36.41	-46.08	-35.72	-43.86	-37.10
Mar	-25.29	-7.63	-31.72	-9.24	-38.09	-16.99	10.644	-24.259	14.40	-16.94	9.04	-18.13	-35.91	-35.20	-35.77	-34.94	-37.07	-36.11
Apr	-30.72	6.27	-36.71	-6.07	-40.34	-29.58	11.429	0.351	17.26	9.92	7.20	8.21	-31.34	-15.13	-29.35	-14.76	-35.99	-16.05
May	-33.80	<b>58.13</b>	<b>-43.72</b>	1.54	-42.17	3.45	1.384	<b>118.855</b>	4.60	<b>139.59</b>	-3.38	<b>136.05</b>	-37.17	<b>83.79</b>	-34.41	<b>84.92</b>	-42.46	<b>82.58</b>
Jun	-35.26	-0.17	-41.61	-0.05	-39.82	0.16	-4.957	1.116	-3.21	1.92	-9.98	2.57	-40.29	-0.01	-39.01	0.77	-44.23	0.87
Jul	-30.19	2.11	-30.31	6.30	-30.64	4.04	-0.035	19.251	2.06	26.36	-5.61	30.15	-36.65	9.06	-37.49	15.38	-43.37	20.05
Aug	-26.02	4.88	-25.80	13.69	-27.63	9.69	-1.383	42.078	-0.06	52.87	-7.16	58.75	-38.75	24.52	-41.01	36.45	-47.69	43.36
Sep	-20.58	5.33	-22.56	<b>15.00</b>	-23.44	<b>10.72</b>	-5.687	44.928	-4.46	56.47	-11.39	58.93	-43.14	27.69	-47.38	40.40	-55.38	42.95
Oct	-18.18	3.55	-20.48	13.21	-21.58	8.72	-11.156	32.033	-15.05	40.55	-20.00	33.68	-46.43	17.21	-54.46	26.23	-61.42	26.72
Nov	-18.98	-1.77	-26.03	4.49	-27.37	1.68	-15.381	-21.487	-20.30	-23.51	-24.63	-21.40	-52.99	-2.12	-60.19	-18.92	-61.52	-38.61
Dec	-12.39	-5.80	-23.53	-9.68	-20.48	-18.90	-2.495	-43.948	-4.23	-36.20	-15.35	-31.46	-48.48	-43.74	-59.77	-46.14	-57.58	-46.47

Another SWAT variable, the surface water flow (SURQ) was decreased for all the future time spans according to GCMs projected data driven simulations under both climate scenarios RCP 4.5 (Table 6.8) and RCP 8.5 (Appendix A). Despite of the SURQ decrease, the LAI increased from May to August and the maximum LAI increase identified by 118.85% according to MIROC5 projections during 2031-2055. However, for same future time span, the SURQ decreased by 65.5% under same projection and climate scenario.

Table 6.8: The LAI changes in response to surface water flow (SURQ) that are simulated using climate data predicted from three different GCMs under RCP 4.5.

RCP 4.5	ACCESS1.0						MIROC5						MK3.6					
	2031-2055		2056-2075		2076-2100		2031-2055		2056-2075		2076-2100		2031-2055		2056-2075		2076-2100	
	SURQ	LAI	SURQ	LAI	SURQ	LAI	SURQ	LAI	SURQ	LAI	SURQ	LAI	SURQ	LAI	SURQ	LAI	SURQ	LAI
Month	SURQ	LAI	SURQ	LAI	SURQ	LAI	SURQ	LAI	SURQ	LAI	SURQ	LAI	SURQ	LAI	SURQ	LAI	SURQ	LAI
Jan	-61.86	-9.79	-61.96	-11.12	-68.76	-19.21	-43.818	-30.903	-29.91	-23.01	-83.55	-23.36	-99.69	-38.79	-98.07	-38.28	-98.43	-39.70
Feb	-98.49	-8.26	-79.54	-9.72	-98.32	-17.45	-96.572	-26.192	-92.94	-18.84	-93.51	-19.95	-99.45	-36.41	-100.00	-35.72	-99.67	-37.10
Mar	-96.11	-7.63	-98.53	-9.24	-99.83	-16.99	-99.598	-24.259	-92.82	-16.94	-92.33	-18.13	-99.92	-35.20	-99.99	-34.94	-99.88	-36.11
Apr	-91.65	6.27	-99.49	-6.07	-98.92	-29.58	-78.923	0.351	-36.80	9.92	-53.73	8.21	-96.91	-15.13	-99.23	-14.76	-97.43	-16.05
May	-97.17	<b>58.13</b>	-99.82	1.54	-99.75	3.45	-65.573	<b>118.855</b>	-60.07	<b>139.59</b>	-82.86	<b>136.05</b>	-99.59	<b>83.79</b>	-98.15	<b>84.92</b>	-100.00	<b>82.58</b>
Jun	-98.85	-0.17	-97.00	-0.05	-93.39	0.16	-89.441	1.116	-93.53	1.92	-92.00	2.57	-99.53	-0.01	-99.73	0.77	-99.82	0.87
Jul	-96.13	2.11	-91.99	6.30	-87.68	4.04	-75.510	19.251	-66.38	26.36	-74.69	30.15	-99.43	9.06	-99.73	15.38	-99.72	20.05
Aug	-94.93	4.88	-90.22	13.69	-95.21	9.69	-46.746	42.078	-16.88	52.87	-46.56	58.75	-99.25	24.52	-98.98	36.45	-99.80	43.36
Sep	-91.34	5.33	-87.05	15.00	-92.50	10.72	-76.029	44.928	-64.02	56.47	-59.17	58.93	-99.87	27.69	-99.28	40.40	-99.97	42.95
Oct	-86.32	3.55	-88.73	13.21	-89.33	8.72	-39.123	32.033	-74.39	40.55	-74.01	33.68	-95.89	17.21	-99.74	26.23	-99.68	26.72
Nov	-90.78	-1.77	-94.86	4.49	-93.70	1.68	-81.702	-21.487	-85.46	-23.51	-91.84	-21.40	-98.90	-2.12	-99.07	-18.92	-99.11	-38.61
Dec	-83.27	-5.80	-90.10	-9.68	-90.20	-18.90	-83.234	-43.948	-78.58	-36.20	-92.54	-31.46	-97.69	-43.74	-100.00	-46.14	-99.45	-46.47

In the study site, the groundwater flow seems to show a decreasing trend in the SWAT simulation while running the model using GCMs projected climate variables as input data. The simulation results show that the maximum GW increase occurs while running model with MIROC5 climate data. The highest increase of GW by 143.29% that triggers an LAI increase by 139.59% in 2056-2075 future time span (Table 6.9). Likewise, these increasing trends are also identified in the months from April to June according to MIROC5 under climate scenario RCP 8.5. The analysis indicates that there will be a significant rise in GW, amounting to a staggering 184.04%, resulting in a corresponding surge of 151.95% in LAI during the period of 2076-2100. (Appendix B).

Table 6.9: The LAI changes in response to groundwater flow (GW) that are simulated using climate data predicted from three different GCMs under RCP 4.5.

RCP 4.5	ACCESS1.0						MIROC5						MK3.6					
	2031-2055		2056-2075		2076-2100		2031-2055		2056-2075		2076-2100		2031-2055		2056-2075		2076-2100	
	Month	GW	LAI	GW	LAI	GW	LAI	GW	LAI	GW	LAI	GW	LAI	GW	LAI	GW	LAI	GW
Jan	-30.13	-9.79	-72.68	-11.12	-71.04	-19.21	-52.175	-30.903	-46.75	-23.01	-70.68	-23.36	-95.34	-38.79	-99.89	-38.28	-99.63	-39.70
Feb	0.86	-8.26	-56.24	-9.72	-50.47	-17.45	-1.657	-26.192	13.32	-18.84	-47.87	-19.95	-94.17	-36.41	-99.75	-35.72	-99.23	-37.10
Mar	-49.63	-7.63	-54.10	-9.24	-60.86	-16.99	0.301	-24.259	24.10	-16.94	-26.00	-18.13	-92.40	-35.20	-99.76	-34.94	-99.39	-36.11
Apr	-71.31	6.27	-73.99	-6.07	-83.73	-29.58	-4.696	0.351	52.63	9.92	15.20	8.21	-90.27	-15.13	-99.33	-14.76	-99.30	-16.05
May	-69.30	58.13	-86.05	1.54	-91.36	3.45	90.456	118.855	143.29	139.59	93.34	136.05	-76.39	83.79	-97.83	84.92	-98.59	82.58
Jun	-79.40	-0.17	-93.77	-0.05	-92.16	0.16	52.229	1.116	55.78	1.92	35.51	2.57	-81.84	-0.01	-95.27	0.77	-99.15	0.87
Jul	-85.39	2.11	-91.66	6.30	-86.31	4.04	-19.274	19.251	-19.82	26.36	-27.44	30.15	-91.40	9.06	-96.45	15.38	-99.48	20.05
Aug	-83.39	4.88	-83.44	13.69	-81.19	9.69	-38.299	42.078	-36.89	52.87	-37.84	58.75	-94.88	24.52	-96.46	36.45	-99.67	43.36
Sep	-77.86	5.33	-78.22	15.00	-78.94	10.72	-46.619	44.928	-45.60	56.47	-44.63	58.93	-97.18	27.69	-97.02	40.40	-99.85	42.95
Oct	-71.10	3.55	-74.52	13.21	-75.41	8.72	-54.957	32.033	-53.90	40.55	-54.73	33.68	-97.36	17.21	-98.76	26.23	-99.95	26.72
Nov	-64.45	-1.77	-70.02	4.49	-70.91	1.68	-57.690	-21.487	-61.83	-23.51	-63.43	-21.40	-96.56	-2.12	-99.88	-18.92	-99.66	-38.61
Dec	-59.98	-5.80	-70.27	-9.68	-72.24	-18.90	-60.065	-43.948	-67.54	-36.20	-74.86	-31.46	-96.45	-43.74	-99.90	-46.14	-98.13	-46.47

## 6.5. Discussion

### 6.5.1. Future climate variables impact on vegetation LAI

This study highlights the following insights of the floodplain vegetation and climate change correlations: i) the climate variables that are tested for, i.e., rainfall and temperature, determine the vegetation greenness LAI which is a surrogate for ecosystem health; and ii) available catchment water added from precipitation and suitable plant growth temperature are primarily responsible for the spatial heterogeneity in response measured by standard deviation of LAI.

The main factor, i.e., precipitation, is limiting the vegetation growth and development in arid and semi-arid areas around the world. Based on the statement, it can be inferred that the growth and development of plants, as well as their greenness, are greatly influenced by the availability of water. This factor appears to have a greater impact than any other factors. Previous studies which outlined this vegetation behaviour is true for different ecosystems such as permanent or semi-permanent floodplain and terrestrial ecosystems (Wen et al., 2012).

The other important factor in vegetation growth is atmospheric temperature, as plants use it for photosynthesis. The minimum and maximum daily temperatures are more important than annual mean temperature, due to direct effects on vegetation growth (Zhang et al., 2006). This study demonstrated that both rainfall and temperature were significantly related to vegetation greenness measured as LAI. However, variation in rainfall during winter and spring were likely to have closer and larger corresponding effect on vegetation growth as suggested

by the SWAT model (Figure 6.7), which is in accordance with results in previous studies (Li et al., 2018). The degree of temporal variations between LAI and precipitation suggests that floodplain vegetations in semi-arid regions may be very sensitive to changes in rainfall patterns at a regional level. Therefore, climate change, which was predicted to induce reduction in precipitation for most of Southeast Australia including the Burrinjuck sub-Catchment (Wen et al., 2012), is anticipated to yield significant consequences for the vegetation greenness of the ecosystem. However, the estimation of climate change impacts on the floodplain vegetation should not be limited solely to hydrological effects, given the direct relationship between vegetation greenness and climatic conditions.

This study identified a decreasing trend in LAI during winter months such as June and July, despite of increasing temperature in these months. Generally, the climate models show a decrease in winter rainfall in the Burrinjuck sub-catchment of the Murrumbidgee River catchment. Likewise, the trend analysis of LAI reveals that the decreasing trend of annual LAI is statistically significant at Burrinjuck floodplain area during 2031–2055 and 2056–2075 under the RCP 4.5 scenario. These results align with a previous study which concluded that vegetation productivity shifts under climate change (Ma et al., 2015). The first objective of this study to understand future climate change impacts on vegetation growth is thus successfully addressed. Previous studies have found a strong correlation between climate change and vegetation LAI (Guli-Jiapaer et al., 2015; Zheng et al., 2021).

### **6.5.2. Seasonal variability in climate change vegetation responses**

In the seasonal domain, the vegetation greenness increases in the spring after the wet season in the study area. Considering precipitation is the only source of soil water in the study area, the average SWC, SURQ, and GW values increased by 52%, 16%, 92%, and 39%, 13%, 148% respectively, during the winter and spring. However, the MODIS LAI analysis shows that the average winter LAI decreased by 10.9% and increased by 12.7% compared to summer LAI. The outcome suggests that the highest temperature for the initiation of vegetation growth occurs during the spring season, while it remains lower during the winter months. During the wet season, the average temperature in the Burrinjuck sub-catchment area is 21.8°C (average from 1980 to 2020), while the average in winter is 13.26°C, which inversely impacts vegetation growth in winter season (He et al., 2017; Huang et al., 2019). However, the average temperature reaches 21.6°C in the spring months that possibly triggers vegetation growth with the help of soil water and groundwater which has already increased during winter rainfall. Therefore, the

vegetation greenness has increased by 12.7% in the spring season when compared to the dry season.

Similarly, vegetation response relationships were analysed against soil water content (SW), surface runoff (SURQ) and groundwater flow (GW) during the dry season for the GCMs climate projections. The vegetation LAI (including all vegetation in the sub-basin) decreased by 65% and 24% during winter and spring seasons, whereas SW and GW decreased by 32% and 82% in winter, and 19% and 71% in spring. The results presented herein demonstrate a strong correlation between soil water and groundwater levels and the responsiveness of vegetation Leaf Area Index (LAI). Previous studies support these findings considering different area of interests (Smettem et al., 2013; He et al., 2017; Huang et al., 2019). This means vegetation can grow well when SWC and groundwater flow has increased after the rainfall in spring and summer seasons. Moreover, this study suggests that vegetation is highly dependent on groundwater during the dry season for their greenness, and any instability or long-term drought can directly affect this floodplain vegetation. The future projections for the Burrinjuck sub-catchment of the Murrumbidgee catchment indicate a decrease in SW, SURQ, and GW based on the climate projections of MIROC5 and MK3.6, as well as the simulated results from SWAT. The future projections for the Burrinjuck sub-catchment of the Murrumbidgee catchment indicate a decrease in SW, SURQ, and GW based on the climate projections of MIROC5 and MK3.6, as well as the simulated results from SWAT. Both climate scenarios RCP 4.5 and RCP 8.5 induced climate change data indicated a warmer future climate with less precipitation for this region. A comprehensive documentation of vegetation and hydrological variables relationships can be prepared for floodplain vegetation management based on the findings in this study.

### ***6.5.3. Vegetation responses to SWAT simulated variables under future climate changes***

This study presents a robust analysis of the relationships between groundwater availability and vegetation responses vigour in the floodplain zone. The SWAT model simulated several hydrological variables in the process of catchment water modelling by calculating a range of basin characteristics and meteorological datasets, which were analysed in relation to vegetation LAI.

Among these SWAT simulated hydrological variables, surface runoff (SURQ) shows a decreasing trend for all three GCMs under two climate scenarios RCP 4.5 and RCP 8.5. The maximum decrease of surface runoff observed were 99.83%, 99.59%, and 100% according to

ACCESS1.0 (2056-2075), MIROC5 (2031-2055), and MK3.6 (2076-2100) respectively, between the month of March and June. The result shows that this runoff reduction is inversely proportionate to the vegetation greenness. The LAI has increased by 58.13% in May during 2031-2055 under ACCESS1.0 climate predictions. A previous study also mentioned that vegetation growth has positively responded to runoff reduction (Shi et al., 2022). Before the analysis, the SWAT model was calibrated and validated with the NSE value 0.79 and 0.76, respectively. These NSE values reflect the model performance can be evaluated as 'very good' for both calibration and validation. A hydrological study in the neighbouring catchment area also documented similar NSE values for SWAT modelling (Saha et al., 2014).

This study found that the simulated variables (SW and GW) and vegetation LAI relationships vary with climate predictions when applied data from the different climate model. The SW decreases from January to December when ACCESS1.0 and MK3 climate predictions were applied for all the future time spans. These decreases vary from 3.15% to 43.72% and 31.34% to 61.52% when considered ACCESS1.0 and MK3.6, respectively. However, SW increases from January to May when model was simulated using MIROC5 climate predictions.

Likewise, GW decreased in most of the months when model was simulated using future climate change projections under two climate scenarios RCP 4.5 and RCP 8.5. The maximum decrease found from June to August for all three GCMs means that GW decreases mostly in the winter season. An exception, MIROC5 projected climate data simulation result shows GW increased between February and June in the 2056-2075 future time span. However, the LAI increased between July and October when simulation was completed using ACCESS1.0 and MK3.6. A warmer climate can be utilised for agricultural production in similar regions around the world by selecting appropriate crops based on their seasonal response to soil water and groundwater.

## **6.6. Conclusion**

The study area Burrinjuck sub-catchment contributes approximately 24% of the total rainfall as runoff to the Murrumbidgee River flow, which is one of the main contributors in the Murray Darling Basin (MDB). Any changes in these rainfall-runoff relationships can cause a major impact on the environment as well as the economy. Understanding future vegetation growth under predicted climate alterations is crucial for developing effective water management policies and climate change mitigation strategies for floodplains and ecosystems.

This study demonstrated that precipitation and temperature were the two primary climatic drivers that impact vegetation growth in the Burrinjuck sub-catchment. Additionally, the analytical results show that the vegetation growth (LAI) is highly responsive to groundwater during the dry season in the study area. The results of this study show that climate change will continue to exert profound effects on vegetation. Further, the results disclosed that the relationship between floodplain vegetation and climate change is two-way, and any change in the climate can directly influence the vegetation growth. For example, the suitable temperature for plant growth (may vary for different plant types) and available soil water can boost vegetation growth which, in turn, contributes to increase in the transpiration rate. Moreover, the grass type vegetation growth helps to increase the infiltration and groundwater recharge.

In this research, the SWAT simulation results suggested that rainfall dominates the Burrinjuck sub-catchment water balance, in which soil water and groundwater flow increase in the wetting period between April and September. The LAI values from the hydrological modelling suggest that changes in soil water, surface water flow, and groundwater in the basin area directly impact vegetation growth conditions. As rainfall dominates the catchment hydrology, future changes in the rainfall pattern may need to be considered for floodplain management. Overall, this study generates valuable contributions to the general understanding of the intricate relationships between climate change and its impact on floodplain vegetation dynamics. In contrast to simply analysing seasonal rainfall variations, this study developed a novel methodology for modelling this relationship. This research findings hold the potential to significantly bolster the development of sustainable floodplain vegetation systems in arid regions, where adverse climate condition is a constant concern. Furthermore, this study offers an impartial assessment of floodplain vegetation greenness, as measured by Leaf Area Index (LAI), and its responses to climate change. These findings carry substantial scientific significance, particularly in the context of enhancing floodplain management within the Burrinjuck sub-catchment.

In addition to shedding light on these critical relationships, this research paves the way for further investigations into other climatic factors, such as evaporation and humidity. This study has integrated vegetation growth responses with variables related to soil water, surface water flow, and groundwater under projected future climatic conditions. It is worth noting that future studies can expand upon this work by incorporating additional factors, including different vegetation types and their respective water requirements. Moreover, this study encourages future research efforts to refine the SWAT modelling results by incorporating more

comprehensive data related to vegetation growth factors, building upon the methodological contributions made in this study. This multifaceted approach will contribute to a more holistic understanding of the intricate interactions between climate change and floodplain vegetation dynamics, ultimately advancing the ability to develop sustainable management strategies in these vulnerable ecosystems.

## CHAPTER 7: CONCLUSION

### 7.1. Introduction

The primary objective of this research was to explore the efficacy of remotely sensed vegetation indices in predicting the impact of climate change on floodplain vegetation in a temperate zone. The study focused on vegetation types for which there was limited knowledge and aimed to answer several research questions. These questions centred on identifying plant types that are more responsive to changes in surface water and groundwater levels, as well as their proximity to water outlets within hydrological response units (HRUs). Additionally, the study examined the hydro-climatic relationships at both local and regional scales. The study was divided into three objectives, as listed in Chapter 1, each objective has been addressed in Chapters 4 to 6, in order to accomplish this goal.

To accomplish these objectives, a comprehensive literature review was performed to ascertain the crucial global factors influencing vegetation response to climate change. Throughout this extensive review, the key observations were identified, the reliability and comprehensiveness of vegetation modelling using remotely sensed data, particularly about different vegetation types. These aspects formed the central focus of the subsequent sections of the thesis, which also incorporated catchment hydrological modelling in the southeast region of Australia. The investigation employed remote-sensing metrics to analyse vegetation response to water availability under projected climate scenarios.

The purpose of this chapter is to summarise the key findings and conclusions that address the research questions of the study. The chapter outlines the outcomes produced from the five stages of research conducted, discusses the limitations, and makes suggestions for future research. Finally, the implications of this study and its broader contributions to the field are also examined. This study was the first to assess the floodplain vegetation and their proximity to the stream flow and their relationships to catchment water availability under future climate scenarios. It also covered, for the first time the investigation of the vegetation types (e.g., grass, shrub, and tree) in the floodplain, considering their location in the watershed. The study was also the first to apply machine learning algorithms to model the observed and predicted NDVI and also the premier to calibrate the SWAT model using MODIS imagery data for LAI in floodplain areas.

This Chapter presents the findings and overall conclusion of the Dissertation, along with suggestions for further investigations. It is divided into four parts: Section 7.2 outlines the findings, Section 7.3 presents the overall conclusion and significant contributions of the study, and Section 7.4 concludes with recommendations for future research.

## **7.2. Summary of findings**

This study provided new knowledge and insights on vegetation responses to different climate scenarios by utilising remotely sensed vegetation indices and hydrological modelling through empirical study. This was accomplished using the triad approach of floodplain hydrological modelling techniques in conjunction with novel application of machine learning algorithms and GIS-based techniques, which have never been applied in previous floodplain vegetation studies.

### ***7.2.1. Modelling floodplain vegetation responses to surface water availability***

The surface water availability at the catchment level was quantified through hydrological modelling using the SIMHYD hydrological model. Machine learning algorithms were employed to correlate vegetation responses to surface water availability by utilising remotely sensed vegetation indices, as discussed in Chapter 4. Climate change can significantly impact precipitation patterns, leading to more intense rainfall events or prolonged droughts in certain regions. Floodplains, being sensitive to changes in water levels, are particularly vulnerable. Increased flooding can drown vegetation, while extended droughts can lead to desiccation and die-off of plants. This altered hydrology disrupts the delicate balance of floodplain ecosystems. This study successfully identified the direct and indirect climatic impacts, specifically the effects of extreme rainfall and drought on vegetation growth. These findings addressed the first objective of the research study and served as a fundamental basis for achieving the subsequent objectives. The key findings of the first objective are summarised below.

The analytical work presented in Chapter 4 (Objective 1) revealed a subset of crucial factors connecting vegetation responses to surface water availability and related climatic changes. These factors encompassed various vegetation types and their reactions in dry and wet conditions, their proximity to stream flow, leaf area, and plant height (categorised by tree, shrub, and grass). During the wet season, grass-type vegetation located far from the stream was

highly correlated with rainfall, while similar vegetation types near the stream were less responsive to rainfall. Furthermore, deep-rooted vegetation such as trees and shrubs near the stream were highly correlated with surface runoff water and streamflow than rainfall. Under reduced precipitation, deep-rooted vegetation types such as trees and shrubs were consistent across floodplains. Other factors linked to climate variables, such as maximum and minimum temperature, relative humidity, wind speed, and solar radiation, require additional data to be included. However, existing studies suggest that under increased temperature, both tree and shrub vegetation types can survive with less rainfall. Under increased rainfall frequency or intensity, grass-type vegetation has growing ability with positive responses.

### ***7.2.2. Modelling floodplain vegetation responses to groundwater variability***

To investigate this research objective, this study employed a process-based ecohydrological river basin model, SWAT hydrological model at the study catchment using remotely sensed vegetation indices (NDVI) and climate variables data presented in Chapter 5. The analytical results highlight the significant correlation between the vegetation system and groundwater hydrology, with a particular emphasis on the substantial reliance on groundwater hydrology in the arid season. The second objective of the research study was effectively addressed by these findings, which laid a crucial foundation for accomplishing the subsequent objectives. Below, the summarised key findings of the second objective are presented.

The robust analysis presented in Chapter 5 (Objective 2) identified crucial findings that establish a reciprocal relationship between floodplain vegetation and groundwater hydrology, whereby changes in the surrounding environment can directly influence the vegetation's reaction to groundwater. Suitable temperature and sufficient water availability can enhance the growth of vegetation, thereby leading to an increase in the potential evapotranspiration rate. Conversely, the growth of grass-type vegetation aids in the augmentation of infiltration. The hydrological simulation findings indicate that rainfall plays a dominant role in the water balance of the study area catchment, with groundwater flow intensifying during the wetting period from April to September. Any changes in the groundwater condition within the basin region can directly impact the state of vegetation. The machine learning data-driven analytics also revealed plant NDVI and SWAT simulated hydrological variables relationships vary with vegetation types. This study also found grass-type vegetation has high correlation to groundwater flow (GW) compared to tree and shrub vegetation. In contrast to basin elevation,

vegetation located in the top point (highland) has high correlation to GW (increased by 42%) than vegetation located in the bottom point (low land).

### **7.2.3. Modelling floodplain vegetation responses to future climate change**

Floodplain vegetation is adapted to specific hydrological conditions. As climate change alters these conditions, certain species may thrive while others decline or disappear. For example, species that are adapted to more frequent flooding may struggle in drier conditions, leading to shifts in species composition and loss of biodiversity. To quantify the vegetation response to future climate change, a hydrological model was set up and run using future climate data projected by different General Circulation Models (GCMs) is presented in Chapter 6. The results highlighted the LAI responses to future precipitation and temperature changes for RCP4.5 and RCP 8.5 climate scenarios for a future period from 2031 to 2100. The third objective of the research study was addressed effectively by critically analysing vegetation-climatic relationships. The key findings of the third objective are presented below.

This study found that the available catchment water added from the precipitation and suitable vegetation growth temperature primarily dictate the spatial heterogeneity, which LAI measures. The maximum and minimum daily temperature has more influence than the annual mean temperature for vegetation growth in the temperate zone. This study also confirms that precipitation variations in winter and spring have a larger impact on vegetation growth in the study floodplain area. The work suggests that there will be a decreasing trend in vegetation growth between 2031 and 2075 according to the RCP4.5 scenario (see details in Chapter 6).

### **7.2.4. Overall summary**

The thesis has shown the following summary findings.

- a) The results presented herein mark the initial attempts to delineate the connections between vegetation and surface water variability across different vegetation types and their proximity to the stream flow, in contrast to previous studies that concentrated on specific vegetation types (such as trees) (Sykes, 2009). The outcomes lend credence to the notion that there exist generalised vegetation-surface water relationships among vegetation types and that relationships may be able to endure or even increase in adaptation to current and future climate shifts.
- b) The hydrological modelling applied in this study, using a combination of station-gauged and remotely sensed meteorological data, generated more reliable model output.

By applying machine learning algorithms in the correlation analysis, the complex relationships between vegetation and groundwater dynamics were analysed. The interrelationships and underlying mechanisms between these processes are likely to influence floodplain vegetation sustainability.

- c) The maximum reduction observed in the study catchment from March to June in south-east Australia. This surface runoff decreasing trend is 43.72 % higher for MK3.6 than ACCESS1.0 climate model predictions. In contrast to groundwater (GW) the reduction is 61.52% more for MK3.6 climate projections than ACCESS1.0. These pointed future scenarios can cause drastic change within floodplain vegetation communities in the temperate zone.

### **7.3. Conclusion**

This study identifies woody vegetation type such as forest and shrub are highly responsive to groundwater and non-woody vegetation such as grass type vegetation responsive to rainfall in temperate zone like south-eastern Australia. This confirms that tree and shrub vegetation can grow well after the rainfall when groundwater flow increases in the dry season. This study also observed vegetation located distant from the water outlet is mainly dependent on the groundwater resources within the catchment. The hydrological modelling applied in this study using combination of station gauged and remotely sensed meteorological data, generated more reliable model output. By applying machine learning algorithms in the correlation analysis, the complex relationships between vegetation and groundwater dynamics were analysed. The interrelationships and underneath mechanisms between these processes are likely to influence floodplain vegetation sustainability.

Knowledge of vegetation types and their proximity to water sources is crucial in various climatic conditions and associated environmental changes. This knowledge plays a vital role in making informed management decisions. For example, it can assist in planning agricultural development with limited irrigation systems during dry seasons, enabling us to adapt to predicted future climate change. Additionally, it can aid in identifying species that are resilient or vulnerable to climatic changes, thus guiding conservation and restoration efforts. Furthermore, this analysis has significant implications for determining which ecosystem services will be more resilient to climate change, as specific aspects such as vegetation types, leaf area, and their transpiration processes regulate climate conditions in ecosystems (Rocca et al., 2014; Moor et al., 2015). However, more effort is required to bridge the knowledge gaps

identified, including a comprehensive understanding of other vegetation conditions and climate scenarios that future studies should focus on. Moreover, it is essential to identify the ecosystems and climatic zones that these studies should target. Notably, vegetation types have been identified as a critical knowledge gap, particularly in comprehending the responses of temperate climatic zones to climate change. Further, understanding floodplain vegetation interactions with catchment water availability under future climate scenarios and thus stability of the catchment water for floodplain vegetation use will become crucial as water resources directly face threats from hydrological alterations due to shifting climate conditions.

This research work has made significant contributions to the field of science, which are as follows:

- An understanding of floodplain vegetation response to the climate change under RCP4.5 and RCP 8.5 climate scenarios based on hydrological modelling.
- Improved understanding of the catchment's surface water modelling with conceptual rainfall-runoff hydrological model in floodplain areas.
- New knowledge on the potential application of MODIS imagery in mapping the vegetation greenness of floodplain areas.
- New knowledge on the potential application of GIS-based hydrological modelling in floodplain areas.
- A novel approach applied in this study to observe vegetation-climate relationships reflected by the leaf area indices (LAI) considering model simulated surface runoff and groundwater flow in a temperate floodplain ecosystem.
- A novel approach applied a comparative model calibration analysis using station gauged flow data and remotely sensed LAI data.

#### **7.4. Recommendations**

Further research is required to fully understand the response of floodplain vegetation to climate change in temperate climate zones such as southeast Australia, utilising remotely sensed data and GIS-based hydrological modelling under future climate scenarios. This area of

study is still in its early stages and additional investigations could provide valuable contributions to the field. Based on the findings of this study, the subsequent recommendations for future investigations are proposed.

- Authorities responsible for managing floodplain ecosystems in the temperate/semi-arid region must undertake a thorough evaluation of the existing policies pertaining to basin water management. This review is necessary to incorporate adaptable water using strategies that can be adjusted in accordance with seasonal demands.
- Management should thoroughly consider any forecasts regarding rainfall pattern alterations in a catchment hydrology where rainfall is the dominant factor, to enhance floodplain management.
- Department of Agriculture can consider small and medium rooted vegetation growth in similar floodplains with possible irrigation adjustment during dry seasons.
- Management authority can review their water management policies and mitigation strategies for climate change for future vegetation growth under predicted climate alterations in floodplains and ecosystems.

The following recommendations are for future research:

- The utilisation of dynamic vegetation and hydrological models based on the study objectives, data accessibility, and computational resources is desired. Among the well-known choices are the Variable Infiltration Capacity (VIC) model for hydrology and the Community Land Model (CLM) for vegetation dynamics. It is essential to establish a framework that integrates the chosen hydrological and vegetation models. This integration should ensure a bidirectional coupling between the models, allowing for reciprocal influences between hydrology and vegetation dynamics. The potential future research question: How do fluctuations in water flow affect the growth and distribution of vegetation in the Burrinjuck sub-catchment and what are the implications for ecosystem resilience and ecosystem services provision under different climate change scenarios?
- Further research on modelling floodplain vegetation response using commercial satellite imagery can explore the utilisation of alternative machine learning algorithms. Additionally, comparing the outcomes of this study with those obtained

from other satellite data sources, including those with higher or lower spatial resolution, can offer insights into the potential options for vegetation hydrology modelling.

- Future studies can consider incorporating remotely sensed LAI data as an input parameter into hydrological models such as SWAT or VIC model. Calibrating the hydrological model using observed hydrological data (e.g., streamflow, runoff) and LAI data and validating model performance against independent datasets is desirable to ensure its accuracy and reliability. A research question can be formed to investigate how changes in groundwater levels influence vegetation dynamics, as captured by variations in LAI.
- Hydrological model calibration can be improved by including measured soil moisture data at field level to compare model simulation to support the output results.
- Future research can consider more comprehensive data related to vegetation growth factors to refine the SWAT modelling results including different vegetation types and their respective water requirements.

## REFERENCES

- Abbaspour, K. C., Johnson, C., & Van Genuchten, M. T. (2004). Estimating uncertain flow and transport parameters using a sequential uncertainty fitting procedure. *Vadose zone journal*, 3(4), 1340-1352.
- Abbaspour, K. C., Rouholahnejad, E., Vaghefi, S., Srinivasan, R., Yang, H., & Kløve, B. (2015). A continental-scale hydrology and water quality model for Europe: Calibration and uncertainty of a high-resolution large-scale SWAT model. *Journal of Hydrology*, 524, 733-752. doi:<https://doi.org/10.1016/j.jhydrol.2015.03.027>
- Abbaspour, K. C., Vaghefi, S. A., & Srinivasan, R. (2018). A Guideline for Successful Calibration and Uncertainty Analysis for Soil and Water Assessment: A Review of Papers from the 2016 International SWAT Conference. *Water*, 10, 6. doi:10.3390/w10010006
- Abdurahman, M. J. (2017). *Long Term Demand-Forecasting and Generation Expansion Planning of the Ethiopian Electric Power (EEP)*. Addis Ababa University,
- Abiodun, B. J., & Adedoyin, A. (2016). A Modelling Perspective of Future Climate Change. In T. M. Letcher (Ed.), *Climate Change (Second Edition)* (pp. 355-371). Boston: Elsevier.
- ABS. (2019). Australian Bureau of Statistics. Retrieved from <https://www.abs.gov.au>
- ABS. (2021). Australian Bureau of Statistics. Retrieved from <https://www.abs.gov.au>
- Acreman, M., & Ferguson, A. (2010). Environmental flows and the European water framework directive. *Freshwater biology*, 55(1), 32-48.
- Adamson, D., Mallawaarachchi, T., & Quiggin, J. (2009). Declining inflows and more frequent droughts in the Murray-Darling Basin: climate change, impacts and adaptation. *Australian Journal of Agricultural and Resource Economics*, 53(3), 345-366. doi:10.1111/j.1467-8489.2009.00451.x
- Adepoju, K., Adelabu, S., & Fashae, O. (2019). Vegetation Response to Recent Trends in Climate and Landuse Dynamics in a Typical Humid and Dry Tropical Region under Global Change. *Advances in Meteorology*, 2019, 4946127. doi:10.1155/2019/4946127
- Adhikari, R. K., Mohanasundaram, S., & Shrestha, S. (2020). Impacts of land-use changes on the groundwater recharge in the Ho Chi Minh city, Vietnam. *Environ Res*, 185, 109-440. doi:10.1016/j.envres.2020.109440
- Afrifa-Yamoah, E., Mueller, U. A., Taylor, S. M., & Fisher, A. J. (2020). Missing data imputation of high-resolution temporal climate time series data. *Meteorological Applications*, 27(1), e1873. doi:<https://doi.org/10.1002/met.1873>
- Aguiar, F. C., Martins, M. J., Silva, P. C., & Fernandes, M. R. (2016). Riverscapes downstream of hydropower dams: Effects of altered flows and historical land-use change. *Landscape and Urban Planning*, 153, 83-98. doi:10.1016/j.landurbplan.2016.04.009
- Aguilar, C., Zinnert, J. C., Polo, M. J., & Young, D. R. (2012). NDVI as an indicator for changes in water availability to woody vegetation. *Ecological Indicators*, 23, 290-300. doi:<https://doi.org/10.1016/j.ecolind.2012.04.008>
- Akitt, J. (2018). Some observations on the greenhouse effect at the Earth's surface. *Spectrochimica Acta Part A: Molecular Biomolecular Spectroscopy*, 188, 127-134.
- Alemayehu, T., van Griensven, A., Woldegiorgis, B. T., & Bauwens, W. (2017). An improved SWAT vegetation growth module and its evaluation for four tropical ecosystems. *Hydrol. Earth Syst. Sci.*, 21(9), 4449-4467. doi:10.5194/hess-21-4449-2017
- Ali, R., McFarlane, D., Varma, S., Dawes, W., Emelyanova, I., Hodgson, G., & Charles, S. (2012). Potential climate change impacts on groundwater resources of south-western Australia. *Journal of Hydrology*, 475, 456-472. doi:10.1016/j.jhydrol.2012.04.043

- Allen, M., Dube, O., Solecki, W., Aragón-Durand, F., Cramer, W., Humphreys, S., & Kainuma, M. (2018). *Special Report: Global Warming of 1.5 C*. Retrieved from
- Alsdorf, D. E., Rodríguez, E., & Lettenmaier, D. P. (2007). Measuring surface water from space. *Reviews of Geophysics*, 45(2). doi:10.1029/2006rg000197
- Anderegg, W. R. L. (2015). Spatial and temporal variation in plant hydraulic traits and their relevance for climate change impacts on vegetation. *New Phytologist*, 205(3), 1008-1014. doi:<https://doi.org/10.1111/nph.12907>
- Andersen, H. E., Kronvang, B., Larsen, S. E., Hoffmann, C. C., Jensen, T. S., & Rasmussen, E. K. (2006). Climate-change impacts on hydrology and nutrients in a Danish lowland river basin. *Science of The Total Environment*, 365(1), 223-237. doi:<https://doi.org/10.1016/j.scitotenv.2006.02.036>
- Andrade, C. W. L. d., Montenegro, S. M. G. L., Montenegro, A. A. A., Lima, J. R. d. S., Srinivasan, R., & Jones, C. A. (2019). Soil moisture and discharge modeling in a representative watershed in northeastern Brazil using SWAT. *Ecohydrology & Hydrobiology*, 19(2), 238-251. doi:<https://doi.org/10.1016/j.ecohyd.2018.09.002>
- Andres, R. J., Boden, T. A., Bréon, F.-M., Ciais, P., Davis, S., Erickson, D., . . . Miller, J. (2012). A synthesis of carbon dioxide emissions from fossil-fuel combustion. *Biogeosciences*, 9(5), 1845-1871.
- Arndt, C., & Tarp, F. (2017). Aid, Environment and Climate Change. *Review of Development Economics*, 21(2), 285-303. doi:<https://doi.org/10.1111/rode.12291>
- Arnold, J. G., Moriasi, D. N., Gassman, P. W., Abbaspour, K. C., White, M. J., Srinivasan, R., . . . Arnold, J.-F. G. (2012). SWAT: Model use, calibration, and validation. *Trans. ASABE*, 55, 1491-1508.
- Arnold, J. G., N. Moriasi, D., W. Gassman, P., C. Abbaspour, K., J. White, M., Srinivasan, R., . . . K. Jha, M. (2012). SWAT: Model Use, Calibration, and Validation. *Transactions of the ASABE*, 55(4), 1491-1508. doi:<https://doi.org/10.13031/2013.42256>
- Arnold, J. G., Srinivasan, R., Muttiah, R. S., & Williams, J. R. (1998). LARGE AREA HYDROLOGIC MODELING AND ASSESSMENT PART I: MODEL DEVELOPMENT1. *JAWRA Journal of the American Water Resources Association*, 34(1), 73-89. doi:<https://doi.org/10.1111/j.1752-1688.1998.tb05961.x>
- Arora, V. (2002). Modeling vegetation as a dynamic component in soil-vegetation-atmosphere transfer schemes and hydrological models. *Reviews of Geophysics*, 40(2). doi:10.1029/2001rg000103
- ASRIS. (2014, 2020). Australian Soil Resource Information System. Retrieved from <https://www.asris.csiro.au/methods.html>
- Awan, U. K., & Ismaeel, A. (2014). A new technique to map groundwater recharge in irrigated areas using a SWAT model under changing climate. *Journal of Hydrology*, 519, 1368-1382. doi:10.1016/j.jhydrol.2014.08.049
- Beare, S., & Heaney, A. (2002). *Climate change and water resources in the Murray Darling Basin, Australia*. Paper presented at the Conference paper.
- Beven, K. (2012). *Rainfall-Runoff Modelling The Primer*. West Sussex, UK: John Wiley & Sons, Ltd.
- Bhanja, S. N., Malakar, P., Mukherjee, A., Rodell, M., Mitra, P., & Sarkar, S. (2019). Using Satellite-Based Vegetation Cover as Indicator of Groundwater Storage in Natural Vegetation Areas. *Geophysical Research Letters*, 46(14), 8082-8092. doi:<https://doi.org/10.1029/2019GL083015>
- Biggs, J., von Fumetti, S., & Kelly-Quinn, M. (2017). The importance of small waterbodies for biodiversity and ecosystem services: implications for policy makers. *Hydrobiologia*, 793(1), 3-39. doi:10.1007/s10750-016-3007-0

- Blöschl, G., Hall, J., Viglione, A., Perdigão, R. A. P., Parajka, J., Merz, B., . . . Živković, N. (2019). Changing climate both increases and decreases European river floods. *Nature*, 573(7772), 108-111. doi:10.1038/s41586-019-1495-6
- Boer, G. J., Flato, G., & Ramsden, D. (2000). A transient climate change simulation with greenhouse gas and aerosol forcing: projected climate to the twenty-first century. *Climate Dynamics*, 16(6), 427-450. doi:10.1007/s003820050338
- BOM. (2021a). Climate Data Online Retrieved from <http://www.bom.gov.au/climate/data/index.shtml>
- BOM. (2021b). Australian Landscape Water Balance Retrieved from <http://www.bom.gov.au/water/landscape/#/etot/Actual/day/-28.4/130.4/3/Point////2021/5/4/>
- BOM. (2023). Australian Landscape Water Balance Retrieved from <http://www.bom.gov.au/water/landscape/#/etot/Actual/day/-28.4/130.4/3/Point////2021/5/4/>
- Bonfils, C. J. W., Santer, B. D., Fyfe, J. C., Marvel, K., Phillips, T. J., & Zimmerman, S. R. H. (2020). Human influence on joint changes in temperature, rainfall and continental aridity. *Nature Climate Change*, 10(8), 726-731. doi:10.1038/s41558-020-0821-1
- Boukal, D. S., Bideault, A., Carreira, B. M., & Sentis, A. (2019). Species interactions under climate change: connecting kinetic effects of temperature on individuals to community dynamics. *Current Opinion in Insect Science*, 35, 88-95. doi:<https://doi.org/10.1016/j.cois.2019.06.014>
- Braatne, J. H., Rood, S. B., Goater, L. A., & Blair, C. L. (2008). Analyzing the impacts of dams on riparian ecosystems: a review of research strategies and their relevance to the Snake River through Hells Canyon. *Environ Manage*, 41(2), 267-281. doi:10.1007/s00267-007-9048-4
- Brock, M. A., Nielsen, D. L., Shiel, R. J., Green, J. D., & Langley, J. D. (2003). Drought and aquatic community resilience: the role of eggs and seeds in sediments of temporary wetlands. *Freshwater biology*, 48(7), 1207-1218. doi:<https://doi.org/10.1046/j.1365-2427.2003.01083.x>
- Broich, M., Tulbure, M. G., Verbesselt, J., Xin, Q., & Wearne, J. (2018). Quantifying Australia's dryland vegetation response to flooding and drought at sub-continental scale. *Remote Sensing of Environment*, 212, 60-78. doi:10.1016/j.rse.2018.04.032
- Brown, A. E., Podger, G. M., Davidson, A. J., Dowling, T. I., & Zhang, L. (2007). Predicting the impact of plantation forestry on water users at local and regional scales: An example for the Murrumbidgee River Basin, Australia. *Forest Ecology and Management*, 251(1), 82-93. doi:<https://doi.org/10.1016/j.foreco.2007.06.011>
- Brown, P. T., Ming, Y., Li, W., & Hill, S. A. (2017). Change in the magnitude and mechanisms of global temperature variability with warming. *Nature Climate Change*, 7(10), 743-748. doi:10.1038/nclimate3381
- Bruijnzeel, L. A. (2004). Hydrological functions of tropical forests: not seeing the soil for the trees? *Agriculture, Ecosystems & Environment*, 104(1), 185-228. doi:10.1016/j.agee.2004.01.015
- Burandt, P., Grzybowski, M., Glińska-Lewczuk, K., Gotkiewicz, W., Szymańska-Walkiewicz, M., & Obolewski, K. (2024). Hydrology as a Determinant of Riparian Habitat Structure in Lowland River Floodplains. *Water*, 16(1). doi:10.3390/w16010164
- Callaghan, T. V., Kulikova, O., Rakhmanova, L., Topp-Jørgensen, E., Labba, N., Kuhmanen, L.-A., . . . Johansson, M. (2020). Improving dialogue among researchers, local and indigenous peoples and decision-makers to address issues of climate change in the North. *Ambio*, 49(6), 1161-1178. doi:10.1007/s13280-019-01277-9

- Cao, R., Chen, J., Shen, M., & Tang, Y. (2015). An improved logistic method for detecting spring vegetation phenology in grasslands from MODIS EVI time-series data. *Agricultural and Forest Meteorology*, 200, 9-20. doi:<https://doi.org/10.1016/j.agrformet.2014.09.009>
- Capon, S. J., Chambers, L. E., Mac Nally, R., Naiman, R. J., Davies, P., Marshall, N., . . . Douglas, M. M. (2013). Riparian ecosystems in the 21st century: hotspots for climate change adaptation? *Ecosystems*, 16, 359-381.
- Capon, S. J., James, C., & Reid, M. (2016). *Vegetation of Australian riverine landscapes: biology, ecology and management*: CSIRO PUBLISHING.
- Capon, S. J., & Reid, M. A. (2016). Vegetation resilience to mega-drought along a typical floodplain gradient of the southern Murray-Darling Basin, Australia. *Journal of Vegetation Science*, 27(5), 926-937. doi:<https://doi.org/10.1111/jvs.12426>
- Cartwright, I., Werner, A. D., & Woods, J. A. (2019). Using geochemistry to discern the patterns and timescales of groundwater recharge and mixing on floodplains in semi-arid regions. *Journal of Hydrology*, 570, 612-622. doi:10.1016/j.jhydrol.2019.01.023
- Catford, J. A., Morris, W. K., Vesk, P. A., Gippel, C. J., & Downes, B. J. (2014). Species and environmental characteristics point to flow regulation and drought as drivers of riparian plant invasion. *Diversity Distributions*, 20(9), 1084-1096.
- Chang, L., Li, Y., Zhang, K., Zhang, J., & Li, Y. (2023). Temporal and Spatial Variation in Vegetation and Its Influencing Factors in the Songliao River Basin, China. *Land*, 12(9). doi:10.3390/land12091692
- Chen, J., Brissette, F. P., Lucas-Picher, P., & Caya, D. (2017). Impacts of weighting climate models for hydro-meteorological climate change studies. *Journal of Hydrology*, 549, 534-546. doi:10.1016/j.jhydrol.2017.04.025
- Chen, J., Brissette, F. P., Poulin, A., & Leconte, R. (2011). Overall uncertainty study of the hydrological impacts of climate change for a Canadian watershed. *Water Resources Research*, 47(12). doi:<https://doi.org/10.1029/2011WR010602>
- Chen, S., Fu, Y. H., Wu, Z., Hao, F., Hao, Z., Guo, Y., . . . Zhang, X. (2023). Informing the SWAT model with remote sensing detected vegetation phenology for improved modeling of ecohydrological processes. *Journal of Hydrology*, 616, 128817. doi:<https://doi.org/10.1016/j.jhydrol.2022.128817>
- Chen, Z., Liu, H., Xu, C., Wu, X., Liang, B., Cao, J., & Chen, D. (2021). Modeling vegetation greenness and its climate sensitivity with deep-learning technology. *Ecol Evol*, 11(12), 7335-7345. doi:10.1002/ece3.7564
- Cheng, Y., Yang, W., Zhan, H., Jiang, Q., Shi, M., & Wang, Y. (2020). On the Origin of Deep Soil Water Infiltration in the Arid Sandy Region of China. *Water*, 12(9), 2409. doi:10.3390/w12092409
- Chi, K., Pang, B., Cui, L., Peng, D., Zhu, Z., Zhao, G., & Shi, S. (2020). Modelling the Vegetation Response to Climate Changes in the Yarlung Zangbo River Basin Using Random Forest. *Water*, 12(5). doi:10.3390/w12051433
- Chiew, F. H. S. (2006). Estimation of rainfall elasticity of streamflow in Australia. *Hydrological Sciences Journal*, 51(4), 613-625. doi:10.1623/hysj.51.4.613
- Chiew, F. H. S., & McMahon, T. A. (2002). Modelling the impacts of climate change on Australian streamflow. *Hydrological Processes*, 16(6), 1235-1245. doi:10.1002/hyp.1059
- Chiew, F. H. S., Peel, M. C., & Western, A. W. (2002). Application and testing of the simple rainfall-runoff model SIMHYD. In (pp. 335-367). Colorado: Water Resources Publications.

- Chiew, F. H. S., Zheng, H., & Potter, N. J. (2018). Rainfall-Runoff Modelling Considerations to Predict Streamflow Characteristics in Ungauged Catchments and under Climate Change. *10*(10), 1319.
- Chung, C. T. Y., & Power, S. B. (2017). The non-linear impact of El Nino, La Nina and the Southern Oscillation on seasonal and regional Australian precipitation. *Journal of Southern Hemisphere Earth Systems Science*, *67*(1), 25-45.
- Cienciala, P., & Pasternack, G. B. (2017). Floodplain inundation response to climate, valley form, and flow regulation on a gravel-bed river in a Mediterranean-climate region. *Geomorphology*, *282*, 1-17. doi:10.1016/j.geomorph.2017.01.006
- Clough, B., Tan, D. T., & Buu, D. C. (2000). Canopy leaf area index and litter fall in stands of the mangrove *Rhizophora apiculata* of different age in the Mekong Delta, Vietnam. *Aquatic Botany*, *66*(4), 311-320.
- Condon, L. E., Atchley, A. L., & Maxwell, R. M. (2020). Evapotranspiration depletes groundwater under warming over the contiguous United States. *Nature Communications*, *11*(1), 873. doi:10.1038/s41467-020-14688-0
- Connor, J., Schwabe, K., King, D., Kaczan, D., & Kirby, M. (2009). Impacts of climate change on lower Murray irrigation. *Australian Journal of Agricultural and Resource Economics*, *53*(3), 437-456. doi:10.1111/j.1467-8489.2009.00460.x
- Cracknell, M. J., & Reading, A. M. (2014). Geological mapping using remote sensing data: A comparison of five machine learning algorithms, their response to variations in the spatial distribution of training data and the use of explicit spatial information. *Computers & Geosciences*, *63*, 22-33. doi:<https://doi.org/10.1016/j.cageo.2013.10.008>
- Craft, C. (2022). Forested wetlands. In C. Craft (Ed.), *Creating and Restoring Wetlands (Second Edition)* (pp. 163-204): Elsevier.
- Crosbie, R. S., Pickett, T., Mpelasoka, F. S., Hodgson, G., Charles, S. P., & Barron, O. V. (2012). An assessment of the climate change impacts on groundwater recharge at a continental scale using a probabilistic approach with an ensemble of GCMs. *Climatic Change*, *117*(1-2), 41-53. doi:10.1007/s10584-012-0558-6
- Cuceloglu, G., Abbaspour, K. C., & Ozturk, I. (2017). Assessing the Water-Resources Potential of Istanbul by Using a Soil and Water Assessment Tool (SWAT) Hydrological Model. *Water*, *9*(10), 814. doi:10.3390/w9100814
- Cui, Y., Liao, Z., Wei, Y., Xu, X., Song, Y., & Liu, H. (2020). The Response of Groundwater Level to Climate Change and Human Activities in Baotou City, China. *Water*, *12*(4). doi:10.3390/w12041078
- Cuo, L., Zhang, Y., Gao, Y., Hao, Z., & Cairang, L. (2013). The impacts of climate change and land cover/use transition on the hydrology in the upper Yellow River Basin, China. *Journal of Hydrology*, *502*, 37-52. doi:10.1016/j.jhydrol.2013.08.003
- Dai, A. (2011). Drought under global warming: a review. *WIREs Climate Change*, *2*(1), 45-65. doi:<https://doi.org/10.1002/wcc.81>
- Dang, T. D., Cochrane, T. A., Arias, M. E., Van, P. D. T., & de Vries, T. T. (2016). Hydrological alterations from water infrastructure development in the Mekong floodplains. *Hydrological Processes*, *30*(21), 3824-3838. doi:10.1002/hyp.10894
- Davies, P. E., Stewardson, M. J., Hilman, T. J., Roberts, J. R., & Thoms, M. C. (2012). *Sustainable Rivers Audit 2. The ecological health of rivers in the Murray-Darling Basin at the end of the Millennium Drought (2008-2010)*. Available at: (75/12). Retrieved from <https://www.mdba.gov.au>
- De Bock, A., Belmans, B., Vanlanduit, S., Blom, J., Alvarado-Alvarado, A. A., & Audenaert, A. (2023). A review on the leaf area index (LAI) in vertical greening systems. *Building and Environment*, *229*, 109926. doi:<https://doi.org/10.1016/j.buildenv.2022.109926>

- de Jong, R., de Bruin, S., de Wit, A., Schaepman, M. E., & Dent, D. L. (2011). Analysis of monotonic greening and browning trends from global NDVI time-series. *Remote Sensing of Environment*, 115(2), 692-702. doi:<https://doi.org/10.1016/j.rse.2010.10.011>
- Dey, P., & Mishra, A. (2017). Separating the impacts of climate change and human activities on streamflow: A review of methodologies and critical assumptions. *Journal of Hydrology*, 548, 278-290. doi:10.1016/j.jhydrol.2017.03.014
- Doody, T. M., Benyon, R. G., Theiveyanathan, S., Koul, V., & Stewart, L. (2014). Development of pan coefficients for estimating evapotranspiration from riparian woody vegetation. *Hydrological Processes*, 28(4), 2129-2149. doi:10.1002/hyp.9753
- Doody, T. M., Colloff, M. J., Davies, M., Koul, V., Benyon, R. G., & Nagler, P. L. (2015). Quantifying water requirements of riparian river red gum (*Eucalyptus camaldulensis*) in the Murray-Darling Basin, Australia - implications for the management of environmental flows. *Ecohydrology*, 8(8), 1471-1487. doi:10.1002/eco.1598
- Duan, Z., Tuo, Y., Liu, J., Gao, H., Song, X., Zhang, Z., . . . Mekonnen, D. F. (2019). Hydrological evaluation of open-access precipitation and air temperature datasets using SWAT in a poorly gauged basin in Ethiopia. *Journal of Hydrology*, 569, 612-626. doi:<https://doi.org/10.1016/j.jhydrol.2018.12.026>
- Ducci, D., & Tranfaglia, G. (2008). Effects of climate change on groundwater resources in Campania (southern Italy). *Geological Society, London, Special Publications*, 288(1), 25-38. doi:10.1144/sp288.3
- Dudgeon, D., Arthington, A. H., Gessner, M. O., Kawabata, Z.-I., Knowler, D. J., Lévêque, C., . . . Stiassny, M. L. (2006). Freshwater biodiversity: importance, threats, status and conservation challenges. *Biological reviews*, 81(2), 163-182.
- Dutta, D., Kundu, A., Patel, N. R., Saha, S. K., & Siddiqui, A. R. (2015). Assessment of agricultural drought in Rajasthan (India) using remote sensing derived Vegetation Condition Index (VCI) and Standardized Precipitation Index (SPI). *The Egyptian Journal of Remote Sensing and Space Science*, 18(1), 53-63. doi:10.1016/j.ejrs.2015.03.006
- Dutta, D., Teng, J., Vaze, J., Hughes, J., Lerat, J., & Marvanek, S. (2013). Building flood inundation modelling capability in river system models for water resources planning and accounting. 359, 205-212.
- Dyer, F., ElSawah, S., Croke, B., Griffiths, R., Harrison, E., Lucena-Moya, P., & Jakeman, A. (2014). The effects of climate change on ecologically-relevant flow regime and water quality attributes. *Stochastic Environmental Research and Risk Assessment*, 28(1), 67-82. doi:10.1007/s00477-013-0744-8
- Eamus, D., Zolfaghar, S., Villalobos-Vega, R., Cleverly, J., & Huete, A. (2015). Groundwater-dependent ecosystems: recent insights from satellite and field-based studies. *Hydrology Earth System Sciences*, 19(10), 4229-4256.
- EarthData. (2021). Application for Extracting and Exploring Analysis Ready Samples (AppEEARS). Retrieved from <https://appeears.earthdatacloud.nasa.gov/>
- Eccles, R., Zhang, H., Hamilton, D., Trancoso, R., & Syktus, J. (2021). Impacts of climate change on streamflow and floodplain inundation in a coastal subtropical catchment. *Advances in Water Resources*, 147, 103825. doi:<https://doi.org/10.1016/j.advwatres.2020.103825>
- Eddy, J. A. (2009). *The sun, the earth, and near-earth space: a guide to the sun-earth system*: Government Printing Office.
- Eibe, F., Mark, A. H., & Ian, H. W. (2016). *The WEKA Workbench. Online Appendix for "Data Mining: Practical Machine Learning Tools and Techniques"* (Fourth ed.). MA, USA: Burlington,.

- Entwistle, N. S., Heritage, G. L., Schofield, L. A., & Williamson, R. J. (2019). Recent changes to floodplain character and functionality in England. *Catena*, *174*, 490-498. doi:10.1016/j.catena.2018.11.018
- Erdal, H. I., & Karakurt, O. (2013). Advancing monthly streamflow prediction accuracy of CART models using ensemble learning paradigms. *Journal of Hydrology*, *477*, 119-128. doi:<https://doi.org/10.1016/j.jhydrol.2012.11.015>
- ESRI. (2019). ArcGIS Desktop (Version 10.7 ). Redlands, CA: Environmental Systems Research Institute.
- Fagandini, C., Todaro, V., Tanda, M. G., Pereira, J. L., Azevedo, L., & Zanini, A. (2023). Missing Rainfall Daily Data: A Comparison Among Gap-Filling Approaches. *Mathematical Geosciences*. doi:10.1007/s11004-023-10078-6
- Fan, Y., Li, H., & Miguez-Macho, G. (2013). Global patterns of groundwater table depth. *Science*, *339*(6122), 940-943. doi:10.1126/science.1229881
- Fang, B., & Lakshmi, V. (2014). Soil moisture at watershed scale: Remote sensing techniques. *Journal of Hydrology*, *516*, 258-272. doi:10.1016/j.jhydrol.2013.12.008
- Fang, H., Baret, F., Plummer, S., & Schaepman-Strub, G. (2019). An Overview of Global Leaf Area Index (LAI): Methods, Products, Validation, and Applications. *Reviews of Geophysics*, *57*(3), 739-799. doi:10.1029/2018rg000608
- Fassò, A., Sommer, M., & von Rohden, C. (2020). Interpolation uncertainty of atmospheric temperature profiles. *Atmos. Meas. Tech.*, *13*(12), 6445-6458. doi:10.5194/amt-13-6445-2020
- Finlayson, C. M. (2005). Plant ecology of Australia's tropical floodplain wetlands: a review. *Ann Bot*, *96*(4), 541-555. doi:10.1093/aob/mci209
- Fischer, E. M., & Knutti, R. (2015). Anthropogenic contribution to global occurrence of heavy-precipitation and high-temperature extremes. *5*(6), 560-564.
- Foley, J. A., Levis, S., Costa, M. H., Cramer, W., & Pollard, D. (2000). Incorporating Dynamic Vegetation Cover within Global Climate Models. *Ecological Applications*, *10*(6), 1620-1632. doi:10.1890/1051-0761(2000)010[1620:Idvewg]2.0.Co;2
- Foley, W. J., McIlwee, A., Lawler, I., Aragonés, L., Woolnough, A. P., & Berding, N. (1998). Ecological applications of near infrared reflectance spectroscopy – a tool for rapid, cost-effective prediction of the composition of plant and animal tissues and aspects of animal performance. *Oecologia*, *116*(3), 293-305. doi:10.1007/s004420050591
- Francesconi, W., Srinivasan, R., Pérez-Miñana, E., Willcock, S. P., & Quintero, M. (2016). Using the Soil and Water Assessment Tool (SWAT) to model ecosystem services: A systematic review. *Journal of Hydrology*, *535*, 625-636. doi:<https://doi.org/10.1016/j.jhydrol.2016.01.034>
- Fu, B., & Burgher, I. (2015). Riparian vegetation NDVI dynamics and its relationship with climate, surface water and groundwater. *Journal of Arid Environments*, *113*, 59-68. doi:10.1016/j.jaridenv.2014.09.010
- Fu, G., Charles, S. P., Chiew, F. H., Teng, J., Zheng, H., Frost, A. J., . . . Kirshner, S. (2013). Modelling runoff with statistically downscaled daily site, gridded and catchment rainfall series. *Journal of Hydrology*, *492*, 254-265.
- Fu, Y., Dong, Y., Xie, Y., Xu, Z., & Wang, L. (2020). Impacts of Regional Groundwater Flow and River Fluctuation on Floodplain Wetlands in the Middle Reach of the Yellow River. *Water*, *12*(7). doi:10.3390/w12071922
- Gao, X., Zhao, Z., Ding, Y., Huang, R., & Giorgi, F. (2001). Climate change due to greenhouse effects in China as simulated by a regional climate model. *Advances in Atmospheric Sciences*, *18*(6), 1224-1230. doi:10.1007/s00376-001-0036-y
- Garnaut, R. (2011). *The Garnaut review 2011: Australia in the global response to climate change*: Cambridge University Press.

- Gassman, P., Sadeghi, A., & Srinivasan, R. (2014). Applications of the SWAT Model Special Section: Overview and Insights. *Journal of environmental quality*, 43, 1-8. doi:10.2134/jeq2013.11.0466
- Gassman, P. W., Reyes, M. E., Green, C. H., & Arnold, J. G. (2007). The Soil and Water Assessment Tool: Historical Development, Applications, and Future Research Directions. *Transactions of the ASABE*, 50(4), 1211-1250. doi:10.13031/2013.23637
- Gassman, P. W., Sadeghi, A. M., & Srinivasan, R. (2014). Applications of the SWAT Model Special Section: Overview and Insights. *Journal of environmental quality*, 43(1), 1-8. doi:<https://doi.org/10.2134/jeq2013.11.0466>
- Gemitzi, A., Ajami, H., & Richnow, H.-H. (2017). Developing empirical monthly groundwater recharge equations based on modeling and remote sensing data – Modeling future groundwater recharge to predict potential climate change impacts. *Journal of Hydrology*, 546, 1-13. doi:10.1016/j.jhydrol.2017.01.005
- Glenn, E. P., Doody, T. M., Guerschman, J. P., Huete, A. R., King, E. A., McVicar, T. R., . . . Zhang, Y. (2011). Actual evapotranspiration estimation by ground and remote sensing methods: the Australian experience. *Hydrological Processes*, 25(26), 4103-4116. doi:10.1002/hyp.8391
- Glenn, E. P., Huete, A. R., Nagler, P. L., & Nelson, S. G. (2008). Relationship Between Remotely-sensed Vegetation Indices, Canopy Attributes and Plant Physiological Processes: What Vegetation Indices Can and Cannot Tell Us About the Landscape. *Sensors*, 8(4), 2136-2160. doi:10.3390/s8042136
- Goesch, T., Hafi, A., Thorpe, S., Gooday, P., & Sanders, O. (2009). Climate change, irrigation and risk management.
- Gonzalez, D., Dillon, P., Page, D., & Vanderzalm, J. (2020). The Potential for Water Banking in Australia's Murray–Darling Basin to Increase Drought Resilience. *Water*, 12(10). doi:10.3390/w12102936
- Goss, K. F. (2003). Environmental flows, river salinity and biodiversity conservation: managing trade-offs in the Murray - Darling basin. *Australian Journal of Botany*, 51(6), 619-625. doi:10.1071/bt03003
- Grafton, R. Q., & Horne, J. (2014). Water markets in the Murray-Darling Basin. *Agricultural Water Management*, 145, 61-71. doi:10.1016/j.agwat.2013.12.001
- Green, D., Petrovic, J., Burrell, M., & Moss, P. (2011). *Water resources and management overview: Murrumbidgee catchment*. Sydney: NSW Office of Water.
- Green, T. R., Taniguchi, M., Kooi, H., Gurdak, J. J., Allen, D. M., Hiscock, K. M., . . . Aureli, A. (2011). Beneath the surface of global change: Impacts of climate change on groundwater. *Journal of Hydrology*, 405(3-4), 532-560. doi:10.1016/j.jhydrol.2011.05.002
- Groeneveld, D., Baugh, W., Sanderson, J., & Cooper, D. (2007). Annual Groundwater Evapotranspiration Mapped from Single Satellite Scenes. *Journal of Hydrology*, 344, 146-156. doi:10.1016/j.jhydrol.2007.07.002
- Groeneveld, D. P. (2008). Remotely-sensed groundwater evapotranspiration from alkali scrub affected by declining water table. *Journal of Hydrology*, 358(3-4), 294-303. doi:10.1016/j.jhydrol.2008.06.011
- Gu, F., Zhang, Y., Huang, M., Tao, B., Guo, R., & Yan, C. (2017). Effects of climate warming on net primary productivity in China during 1961-2010. *Ecol Evol*, 7(17), 6736-6746. doi:10.1002/ece3.3029
- Guli-Jiapaer, Liang, S., Yi, Q., & Liu, J. (2015). Vegetation dynamics and responses to recent climate change in Xinjiang using leaf area index as an indicator. *Ecological Indicators*, 58, 64-76. doi:<https://doi.org/10.1016/j.ecolind.2015.05.036>

- Gupta, R., Bhattarai, R., & Mishra, A. (2019). Development of Climate Data Bias Corrector (CDBC) Tool and Its Application over the Agro-Ecological Zones of India. *Water*, 11(5). doi:10.3390/w11051102
- Gurdak, J., McMahon, P., & Bruce, B. W. (2012). *Vulnerability of Groundwater Quality to Human Activity and Climate Change and Variability, High Plains Aquifer, USA*. Retrieved from
- Habibie, M., I, Noguchi, R., & Ahamed, T. (2022). Drought Estimation from Vegetation Phenology Analysis of Maize in Indonesia Using Deep Learning Algorithm. In T. Ahamed (Ed.), *Remote Sensing Application: Regional Perspectives in Agriculture and Forestry* (pp. 133-148). Singapore: Springer Nature Singapore.
- Hall, M., Frank, E., Holmes, G., Pfahringer, B., Reutemann, P., & Witten, I. H. (2009). The WEKA data mining software. *ACM SIGKDD Explorations Newsletter*, 11(1), 10-18. doi:10.1145/1656274.1656278
- Hallouz, F., Meddi, M., Mahé, G., Alirahmani, S., & Keddar, A. (2019). Modeling of discharge and sediment transport through the SWAT model in the basin of Harraza (Northwest of Algeria). *Water Science*, 32(1), 79-88. doi:10.1016/j.wsj.2017.12.004
- Hamed, K. H. (2009). Exact distribution of the Mann–Kendall trend test statistic for persistent data. *Journal of Hydrology*, 365(1), 86-94. doi:<https://doi.org/10.1016/j.jhydrol.2008.11.024>
- Hamed, M. M., Nashwan, M. S., Shahid, S., Ismail, T. b., Wang, X.-j., Dewan, A., & Asaduzzaman, M. (2022). Inconsistency in historical simulations and future projections of temperature and rainfall: A comparison of CMIP5 and CMIP6 models over Southeast Asia. *Atmospheric Research*, 265, 105927. doi:<https://doi.org/10.1016/j.atmosres.2021.105927>
- Hamlet, A. F., & Lettenmaier, D. P. (1999). EFFECTS OF CLIMATE CHANGE ON HYDROLOGY AND WATER RESOURCES IN THE COLUMBIA RIVER BASIN1. *JAWRA Journal of the American Water Resources Association*, 35(6), 1597-1623. doi:<https://doi.org/10.1111/j.1752-1688.1999.tb04240.x>
- Han, B., Benner, S. G., & Flores, A. N. (2018). Evaluating impacts of climate change on future water scarcity in an intensively managed semi-arid region using a coupled model of biophysical processes and water rights. 1-53. doi:10.5194/hess-2018-140
- Hartmann, D. L. (2016). Global Physical Climatology. In D. L. Hartmann (Ed.), (pp. 1-23). Boston: Elsevier.
- Harvey, J. W., Schaffranek, R. W., Noe, G. B., Larsen, L. G., Nowacki, D. J., & O'Connor, B. L. (2009). Hydroecological factors governing surface water flow on a low-gradient floodplain. *Water Resources Research*, 45(3). doi:10.1029/2008wr007129
- He, B., Chen, A., Jiang, W., & Chen, Z. (2017). The response of vegetation growth to shifts in trend of temperature in China. *Journal of Geographical Sciences*, 27(7), 801-816. doi:10.1007/s11442-017-1407-3
- Head, L., Adams, M., McGregor, H. V., & Toole, S. (2014). Climate change and Australia. *WIREs Climate Change*, 5(2), 175-197. doi:<https://doi.org/10.1002/wcc.255>
- Hein, L., Metzger, M. J., & Leemans, R. (2009). The local impacts of climate change in the Ferlo, Western Sahel. 93(3), 465-483.
- Herrera-Pantoja, M., & Hiscock, K. M. (2015). Projected impacts of climate change on water availability indicators in a semi-arid region of central Mexico. *Environmental Science & Policy*, 54, 81-89. doi:<https://doi.org/10.1016/j.envsci.2015.06.020>
- Hillman, T. J., & Shiel, R. J. (2017, 6). *Macro and microinvertebrates in Australian billabongs*. Paper presented at the Internationale Vereinigung für theoretische und angewandte Limnologie: Verhandlungen.

- Hofstra, N., Haylock, M., New, M., Jones, P., & Frei, C. (2008). Comparison of six methods for the interpolation of daily, European climate data. *Journal of Geophysical Research: Atmospheres*, 113(D21). doi:<https://doi.org/10.1029/2008JD010100>
- Houghton, R. A., Byers, B., & Nassikas, A. A. J. N. C. C. (2015). A role for tropical forests in stabilizing atmospheric CO<sub>2</sub>. 5(12), 1022-1023.
- House, A. R., Thompson, J. R., Sorensen, J. P. R., Roberts, C., & Acreman, M. C. (2016). Modelling groundwater/surface water interaction in a managed riparian chalk valley wetland. *Hydrological Processes*, 30(3), 447-462. doi:10.1002/hyp.10625
- Howden, S., Crimp, S., & Nelson, R. (2010). *Australian agriculture in a climate of change*. Paper presented at the Managing climate change: papers from the Greenhouse 2009 conference.
- Huang, C., Chen, Y., & Wu, J. (2014). Mapping spatio-temporal flood inundation dynamics at large river basin scale using time-series flow data and MODIS imagery. *International Journal of Applied Earth Observation and Geoinformation*, 26, 350-362. doi:10.1016/j.jag.2013.09.002
- Huang, F., Zhang, D., & Chen, X. (2019). Vegetation Response to Groundwater Variation in Arid Environments: Visualization of Research Evolution, Synthesis of Response Types, and Estimation of Groundwater Threshold. *International Journal of Environmental Research and Public Health*, 16(10). doi:10.3390/ijerph16101849
- Huang, K., Zhang, Y., Zhu, J., Liu, Y., Zu, J., & Zhang, J. (2016). The Influences of Climate Change and Human Activities on Vegetation Dynamics in the Qinghai-Tibet Plateau. *Remote Sensing*, 8(10). doi:10.3390/rs8100876
- Hughes, F. M., & Rood, S. B. (2003). Allocation of river flows for restoration of floodplain forest ecosystems: a review of approaches and their applicability in Europe. *Environmental Management*, 32, 12-33.
- Ines, A. V. M., & Hansen, J. W. (2006). Bias correction of daily GCM rainfall for crop simulation studies. *Agricultural and Forest Meteorology*, 138(1), 44-53. doi:<https://doi.org/10.1016/j.agrformet.2006.03.009>
- IPCC. (2007). *IPCC fourth assessment report*. Retrieved from Geneva:
- IPCC. (2014). *Climate Change 2013 – The Physical Science Basis: Working Group I Contribution to the Fifth Assessment Report of the Intergovernmental Panel on Climate Change*. Cambridge: Cambridge University Press.
- IPCC. (2014). *Climate Change 2014: Synthesis Report. Contribution of Working Groups I, II and III to the Fifth Assessment Report of the Intergovernmental Panel on Climate Change. (AR5 SYNTHESIS REPORT)*. doi:10.1017/CBO9781107415324.
- IPCC. (2021). *Summary for Policymakers. In: Climate Change 2021: The Physical Science Basis. Contribution of Working Group I to the Sixth Assessment Report of the Intergovernmental Panel on Climate Change*. Retrieved from Cambridge University Press:
- Jeffrey, S., Carter, J., Moodie, K., & Beswick, A. (2001). Using spatial interpolation to construct a comprehensive archive of Australian climate data. *Environmental Modelling & Software*, 16, 309-330. doi:10.1016/S1364-8152(01)00008-1
- Jia, K., Ruan, Y., Yang, Y., & Zhang, C. (2019). Assessing the Performance of CMIP5 Global Climate Models for Simulating Future Precipitation Change in the Tibetan Plateau. *Water*, 11(9). doi:10.3390/w11091771
- Jia, Y., Ge, Y., Ling, F., Guo, X., Wang, J., Wang, L., . . . Li, X. (2018). Urban Land Use Mapping by Combining Remote Sensing Imagery and Mobile Phone Positioning Data. *Remote Sensing*, 10(3). doi:10.3390/rs10030446

- Jiang, L., Guli-Jiapaer, Bao, A., Guo, H., & Ndayisaba, F. (2017). Vegetation dynamics and responses to climate change and human activities in Central Asia. *Science of The Total Environment*, 599-600, 967-980. doi:<https://doi.org/10.1016/j.scitotenv.2017.05.012>
- Jiang, Q., & Grafton, R. Q. (2012). Economic effects of climate change in the Murray–Darling Basin, Australia. *Agricultural Systems*, 110, 10-16. doi:10.1016/j.agry.2012.03.009
- Jiao, L., An, W., Li, Z., Gao, G., & Wang, C. (2020). Regional variation in soil water and vegetation characteristics in the Chinese Loess Plateau. *Ecological Indicators*, 115, 106399. doi:<https://doi.org/10.1016/j.ecolind.2020.106399>
- Jose, D. M., & Dwarakish, G. S. (2022). Ranking of downscaled CMIP5 and CMIP6 GCMs at a basin scale: case study of a tropical river basin on the South West coast of India. *Arabian Journal of Geosciences*, 15(1), 120. doi:10.1007/s12517-021-09289-0
- Jung, I., Bae, D., & Lee, B. (2013). Possible change in Korean streamflow seasonality based on multi-model climate projections. *Hydrological Processes*, 27(7), 1033-1045.
- Junk, W. J. (1989). *Flood tolerance and tree distribution in central Amazonian floodplains*.
- Junk, W. J., & Wantzen, K. M. (2004). *The flood pulse concept: new aspects, approaches and applications-an update*. Paper presented at the Second international symposium on the management of large rivers for fisheries.
- Kandasamy, J., Sountharajah, D., Sivabalan, P., Chanan, A., Vigneswaran, S., & Sivapalan, M. (2014). Socio-hydrologic drivers of the pendulum swing between agricultural development and environmental health: a case study from Murrumbidgee River basin, Australia. *Hydrology Earth System Sciences*, 18(3), 1027-1041.
- Karwa, R. (2020). Laws of Thermal Radiation. In R. Karwa (Ed.), *Heat and Mass Transfer* (pp. 733-765). Singapore: Springer Singapore.
- Kath, J., Le Brocque, A. F., Reardon-Smith, K., & Apan, A. (2019). Remotely sensed agricultural grassland productivity responses to land use and hydro-climatic drivers under extreme drought and rainfall. *Agricultural and Forest Meteorology*, 268, 11-22. doi:<https://doi.org/10.1016/j.agrformet.2019.01.007>
- Khan, S., Akbar, S., Rana, T., Abbas, A., Robinson, D., Paydar, Z., . . . Xevi, E. (2005). Off-and-on farm savings of irrigation water. Murrumbidgee Valley water efficiency feasibility project.
- Khoi, D. N., & Hang, P. T. T. (2015). Uncertainty Assessment of Climate Change Impacts on Hydrology: A Case Study for the Central Highlands of Vietnam. In S. Shrestha, A. K. Anal, P. A. Salam, & M. van der Valk (Eds.), *Managing Water Resources under Climate Uncertainty: Examples from Asia, Europe, Latin America, and Australia* (pp. 31-44). Cham: Springer International Publishing.
- Kim, H.-Y., Ko, J., Kang, S., & Tenhunen, J. (2013). Impacts of climate change on paddy rice yield in a temperate climate. *Global Change Biology*, 19(2), 548-562. doi:<https://doi.org/10.1111/gcb.12047>
- Kim, K. B., Hyun-Han, K., & Han, D. (2016). Hydrological modelling under climate change considering nonstationarity and seasonal effects. *Hydrology Research*, 47(2), 260-273. doi:<https://doi.org/10.2166/nh.2015.103>
- King, A. D., Klingaman, N. P., Alexander, L. V., Donat, M. G., Jourdain, N. C., & Maher, P. (2014). Extreme Rainfall Variability in Australia: Patterns, Drivers, and Predictability. *Journal of Climate*, 27(15), 6035-6050. doi:<https://doi.org/10.1175/JCLI-D-13-00715.1>
- Kingsford, R. T. (2000). Ecological impacts of dams, water diversions and river management on floodplain wetlands in Australia. *Austral Ecology*, 25(2), 109-127. doi:10.1046/j.1442-9993.2000.01036.x
- Kingsford, R. T. (2000). Protecting rivers in arid regions or pumping them dry? *Hydrobiologia*, 427(1), 1-11. doi:10.1023/a:1004033915662

- Kirby, J. M., Mainuddin, M., Ahmad, M. D., & Gao, L. (2013). Simplified Monthly Hydrology and Irrigation Water Use Model to Explore Sustainable Water Management Options in the Murray-Darling Basin. *Water Resources Management*, 27(11), 4083-4097. doi:10.1007/s11269-013-0397-x
- Kitessa, B. D., Ayalew, S. M., Gebrie, G. S., & Teferi, S. T. (2021). Long-term water-energy demand prediction using a regression model: a case study of Addis Ababa city. *Journal of Water and Climate Change*, 12(6), 2555-2578. doi:10.2166/wcc.2021.012 %J Journal of Water and Climate Change
- Kitoh, A., Endo, H., Krishna Kumar, K., Cavalcanti, I. F., Goswami, P., & Zhou, T. (2013). Monsoons in a changing world: A regional perspective in a global context. *Journal of Geophysical Research: Atmospheres*, 118(8), 3053-3065.
- Klein, C., Bliefernicht, J., Heinzeller, D., Gessner, U., Klein, I., & Kunstmann, H. (2017). Feedback of observed interannual vegetation change: a regional climate model analysis for the West African monsoon. *Climate Dynamics*, 48(9), 2837-2858. doi:10.1007/s00382-016-3237-x
- Kløve, B., Ala-Aho, P., Bertrand, G., Gurdak, J. J., Kupfersberger, H., Kværner, J., . . . Pulido-Velazquez, M. (2014). Climate change impacts on groundwater and dependent ecosystems. *Journal of Hydrology*, 518, 250-266. doi:10.1016/j.jhydrol.2013.06.037
- Konikow, L. F., & Kendy, E. (2005). Groundwater depletion: A global problem. *Hydrogeology Journal*, 13(1), 317-320. doi:10.1007/s10040-004-0411-8
- Kopeć, D., Ratajczyk, N., Wolańska-Kamińska, A., Walisch, M., & Kruk, A. (2014). Floodplain forest vegetation response to hydroengineering and climatic pressure – A five decade comparative analysis in the Bzura River valley (Central Poland). *Forest Ecology and Management*, 314, 120-130. doi:10.1016/j.foreco.2013.11.033
- Kretz, L., Bondar-Kunze, E., Hein, T., Richter, R., Schulz-Zunkel, C., Seele-Dilbat, C., . . . Wirth, C. (2021). Vegetation characteristics control local sediment and nutrient retention on but not underneath vegetation in floodplain meadows. *PLoS ONE*, 16(12), e0252694. doi:10.1371/journal.pone.0252694
- Kumar, S. V., M. Mocko, D., Wang, S., Peters-Lidard, C. D., & Borak, J. (2019). Assimilation of Remotely Sensed Leaf Area Index into the Noah-MP Land Surface Model: Impacts on Water and Carbon Fluxes and States over the Continental United States. *Journal of Hydrometeorology*, 20(7), 1359-1377. doi:<https://doi.org/10.1175/JHM-D-18-0237.1>
- Kushwaha, N. L., Rajput, J., Elbeltagi, A., Elnaggar, A. Y., Sena, D. R., Vishwakarma, D. K., . . . Hussein, E. E. (2021). Data Intelligence Model and Meta-Heuristic Algorithms-Based Pan Evaporation Modelling in Two Different Agro-Climatic Zones: A Case Study from Northern India. *12(12)*, 1654.
- Labat, D., Goddérís, Y., Probst, J. L., & Guyot, J. L. (2004). Evidence for global runoff increase related to climate warming. *Advances in Water Resources*, 27(6), 631-642. doi:10.1016/j.advwatres.2004.02.020
- Lauri, H., de Moel, H., Ward, P. J., Räsänen, T. A., Keskinen, M., & Kummu, M. (2012). Future changes in Mekong River hydrology: impact of climate change and reservoir operation on discharge. *Hydrol. Earth Syst. Sci.*, 16(12), 4603-4619. doi:10.5194/hess-16-4603-2012
- Lawrence, D., Coe, M., Walker, W., Verchot, L., & Vandecar, K. (2022). The Unseen Effects of Deforestation: Biophysical Effects on Climate. 5. doi:10.3389/ffgc.2022.756115
- Le Treut, H., Somerville, R., Cubasch, U., Ding, Y., Mauritzen, C., Mokssit, A., . . . Prather, M. (2007). *Historical Overview of Climate Change Science. Chapter 1*. Retrieved from Cambridge, United Kingdom and New York, NY, USA:
- Leauthaud, C., Kergoat, L., Hiernaux, P., Grippa, M., Musila, W., Duvail, S., & Albergel, J. (2018). Modelling the growth of floodplain grasslands to explore the impact of

- changing hydrological conditions on vegetation productivity. *Ecological Modelling*, 387, 220-237. doi:10.1016/j.ecolmodel.2018.09.015
- Lee, J.-Y., & Wang, B. (2012). Future change of global monsoon in the CMIP5. *Climate Dynamics*, 42(1-2), 101-119. doi:10.1007/s00382-012-1564-0
- Leenaars, J. G., Claessens, L., Heuvelink, G., Hengl, T., González, M., van Bussel, L. G., . . . Cassman, K. (2018). Mapping rootable depth and root zone plant-available water holding capacity of the soil of sub-Saharan Africa. *Geoderma*, 324, 18-36.
- Lees, T., Tseng, G., Atzberger, C., Reece, S., & Dadson, S. (2022). Deep Learning for Vegetation Health Forecasting: A Case Study in Kenya. *14*(3), 698.
- Leigh, C., Sheldon, F., Kingsford, R. T., & Arthington, A. H. (2010). Sequential floods drive 'booms' and wetland persistence in dryland rivers: a synthesis. *Marine and Freshwater Research*, 61(8), 896-908. doi:10.1071/mf10106
- Lewin, J. (2013). Enlightenment and the GM floodplain. *Earth Surface Processes and Landforms*, 38(1), 17-29. doi:10.1002/esp.3230
- Li, D., Sharp, J. O., & Drewes, J. E. (2016). Influence of Wastewater Discharge on the Metabolic Potential of the Microbial Community in River Sediments. *Microb Ecol*, 71(1), 78-86. doi:10.1007/s00248-015-0680-x
- Li, H., Sheffield, J., & Wood, E. F. (2010). Bias correction of monthly precipitation and temperature fields from Intergovernmental Panel on Climate Change AR4 models using equidistant quantile matching. *Journal of Geophysical Research: Atmospheres*, 115(D10). doi:<https://doi.org/10.1029/2009JD012882>
- Li, L., Zha, Y., Zhang, J., Li, Y., & Lyu, H. (2020). Effect of terrestrial vegetation growth on climate change in China. *Journal of Environmental Management*, 262, 110321. doi:<https://doi.org/10.1016/j.jenvman.2020.110321>
- Li, L., Zhang, Y., Liu, L., Wu, J., Wang, Z., Li, S., . . . Paudel, B. (2018). Spatiotemporal Patterns of Vegetation Greenness Change and Associated Climatic and Anthropogenic Drivers on the Tibetan Plateau during 2000–2015. *Remote Sensing*, 10(10). doi:10.3390/rs10101525
- Li, P., Hua, P., Zhang, J., & Krebs, P. (2022). Ecological risk and machine learning based source analyses of trace metals in typical surface water. *Science of The Total Environment*, 838, 155944. doi:<https://doi.org/10.1016/j.scitotenv.2022.155944>
- Li, S., Asanuma, J., Kotani, A., Davaa, G., & Oyunbaatar, D. (2007). Evapotranspiration from a Mongolian steppe under grazing and its environmental constraints. *Journal of Hydrology*, 333(1), 133-143. doi:<https://doi.org/10.1016/j.jhydrol.2006.07.021>
- Li, X., Yuan, W., & Dong, W. (2021). A Machine Learning Method for Predicting Vegetation Indices in China. *Remote Sensing*, 13(6). doi:10.3390/rs13061147
- Li, Z., Liu, W.-z., Zhang, X.-c., & Zheng, F.-l. (2009). Impacts of land use change and climate variability on hydrology in an agricultural catchment on the Loess Plateau of China. *Journal of Hydrology*, 377(1), 35-42. doi:<https://doi.org/10.1016/j.jhydrol.2009.08.007>
- Lian, X., Jeong, S., Park, C.-E., Xu, H., Li, L. Z. X., Wang, T., . . . Piao, S. (2022). Biophysical impacts of northern vegetation changes on seasonal warming patterns. *Nature Communications*, 13(1), 3925. doi:10.1038/s41467-022-31671-z
- Liang, W., Bai, D., Wang, F., Fu, B., Yan, J., Wang, S., . . . Feng, M. (2015). Quantifying the impacts of climate change and ecological restoration on streamflow changes based on a Budyko hydrological model in China's Loess Plateau. *Water Resources Research*, 51(8), 6500-6519. doi:<https://doi.org/10.1002/2014WR016589>
- Lin, Y.-S., Medlyn, B. E., & Ellsworth, D. S. (2012). Temperature responses of leaf net photosynthesis: the role of component processes. *Tree Physiology*, 32(2), 219-231. doi:10.1093/treephys/tp141 %J Tree Physiology

- Liou, Y. A., & Kar, S. K. (2014). Evapotranspiration Estimation with Remote Sensing and Various Surface Energy Balance Algorithms—A Review. *Energies*, 7(5), 2821-2849. doi:<https://doi.org/10.3390/en7052821>
- Liu, J., Gao, G., Wang, S., Jiao, L., Wu, X., & Fu, B. (2018). The effects of vegetation on runoff and soil loss: Multidimensional structure analysis and scale characteristics. *Journal of Geographical Sciences*, 28(1), 59-78. doi:10.1007/s11442-018-1459-z
- Liu, Z., Herman, J. D., Huang, G., Kadir, T., & Dahlke, H. E. (2021). Identifying climate change impacts on surface water supply in the southern Central Valley, California. *Science of The Total Environment*, 759, 143429. doi:<https://doi.org/10.1016/j.scitotenv.2020.143429>
- Long, D., Longuevergne, L., & Scanlon, B. R. (2014). Uncertainty in evapotranspiration from land surface modeling, remote sensing, and GRACE satellites. *Water Resources Research*, 50(2), 1131-1151. doi:10.1002/2013wr014581
- López-Serrano, P. M., López-Sánchez, C. A., Álvarez-González, J. G., & García-Gutiérrez, J. (2016). A Comparison of Machine Learning Techniques Applied to Landsat-5 TM Spectral Data for Biomass Estimation. *Canadian Journal of Remote Sensing*, 42(6), 690-705. doi:10.1080/07038992.2016.1217485
- López, J. L., Hernández, S., Urrutia, A., López-Cortés, X. A., Araya, H., & Morales-Salinas, L. (2021). Effect of missing data on short time series and their application in the characterization of surface temperature by detrended fluctuation analysis. *Computers & Geosciences*, 153, 104794. doi:<https://doi.org/10.1016/j.cageo.2021.104794>
- Lu, Y., & Qin, X. S. (2014). A coupled K-nearest neighbour and Bayesian neural network model for daily rainfall downscaling. *International Journal of Climatology*, 34(11), 3221-3236. doi:10.1002/joc.3906
- Ma, T., Duan, Z., Li, R., & Song, X. (2019). Enhancing SWAT with remotely sensed LAI for improved modelling of ecohydrological process in subtropics. *Journal of Hydrology*, 570, 802-815. doi:<https://doi.org/10.1016/j.jhydrol.2019.01.024>
- Ma, X., Huete, A., Moran, S., Ponce-Campos, G., & Eamus, D. (2015). Abrupt shifts in phenology and vegetation productivity under climate extremes. *Journal of Geophysical Research: Biogeosciences*, 120(10), 2036-2052. doi:<https://doi.org/10.1002/2015JG003144>
- Mackay, A. (2008). Climate Change 2007: Impacts, Adaptation and Vulnerability. Contribution of Working Group II to the Fourth Assessment Report of the Intergovernmental Panel on Climate Change. *Journal of environmental quality*, 37(6), 2407-2407. doi:<https://doi.org/10.2134/jeq2008.0015br>
- Madronich, S., & Flocke, S. (1999). The role of solar radiation in atmospheric chemistry. *Environmental photochemistry*, 1-26.
- Makumbura, R. K., & Rathnayake, U. (2022). Variation of Leaf Area Index (LAI) under Changing Climate: Kadolkele Mangrove Forest, Sri Lanka. *Advances in Meteorology*, 2022, 9693303. doi:10.1155/2022/9693303
- Mallick, J., AlMesfer, M. K., Singh, V. P., Falqi, I. I., Singh, C. K., Alsubih, M., & Kahla, N. B. (2021). Evaluating the NDVI–Rainfall Relationship in Bisha Watershed, Saudi Arabia Using Non-Stationary Modeling Technique. *Atmosphere*, 12(5), 593. doi:10.3390/atmos12050593
- Mancini, M., & Corbari, C. (2014). Calibration and Validation of a Distributed Energy–Water Balance Model Using Satellite Data of Land Surface Temperature and Ground Discharge Measurements. *Journal of Hydrometeorology*, 15(1), 376-392. doi:10.1175/jhm-d-12-0173.1
- Mann, H. B. (1945). Nonparametric Tests Against Trend. *Econometrica*, 13(3), 245-259. doi:10.2307/1907187

- Mann, M. E., Steinman, B. A., Brouillette, D. J., & Miller, S. K. (2021). Multidecadal climate oscillations during the past millennium driven by volcanic forcing. *Science*, *371*(6533), 1014-1019. doi:10.1126/science.abc5810
- Marin, D. B., Ferraz, G. A. e. S., Santana, L. S., Barbosa, B. D. S., Barata, R. A. P., Osco, L. P., . . . Guimarães, P. H. S. (2021). Detecting coffee leaf rust with UAV-based vegetation indices and decision tree machine learning models. *Computers and Electronics in Agriculture*, *190*, 106476. doi:<https://doi.org/10.1016/j.compag.2021.106476>
- Martinetti, S., Fatichi, S., Floriancic, M., Burlando, P., & Molnar, P. (2021). Field evidence of riparian vegetation response to groundwater levels in a gravel-bed river. *14*(2), e2264. doi:<https://doi.org/10.1002/eco.2264>
- Martiny, N., Camberlin, P., Richard, Y., & Philippon, N. (2007). Compared regimes of NDVI and rainfall in semi-arid regions of Africa. *International Journal of Remote Sensing*, *27*(23), 5201-5223. doi:10.1080/01431160600567787
- Marvel, K., Cook, B. I., Bonfils, C. J. W., Durack, P. J., Smerdon, J. E., & Williams, A. P. (2019). Twentieth-century hydroclimate changes consistent with human influence. *Nature*, *569*(7754), 59-65. doi:10.1038/s41586-019-1149-8
- McKay, R. C., Boschat, G., Rudeva, I., Pepler, A., Purich, A., Dowdy, A., . . . Rauniyar, S. (2023). Can southern Australian rainfall decline be explained? A review of possible drivers. *WIREs Climate Change*, *14*(2), e820. doi:<https://doi.org/10.1002/wcc.820>
- McLaughlin, D. L., & Cohen, M. J. (2013). Realizing ecosystem services: wetland hydrologic function along a gradient of ecosystem condition. *Ecol Appl*, *23*(7), 1619-1631. doi:10.1890/12-1489.1
- McMahon, T. A., Vogel, R. M., Peel, M. C., & Pegram, G. G. (2007). Global streamflows—Part 1: Characteristics of annual streamflows. *Journal of Hydrology*, *347*(3-4), 243-259.
- MDBA. (2023, 24 June 2023). Murrumbidgee catchment. Retrieved from <https://www.mdba.gov.au/basin/catchments/southern-basin-catchments/murrumbidgee-catchment>
- Mekis, É., & Vincent, L. A. (2011). An Overview of the Second Generation Adjusted Daily Precipitation Dataset for Trend Analysis in Canada. *Atmosphere-Ocean*, *49*(2), 163-177. doi:10.1080/07055900.2011.583910
- Mekonnen, D. F., Duan, Z., Rientjes, T., & Disse, M. (2018). Analysis of combined and isolated effects of land-use and land-cover changes and climate change on the upper Blue Nile River basin's streamflow. *Hydrol. Earth Syst. Sci.*, *22*(12), 6187-6207. doi:10.5194/hess-22-6187-2018
- Mengistu, A. G., Woldesenbet, T. A., Dile, Y. T., & Bayabil, H. K. (2023). Modeling the impacts of climate change on hydrological processes in the Baro–Akobo River basin, Ethiopia. *Acta Geophysica*, *71*(4), 1915-1935. doi:10.1007/s11600-022-00956-8
- Merritt, D. M., Scott, M. L., LeROY P, N., Auble, G. T., & Lytle, D. A. (2010). Theory, methods and tools for determining environmental flows for riparian vegetation: riparian vegetation-flow response guilds. *55*(1), 206-225. doi:<https://doi.org/10.1111/j.1365-2427.2009.02206.x>
- Microsoft Corporation. (2018). Microsoft Excel. Redmond, WA, USA: Microsoft Corporation. Retrieved from <https://office.microsoft.com/excel>
- Mohammadi Igder, O., Alizadeh, H., Mojaradi, B., & Bayat, M. (2022). Multivariate assimilation of satellite-based leaf area index and ground-based river streamflow for hydrological modelling of irrigated watersheds using SWAT+. *Journal of Hydrology*, *610*, 128012. doi:<https://doi.org/10.1016/j.jhydrol.2022.128012>

- Mohammed, B., Salah, O., Driss, O., & Abdelghani, C. (2020). Global warming and groundwater from semi-arid areas: Essaouira region (Morocco) as an example. *SN Applied Sciences*, 2(7), 1245. doi:10.1007/s42452-020-3014-7
- Mohanty, B. P., Cosh, M., Lakshmi, V., & Montzka, C. (2013). Remote Sensing for Vadose Zone Hydrology-A Synthesis from the Vantage Point. *Vadose zone journal*, 12(3), vzj2013.2007.0128. doi:10.2136/vzj2013.07.0128
- Montazerolghaem, M., Vervoort, W., Minasny, B., & McBratney, A. (2016). Long-term variability of the leading seasonal modes of rainfall in south-eastern Australia. *Weather and Climate Extremes*, 13, 1-14. doi:<https://doi.org/10.1016/j.wace.2016.04.001>
- Moomaw, W. R., Chmura, G. L., Davies, G. T., Finlayson, C. M., Middleton, B. A., Natali, S. M., . . . Sutton-Grier, A. E. (2018). Wetlands In a Changing Climate: Science, Policy and Management. *Wetlands*, 38(2), 183-205. doi:10.1007/s13157-018-1023-8
- Moor, H., Hylander, K., & Norberg, J. (2015). Predicting climate change effects on wetland ecosystem services using species distribution modeling and plant functional traits. *Ambio*, 44(1), 113-126. doi:10.1007/s13280-014-0593-9
- Moriasi, D., Arnold, J., Van Liew, M., Bingner, R., Harmel, R. D., & Veith, T. (2007). Model Evaluation Guidelines for Systematic Quantification of Accuracy in Watershed Simulations. *Transactions of the ASABE*, 50, 885–900. doi:10.13031/2013.23153
- Mosner, E., Weber, A., Carambia, M., Nilson, E., Schmitz, U., Zelle, B., . . . Horchler, P. (2015). Climate change and floodplain vegetation—future prospects for riparian habitat availability along the Rhine River. *Ecological Engineering*, 82, 493-511. doi:10.1016/j.ecoleng.2015.05.013
- Moxham, C., Kenny, S. A., Beesley, L. S., & Gwinn, D. C. (2019). Large-scale environmental flow results in mixed outcomes with short-term benefits for a semi-arid floodplain plant community. *Freshwater biology*, 64(1), 24-36. doi:10.1111/fwb.13191
- Muhury, N., Apan, A. A., Marasani, T. N., & Ayele, G. T. (2022). Modelling Floodplain Vegetation Response to Groundwater Variability Using the ArcSWAT Hydrological Model, MODIS NDVI Data, and Machine Learning. *Land*, 11(12). doi:10.3390/land11122154
- Muhury, N., Ayele, G. T., Balcha, S. K., Jemberie, M. A., & Teferi, E. (2023). Basin Runoff Responses to Climate Change Using a Rainfall-Runoff Hydrological Model in Southeast Australia. *Atmosphere*, 14(2). doi:10.3390/atmos14020306
- Muñoz, P., Orellana-Alvear, J., Willems, P., & Célleri, R. (2018). Flash-Flood Forecasting in an Andean Mountain Catchment—Development of a Step-Wise Methodology Based on the Random Forest Algorithm. *Water*, 10(11). doi:10.3390/w10111519
- Nan, Y., Bao-hui, M., & Chun-kun, L. (2011). Impact Analysis of Climate Change on Water Resources. *Procedia Engineering*, 24, 643-648. doi:<https://doi.org/10.1016/j.proeng.2011.11.2710>
- Nanzad, L., Zhang, J., Tuvdendorj, B., Nabil, M., Zhang, S., & Bai, Y. (2019). NDVI anomaly for drought monitoring and its correlation with climate factors over Mongolia from 2000 to 2016. *Journal of Arid Environments*, 164, 69-77. doi:<https://doi.org/10.1016/j.jaridenv.2019.01.019>
- Narasimhan, B., & Srinivasan, R. (2005). Development and evaluation of Soil Moisture Deficit Index (SMDI) and Evapotranspiration Deficit Index (ETDI) for agricultural drought monitoring. *Agricultural and Forest Meteorology*, 133(1), 69-88. doi:<https://doi.org/10.1016/j.agrformet.2005.07.012>
- Nash, J. E., & Sutcliffe, J. V. (1970). River flow forecasting through conceptual models part I — A discussion of principles. *Journal of Hydrology*, 10(3), 282-290. doi:[https://doi.org/10.1016/0022-1694\(70\)90255-6](https://doi.org/10.1016/0022-1694(70)90255-6)

- Naumburg, E., Mata-gonzalez, R., Hunter, R. G., McLendon, T., & Martin, D. W. (2005). Phreatophytic Vegetation and Groundwater Fluctuations: A Review of Current Research and Application of Ecosystem Response Modeling with an Emphasis on Great Basin Vegetation. *Environmental Management*, 35(6), 726-740. doi:10.1007/s00267-004-0194-7
- Neitsch, S. L., Arnold, J. G., Kiniry, J. R., & Williams, J. R. (2011). *SWAT Theoretical Documentation Version 2009*. Retrieved from College Station, TX, USA, 2011: <http://swat.tamu.edu/documentation/>
- Nielsen, U. N., & Ball, B. A. (2015). Impacts of altered precipitation regimes on soil communities and biogeochemistry in arid and semi-arid ecosystems. *Global Change Biology*, 21(4), 1407-1421. doi:<https://doi.org/10.1111/gcb.12789>
- Nijssen, B., O'Donnell, G. M., Hamlet, A. F., & Lettenmaier, D. P. (2001). Hydrologic sensitivity of global rivers to climate change. *Climatic Change*, 50(1/2), 143-175. doi:10.1023/a:1010616428763
- Noor, M., Rehman, N. u., Jalil, A., Fahad, S., Adnan, M., Wahid, F., . . . Hassan, S. (2020). Climate Change and Costal Plant Lives. In S. Fahad, M. Hasanuzzaman, M. Alam, H. Ullah, M. Saeed, I. Ali Khan, & M. Adnan (Eds.), *Environment, Climate, Plant and Vegetation Growth* (pp. 93-108). Cham: Springer International Publishing.
- Norris, R. H., Prosser, I. P., Young, W. J., Liston, P., Bauer, N., Davies, N., . . . Thoms, M. C. (2001). The assessment of river condition (ARC): an audit of the ecological condition of Australian rivers.
- Nouri, H., Anderson, S., Sutton, P., Beecham, S., Nagler, P., Jarchow, C. J., & Roberts, D. A. (2017). NDVI, scale invariance and the modifiable areal unit problem: An assessment of vegetation in the Adelaide Parklands. *Sci Total Environ*, 584-585, 11-18. doi:10.1016/j.scitotenv.2017.01.130
- Okujeni, A., van der Linden, S., & Hostert, P. (2015). Extending the vegetation–impervious–soil model using simulated EnMAP data and machine learning. *Remote Sensing of Environment*, 158, 69-80. doi:<https://doi.org/10.1016/j.rse.2014.11.009>
- Olley, J. M., & Wasson, R. J. (2003). Changes in the flux of sediment in the Upper Murrumbidgee catchment, Southeastern Australia, since European settlement. *Hydrological Processes*, 17(16), 3307-3320. doi:<https://doi.org/10.1002/hyp.1388>
- Ouyang, F., Zhu, Y., Fu, G., Lü, H., Zhang, A., Yu, Z., & Chen, X. (2015). Impacts of climate change under CMIP5 RCP scenarios on streamflow in the Huangnizhuang catchment. *Stochastic Environmental Research and Risk Assessment*, 29(7), 1781-1795. doi:10.1007/s00477-014-1018-9
- Paillex, A., Dolédec, S., Castella, E., Mérigoux, S., Aldridge, D. C., & Arnott, S. (2013). Functional diversity in a large river floodplain: anticipating the response of native and alien macroinvertebrates to the restoration of hydrological connectivity. *Journal of Applied Ecology*, 50(1), 97-106. doi:10.1111/1365-2664.12018
- Pall, P., Aina, T., Stone, D. A., Stott, P. A., Nozawa, T., Hilberts, A. G., . . . Allen, M. R. (2011). Anthropogenic greenhouse gas contribution to flood risk in England and Wales in autumn 2000. *Nature Communications*, 470(7334), 382-385.
- Panwar, S. C., G. J. . (2013). Climate change and its influence on groundwater resources. 105, 37-46.
- Park, J.-Y., Ahn, S.-R., Hwang, S.-J., Jang, C.-H., Park, G.-A., & Kim, S.-J. (2014). Evaluation of MODIS NDVI and LST for indicating soil moisture of forest areas based on SWAT modeling. *Paddy and Water Environment*, 12(1), 77-88. doi:10.1007/s10333-014-0425-3

- Parsons, M., & Thoms, M. C. (2013). Patterns of vegetation greenness during flood, rain and dry resource states in a large, unconfined floodplain landscape. *Journal of Arid Environments*, 88, 24-38. doi:10.1016/j.jaridenv.2012.07.023
- Patil, R., Wei, Y., Pullar, D., & Shulmeister, J. (2020). Evolution of streamflow patterns in Goulburn-Broken catchment during 1884–2018 and its implications for floodplain management. *Ecological Indicators*, 113. doi:10.1016/j.ecolind.2020.106277
- Pechlivanidis, I. G., Jackson, B. M., McIntyre, N. R., & Wheater, H. S. (2011). Catchment scale hydrological modelling: a review of model types, calibration approaches and uncertainty analysis methods in the context of recent developments in technology and applications. *Global Nest*, 13(3), 193 - 214.
- Peel, M., Finlayson, B., & McMahon, T. (2007). Updated world map of the Köpper-Geiger climate classification. *Hydrol Earth Syst Sci Discuss*, 11, 439-472.
- Peel, M. C., Chiew, F. H. S., Western, A. W., & McMahon, T. A. (2000). Extension of Unimpaired Monthly Streamflow Data and Regionalisation of Parameter Values to Estimate Streamflow in Ungauged Catchments. 1-37.
- Pei, Z., Fang, S., Yang, W., Wang, L., Wu, M., Zhang, Q., . . . Khoi, D. N. (2019). The Relationship between NDVI and Climate Factors at Different Monthly Time Scales: A Case Study of Grasslands in Inner Mongolia, China (1982–2015). *11*(24), 7243.
- Penman, H. L. (1948). Natural evaporation from open water, bare soil and grass. *Proceedings of the Royal Society of London. Series A. Mathematical Physical Sciences*, 193(1032), 120-145.
- Pérez, G., Coma, J., Chàfer, M., & Cabeza, L. F. (2022). Seasonal influence of leaf area index (LAI) on the energy performance of a green facade. *Building and Environment*, 207, 108497. doi:<https://doi.org/10.1016/j.buildenv.2021.108497>
- Peters, D. L., Caissie, D., Monk, W. A., Rood, S. B., & St-Hilaire, A. (2016). An ecological perspective on floods in Canada. *Canadian Water Resources Journal / Revue canadienne des ressources hydriques*, 41(1-2), 288-306. doi:10.1080/07011784.2015.1070694
- Pflugmacher, D., Cohen, W. B., & E. Kennedy, R. (2012). Using Landsat-derived disturbance history (1972–2010) to predict current forest structure. *Remote Sensing of Environment*, 122, 146-165. doi:10.1016/j.rse.2011.09.025
- Pisinaras, V., Petalas, C., Gikas, G. D., Gemitzi, A., & Tsihrintzis, V. A. (2010). Hydrological and water quality modeling in a medium-sized basin using the Soil and Water Assessment Tool (SWAT). *Desalination*, 250(1), 274-286. doi:<https://doi.org/10.1016/j.desal.2009.09.044>
- Politti, E., Egger, G., Angermann, K., Rivaes, R., Blamauer, B., Klösch, M., . . . Habersack, H. (2014). Evaluating climate change impacts on Alpine floodplain vegetation. *Hydrobiologia*, 737(1), 225-243. doi:10.1007/s10750-013-1801-5
- Ponting, J., Kelly, T. J., Verhoef, A., Watts, M. J., & Sizmur, T. (2021). The impact of increased flooding occurrence on the mobility of potentially toxic elements in floodplain soil – A review. *Science of The Total Environment*, 754, 142040. doi:<https://doi.org/10.1016/j.scitotenv.2020.142040>
- Porporato, A., Daly, E., & Rodriguez-Iturbe, I. (2004). Soil water balance and ecosystem response to climate change. *The American Naturalist*, 164(5), 625-632.
- Potter, N. J., Chiew, F. H. S., & Frost, A. J. (2010). An assessment of the severity of recent reductions in rainfall and runoff in the Murray–Darling Basin. *Journal of Hydrology*, 381(1), 52-64. doi:<https://doi.org/10.1016/j.jhydrol.2009.11.025>
- Potter, N. J., & Zhang, L. (2009). Interannual variability of catchment water balance in Australia. *Journal of Hydrology*, 369(1-2), 120-129. doi:10.1016/j.jhydrol.2009.02.005

- Probst, E., & Mauser, W. (2023). Climate Change Impacts on Water Resources in the Danube River Basin: A Hydrological Modelling Study Using EURO-CORDEX Climate Scenarios. *Water*, 15(1), 8. doi:<https://doi.org/10.3390/w15010008>
- Prosser, I. P., Chiew, F. H. S., & Stafford Smith, M. (2021). Adapting Water Management to Climate Change in the Murray–Darling Basin, Australia. *13*(18), 2504.
- Qaderi, M. M., Martel, A. B., & Dixon, S. L. (2019). Environmental Factors Influence Plant Vascular System and Water Regulation. *Plants (Basel)*, 8(3), 65. doi:10.3390/plants8030065
- Qu, S., Wang, L., Lin, A., Yu, D., Yuan, M., & Li, C. a. (2020). Distinguishing the impacts of climate change and anthropogenic factors on vegetation dynamics in the Yangtze River Basin, China. *Ecological Indicators*, 108, 105724. doi:<https://doi.org/10.1016/j.ecolind.2019.105724>
- Qureshi, M. E., & Whitten, S. M. (2014). Regional impact of climate variability and adaptation options in the southern Murray–Darling Basin, Australia. *Water Resources and Economics*, 5, 67-84. doi:10.1016/j.wre.2013.12.002
- Rahim, H. R. B. A., Muhammad Quisar Bin, L., Sulaiman Wadi, H., Gabor Louis, H., Karel, S., Waleed Soliman, M., & Joydeep, D. (2016). Applied light-side coupling with optimized spiral-patterned zinc oxide nanorod coatings for multiple optical channel alcohol vapor sensing. *Journal of Nanophotonics*, 10(3), 036009. doi:10.1117/1.JNP.10.036009
- Raje, D., Priya, P., & Krishnan, R. (2014). Macroscale hydrological modelling approach for study of large scale hydrologic impacts under climate change in Indian river basins. *Hydrological Processes*, 28(4), 1874-1889. doi:<https://doi.org/10.1002/hyp.9731>
- Rajib, A., Kim, I. L., Golden, H. E., Lane, C. R., Kumar, S. V., Yu, Z., & Jeyalakshmi, S. (2020). Watershed Modeling with Remotely Sensed Big Data: MODIS Leaf Area Index Improves Hydrology and Water Quality Predictions. *Remote Sensing*, 12(13). doi:10.3390/rs12132148
- Ramanathan, V., Chung, C., Kim, D., Bettge, T., Buja, L., Kiehl, J. T., . . . Wild, M. (2005). Atmospheric brown clouds: impacts on South Asian climate and hydrological cycle. *Proc Natl Acad Sci U S A*, 102(15), 5326-5333. doi:10.1073/pnas.0500656102
- Reichstein, M., Bahn, M., Ciais, P., Frank, D., Mahecha, M. D., Seneviratne, S. I., . . . Wattenbach, M. (2013). Climate extremes and the carbon cycle. *Nature*, 500(7462), 287-295. doi:10.1038/nature12350
- Reid, M. A., Delong, M. D., & Thoms, M. C. (2012). The Influence of Hydrological Connectivity on Food Web Structure in Floodplain Lakes. *River Research and Applications*, 28(7), 827-844. doi:10.1002/rra.1491
- Reinfelds, I., Swanson, E., Cohen, T., Larsen, J., & Nolan, A. (2014). Hydrospatial assessment of streamflow yields and effects of climate change: Snowy Mountains, Australia. *Journal of Hydrology*, 512, 206-220. doi:10.1016/j.jhydrol.2014.02.038
- Ren, S., & Kingsford, R. T. (2014). Modelling impacts of regulation on flows to the Lowbidgee floodplain of the Murrumbidgee River, Australia. *Journal of Hydrology*, 519, 1660-1667. doi:10.1016/j.jhydrol.2014.09.003
- Reshmidevi, T. V., Nagesh Kumar, D., Mehrotra, R., & Sharma, A. (2018). Estimation of the climate change impact on a catchment water balance using an ensemble of GCMs. *Journal of Hydrology*, 556, 1192-1204. doi:<https://doi.org/10.1016/j.jhydrol.2017.02.016>
- Richardson, D. M., & Pysek, P. (2012). Naturalization of introduced plants: ecological drivers of biogeographical patterns. *New Phytol*, 196(2), 383-396. doi:10.1111/j.1469-8137.2012.04292.x

- Rivaes, R., Rodríguez-González, P. M., Albuquerque, A., Pinheiro, A. N., Egger, G., & Ferreira, M. T. (2013). Riparian vegetation responses to altered flow regimes driven by climate change in Mediterranean rivers. *Ecohydrology*, 6(3), 413-424. doi:10.1002/eco.1287
- Roberts, J., & Marston, F. (2011). *Water regime for Wetland and floodplain plants* (9781921853036). Retrieved from Canberra: [www.ag.gov.au/cca](http://www.ag.gov.au/cca)
- Rocca, M. E., Brown, P. M., MacDonald, L. H., & Carrico, C. M. (2014). Climate change impacts on fire regimes and key ecosystem services in Rocky Mountain forests. *Forest Ecology and Management*, 327, 290-305. doi:<https://doi.org/10.1016/j.foreco.2014.04.005>
- Rogers, K., Saintilan, N., Colloff, M., & Wen, L. (2013). Application of thresholds of potential concern and limits of acceptable change in the condition assessment of a significant wetland. *Environmental monitoring and assessment*, 185. doi:10.1007/s10661-013-3197-0
- Rosenberg, D. M., McCully, P., & Pringle, C. M. (2000). Global-Scale Environmental Effects of Hydrological Alterations: Introduction. *BioScience*, 50(9), 746-751. doi:10.1641/0006-3568(2000)050[0746:Gseeoh]2.0.Co;2
- Sa'adi, Z., Shiru, M. S., Shahid, S., & Ismail, T. (2020). Selection of general circulation models for the projections of spatio-temporal changes in temperature of Borneo Island based on CMIP5. *Theoretical and Applied Climatology*, 139(1), 351-371. doi:10.1007/s00704-019-02948-z
- Saha, P., & Zeleke, K. (2014). Assessment of streamflow and catchment water balance sensitivity to climate change for the Yass River catchment in south eastern Australia. *Environmental Earth Sciences*, 73, 6229-6242. doi:10.1007/s12665-014-3846-9
- Saha, P., Zeleke, K., & Hafeez, M. (2013). Streamflow modeling in a fluctuant climate using SWAT: Yass River catchment in south eastern Australia. *Environmental Earth Sciences*, 71(12), 5241-5254. doi:10.1007/s12665-013-2926-6
- Saha, P. P., Zeleke, K., & Hafeez, M. (2014). Streamflow modeling in a fluctuant climate using SWAT: Yass River catchment in south eastern Australia. *Environmental Earth Sciences*, 71(12), 5241-5254.
- Sandi, S. G., Rodriguez, J. F., Saintilan, N., Wen, L., Kuczera, G., Riccardi, G., & Saco, P. M. (2020). Resilience to drought of dryland wetlands threatened by climate change. *Scientific Reports*, 10(1), 13232. doi:10.1038/s41598-020-70087-x
- Santos, J. F., Schickhoff, U., ul Hasson, S., & Böhner, J. (2023). Biogeophysical Effects of Land-Use and Land-Cover Changes in South Asia: An Analysis of CMIP6 Models. *12*(4), 880.
- Sarkar, A. (2021). Deep Learning and the Evolution of Useful Information. *Inf. Matters*, 1, 6.
- Sarker, I. H. (2021). Machine Learning: Algorithms, Real-World Applications and Research Directions. *SN Computer Science*, 2(3), 160. doi:10.1007/s42979-021-00592-x
- Schlaepfer, D. R., Bradford, J. B., Lauenroth, W. K., Munson, S. M., Tietjen, B., Hall, S. A., . . . Jamiyansharav, K. (2017). Climate change reduces extent of temperate drylands and intensifies drought in deep soils. *Nature Communications*, 8(1), 14196. doi:10.1038/ncomms14196
- Schmidt, G. A., Ruedy, R. A., Miller, R. L., & Lacis, A. A. (2010). Attribution of the present-day total greenhouse effect. *Journal of Geophysical Research: Atmospheres*, 115(D20).
- Schmidt, K. S., & Skidmore, A. K. (2003). Spectral discrimination of vegetation types in a coastal wetland. *Remote Sensing of Environment*, 85(1), 92-108. doi:10.1016/s0034-4257(02)00196-7

- Schmugge, T. J., Jackson, T. J., & McKim, H. L. (1980). Survey of methods for soil moisture determination. *Water Resources Research*, 16(6), 961-979. doi:<https://doi.org/10.1029/WR016i006p00961>
- Seeyan, S., Merkel, B., & Abo, R. (2014). Investigation of the Relationship between Groundwater Level Fluctuation and Vegetation Cover by using NDVI for Shaqlawa Basin, Kurdistan Region – Iraq. *Journal of Geography and Geology*, 6, 187. doi:10.5539/jgg.v6n3p187
- Setegn, S., Srinivasan, R., Melesse, A., & Dargahi, B. (2009). SWAT Model Application and Prediction Uncertainty Analysis in the Lake Tana Basin, Ethiopia. *Hydrological Processes*, 24, 357-367. doi:10.1002/hyp.7457
- Sharma, A. K., Kumar, A., Saxena, S., Beniwal, M. J. I. J. o. E. R., & Technology. (2015). Evaluating WEKA over the Open Source Web Data Mining Tools. 8(1), 128-132.
- Sharmila, S., Joseph, S., Sahai, A., Abhilash, S., & Chattopadhyay, R. (2015). Future projection of Indian summer monsoon variability under climate change scenario: An assessment from CMIP5 climate models. *Global Planetary Change*, 124, 62-78.
- Sheykhmousa, M. R., Mahdianpari, M., Ghanbari, H., Mohammadimanesh, F., Ghamisi, P., & Homayouni, S. (2020). Support Vector Machine Versus Random Forest for Remote Sensing Image Classification: A Meta-Analysis and Systematic Review. *IEEE Journal of Selected Topics in Applied Earth Observations and Remote Sensing*, 13, 6308-6325. doi:10.1109/jstars.2020.3026724
- Shi, P., Li, P., Li, Z., Sun, J., Wang, D., & Min, Z. (2022). Effects of grass vegetation coverage and position on runoff and sediment yields on the slope of Loess Plateau, China. *Agricultural Water Management*, 259, 107231. doi:<https://doi.org/10.1016/j.agwat.2021.107231>
- Shi, Y., Shen, Y., Kang, E., Li, D., Ding, Y., Zhang, G., & Hu, R. (2007). Recent and Future Climate Change in Northwest China. *Climatic Change*, 80(3), 379-393. doi:10.1007/s10584-006-9121-7
- Short, F. T., Kosten, S., Morgan, P. A., Malone, S., & Moore, G. E. (2016). Impacts of climate change on submerged and emergent wetland plants. *Aquatic Botany*, 135, 3-17. doi:<https://doi.org/10.1016/j.aquabot.2016.06.006>
- Shrestha, U. B., Sharma, K. P., Devkota, A., Siwakoti, M., & Shrestha, B. B. (2018). Potential impact of climate change on the distribution of six invasive alien plants in Nepal. *Ecological Indicators*, 95, 99-107. doi:<https://doi.org/10.1016/j.ecolind.2018.07.009>
- Silva Jr, R., Souza F, P. W., Salomão, G., Tavares, A., Santos, J., Santos, D., . . . Rocha, E. (2021). Response of Water Balance Components to Changes in Soil Use and Vegetation Cover Over Three Decades in the Eastern Amazon. *Frontiers in Water*, 3, 1. doi:10.3389/frwa.2021.749507
- Simpson, P. ( 2022). *Murrumbidgee Bulk Entitlement Delivery Trials 2016 & 2017*. Retrieved from [https://www.industry.nsw.gov.au/data/assets/pdf\\_file/0004/515218/BED-trial.pdf](https://www.industry.nsw.gov.au/data/assets/pdf_file/0004/515218/BED-trial.pdf)
- Sims, N. C., & Colloff, M. J. (2012). Remote sensing of vegetation responses to flooding of a semi-arid floodplain: Implications for monitoring ecological effects of environmental flows. *Ecological Indicators*, 18, 387-391. doi:10.1016/j.ecolind.2011.12.007
- Singh, A. A., & Singh, A. K. (2021). Chapter 6 - Climatic controls on water resources and its management: challenges and prospects of sustainable development in Indian perspective. In B. Thokchom, P. Qiu, P. Singh, & P. K. Iyer (Eds.), *Water Conservation in the Era of Global Climate Change* (pp. 121-145): Elsevier.
- Smettem, K. R. J., Waring, R. H., Callow, J. N., Wilson, M., & Mu, Q. (2013). Satellite-derived estimates of forest leaf area index in southwest Western Australia are not tightly coupled to interannual variations in rainfall: implications for groundwater decline in a

- drying climate. *Global Change Biology*, 19(8), 2401-2412. doi:<https://doi.org/10.1111/gcb.12223>
- Smith, T. C., & Frank, E. (2016). Introducing machine learning concepts with WEKA. In *Statistical genomics* (pp. 353-378). Totowa, NJ, USA: Humana Press.
- Song, Y., Jin, L., & Wang, H. (2018). Vegetation Changes along the Qinghai-Tibet Plateau Engineering Corridor Since 2000 Induced by Climate Change and Human Activities. *Remote Sensing*, 10(1). doi:10.3390/rs10010095
- Song, Y. H., Chung, E. S., & Shahid, S. (2021). Spatiotemporal differences and uncertainties in projections of precipitation and temperature in South Korea from CMIP6 and CMIP5 general circulation models. *International Journal of Climatology*, 41(13), 5899-5919. doi:10.1002/joc.7159
- Sperber, K., Annamalai, H., Kang, I.-S., Kitoh, A., Moise, A., Turner, A., . . . Zhou, T. (2013). The Asian summer monsoon: an intercomparison of CMIP5 vs. CMIP3 simulations of the late 20th century. *Climate Dynamics*, 41(9), 2711-2744.
- Spracklen, D. V., Baker, J. C. A., Garcia-Carreras, L., & Marsham, J. H. (2018). The Effects of Tropical Vegetation on Rainfall. *Annual Review of Environment and Resources*, 43(1), 193-218. doi:10.1146/annurev-environ-102017-030136
- Starr, B. (1999). Soil erosion, phosphorous and dryland salinity in the upper Murrumbidgee: past changes and findings.
- Stas, M., Orshoven, J., Dong, Q., Heremans, S., & Zhang, B. (2016). *A comparison of machine learning algorithms for regional wheat yield prediction using NDVI time series of SPOT-VGT*.
- Strauch, M., & Volk, M. (2013). SWAT plant growth modification for improved modeling of perennial vegetation in the tropics. *Ecological Modelling*, 269, 98-112. doi:<https://doi.org/10.1016/j.ecolmodel.2013.08.013>
- Sun, L., Yang, L., Hao, L., Fang, D., Jin, K., & Huang, X. (2017). Hydrological Effects of Vegetation Cover Degradation and Environmental Implications in a Semiarid Temperate Steppe, China. *Sustainability*, 9(2). doi:10.3390/su9020281
- Sutanudjaja, E. H., van Beek, L. P. H., de Jong, S. M., van Geer, F. C., & Bierkens, M. F. P. (2014). Calibrating a large-extent high-resolution coupled groundwater-land surface model using soil moisture and discharge data. *Water Resources Research*, 50(1), 687-705. doi:10.1002/2013wr013807
- Sykes, M. T. (2009). Climate Change Impacts: Vegetation. In *Encyclopedia of Life Sciences*.
- Tan, M. L., Gassman, P. W., Yang, X., & Haywood, J. (2020). A review of SWAT applications, performance and future needs for simulation of hydro-climatic extremes. *Advances in Water Resources*, 143, 103662. doi:<https://doi.org/10.1016/j.advwatres.2020.103662>
- Tang, W., Liu, S., Kang, P., Peng, X., Li, Y., Guo, R., . . . Zhu, L. (2021). Quantifying the lagged effects of climate factors on vegetation growth in 32 major cities of China. *Ecological Indicators*, 132, 108290. doi:<https://doi.org/10.1016/j.ecolind.2021.108290>
- Taylor, K. E., Stouffer, R. J., & Meehl, G. A. (2012). An Overview of CMIP5 and the Experiment Design. *Bulletin of the American meteorological Society*, 93(4), 485-498. doi:10.1175/bams-d-11-00094.1
- Thapa, R., Thoms, M. C., & Parsons, M. (2016). The response of dryland floodplain vegetation productivity to flooding and drying. *Journal of Arid Environments*, 129, 42-55. doi:10.1016/j.jaridenv.2016.02.007
- Thomey, M. L., Collins, S. L., Vargas, R., Johnson, J. E., Brown, R. F., Natvig, D. O., & Friggens, M. T. (2011). Effect of precipitation variability on net primary production and soil respiration in a Chihuahuan Desert grassland. 17(4), 1505-1515.

- Thompson, J. R., Gavin, H., Refsgaard, A., Refstrup Sørensen, H., & Gowing, D. J. (2009). Modelling the hydrological impacts of climate change on UK lowland wet grassland. *Wetlands Ecology and Management*, 17(5), 503-523. doi:10.1007/s11273-008-9127-1
- Tian, S., Renzullo, L. J., van Dijk, A. I. J. M., Tregoning, P., & Walker, J. P. (2019). Global joint assimilation of GRACE and SMOS for improved estimation of root-zone soil moisture and vegetation response. *Hydrol. Earth Syst. Sci.*, 23(2), 1067-1081. doi:10.5194/hess-23-1067-2019
- Tockner, K., & Stanford, J. A. (2002). Riverine flood plains: present state and future trends. *Environmental Conservation*, 29(3), 308-330. doi:10.1017/s037689290200022x
- Tomlinson, M., & Boulton, A. J. (2010). Ecology and management of subsurface groundwater dependent ecosystems in Australia—a review. *Marine Freshwater Research*, 61(8), 936-949.
- Tucker, C. J. (1979). Red and photographic infrared linear combinations for monitoring vegetation. *Remote Sensing of Environment*, 8(2), 127-150. doi:10.1016/0034-4257(79)90013-0
- Tucker, C. J., Slayback, D. A., Pinzon, J. E., Los, S. O., Myneni, R. B., & Taylor, M. G. (2001). Higher northern latitude normalized difference vegetation index and growing season trends from 1982 to 1999. *International Journal of Biometeorology*, 45(4), 184-190. doi:10.1007/s00484-001-0109-8
- Ummenhofer, C. C., & Meehl, G. A. (2017). Extreme weather and climate events with ecological relevance: a review. *Philos Trans R Soc Lond B Biol Sci*, 372(1723). doi:10.1098/rstb.2016.0135
- Uniyal, B., Dietrich, J., Vasilakos, C., & Tzoraki, O. (2017). Evaluation of SWAT simulated soil moisture at catchment scale by field measurements and Landsat derived indices. *Agricultural Water Management*, 193, 55-70. doi:<https://doi.org/10.1016/j.agwat.2017.08.002>
- USGS. (2021). Earth explorer. US Geological Survey. Retrieved from <https://earthexplorer.usgs.gov/>
- Valencia, S., Salazar, J. F., Villegas, J. C., Hoyos, N., & Duque-Villegas, M. J. A. P. (2022). SWAT-Tb with improved LAI representation in the tropics highlights the role of forests in watershed regulation.
- van der Velde, M., Tubiello, F. N., Vrieling, A., & Bouraoui, F. (2012). Impacts of extreme weather on wheat and maize in France: evaluating regional crop simulations against observed data. *113*(3), 751-765.
- van Dijk, A. I. J. M., Beck, H. E., Crosbie, R. S., de Jeu, R. A. M., Liu, Y. Y., Podger, G. M., . . . Viney, N. R. (2013). The Millennium Drought in southeast Australia (2001–2009): Natural and human causes and implications for water resources, ecosystems, economy, and society. *Water Resources Research*, 49(2), 1040-1057. doi:<https://doi.org/10.1002/wrcr.20123>
- Van Meerveld, H., Seibert, J., & Peters, N. E. (2015). Hillslope–riparian-stream connectivity and flow directions at the Panola Mountain Research Watershed. *Hydrol. Processes*, 29(16), 3556-3574.
- Vaze, J., Davidson, A., Teng, J., & Podger, G. (2011). Impact of climate change on water availability in the Macquarie-Castlereagh River Basin in Australia. *Hydrological Processes*, 25(16), 2597-2612. doi:<https://doi.org/10.1002/hyp.8030>
- Verstraeten, G., Prosser, I. P., & Fogarty, P. (2007). Predicting the spatial patterns of hillslope sediment delivery to river channels in the Murrumbidgee catchment, Australia. *Journal of Hydrology*, 334(3), 440-454. doi:<https://doi.org/10.1016/j.jhydrol.2006.10.025>

- Vigiak, O., Malago, A., Bouraoui, F., Vanmaercke, M., & Poesen, J. (2015). Adapting SWAT hillslope erosion model to predict sediment concentrations and yields in large Basins. *Sci Total Environ*, 538, 855-875. doi:10.1016/j.scitotenv.2015.08.095
- Vincent, L. A., Wang, X. L., Milewska, E. J., Wan, H., Yang, F., & Swail, V. (2012). A second generation of homogenized Canadian monthly surface air temperature for climate trend analysis. *Journal of Geophysical Research: Atmospheres*, 117(D18). doi:<https://doi.org/10.1029/2012JD017859>
- Virnodkar, S. S., Pachghare, V. K., Patil, V., C., & Jha, S. K. (2020). Remote sensing and machine learning for crop water stress determination in various crops: a critical review. *Precision Agriculture*, 21(5), 1121-1155. doi:10.1007/s11119-020-09711-9
- Von Freyberg, J., Radny, D., Gall, H. E., & Schirmer, M. (2014). Implications of hydrologic connectivity between hillslopes and riparian zones on streamflow composition. *J. Contam. Hydrol*, 169, 62-74.
- Vörösmarty, C. J., McIntyre, P. B., Gessner, M. O., Dudgeon, D., Prusevich, A., Green, P., . . . Liermann, C. R. (2010). Global threats to human water security and river biodiversity. *Nature*, 467(7315), 555-561.
- Vrieling, A., de Leeuw, J., & Said, M. (2013). Length of Growing Period over Africa: Variability and Trends from 30 Years of NDVI Time Series. *Remote Sensing*, 5(2), 982-1000. doi:10.3390/rs5020982
- Wallbrink, P. J., Olley, J. M., Murray, A. S., & Olive, L. J. (1996). *The contribution of subsoil to sediment yield in the Murrumbidgee River basin, New South Wales, Australia*, Wallingford, UK, .
- Wanders, N., Bierkens, M. F. P., de Jong, S. M., de Roo, A., & Karssenber, D. (2014). The benefits of using remotely sensed soil moisture in parameter identification of large-scale hydrological models. *Water Resources Research*, 50(8), 6874-6891. doi:10.1002/2013wr014639
- Wang, B., Yim, S.-Y., Lee, J.-Y., Liu, J., & Ha, K.-J. (2014). Future change of Asian-Australian monsoon under RCP 4.5 anthropogenic warming scenario. *Climate Dynamics*, 42(1), 83-100. doi:10.1007/s00382-013-1769-x
- Wang, P., Zhang, Y., Yu, J., Fu, G., & Ao, F. (2011). Vegetation dynamics induced by groundwater fluctuations in the lower Heihe River Basin, northwestern China. *Journal of Plant Ecology*, 4(1-2), 77-90. doi:10.1093/jpe/rtr002
- Wang, S., Kang, S., Zhang, L., & Li, F. (2008). Modelling hydrological response to different land-use and climate change scenarios in the Zamu River basin of northwest China. *Hydrological Processes*, 22(14), 2502-2510. doi:<https://doi.org/10.1002/hyp.6846>
- Ward, D. P., Petty, A., Setterfield, S. A., Douglas, M. M., Ferdinands, K., Hamilton, S. K., & Phinn, S. (2014). Floodplain inundation and vegetation dynamics in the Alligator Rivers region (Kakadu) of northern Australia assessed using optical and radar remote sensing. *Remote Sensing of Environment*, 147, 43-55. doi:<https://doi.org/10.1016/j.rse.2014.02.009>
- Ward, J. V., Malard, F., Tockner, K., & Uehlinger, U. (1999). Influence of ground water on surface water conditions in a glacial flood plain of the Swiss Alps. *Hydrological Processes*, 13(3), 277-293. doi:10.1002/(sici)1099-1085(19990228)13:3<277::Aid-hyp738>3.0.Co;2-n
- Watson, D. J. (1947). Comparative physiological studies on the growth of field crops: I. Variation in net assimilation rate and leaf area between species and varieties, and within and between years. *Annals of botany*, 11(41), 41-76.
- Wedajo, G. K., Muleta, M. K., Gessesse, B., & Koriche, S. A. (2019). Spatiotemporal climate and vegetation greenness changes and their nexus for Dhidhessa River Basin, Ethiopia. *Environmental Systems Research*, 8(1), 31. doi:10.1186/s40068-019-0159-8

- Wen, L., Macdonald, R., Morrison, T., Hameed, T., Saintilan, N., & Ling, J. (2013). From hydrodynamic to hydrological modelling: Investigating long-term hydrological regimes of key wetlands in the Macquarie Marshes, a semi-arid lowland floodplain in Australia. *Journal of Hydrology*, 500, 45-61. doi:10.1016/j.jhydrol.2013.07.015
- Wen, L., Yang, X., & Saintilan, N. (2012). Local climate determines the NDVI-based primary productivity and flooding creates heterogeneity in semi-arid floodplain ecosystem. *Ecological Modelling*, 242, 116-126. doi:<https://doi.org/10.1016/j.ecolmodel.2012.05.018>
- Williams, J. R. (2017). Water reform in the Murray-Darling Basin: A challenge in complexity in balancing social, economic and environmental perspectives. *150*, 68-92.
- Wu, C., Webb, J. A., & Stewardson, M. J. (2022). Modelling Impacts of Environmental Water on Vegetation of a Semi-Arid Floodplain; Lakes System Using 30-Year Landsat Data. *Remote Sensing*, 14(3). doi:10.3390/rs14030708
- Wu, L., Liu, X., Yang, Z., Yu, Y., & Ma, X. (2022). Effects of single- and multi-site calibration strategies on hydrological model performance and parameter sensitivity of large-scale semi-arid and semi-humid watersheds. *Hydrol. Processes*, 36(6), e14616. doi:<https://doi.org/10.1002/hyp.14616>
- Wu, T., Lu, Y., Fang, Y., Xin, X., Li, L., Li, W., . . . Liu, X. (2019). The Beijing Climate Center Climate System Model (BCC-CSM): The main progress from CMIP5 to CMIP6. *Geoscientific Model Development*, 12(4), 1573-1600. doi:10.5194/gmd-12-1573-2019
- Wu, W., Tao, Z., Chen, G., Meng, T., Li, Y., Feng, H., . . . Meteorology, F. (2022). Phenology determines water use strategies of three economic tree species in the semi-arid Loess Plateau of China. *312*, 108716.
- Wu, X., Dong, W., Lin, X., Liang, Y., Meng, Y., & Xie, W. (2017). Evolution of wetland in Honghe National Nature Reserve from the view of hydrogeology. *Science of The Total Environment*, 609, 1370-1380. doi:<https://doi.org/10.1016/j.scitotenv.2017.07.260>
- Xiang, K., Li, Y., Horton, R., & Feng, H. (2020). Similarity and difference of potential evapotranspiration and reference crop evapotranspiration – a review. *Agricultural Water Management*, 232, 106043. doi:<https://doi.org/10.1016/j.agwat.2020.106043>
- Xiaomei, J., Li, W., Zhang, Y., Zhongqi, X., & Ying, Y. (2007). A study of the relationship between vegetation growth and groundwater in the Yinchuan Plain. *Earth Science Frontiers*, 14(3), 197-203.
- Xu, G., Zhang, H., Chen, B., Zhang, H., Innes, J. L., Wang, G., . . . Myneni, R. B. (2014). Changes in Vegetation Growth Dynamics and Relations with Climate over China's Landmass from 1982 to 2011. *Remote Sensing*, 6(4), 3263-3283. doi:10.3390/rs6043263
- Xu, K., Wang, X., Jiang, C., & Sun, O. J. (2020). Assessing the vulnerability of ecosystems to climate change based on climate exposure, vegetation stability and productivity. *Forest Ecosystems*, 7(1), 23. doi:10.1186/s40663-020-00239-y
- Xu, R., Yu, P., Liu, Y., Chen, G., Yang, Z., Zhang, Y., . . . Guo, Y. (2023). Climate change, environmental extremes, and human health in Australia: challenges, adaptation strategies, and policy gaps. *The Lancet Regional Health - Western Pacific*, 40, 100936. doi:<https://doi.org/10.1016/j.lanwpc.2023.100936>
- Xue, J., & Su, B. (2017). Significant Remote Sensing Vegetation Indices: A Review of Developments and Applications. *Journal of Sensors*, 2017, 1353691. doi:10.1155/2017/1353691
- Xue, J., Wang, Y., Teng, H., Wang, N., Li, D., Peng, J., . . . Shi, Z. (2021). Dynamics of Vegetation Greenness and Its Response to Climate Change in Xinjiang over the Past Two Decades. *Remote Sensing*, 13(20). doi:10.3390/rs13204063

- Yang, D., Shao, W., Yeh, P. J. F., Yang, H., Kanae, S., & Oki, T. (2009). Impact of vegetation coverage on regional water balance in the nonhumid regions of China. *Water Resources Research*, 45(7), W00A14-n/a. doi:10.1029/2008WR006948
- Yang, D., Yang, Y., & Xia, J. (2021). Hydrological cycle and water resources in a changing world: A review. *Geography and Sustainability*, 2(2), 115-122. doi:<https://doi.org/10.1016/j.geosus.2021.05.003>
- Yin, L., Zhou, Y., Huang, J., Wenninger, J., Zhang, E., Hou, G., & Dong, J. (2015). Interaction between groundwater and trees in an arid site: Potential impacts of climate variation and groundwater abstraction on trees. *Journal of Hydrology*, 528, 435-448. doi:10.1016/j.jhydrol.2015.06.063
- Yonaba, R., Biauou, A. C., Koïta, M., Tazen, F., Mounirou, L. A., Zouré, C. O., . . . Yacouba, H. (2021). A dynamic land use/land cover input helps in picturing the Sahelian paradox: Assessing variability and attribution of changes in surface runoff in a Sahelian watershed. *Science of The Total Environment*, 757, 143792. doi:<https://doi.org/10.1016/j.scitotenv.2020.143792>
- Yuan, F., Sawaya, K. E., Loeffelholz, B. C., & Bauer, M. E. (2005). Land cover classification and change analysis of the Twin Cities (Minnesota) Metropolitan Area by multitemporal Landsat remote sensing. *Remote Sensing of Environment*, 98(2-3), 317-328. doi:10.1016/j.rse.2005.08.006
- Yuan, Q., Li, S., Yue, L., Li, T., Shen, H., & Zhang, L. (2019). Monitoring the Variation of Vegetation Water Content with Machine Learning Methods: Point–Surface Fusion of MODIS Products and GNSS-IR Observations. *11*(12), 1440.
- Zachos, J., Pagani, M., Sloan, L., Thomas, E., & Billups, K. J. s. (2001). Trends, rhythms, and aberrations in global climate 65 Ma to present. *292*(5517), 686-693.
- Zhang, D., Lin, Q., Chen, X., & Chai, T. (2019). Improved Curve Number Estimation in SWAT by Reflecting the Effect of Rainfall Intensity on Runoff Generation. *Water*, 11(1). doi:10.3390/w11010163
- Zhang, J.-T., Ru, W., & Li, B. (2006). Relationships between vegetation and climate on the Loess Plateau in China. *Folia Geobotanica*, 41(2), 151-163. doi:10.1007/BF02806476
- Zhang, L., Walker, G. R., & Dawes, W. (1999). Predicting the effect of vegetation changes on catchment average water balance.
- Zhang, R., Ouyang, Z.-T., Xie, X., Guo, H. Q., Tan, D. Y., Xiao, X. M., . . . Zhao, B. (2016). Impact of Climate Change on Vegetation Growth in Arid Northwest of China from 1982 to 2011. *Remote Sensing*, 8(5). doi:10.3390/rs8050364
- Zhang, Y., Chiew, F. H. S., Zhang, L., & Li, H. (2009). Use of Remotely Sensed Actual Evapotranspiration to Improve Rainfall Runoff Modeling in Southeast Australia. *Journal of Hydrometeorology*, 10(4), 969-980. doi:10.1175/2009jhm1061.1
- Zhang, Y., Gentine, P., Luo, X., Lian, X., Liu, Y., Zhou, S., . . . Keenan, T. F. (2022). Increasing sensitivity of dryland vegetation greenness to precipitation due to rising atmospheric CO<sub>2</sub>. *Nature Communications*, 13(1), 4875. doi:10.1038/s41467-022-32631-3
- Zheng, K., Tan, L., Sun, Y., Wu, Y., Duan, Z., Xu, Y., & Gao, C. (2021). Impacts of climate change and anthropogenic activities on vegetation change: Evidence from typical areas in China. *Ecological Indicators*, 126, 107648. doi:<https://doi.org/10.1016/j.ecolind.2021.107648>
- Zhong, L., Ma, Y., Salama, M. S., & Su, Z. (2010). Assessment of vegetation dynamics and their response to variations in precipitation and temperature in the Tibetan Plateau. *Climatic Change*, 103(3), 519-535. doi:10.1007/s10584-009-9787-8
- Zhou, W., Gang, C., Zhou, L., Chen, Y., Li, J., Ju, W., & Odeh, I. (2014). Dynamic of grassland vegetation degradation and its quantitative assessment in the northwest China. *Acta Oecologica*, 55, 86-96. doi:<https://doi.org/10.1016/j.actao.2013.12.006>

- Zhou, X., Yang, W., Luo, K., & Tang, X. (2022). Estimation of Aboveground Vegetation Water Storage in Natural Forests in Jiuzhaigou National Nature Reserve of China Using Machine Learning and the Combination of Landsat 8 and Sentinel-2 Data. *13*(4), 507.
- Zhu, L., Gong, H., Dai, Z., Xu, T., & Su, X. (2015). An integrated assessment of the impact of precipitation and groundwater on vegetation growth in arid and semiarid areas. *Environmental Earth Sciences*, *74*(6), 5009-5021. doi:10.1007/s12665-015-4513-5
- Zhu, Y., Chen, Y., Ren, L., Lü, H., Zhao, W., Yuan, F., & Xu, M. (2016). Ecosystem restoration and conservation in the arid inland river basins of Northwest China: Problems and strategies. *Ecological Engineering*, *94*, 629-637.
- Zhu, Y., Wu, Y., & Drake, S. (2004). A survey: obstacles and strategies for the development of ground-water resources in arid inland river basins of Western China. *Journal of Arid Environments*, *59*(2), 351-367.
- Zhu, Y. Y., & Yang, S. (2020). Evaluation of CMIP6 for historical temperature and precipitation over the Tibetan Plateau and its comparison with CMIP5. *Advances in Climate Change Research*, *11*(3), 239-251. doi:10.1016/j.accr.2020.08.001
- Ziadat, F. M., & Taimeh, A. Y. (2013). Effect of Rainfall Intensity, Slope, Land Use and Antecedent Soil Moisture on Soil Erosion in an Arid Environment. *Land Degradation & Development*, *24*(6), 582-590. doi:10.1002/ldr.2239
- Zubieta, R., Saavedra, M., Silva, Y., & Giráldez, L. (2017). Spatial analysis and temporal trends of daily precipitation concentration in the Mantaro River basin: central Andes of Peru. *Stochastic Environmental Research and Risk Assessment*, *31*(6), 1305-1318. doi:10.1007/s00477-016-1235-5

## APPENDIX A

The LAI changes in response to groundwater flow (GW) are simulated using climate data predicted from three different GCMs under RCP 8.5.

RCP 8.5	ACCESS1.0						MIROC5						MK3					
	2031-2055		2056-2075		2076-2100		2031-2055		2056-2075		2076-2100		2031-2055		2056-2075		2076-2100	
Month	SURQ	LAI																
Jan	-61.19	-10.76	-64.25	-11.12	-68.39	-19.21	-40.45	-29.60	8.07	-25.91	-9.81	-19.75	-89.68	-41.05	-98.25	-32.24	-85.41	-38.16
Feb	-98.37	-8.96	-78.46	-9.72	-98.25	-17.45	-89.59	-24.05	-94.75	-21.45	-87.33	-14.78	-99.20	-37.06	-98.09	-29.19	-99.08	-34.28
Mar	-96.09	-8.23	-98.39	-9.24	-99.75	-16.99	-95.65	-21.69	-98.29	-19.35	-86.19	-12.69	-99.47	-35.67	-98.31	-27.88	-97.51	-32.61
Apr	-91.60	5.89	-99.49	-6.07	-98.54	-29.58	-75.22	3.85	-72.90	6.67	-9.34	15.64	-94.60	-15.33	-98.01	-5.09	-95.73	-10.92
May	-97.12	49.05	-99.83	1.54	-99.75	3.45	-80.33	126.28	-88.21	132.30	-75.53	151.95	-98.09	83.61	-99.97	106.03	-99.98	94.08
Jun	-98.71	-0.16	-96.96	-0.05	-93.27	0.16	-91.74	1.85	-82.00	3.23	-71.71	3.85	-99.62	0.01	-100.00	0.72	-100.00	1.42
Jul	-96.11	2.13	-91.91	6.30	-87.52	4.04	-76.60	22.34	-80.47	30.55	-52.46	37.57	-99.41	11.95	-99.19	19.29	-99.70	24.30
Aug	-94.91	4.85	-90.21	13.69	-95.22	9.69	-55.04	45.30	-67.47	58.76	-46.29	69.88	-98.19	30.08	-99.77	42.05	-99.09	48.49
Sep	-91.35	4.60	-87.03	15.00	-92.49	10.72	-66.36	47.95	-74.46	60.29	-21.69	66.02	-99.83	32.96	-99.48	43.91	-98.96	45.36
Oct	-86.39	2.02	-88.81	13.21	-88.28	8.72	-61.03	34.51	-65.43	43.04	-37.82	28.09	-98.03	21.01	-97.97	28.45	-98.45	23.31
Nov	-90.78	-4.16	-94.82	4.49	-93.52	1.68	-77.92	-24.14	-80.50	-29.97	-74.03	-24.00	-98.64	-0.64	-99.18	-30.77	-99.37	-40.28
Dec	-83.38	-7.48	-90.03	-9.68	-89.03	-18.90	-79.69	-40.11	-62.28	-38.94	-76.36	-33.72	-95.55	-46.61	-99.54	-39.63	-99.97	-47.92

## APPENDIX B

The LAI changes in response to groundwater flow (GW) are simulated using climate data predicted from three different GCMs under RCP 8.5.

RCP 8.5	ACCESS1.0						MIROC5						MK3					
	2031-2055		2056-2075		2076-2100		2031-2055		2056-2075		2076-2100		2031-2055		2056-2075		2076-2100	
	GW	LAI																
<b>Month</b>	GW	LAI																
<b>Jan</b>	-29.67	-10.76	-73.04	-11.12	-67.86	-19.21	-27.01	-29.60	-31.53	-25.91	-29.02	-19.75	-82.32	-41.05	-98.85	-32.24	-96.85	-38.16
<b>Feb</b>	2.51	-8.96	-56.95	-9.72	-47.33	-17.45	14.79	-24.05	36.13	-21.45	31.33	-14.78	-66.55	-37.06	-88.12	-29.19	-86.13	-34.28
<b>Mar</b>	-47.52	-8.23	-53.15	-9.24	-59.94	-16.99	21.98	-21.69	14.09	-19.35	38.50	-12.69	-69.33	-35.67	-78.34	-27.88	-74.37	-32.61
<b>Apr</b>	-71.95	5.89	-71.12	-6.07	-83.51	-29.58	31.22	3.85	6.74	6.67	91.06	15.64	-54.18	-15.33	-54.45	-5.09	-67.28	-10.92
<b>May</b>	-68.90	49.05	-84.93	1.54	-90.48	3.45	100.44	126.28	85.75	132.30	184.08	151.95	-20.89	83.61	-31.69	106.03	-52.46	94.08
<b>Jun</b>	-78.77	-0.16	-93.58	-0.05	-91.67	0.16	36.24	1.85	24.05	3.23	58.40	3.85	-51.09	0.01	-61.76	0.72	-79.00	1.42
<b>Jul</b>	-85.10	2.13	-91.62	6.30	-85.73	4.04	-28.36	22.34	-28.94	30.55	-17.98	37.57	-79.94	11.95	-84.10	19.29	-93.61	24.30
<b>Aug</b>	-83.22	4.85	-83.26	13.69	-80.41	9.69	-42.31	45.30	-43.68	58.76	-41.68	69.88	-88.20	30.08	-91.93	42.05	-98.00	48.49
<b>Sep</b>	-77.71	4.60	-77.99	15.00	-78.12	10.72	-48.91	47.95	-49.92	60.29	-49.45	66.02	-93.58	32.96	-97.23	43.91	-98.74	45.36
<b>Oct</b>	-70.92	2.02	-74.43	13.21	-75.03	8.72	-54.19	34.51	-60.39	43.04	-54.24	28.09	-97.89	21.01	-99.34	28.45	-99.21	23.31
<b>Nov</b>	-64.23	-4.16	-70.23	4.49	-70.46	1.68	-55.18	-24.14	-68.20	-29.97	-58.50	-24.00	-97.49	-0.64	-98.10	-30.77	-99.31	-40.28
<b>Dec</b>	-59.62	-7.48	-70.36	-9.68	-70.46	-18.90	-57.24	-40.11	-63.30	-38.94	-59.95	-33.72	-94.19	-46.61	-98.34	-39.63	-98.89	-47.92